Cranfield University

School of Industrial and Manufacturing Science

PhD THESIS

Academic year 1993-1994

Thierry CHEVROT

Pressure effects on the hot-salt stress-corrosion cracking of titanium alloys

Supervisor: Professor J. R. Nicholls

March 1994

ABSTRACT

Benefiting from good specific mechanical properties, exceptional oxidation resistance, and high temperature capability, Titanium Alloys are used in Gas Turbine Engines, especially in the early stages of the compressor. However they are subject to stress-corrosion cracking in the laboratory when subjected to stresses and contaminated with salts at elevated temperatures. The lack of in-service failures of titanium components due to Hot-Salt Stress-Corrosion Cracking (HSSCC) is not yet understood.

The parameters influencing the HSSCC of titanium alloys (temperature, load, stress and temperature cycling, quantity and kind of salt, air velocity, water vapour or oxygen content of the atmosphere, composition, texture, and microstructure of the alloy, surface conditions), cannot account for the lack of in-service failure. After an examination of the service conditions within a typical gas turbine engine compressor, it was considered that the high pressures prevailing may extend the life of titanium alloys subjected to HSSCC.

This work used a unique high temperature, high pressure, servo-hydraulic facility in order to carry out hot-salt stress-corrosion testing on titanium alloy IMI 834 at high pressure. The results obtained show that high oxygen partial pressures extend significantly the life of IMI 834 subjected to HSSCC.

Continuous thermogravimetric measurements both in oxidising and salt-corroding environments were carried out to study the kinetics of the hot-salt attack of IMI 834. Basic metallography revealed the formation of channels which extend deep into the metal during the initial stages of hot-salt-corrosion.

Theoretical thermodynamic studies highlighted the role of alloying elements and vapour phase metallic chlorides in the mechanisms of the HSSCC of titanium alloys.

A new model for the hot-salt stress-corrosion of titanium alloys is proposed. It is based on the establishment of a self sustaining cycle where vapour phase metallic chlorides act as hydrogen carriers and can diffuse quickly into the material through channels.

ACKNOWLEDGEMENTS

The author would like to express his gratitude to Professor J. R. Nicholls for providing expert and enthusiastic supervision throughout this work. It really is a pleasure to work with him.

Thanks also to Rolls Royce plc. for supporting this work, and especially to Mr R. Wing, Mr P. Webster, and Mr T. Cuningham for many helpful discussions.

Thank you also to my friends Mr J. Hedge and T. Pryor, and M. Deakin who have provided efficient technical support throughout this work. Their input has been invaluable.

Lastly but not least, thanks to my future wife, Helen, who has given me unconditional support during these three years and helped me when times were hard.

To Helen,

TABLE OF CONTENTS

LIST OF FIGURES

LIST OF TABLES

LIST OF PHOTOGRAPHS

NOTATIONS

m_y	Mass of species y deposited during salt spraying	(g)
M_y	Molar mass of species y	(g/mole)
[Salt]	Salt concentration deposited	(g/cm^2)
L(P)	Pressure load applied on the lower pulling rod	(kN)
P, P_{tot}	Total pressure	(bars)
A	Effective section of the lower pulling rod	(mm^2)
Kp	Parabolic rate constant based on mass gain data	($mg^2.cm^{-4}.s^{-1}$)
x	Depth of alpha case	(µm)
T	Temperature	(°K)
σ	Stress	(MPa)
σ_0	Normalised stress	(MPa)
σ_{0atm}	Normalised stress at atmospheric pressure	(MPa)
σ^*	Normalised stress at 1 bar partial pressure of oxygen	(MPa)
t	Time of exposure or time to failure	(h)
t_{exp}	Experimental time to failure	(h)
t_{calc}	Calculated time to failure	(h)
a, b, c, C	Linear regression parameters	
Patm=1 bar	Atmospheric pressure	
P(Y)	Partial pressure of gas Y	(bars)
Vol%(O_2)	Volumetric oxygen content	(%)
X	Mass gain	(µg/cm^2)
R=8.32	Gas constant	(J/mole/°K)
ΔG	Activation energy	(J/mole)
ΔG^0	Standard free energy of formation	(J/mole)
K	Equilibrium rate constant	
a(Y)	Activity of compound Y	

INTRODUCTION

The development of military and civil supersonic aircraft after world war II underlined the need for a new generation of materials which could provide high mechanical properties for airframe and gas turbine engine applications, while keeping the weight of such aircraft to a minimum (Jaffee 1980). In most aerospace applications, aluminium alloys are therefore used to temperatures up to 150 °C. Benefiting from a high strength-to-weight ratio, titanium alloys are currently used at temperatures up to about 600 °C. Above this limit, Nickel based alloys are the best candidate but because of their higher density, there is a penalty to pay in terms of the aircraft's fuel efficiency.

The substitution of titanium for nickel in gas turbine engine components results in significant weight savings and has therefore been an important trend in the development of new engines offering better efficiency on a thrust-to-weight basis. This tendency is indicated in Figure (i), which compares titanium usage in the Rolls Royce RB211-22B which entered service in 1972 with the TRENT 700 which is due to enter service later this year. It can be seen that on the later engine the development of titanium alloys has enabled their use throughout the compressor module of the engine.

However, substitution of titanium for nickel based alloys is far from being direct. In order to achieve this technological advance, limitations of the high temperature use of titanium have to be overcome. These include the possibility of catastrophic titanium fires, creep limitations at very high temperatures, as well as Hot-Salt Stress-Corrosion Cracking (HSSCC) susceptibility (Huron 1988). Titanium fires are currently avoided through careful design, while creep properties have been addressed through alloy development (Eylon 1984, Neal 1989). Indeed IMI 834, the subject alloy of this investigation, and that employed in the later stage of the TRENT high pressure compressor, is an excellent example of a titanium alloy with a usable temperature capability above 600 °C. Hot-salt stress-corrosion cracking still remains a major problem to be addressed.

The problem of HSSCC of titanium alloys has been a worrying concern to the aerospace industry for almost forty years but has not yet been considered as critical.

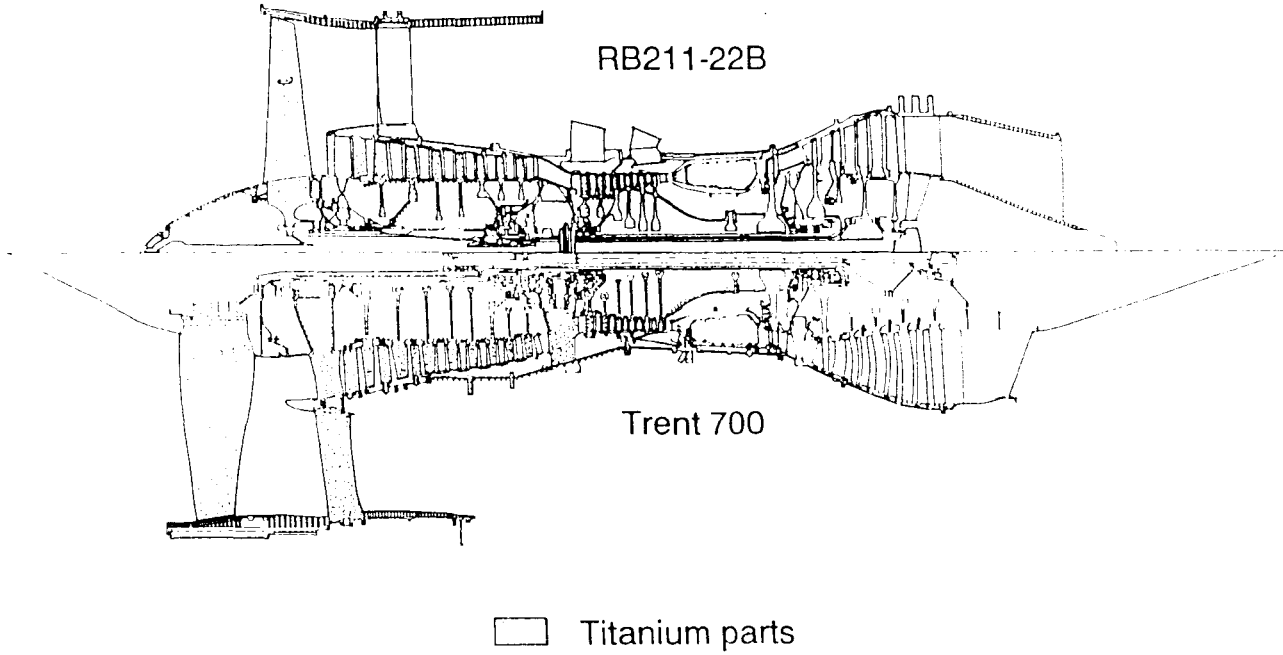

Figure (i): Usage of titanium in gas turbine engine technology
(Used with the permission of Rolls-Royce plc.)

The first report of hot-salt cracking of titanium was made in 1955 by G.W.Bauer when he observed cracking of the material at stresses far below the yield stress of the alloy. This unexpected initiation of cracks was correctly traced back to salty fingerprints and his discovery initiated a considerable amount of research in this field. However, if laboratory failures of titanium alloys exposed to hot-salt are now a well known phenomenon, gas turbines manufacturers have in fact used this class of materials in the high temperature compressor parts of gas turbine engines without reporting any incidents due to stress-corrosion, even after tens of millions of flight hours (King 1966). Several explanations were given for this lack of in-service failures: Some designers stated that stresses and temperatures operating in flight are lower than those expected, others claimed that high airflows encountered in service prevent salt deposition, while a third school of thought is based on the existence of temperature and stress cycles induced by the discontinuous operation of the engine. However because the mechanisms of the HSSCC of titanium alloys have not yet been fully explained, and because the high temperature capability of these materials has been extended, there are growing concerns that hot-salt stress-corrosion may after all become a serious problem. A full understanding of the phenomenon is therefore required in order to specify a "titanium strategy" for the development of even more efficient aircraft.

After an examination of the in-service conditions that prevail within a typical gas turbine engine, it was considered that high pressures encountered in a compressor environment may actually influence the life of titanium components subjected to HSSCC conditions. This study which was carried out using a unique high temperature, high pressure, servo hydraulic facility aimed to characterise the possible interactions between pressure effects and hot-salt stress-corrosion cracking mechanisms. Kinetics studies using continuous thermogravimetric studies and theoretical thermodynamic analyses are used to develop an understanding of the mechanisms of the HSSCC of titanium alloys.

The first three chapters of this work will review the main characteristics of titanium and its alloys, the current knowledge of hot-salt stress-corrosion cracking of titanium alloys and the mechanisms which have been put forward by previous workers for this phenomena. The fourth chapter describes the experimental apparatus and procedures which have been used in the course of this study, while chapter V focuses on the results obtained. In chapter VI, these results will be discussed, and theoretical thermodynamical studies will be introduced in order to develop a new model for the HSSCC of titanium alloys.

CHAPTER I

METALLURGY, MECHANICAL PROPERTIES, AND APPLICATIONS OF COMMERCIAL TITANIUM ALLOYS

" Titanium is not in any sense of the word a wonder metal. Take the rigidity and strength of steel, combine it with the ductility of aluminium, the light weight of magnesium, the corrosion resistance of platinum, add creep resistance at high temperature, high impact resistance at sub-zero temperature, blend these together and only then, might we employ the term wonder metal."

S.Abkowitz, J.J.Burke, R.H.Hiltz Jr. (Abkowitz 1955)

I.a. Introduction

Titanium was first recognised in 1791 by W.Mc Gregor who detected the oxide of a new metal in Ilmenite ($FeOTiO_2$) and was first extracted in any quality in 1937 by Kroll. However the metal was not produced in quantity until the late 40's when it started to be substituted for aluminium for the skin and structure of high-speed aircraft subjected to aerodynamic heating (Polmear 1989).

The metal is extracted from the ore by the production of titanium tetrachloride ($TiCl_4$) and its subsequent reduction by either interaction with magnesium (Kroll process) or Sodium (Hunter process), or by electrolytic reduction (Dow-Howmet process). (Donachie 1982). These extraction processes make titanium a relatively expensive metal (the amount of energy required to produce titanium is currently 70% higher than that needed to extract an equal weight of aluminium), but its high specific mechanical properties may make it more cost effective than other materials, especially in aerospace applications where weight considerations are a major concern (see Figure I.a.).

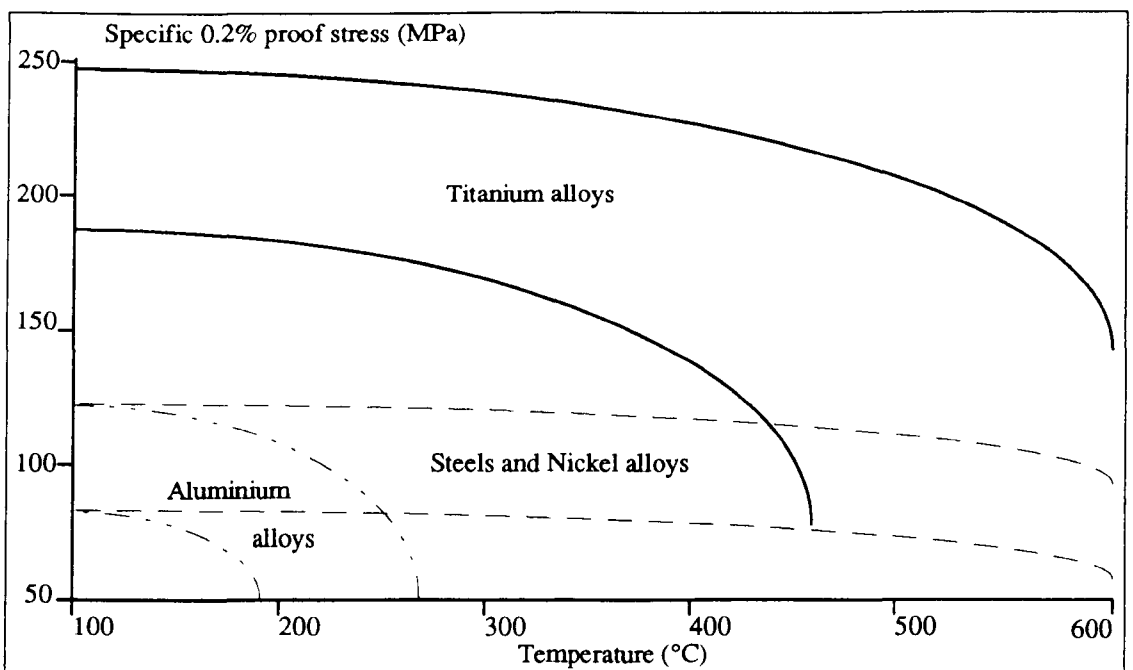

Figure I.a.: Relationship of specific 0.2% proof stress (ratio of proof stress to relative density) with temperature for titanium alloys, aluminium alloys, nickel alloys, and steels (Polmear 1989)

After a brief review of the main physical, chemical, and mechanical properties of pure titanium, the attention will be focused on the different types of commercially available alloys. The mechanical properties of such alloys are intricately dependent on their composition and heat treatment, and a detailed description of these relationships will be given. Finally, the different fields of application for such alloys will be reviewed.

I.b. Titanium metal

Titanium is a low density metallic element which is abundant in the earth's crust but which became available only at the beginning of the century. However its remarkable specific mechanical properties have contributed to its rapid development and use, to make it one of the most successful metals of the past fifty years.

I.b.1 Physical properties

Some of the physical properties of titanium which are relevant to the work achieved in this study are:

Density: With a relative density of 4.51 titanium is considered a light metal. This, combined with good mechanical properties and outstanding corrosion resistance has been the driving force for the use of this metal in the past fifty years.

Crystal structure: At 882 °C, titanium undergoes an allotropic transformation from a low temperature, hexagonal-close-packed structure called Alpha Phase to a body centred cubic Beta Phase that remains stable until the melting point (1678 °C). This transformation from alpha phase to beta phase allows one to heat treat titanium alloys in order to optimise their mechanical properties according to the application considered (Seagle 1968).

Atomic structure: Titanium is a transition metal with an incomplete inner shell in its electronic structure which enables it to form solid solutions with most substitutional elements having a size factor within 20%.

Titanium can therefore form solid solutions with other metallic elements which stabilise either the alpha or the beta phase. For example, one can see on Figure I.b. which

shows the Ti-Al phase diagram that aluminium is an alpha stabiliser. Indeed, aluminium raises the α/β transition from 882 °C for pure titanium to 1240 °C for the alloy containing 29 wt% of Al. Aluminium can also form the γ phase TiAl and another titanium aluminide Ti_3Al (α_2). These two phases are currently investigated in order to produce a new generation of aerospace materials possessing even higher specific properties than currently available commercial titanium alloys.

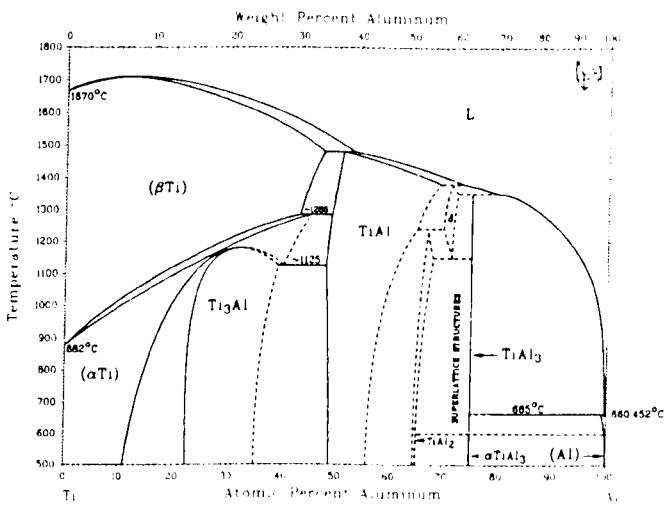

Figure I.b.: Phase diagram of the Ti-Al system (Grahle 1991)

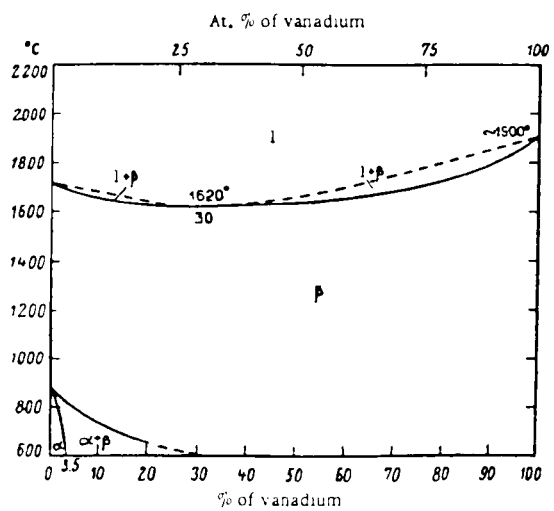

Figure I.c.: Ti-V phase diagram (Molchanova 1964)

Figure I.c. shows the Ti-V diagram. One can see that unlike aluminium, vanadium depresses the temperature of the α/β transus and therefore stabilises the beta phase. This element is actually one of the most active beta stabilisers and decreases very sharply this transition temperature.

I.b.2. Oxidation of titanium

Figure I.d. shows the Ti-O phase diagram up to 35 wt% oxygen (Schofield 1955). Oxygen stabilises the alpha phase which results in a brittle layer called alpha case. The solid solubility of oxygen in the alpha phase increases slightly with temperature. The solid solubility of oxygen in the beta phase is much lower than in the alpha phase and increases with temperature.

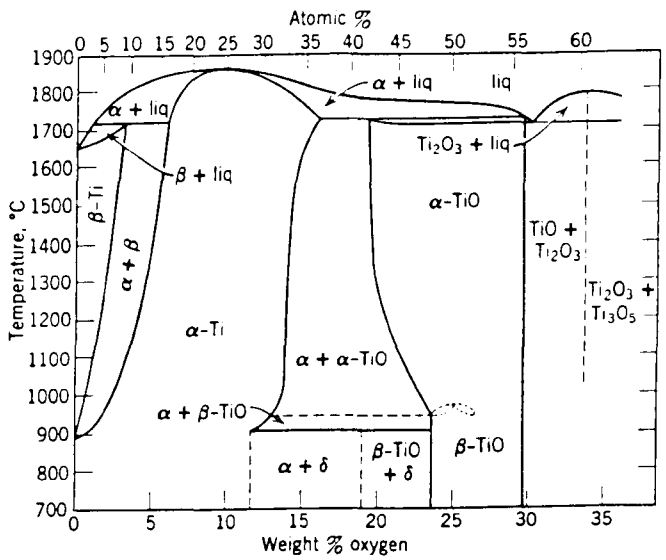

Figure I.d.: The Ti-O phase diagram up to 35 wt% oxygen (Schofield 1955)

The formation of a sequence of layers of the different titanium oxides (TiO, Ti_2O_3, Ti_3O_5, TiO_2) has been reported for oxidation in air and in the presence of water vapour (Kofstad 1966), although the surface scale that is usually observed is TiO_2. Oxidation is governed by a series of rate equations which depend on the temperature and time of exposure (Figure I.e.). However, the observed behaviour will be affected by the purity of the metal and the amounts of alloying additions. In particular, a recent study on the influence of aluminium on the oxidation of titanium showed that parabolic rate oxidation could be extended to temperatures as low as 550 °C (Chaze 1990).

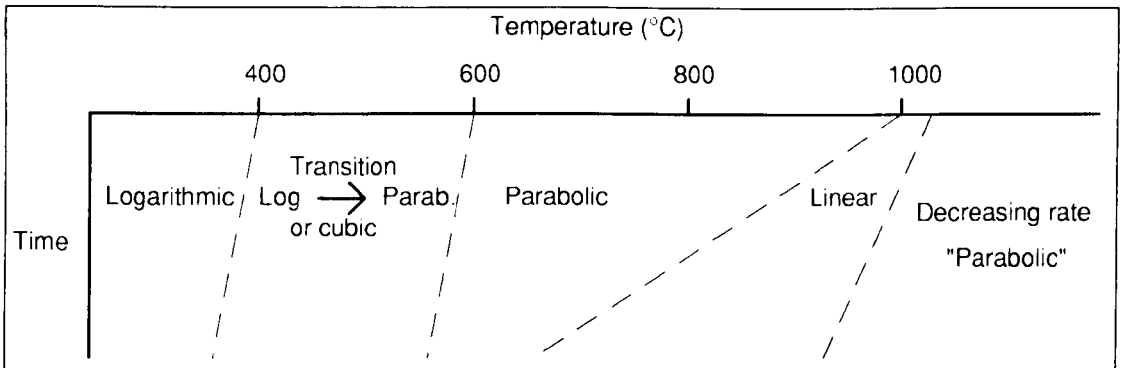

Figure I.e.: Schematic diagram of rate equations observed in oxidation of titanium (Kofstad 1966)

Parabolic oxidation involves in fact two simultaneous processes which are oxygen solution (or formation of alpha case), and oxide growth. Since both of these processes are parabolic, the overall rate behaviour is also parabolic (Kofstad 1966). The oxidation of titanium and its alloys will be discussed in more details in paragraph VI.c.2.

I.b.3. Chemical properties

Corrosion: Titanium passivates in solutions and because of its highly stable oxide film the metal can resist the attack of oxidising solutions, particularly those containing chloride ions. Therefore, titanium is remarkably resistant to wet chlorine gas, bleaching solutions, hypochlorates and chlorine dioxide, although it suffers catastrophic attack in dry chlorine gas. Its resistance to sea water is virtually unsurpassed by other structural materials. However titanium is attacked by reducing environments in which its rutile film (TiO_2) becomes unstable (Bomberger 1968).

Acids: Hydrofluoric acid is the basic agent for the dissolution of titanium and is used as a general etchant and descaling agent. The attack of hydrochloric and sulphuric acids proceeds slowly at room temperature but can be accelerated with a small input of heat. Other inorganic acids have either limited or no appreciable reactivity with the metal.

Gases: The chemical reactivity of titanium with gaseous atmospheres at high temperature is especially important and often necessitates the use of inert atmospheres for hot-working. These reactions may cause dramatic failures in some high temperature applications. Table I.a. compares the solubility of interstitial elements in titanium at room temperature with values reported for iron and aluminium. This table clearly

shows the affinity of titanium for interstitial gases atoms, especially oxygen and nitrogen.

	Interstitial element			
Metal	Oxygen	Nitrogen	Carbon	Hydrogen
Titanium	14.5 wt%	~ 20 wt%	0.5 wt%	~ 100 ppm
Iron	~ 1 ppm	< 5 ppm	100 ppm	< 1 ppm
Aluminium	< 1 ppm	< 1 ppm	< 1 ppm	< 1 ppm

Table I.a. Solubility at room temperature of some interstitial elements in titanium, iron, and aluminium. (Morton 1976)

Titanium combines with oxygen to form a series of oxides from TiO to TiO_2. Ignition can occur in air at 1204 °C and at 610 °C in a pure oxygen atmosphere. The reactivity with nitrogen is similar and is often used for nitride coating of the metal.

Reactions between titanium and hydrogen are a potential problem as they start slightly above room temperature, and can result in brittle failure of titanium alloys. Large amounts of hydrogen can be absorbed either interstitially or with the formation of hydrides (TiH and TiH_3). Indeed hydrogen is a beta stabiliser and in the β phase titanium can dissolve up to 50 at% in solution, equivalent to the hydride TiH. The maximum solubility of hydrogen in alpha titanium is 0.18 wt% (7.8 at.%). This solubility decreases sharply at lower temperatures in the range 320 to 125 °C (see Figure I.f.). It has also been shown that impurities contained in commercial titanium decrease the hydrogen solubility in alpha titanium (Mc Quillan 1951). Unfortunately apart from the above work, studies on the effects of alloying additions on the solubility of hydrogen in titanium are rare. Above 815 °C water vapour and titanium can also combine to form oxides and evolve hydrogen, which is absorbed in the base metal (Abkowitz 1955).

Finally, titanium readily combines with chlorine to form tetrachlorides at temperatures as low as 349 °C (Abkowitz 1955).

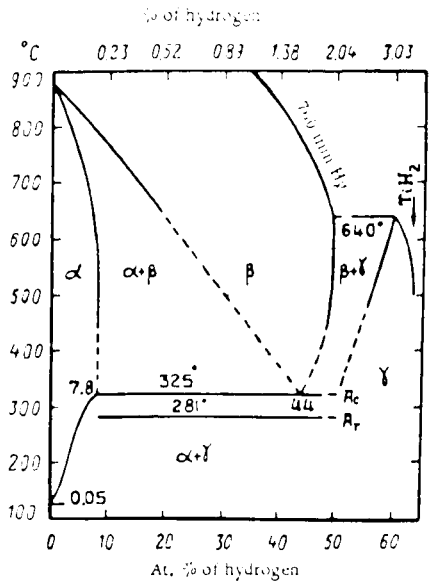

Figure I.f.: Ti-H phase diagram (Molchanova 1964)

I.b.4. Mechanical properties

The mechanical properties of titanium alloys will be discussed later (paragraph I.c.5.) and the purpose of the current discussion is only to present some of the more remarkable features of the unalloyed metal, which is compared with other metallic elements in table I.b.

Tensile properties, ductility, and modulus of elasticity: Unalloyed titanium can have tensile strength ranging from 241 to 689 MPa, depending on the process used for its production. Its ductility ranges from 20 to 40% elongation and 45 to 65% reduction in area, depending upon the interstitial content. The modulus of elasticity is of about 103 GPa. This compares favourably with aluminium and magnesium, but poorly with steel (Table I.b.). Like the modulus of elasticity, the modulus in shear (modulus of rigidity) falls between that of aluminium and that of steel with a value of about 41 GPa.

Creep: The creep strength seems to be the major weakness of unalloyed titanium. This has led to a considerable amount of work to develop alloys with good creep resistance, and is still one of the most active area of research with the metal. In particular the addition of elements such as aluminium and limited amounts of silicon have successfully increased the creep resistance of modern titanium alloys, especially with a view to use in gas turbine engine applications.

Metal	Ratio of Mechanical property to specific density					
	UTS (MPa)	Yield stress (MPa)	Elasticity modulus (MPa)	Rigidity modulus (MPa)	Elongation (%)	Reduction of area (%)
Aluminium	23	7.7	25.5	10	60	70
Copper	28.47	10.77	12.31	4.62	15	52
Iron (pure)	35	17.5	26	8.75	40	80
Magnesium	107	39.6	24.77	9.48	15	50
Titanium (pure)	53.5	30.58	22.9	7.65	55	80

Table I.b. Comparative selected properties (Ratio of mechanical property to specific density) of metals (From Abkowitz 1955)

I.c Titanium alloys

Titanium alloys possess mechanical properties which depend strongly on their composition and microstructure (or heat treatment) (Huron 1988). There are, many combinations possible between these two parameters, and an extensive range of alloys, each with its own characteristics, is currently available.

I.c.1 Classification of titanium alloys

The different alloying elements encountered in titanium alloys either raise or depress the temperature at which titanium metal undergoes the allotropic transformation from its hexagonal-close-packed structure (α phase) to the body centred cubic β phase. Hence titanium alloys are classified according to their respective amounts of α and β phase at room temperature, amounts which depend solely on the composition and heat treatment of the alloy. Three classes are to be distinguished:

α *alloys:* These alloys contain elements which dissolve preferentially in the alpha phase and raise the α/β transus. The main alpha stabilisers are aluminium and tin, but also interstitial elements such as oxygen, carbon, and nitrogen.

β *alloys:* They contain high amounts of beta stabilisers which depress the α/β transus. These alloying elements are mainly molybdenum, tungsten, vanadium, and tantalum which form binary solid solutions with titanium, and copper, manganese, chromium, iron, nickel, cobalt, and hydrogen which form a β eutectoid phase.

$\alpha + \beta$ *alloys:* They usually contain alpha stabilisers, together with 4 to 6 % of beta stabilisers.

Other alloying elements which have no influence on the amounts of α and β phases in the alloy are also used. Two typical examples are zirconium and silicon which acts as a solid solution strengthener for both phases.

I.c.2. Alpha alloys

All α stabilising elements (Al, Sn, O) cause solid solution strengthening and increase the tensile strength of the material by 35 to 70 MPa for each 1 wt% of the added element. However there is a limit to the amount of α stabilising elements which can be added to titanium. Hence, the 'aluminium equivalent content' calculated as

$$\text{Al equivalent} = \text{Al} + \frac{1}{3}\text{Sn} + \frac{1}{6}\text{Zr} + 10\ (\text{C} + \text{O} + 2\times\text{N}) \qquad \text{(I.1)}$$

must be less than 9 wt%. (Rosenberg 1970)

Another limitation for α alloys lies in the amount of aluminium which can be added, as elevated temperature ageing of alloys containing more than 5-6 wt% of Al can lead to the formation of titanium aluminide Ti_3Al and can induce poor ductility.

Finally, the hydrogen content of titanium alloys has to be kept relatively low to avoid the formation of hydrides which play an important role in fracture phenomena with titanium and its alloys (see paragraph I.b.3.).

The class of alpha alloys can in turn be subdivided in three groups:

Fully alpha alloys: These include all grades of commercially pure titanium (i.e. Ti-O alloys), and the alloy Ti-5Al-2.5Sn. In general, fully alpha alloys have relatively low tensile strengths, reasonable creep strengths in the upper temperature range, and good ductilities down to very low temperatures. Their mechanical properties are relatively insensitive to their microstructure. They are readily weldable, but hot-work must be limited to temperatures below the α/β transus to prevent excessive grain growth. Their formability is also limited, and they exhibit a high rate of strain hardening. Three microstructures are to be distinguished (ASTM 1972, Reinsch 1982):

The equiaxed structure is obtained after annealing in the α field and contains relatively small grains. This results in better tensile strength and ductility.

The hexagonal martensitic α' phase is obtained by quenching the alloy after processing the alloy in the β phase field.

Serrated α (or Widmanstätten α plates) is obtained through slow cooling from the β phase field and provides better toughness and creep resistance.

Near alpha alloys: They contain up to 2% of β stabilising elements and can therefore be processed either in the $(\alpha+\beta)$ field or above the α/β transus.

The microstructure of alloys processed in the $(\alpha+\beta)$ field depends mainly on alloy composition and on the cooling rate. Rapid cooling from the processing temperature results in the formation of martensitic α' phase and provides high creep resistance and increased strength. For alloys containing large amounts of aluminium and for relatively slow cooling rates, precipitation of the α_2 phase (Ti_3Al) takes place and induces a loss of ductility but improves weldability and forging characteristics.

Some alloys can be processed in the β field, at temperatures close to the α/β transus. Quenching at these temperatures results in the formation of laths of martensitic α' phase which decomposes on subsequent ageing treatments. The final microstructure consists of laths of α phase delineated by a dispersion of fine β phase, and allows the alloy to reach optimum levels of creep resistance and fatigue strength. It has been suggested that IMI 834 has reached the limit for the optimisation of near alpha alloys (Neal 1989).

More generally, near alpha alloys possess high tensile strengths at room temperature and show the best creep resistance of all titanium alloys from 400 °C up to 650 °C. (Eylon 1984)

Ti-Cu age hardening alloys: Additions of copper to titanium as in IMI 230 (Ti-2.5Cu) induces an increase in the tensile strength of the material by about 150 to 170 MPa. This is accomplished after solution treatment and air cooling or oil quenching, followed by a double ageing treatment which promotes the precipitation of the metastable $TiCu_2$ phase.

I.c.3 Beta alloys

The main characteristic of beta alloys is that they contain large amounts of metastable β phase whose decomposition provokes the precipitation of secondary α phase which can be used to strengthen the material. However the high content of β stabilisers usually results in a higher density, and the instability of such alloys limits their use to relatively low temperatures. So far this class of materials has found few applications, but its use is expected to increase especially as biomaterials due to this classes excellent corrosion resistance and superior forming capabilities.

I.c.4. (α+β) alloys

This class represents more than 70% of all the titanium used in industry. These materials possess a wide range of compositions from highly β stabilised alloys to lean α /β phase contents. Their properties are highly dependent on their heat treatment and on the decomposition of the β phase. (Seagle 1968)

Annealed alloys: Annealing is used primarily to increase fracture toughness, ductility at room temperature, dimensional and metallurgical stability, and creep resistance. Several treatments are to be distinguished:

Mill annealing is a partial annealing which is used for general purposes. Exposure of the alloy to temperatures of about 700 °C results in an equiaxed structure of α grains and grains of transformed β (Widmanstätten α).

Duplex and triplex annealing cause further partitioning of alloying elements between the α and β phases. This improves the stability of the alloy and results in better ductility and low cycle fatigue strength.

Beta annealing causes the formation of Widmanstätten alpha phase laths, whose size depends on the cooling rate, in a beta phase matrix. The resulting improvement in fracture toughness and fatigue strength has been associated with slower rates of crack propagation, despite a lower crack initiation resistance.

Quenching from the Beta phase field: This treatment relies on the subsequent decomposition of the quenched structure during tempering or ageing at elevated temperatures. The microstructures obtained are complex and lead to the formation of

different martensitic alpha phases, depending on the amount of β stabilisers in the alloy (Figure I.g.).

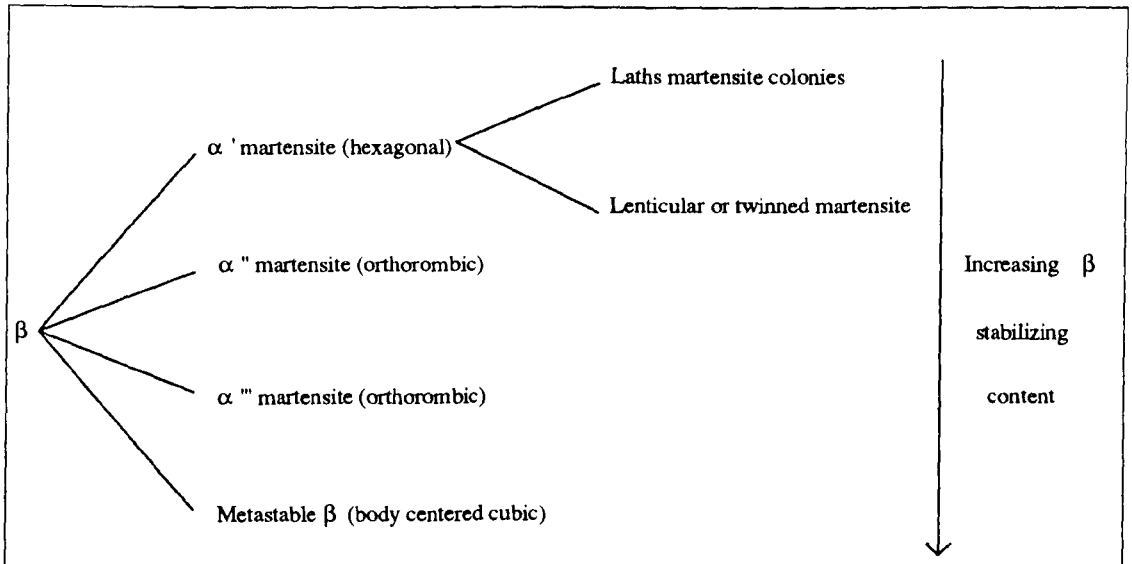

Figure I.g. Phases obtained by quenching (α+β) alloys (Polmear 1989)

Tempering: The reactions leading to the decomposition of titanium martensites at elevated temperatures are complex and are summarised in figure I.h. Tempering of titanium alloys softens the material and usually results in a significant increase in strength.

Ageing: The response of the alloy to ageing lies in the instability of the beta phase at lower temperatures, which causes its decomposition and results in higher values of strength, along with adequate ductility and good metallurgical stability (Figure I.i.). Again, this process is dependent on alloy composition and some of the products resulting from the different microstuctural reactions are to be avoided in order to prevent embrittlement. This is the case for the ω phase which consists of a very fine dispersion of particle formed from the metastable beta phase, and also for the β_1 phase which occurs as a uniformly dispersed precipitate in alloys containing sufficient amounts of beta stabilisers. The formation of such phases is usually avoided by choosing correct ageing temperatures and times, or through varying the alloy composition.

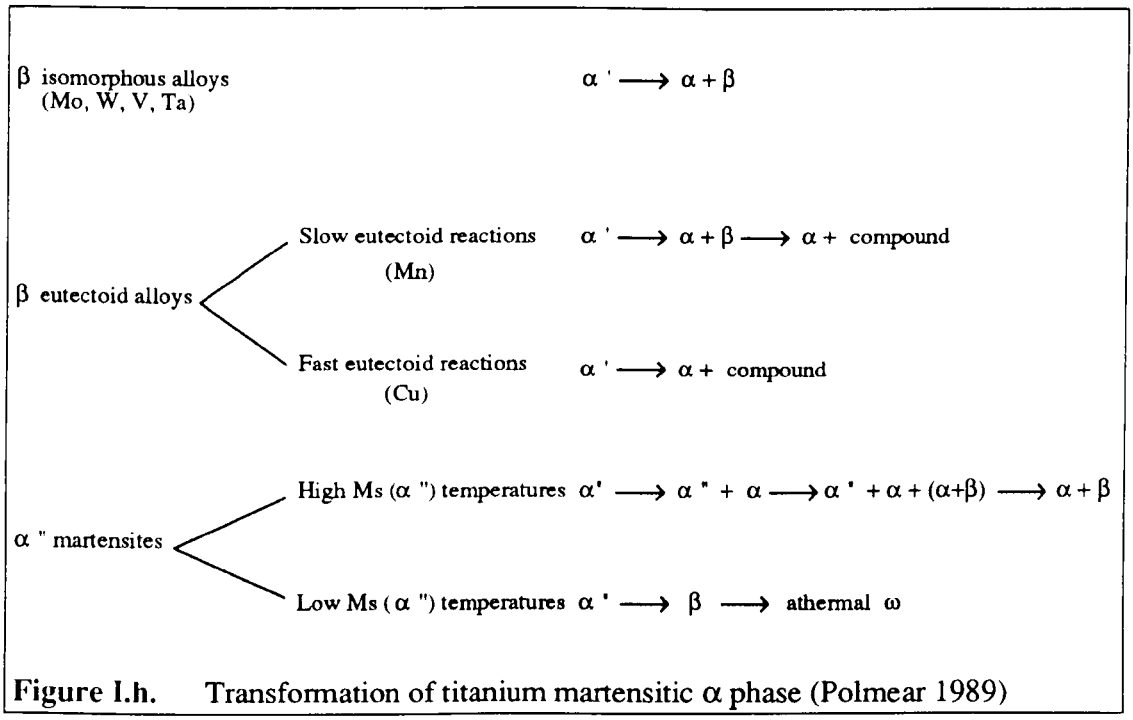

Figure I.h. Transformation of titanium martensitic α phase (Polmear 1989)

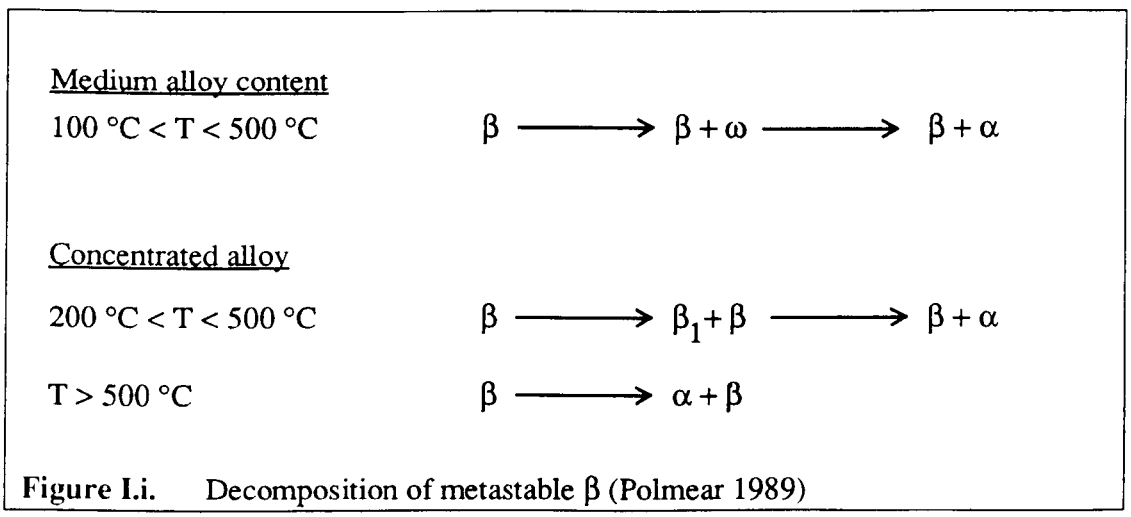

Figure I.i. Decomposition of metastable β (Polmear 1989)

I.c.5. Engineering performances

The chemical and mechanical properties described earlier for titanium metal are obviously retained by its alloys to different degrees. The two most interesting features are the exceptional corrosion resistance and the high strength-to-weight ratio (Figure I.a) associated with these materials. Table I.c summarises the compositions and tensile properties of commercial titanium alloys which are currently available to industry. The behaviour of these alloys is related to the main industrial requirements as follows:

Creep properties: The improvement of creep resistance has been the main objective in the evolution of new titanium alloys with IMI 834 being currently the state of the art with a temperature capability of about 650 °C. The development of titanium aluminides should represent significant progress and establish a new limit at 1000 °C (Walker 1994).

Fatigue resistance: This feature is greatly influenced by the texture and the microstructure of the alloy: A coarse, basket weave type microstructure is resistant to crack propagation, whereas a finer microstructure tends to delay crack initiation. For alloys containing large amounts of alpha phase, the effect of dwell periods at high loads increases the growth of fatigue cracks immediately after the dwell period by as much as fifty times. These so-called 'dwell effects' can occur at temperatures as low as 75 °C and seem to be related to the presence of hydrogen in the material (Polmear 1989). Titanium alloys also suffer from fretting fatigue which can reduce their life by as much as eight times.

Stress-corrosion cracking: Although titanium alloys exhibit good resistance to cracking in many environments able to induce cracking in stainless steels, they are prone to stress-corrosion cracking in red fuming nitric acid and in the presence of chloride salt deposits (Miska 1974). Alpha alloys show the greatest susceptibility and aluminium contents in excess of 5 to 6% are considered to be detrimental as they induce the precipitation of the aluminide Ti_3Al (also called α_2 phase). Stress-corrosion cracking in titanium is considered to result from the absorption of hydrogen and the precipitation of titanium hydrides, or even from the direct diffusion of hydrogen to crack tips (Beck 1969, Boyd 1969).

Corrosion fatigue: This is one of the better properties of these alloys combining their high fatigue strength with their excellent corrosion resistance.

Alloy	Composition (%)							Tensile properties		
	Al	Sn	Zr	Mo	V	Si	other	0.2% Proof stress (MPa)	Tensile strength (MPa)	Elongation (%)
α alloys										
CP Ti 99.5%								170	240	25
CP Ti 99.0%								480	550	15
IMI 260							0.2 Pd	315	425	25
IMI 317	5	2.5						800	860	15
IMI 230							2.5 Cu	630	790	84
Near α alloys										
Ti-8-1-1	8			1	1			980	1060	15
IMI 679	2.25	11	5	1		0.25		990	1100	15
IMI 685	6		5	0.5		0.25		900	1020	12
Ti-6-2-4-2S	6	2	4	2		0.2		960	1030	15
Ti-11	6	2	1.5	1		0.1	0.35 Bi	850	940	15
IMI 829	5.5	3.5	3	0.3		0.3	1 Nb	860	910	15
Ti-1100	6.0	2.75	4.0			0.45	0.4 Nb			
							0.07 C	860	960	11
IMI 834	5.8	4.0	4.0	0.5		0.4	0.75Nb	910	1030	10
							0.06C			

Table I.c. Compositions and typical room temperature mechanical properties of selected wrought titanium alloys

Alloy	Composition (%)							Tensile properties		
	Al	Sn	Zr	Mo	V	Si	other	0.2% Proof stress (MPa)	Tensile strength (MPa)	Elongation (%)
α/β alloys										
IMI 318 / Ti-6-4	6				4			925	990	14
IMI 550	4	2		4		0.5		1000	1100	14
IMI 680	2.25	11		4		0.2		1190	1310	15
Ti-6-6-2	6	2			6			1170	1275	15
Ti-6-2-4-6	6	2	4	6				1170	1270	15
IMI 551	4	4		4		0.5		1200	1310	13
Ti-8Mn							8 Mn	860	945	15
β alloys										
Ti-13-11-3	3				13		11 Cr	1200	1280	8
Beta III		4.5	6	11.5				1315	1390	10
Ti-8-8-2-3	3			8	8		2 Fe	1240	1310	8
Transage 129	2	2	11		11			1280	1400	6
Beta C	3		4	4	8		6 Cr	1130	1225	10
Ti-10-2-3	3				10		2 Fe	1250	1320	8

Table I.c. (continued)

I.d. Applications of titanium alloys

I.d.1 Aerospace industry

Titanium alloys were first introduced in aircraft gas turbine engines in 1952 and now make up 25% to 30% of the weight of most modern engines. The alloy Ti-6Al-4V (equivalent to IMI 318) is the most widely used especially in the cooler parts of the compressor whereas near alpha alloys such as IMI 834 are used where greater strength and creep resistance are required. Commercially pure titanium is used for casing and ductings.

Titanium alloys are also used for structural purposes in other aerospace applications, such as sheets for nacelles, exhaust shrouds, fire walls, and fuel storage tanks in rockets. Forgings are now used for critical applications: Undercarriage components, flap and slat tracks in wings, engine mountings and fasteners.

I.d.2 Chemical industry

Because of its outstanding corrosion resistance, many chemical applications involve commercially pure titanium and include storage tanks for bleaching agents, hot brine, ferric chlorides, and chlorinated hydrocarbons. Titanium is also used for tubing in steam condensers and heat exchangers for the offshore oil industry.

I.d.3 General engineering

Titanium alloys are used in deep sea submersible vessels, hydrofoil struts, yacht fittings, and components for mine sweepers. The metal finishing industry takes advantage of the electrical conductivity of rutile (TiO_2) and uses titanium for aluminium anodising jigs, anode baskets, and cathodes.

I.d.4. Biomaterials

The use of titanium in vitro is due to its excellent corrosion resistance to body fluids along with good stress-corrosion resistance, high mechanical strength, and acceptable tissue tolerance.

I.e. Conclusion

The main characteristics of titanium are its outstanding corrosion resistance, its high strength-to-weight ratio and its good tensile properties.

There are three classes of titanium alloys: Alpha alloys, beta alloys, and (alpha+beta) alloys. The mechanical properties of titanium alloys greatly depend on alloy composition and heat treatment.

Titanium alloys suffer from stress-corrosion cracking in red fuming nitric acid and hot salt environments.

The main applications of titanium alloys are found in the aerospace and chemical industries.

CHAPTER II

THE PHENOMENON OF HOT-SALT STRESS-CORROSION CRACKING OF TITANIUM ALLOYS

"In any case, the problem of titanium in a Mach 3 supersonic transport must be faced now. The fact is yet to be established that the hot-salt problem exists in service."

W.K.Boyd, F.W.Fink (Boyd 1964)

II.a. Introduction

The first report of hot-salt stress-corrosion cracking (HSSCC) of titanium alloys was made in 1955 by G.W.Bauer after he noticed severe surface cracking of Ti-6Al-4V while carrying out basic creep testing of this alloy at 370 °C and at stresses ranging from 345 to 413 MPa (Boyd 1964). The local attack which led to the premature failure of the material originated from the surface and was associated with a mottled grey deposit in the pattern of fingerprints. Bauer therefore attributed the phenomenon to salt contamination from perspiration.

This matter led to a considerable amount of research during the sixties and the seventies, and investigators at companies such as Pratt & Whitney, ITT Research Fundation, The Titanium Producers' Laboratories, Rolls Royce, Lockheed, NASA, developed programmes aimed at gathering an understanding of HSSCC of titanium (Boyd 1964, Blackburn 1973, Rideout 1968). However, although cracking was observed in the laboratory and was also observed on hot-formed sheet materials associated with the use of temperature-indicating compounds containing chloride salts (Boyd 1964), no in-service failure was ever detected, indicating either that the conditions necessary to induce cracking are not met under flight conditions, or that an inhibitor which exists under these conditions is absent during laboratory testing.

The main problem encountered by reviewers when dealing with this phenomenon is the large scatter in the published laboratory results. This scatter is mainly due to three reasons:

Lack of standardised testing: Creep testing of titanium alloys exposed to HSSCC conditions is by far the most popular technique used. The test piece is usually precoated with salt and exposed in a creep furnace at elevated temperatures in the presence of a tensile stress. However numerous other methods have been developed where the method of applying the stress also include bent beam (Rideout 1966), residual stress bend (Heimerl 1966), self stressed bend (Weber 1967), cantilever beam (Martin 1966), and U-bend specimens (Siniglia 1978). When one considers also the differences related to the type of salt employed and the manner in which it is deposited, the material and its relevant heat treatments, and the many designs used for test pieces, it becomes extremely difficult to compare the results obtained by different workers.

Hot-salt stress-corrosion threshold considerations: Stress threshold curves for HSSCC separate regions where the material is considered to be susceptible to hot-salt stress-corrosion from regions where it is considered to be immune. However, as one can see in Figure II.a. where different criteria have been used to determine the threshold curves of the same alloy in the same test conditions, the results are very much dependent on the parameter used to describe the susceptibility to HSSCC (see paragraph II.b.1) : residual mechanical ductility, stress-rupture, crack observation, and/or the presence of corrosion products (Gray 1969a). Therefore the works achieved by different investigators can usually be only compared on a qualitative basis rather than quantitatively.

Genuine experimental error: Because of its nature, hot-salt stress-corrosion testing can itself produce considerable scatter. This is often due to the use of heavy engineering equipment, the existence of long transitory states before test conditions are reached, and the difficult control of parameters such as uniform salt deposition or salt coating thickness. Hence, relatively long times are usually chosen in order to diminish these experimental errors.

The large amount of research carried out by numerous investigators represents a wealth of data pertinent to the understanding of HSSCC and describes three main objectives (ASTM 1966):

-1- To tackle the influence of environmental factors on the phenomenon.

-2- To determine the relative susceptibility of alloys as related to their compositions and their metallurgical features.

-3- To develop suitable models describing the mechanisms.

The latter point will be reported in chapter III. The influence of the environment and of the materials will be discussed here after a brief description of the characteristics of HSSCC of titanium alloys.

II.b. Characteristics of the hot-salt stress-corrosion cracking of titanium alloys.

II.b.1. General conditions inducing HSSCC

Titanium alloys tested in the laboratory suffer from hot-salt stress-corrosion when stressed and exposed at elevated temperature in the presence of salts. The lower temperature threshold to induce cracking is alloy dependent and is fixed by the necessity of forming the required corrosion products (Petersen 1971). Such thresholds were found to be around 230 °C for Ti-8Al-1Mo-1V and 260 °C for Ti-6Al-4V, both in the mill anneal condition. In the 260 °C to 500 °C range, the stresses required to produce HSSCC are well below those for design creep. At about 500 °C, creep relaxes the stress concentration necessary for cracking to occur in most conventional alloys. However, the development of more creep resistant alloys such as IMI 834, the subject of this investigation, has increased this limit to about 600 °C when appropriate heat treatments are used.

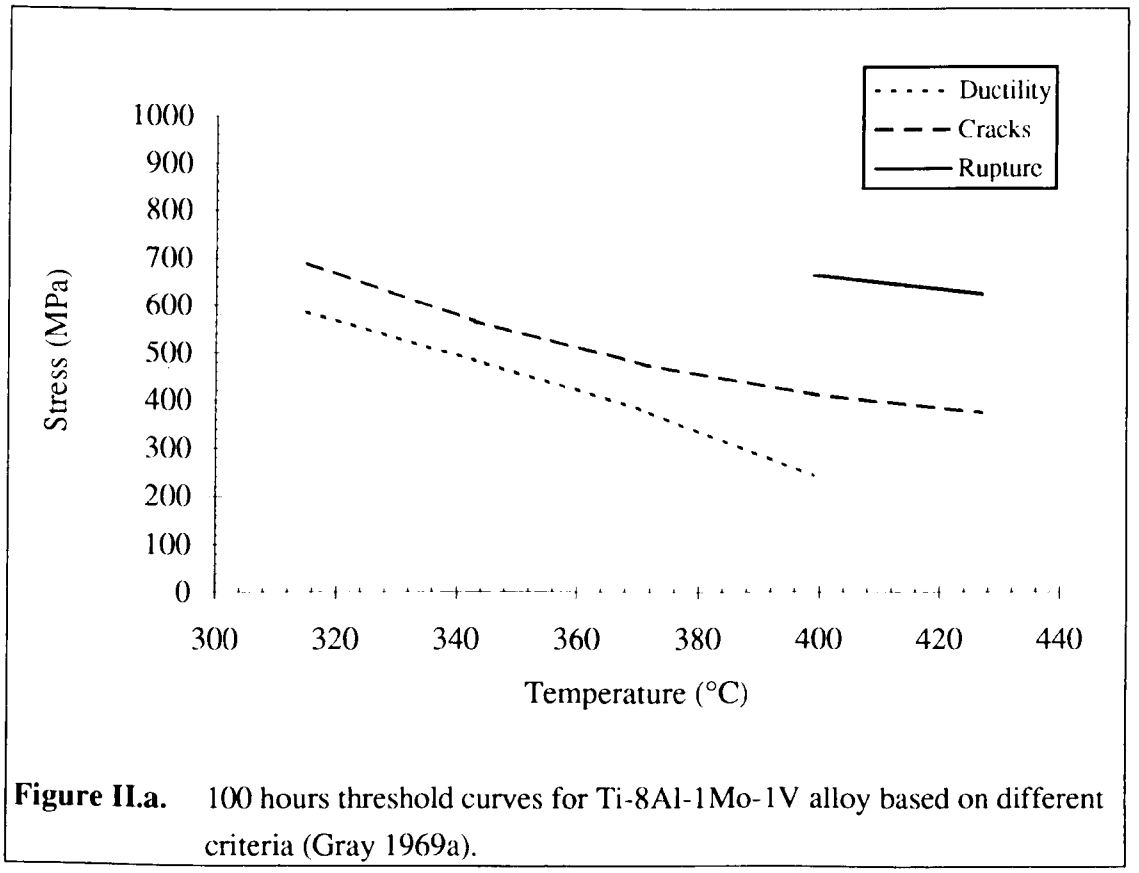

Figure II.a. 100 hours threshold curves for Ti-8Al-1Mo-1V alloy based on different criteria (Gray 1969a).

The threshold stresses required for hot-salt stress-corrosion cracking are of course dependent on factors such as temperature, exposure time, alloy microstructure, and salt concentration. Figure II.a. illustrates a typical threshold curve for Ti-8Al-1Mo-1V. Gray showed that stresses as low as 470 MPa for Ti-6Al-4V (i.e. 55% of its yield stress) and 270 MPa for Ti-8Al-1Mo-1V (i.e. 33% of its yield stress) could produce HSSCC damage during 96 hours exposure at 400 °C (Gray 1973). Furthermore a letter survey of engine manufacturers revealed that the maximum temperature and stress conditions of Ti-6Al-4V components in engines were operating at stresses and temperatures above the most pessimistic of the reported laboratory threshold curves.

As will be discussed later, minute amounts of a wide range of salts can cause HSSCC of titanium. Ashbrook carried out a field survey at engine overhaul depots to determine the actual salt deposition on compressor airfoils after exposure to a variety of flight conditions (Ashbrook 1969). Average concentrations of 0.155 mg/cm^2 were measured after severe flight conditions such as pilot training in the Caribbean, and local concentrations of 1.55 mg/cm^2 were detected in many instances.

II.b.2. Fracture characteristics.

As pointed out by Dinnappa, hot-salt stress-corrosion failure consists of two zones (Dinnappa 1988): A brittle outer zone, covered with corrosion products and which is produced by HSSCC mechanisms, and an inner ductile zone which results from pure mechanical cracking and overloading.

General corrosion and pitting are observed on the surface of the salt coated material before the occurrence of cracking, accompanied by surface roughening and discoloration from straw yellow through peacock blue to grey (Hatch 1966). Cracking initiates rapidly at relatively corrosion-free areas, dip-shaped depressions, and pits are formed usually below or at the edge of salt beads in a random fashion. Hot-salt stress-corrosion appears to be insensitive to surface roughness or cracks (Turley 1966).

Propagation of cracks is intergranular in nature, with limited transgranular cleavage and is often accompanied by crack branching. It is considered to be relatively slow compared with the short times required for initiation. Turley et al. associated increasing amounts of transgranular propagation with an increased sensitivity of the alloy to hot-salt stress-corrosion and argue that the beta phase of the material is not related to

increased susceptibility (Turley 1966). In addition, Lapasset associates transgranular propagation with cleavage of the alpha phase (Lapasset 1979).

Finally, Turvey et al. noticed the presence of fine precipitates along the crack at grain boundaries which were also associated with susceptibility of the alloy to HSSCC but these could not be identified (Turley 1966).

From these early observations, one can draw two conclusions:

-1- Hot-salt-stress-corrosion cracking failure characteristics have been well identified by previous workers.

-2- It appears that even during the late sixties, the conditions necessary to induce HSSCC of titanium were met during a typical flight.

In spite of the constant improvement in gas turbine engine technology which has produced even more severe operating conditions in the past twenty years, no in-service failure has yet been recorded. Therefore, one has to carry out a systematic study of the many environmental parameters which may take part in the phenomenon, and look for the possible existence of HSSCC inhibitors.

II.c. Effect of environmental parameters.

II.c.1. Static temperature, static load, and exposure time.

Under static hot-salt stress-corrosion cracking conditions, temperature, stress, and exposure time are of course closely related. This allowed investigators to carry out two radically different types of testing: Long term exposures (up to 30000 hours) at relatively low stresses and temperatures (Martin 1966), or short term exposures (96 hours to 1000 hours) in more severe conditions (Gray 1970, Simenz 1966). The advantage of the former is to reduce the scatter encountered in short term HSSCC testing. However, the latter technique is considerably more practical, as testing times are significantly reduced.

Figure II.b shows the evolution of 100 hours exposure threshold curves for hot-salt stress-corrosion cracking failures and 0.1% creep strength of two titanium alloys Ti-6Al-4V and Ti-8Al-1Mo-1V (Petersen 1971). One can observe that for a given stress, two temperature thresholds have to be considered: The lower threshold is believed to represent the temperature at which the chemical reactions between the salt and the alloy are activated (Rideout 1966). Above the upper threshold, creep resistance becomes the limiting factor.

Several workers have attempted to use rate-process parameters in order to predict hot-salt stress-corrosion cracking initiation over a wide range of stresses, times, and temperatures. The best results, which are represented in figure II.c and II.d were obtained by Turley et al. (Turley 1966) and Royster (Royster 1968) using the Larson-Miller parameter for test durations in the range of 100 to 7000 hours and the Orr-Sherby-Dorn parameter for exposures of 5 minutes to 20000 hours respectively. These criteria provide a method with which to compare works achieved by different workers provided that the testing techniques, the alloy, and the threshold criterion are identical. Hence, the wide variations in threshold stresses which are usually encountered when using different exposure times (Gray 1969b) can be overcome, and an approximate standardisation of the results can be achieved.

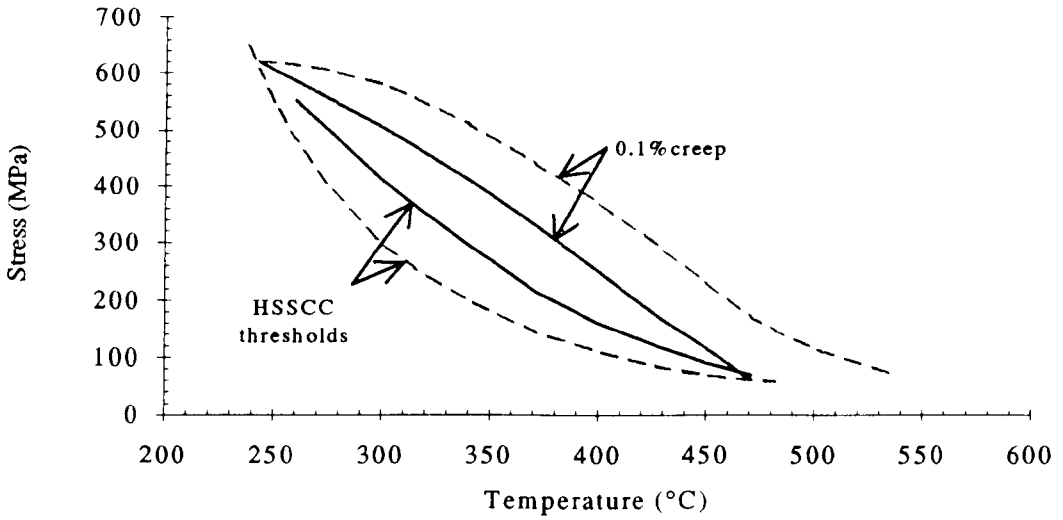

Figure II.b. 100 hours exposure salt-stress corrosion and 0.1% creep strength for Ti-8Al-1Mo-1V (-----) and Ti-6Al-4V (——) (Petersen 1971)

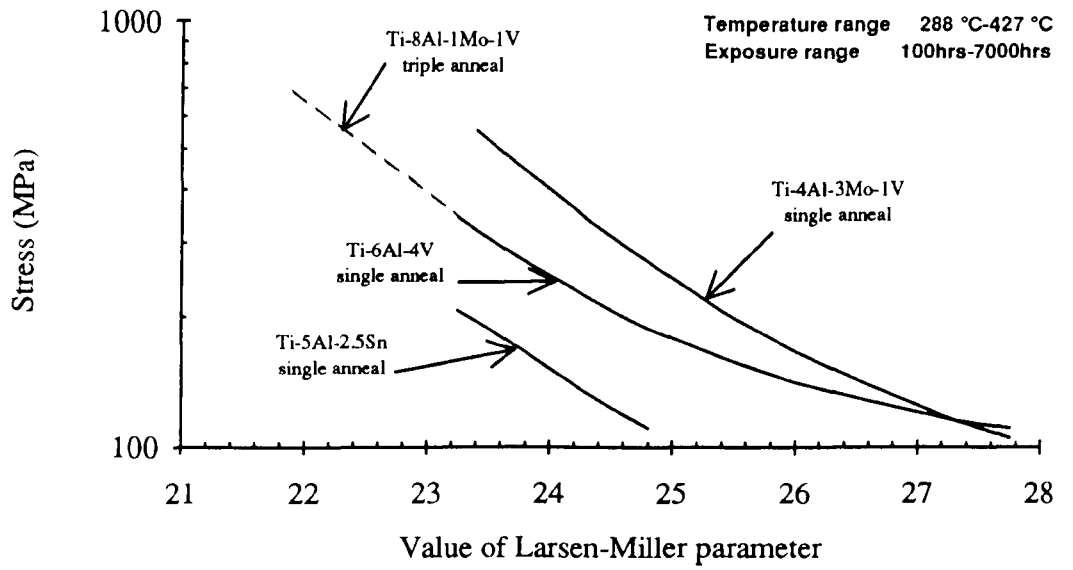

Figure II.c. Application of Larsen-Miller parameter ($P = T(20 + Logt) \times 10^{-3}$) to salt stress-corrosion cracking thresholds in titanium alloys. (Turley 1966).

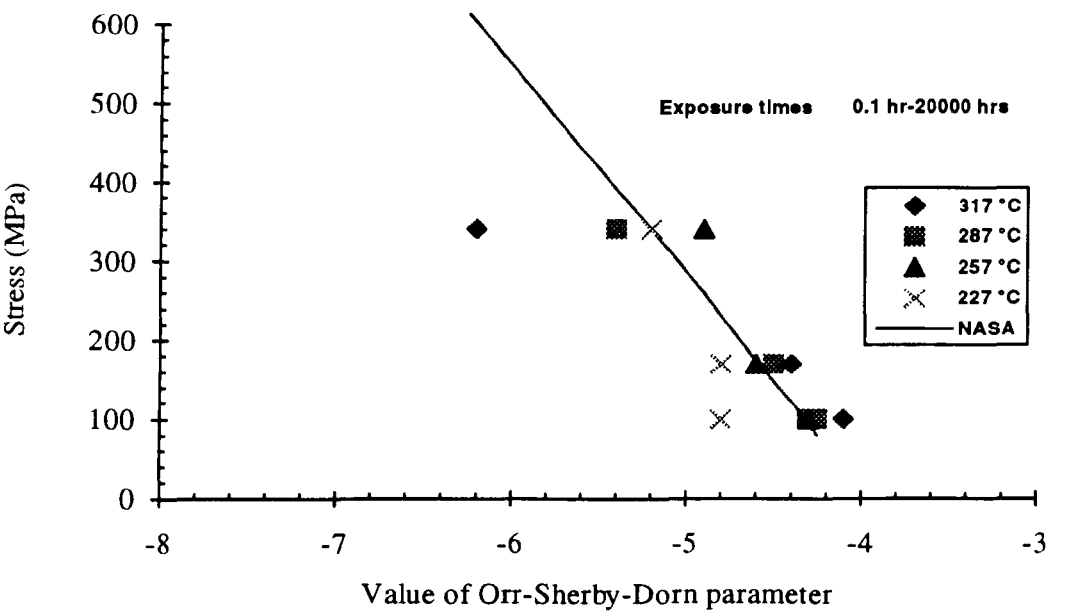

Figure II.d. Application of Orr-Sherby-Dorn parameter ($P = Logt - \frac{\Delta H}{2.3RT_K}$) for predicting stress-corrosion cracking initiation in Ti-8Al-1Mo-1V titanium alloy sheet; Each marker style represents a different experiment (Royster 1968).

II.c.2 Salts and other contaminants

As no in-service failures had been detected, several workers investigated the possible influence of the type of salt used, its concentration, and the mode of its deposition on HSSCC. Furthermore, there was a need to determine whether other contaminants, and particularly those containing chlorides, could provoke similar effects in titanium.

Salt type: The numerous salts used in testing by previous investigators with their respective melting points and ionic conductivity are indicated in table II.a. There is general agreement that pure sodium chloride (NaCl) is the most aggressive salt, although natural sea salt, potassium chloride (KCl), and ASTM synthetic salt can produce considerable damage (Rideout 1966, Piper 1966, Simenz 1966). Heimerl and Turley also tested specimens exposed to natural atmospheric conditions at Langley, Virginia and at El Segundo Beach, California, and detected extensive damage after exposure to elevated temperatures under stress (Heimerl 1966, Turley 1966). However Ondrejcin reported the inability of fluoride salts to induce HSSCC in titanium alloys (Ondrejcin 1967).

Most aggressive salts			Least aggressive salts		
Salt	Melting point (°C)	Infinite ionic conductivity ($10^{-4}m^2.s.mol^{-1}$)	Salt	Melting point (°C)	Infinite ionic conductivity ($10^{-4}m^2.s.mol^{-1}$)
NaCl	455	126.39	$CaCl_2$	782	135.77
LiCl	605	114.97	CaCl	646	-
KCl	770	149.79	$SrCl_2$	875	135.73
LiCl-KCl	354	-	$MgCl_2$	714	129.34
AgCl	455	-	CsCl	645	-
NaBr	747	-			
NaI	661	126.88			
$BaCl_2$	963	139.91			

Table II.a. Melting point and ionic conductivity of salts used in HSSCC testing.

There is speculation in the literature about these differences in salt agressivity. Garfinkle attributes the passivity of fluoride salts to the fact that they are not

hydrolisable (Garfinkle 1972), while Logan explains the "weakness" of magnesium chloride ($MgCl_2$) by its glassy nature which would act as a protective coating for the metal until it is oxidised (Logan 1966). In any case it seems obvious from table II.a. that neither the melting point nor the ionic conductivity of the salt can be related to its effects. Rideout et al. provide the most satisfactory explanation by relating the extent of damage caused by a salt to the high chemical reactivity of its oxides and hydroxides (Rideout 1966).

Salt concentration: It has already been mentioned that significant quantities of salts have been measured in titanium parts of compressor engines during field surveys, and that the amounts detected were sufficient to induce HSSCC in laboratory testing (see § II.b.1). A number of investigators also studied the influence of salt concentration or salt coating thickness on the extent of hot-salt stress-corrosion cracking damage in titanium alloys.

Damage was reported in a titanium alloy with a salt coating as low as 0.008 mg/cm^2 in a laboratory test (Boudreau 1968). However most of the testing achieved to date used salt concentrations ranging from 0.03 mg/cm^2 to 1 mg/cm^2. Gray reports that hot-salt stress-corrosion thresholds are unchanged when the salt concentration is increased from 0.03 mg/cm^2 to 0.3 mg/cm^2. Even concentrations of 1.5 mg/cm^2 did not lower the stress required to cause HSSCC at 371 °C (Gray 1969b).

Other workers studied the influence of salt coating thickness. They report that a thin salt coating gives earlier cracking than a heavy brush coat when short exposure times (100 hours) are considered (Simenz 1966, Heimerl 1966). However, it appears that as the exposure time is increased, the aggressivities of a thin and a thick salt coating become equivalent. Heimerl et al. attribute this behaviour to the greater availability of oxygen for a thin salt coating and hence, the need for longer exposure times in the case of heavier coats.

Salt depositions: A wide range of salt deposition techniques have been used to achieve the desired salt concentration on test pieces: They include spraying in a salt fog atmosphere (Lapasset 1979), placing a salt solution on the specimen with subsequent heating (Kolachev 1977), continuous spraying during the test (Gray 1969b), brushing a salt slurry on the gauge length (Turley 1966), and dipping the test piece in a salt solution (Heimerl 1966).

The most interesting mode of salt deposition in view of in-service conditions is of course spraying the test piece in a salt fog atmosphere at elevated temperature. Gray carried out a systematic study of this technique by testing a titanium alloy sprayed under a range of conditions (Gray 1969b). He observed that salt coatings deposited at higher temperatures (316 °C and 371 °C) produce less damage than these deposited at lower temperatures (204 °C). However this effect tends to disappear around 400 °C. The author concludes that this phenomenon is probably due to the amount of moisture retained by the salt for each of these temperatures. Gray also compared the effect of precoating the specimen prior to testing and coating the test piece in a continuous manner during HSSCC exposure. The two techniques produced similar results except at the highest temperature of 427 °C where a tenfold increase of the threshold stress was obtained with the second method. This was attributed to the growth of a protective oxide on the test piece before the salt is present in sufficient quantities to initiate damage.

Other contaminants: The occurrence of hot-salt stress-corrosion cracking during laboratory testing of titanium alloys urged several investigators to look for similar problems in the titanium industry and to identify other potential contaminants.

Convair reported the susceptibility of three titanium alloys to hot-cracking due to salt deposits or experimental rinse water containing as little as 100 ppm sodium chloride during hot-forming and hot-sizing (Boyd 1964). Simenz et al. showed that several alloys were also susceptible to stress-corrosion cracking at elevated temperature in the presence of cabin and tank sealing compounds, while Martin detected the same effects with braze coatings on Ti-8Al-1Mo-1V (Simenz 1966, Martin 1966).

II.c.3. Water vapour

There is a general view that water vapour is not only a prerequisite for the hot-salt stress-corrosion cracking of titanium alloys, but that its role in the mechanisms of HSSCC is of considerable importance. However, studies on the influence of water vapour on the phenomenon have been both extremely difficult and somewhat contradictory.

In 1964, Boyd and Fink mentioned that although water usually had a beneficial effect on corrosion problems in titanium, there was a possibility that for hot-salt stress-

corrosion, cracking may occur quickly if a critical moisture level was exceeded (Boyd 1964).

A number of investigators tried to demonstrate this concept by carrying out testing in so-called "wet " and "dry" conditions. However it became rapidly obvious that even minute amounts of moisture were sufficient to induce HSSCC of titanium, which rendered the task rather difficult.

Hatch et al. claim that no cracking was observed in the alloy Ti-5Al-2.5Sn at 427 °C when both the specimens and the salt were baked out prior to testing and kept in an anhydrous state during stressed exposure (Hatch 1966). However, their results were obtained using an exposure time of two hours, and there is a possibility that cracking may only have been delayed rather than entirely stopped. Ondrejcin's results are more convincing: Using the same conditions as Hatch et al. but with alloy Ti-8Al-1Mo-1V at 343 °C, no cracking was observed after seven days exposure in "dry" conditions, whereas the moist system showed attack and cracking in ninety minutes (Ondrejcin 1967).

On the other hand, the results obtained by Gray and Johnston which are represented in figure II.e. show that for two significantly different moisture contents (1 ppm and 5300 ppm) the threshold stresses were not consistently affected (Gray 1969b). Similar results have also been reported in another study (Heimerl 1966). However Kirchner and Ripling claim that if cracking still occurs in "dry" conditions, it can be significantly delayed by as much as fifteen times compared with "wet" exposures (Kirchner 1966).

The reason behind these conflicting results is probably due to the numerous forms in which water can be found in the process. Hence water can be present as vapour, but also as crystallisation water in the salt (Rideout 1966) or even occluded in the metal oxide scale (Logan 1966). Lapasset tried to isolate the different effects of moisture according to the form under which it is present (Lapasset 1979). His work used infrared spectrometry to measure the average amount of water retained by sodium chloride crystals. A value of 40 mg/cm^3 of salt was obtained. He also tried to eliminate this crystallisation water in order to measure the influence of atmospheric moisture on the HSSCC of titanium. Lapasset concludes that the role played by atmospheric water vapour seems to be minor compared with the role of crystallisation water, especially during the initiation stage of hot-salt stress-corrosion.

Therefore, it appears that the amounts of moisture required to induce HSSCC in titanium are so low, that the crystallisation water present in the salt itself is largely sufficient to cause cracking.

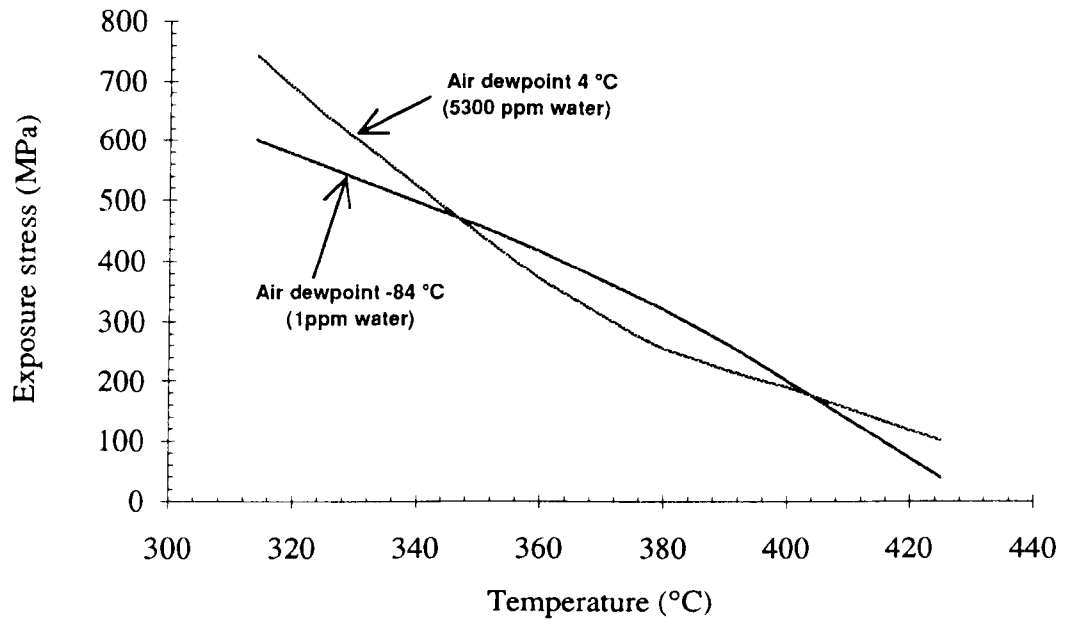

Figure II.e. Effect of hygrometry levels on threshold curves of titanium alloy Ti-8Al-1Mo-1V (Gray 1969b).

II.c.4. Oxygen

It is obvious from the literature that there is a considerable need for oxygen, either in its gaseous form or supplied by a reducible oxide, in order to induce hot-salt stress-corrosion of a titanium alloy (Boyd 1964, Petersen 1966, Garfinkle 1972). Indeed, Petersen points out that the greatest amount of corrosion produced on materials exposed to hot-salt stress-corrosion is found near the edge of large salt deposits where oxygen from the atmosphere is readily available. He concludes that oxygen is probably required to maintain the corrosion reaction between the alloy and the salt.

Logan claims to have produced cracking in the absence of gaseous oxygen in Ti-8Al-1Mo-1V (Logan 1966). In his experiment, the only source of oxygen consisted of a rutile layer formed on the surface of the specimen during a preoxidising treatment.

From these results, he concludes that a solid-state reaction took place between the crystalline sodium chloride, the oxide layer, and the base metal.

Heimerl et al. studied the influence of oxygen on HSSCC by testing the same alloy in three different gas atmospheres (Figure II.f). Their results indicate similar susceptibilities of the material to hot-salt stress-corrosion cracking when normal air (21% O_2) or pure oxygen (100% O_2) environments are used. However, a net improvement was obtained when the oxygen content was reduced to 0.1% (Heimerl 1966). Lapasset repeated this work with another alloy (Ti-6Al-4V) using atmospheric oxygen contents ranging from 0.3 ppm (2.3×10^{-4} torr) to 700 ppm (5.3×10^{-1} torr). His results show a considerable influence of oxygen in the range 0.3 ppm to 70 ppm, this effect tending to flatten out above this value. Lapasset also claims that the lower oxygen threshold below which HSSCC would be inhibited for his experimental conditions lies somewhere around 2×10^{-4} torr (Lapasset 1979).

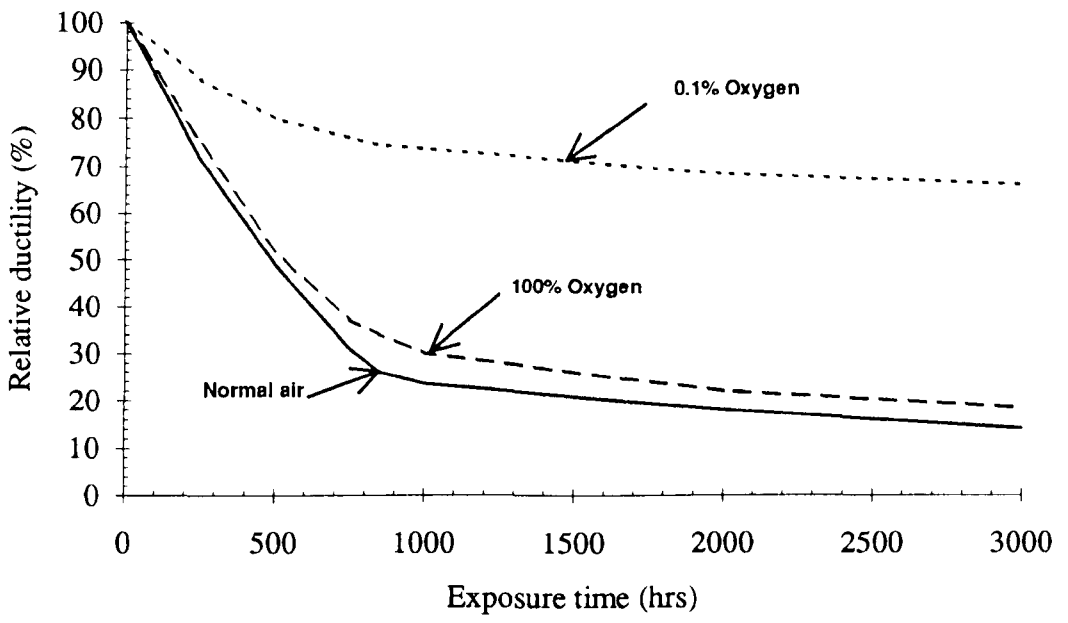

Figure II.f.: Effect of oxygen on hot-salt stress-corrosion of Ti-8Al-1Mo-1V alloy sheet at 288°C (Heimerl 1966).

II.c.5. Environmental pressure.

The use of titanium alloys in the manufacture of blades and discs for the early stages of gas-turbine engine compressors is one of the main applications for this class of materials in the aerospace industry. It may therefore seem surprising that only a very limited amount of HSSCC testing under high pressure conditions has been achieved to date. The reason for this lack of data is of course due to the particularly difficult task of working with high temperatures, high pressures, and mechanical loads at the same time.

The first attempt to characterise the influence of environmental pressure on the hot-salt stress-corrosion of titanium alloys came from Heimerl et al. who carried out tests at low pressures representing atmospheres equivalent to those encountered at altitudes of 21,300 m and 116,000 m (Heimerl 1966). The results showed a consistent decrease in stress-corrosion at low pressures (Figure II.g.). Heimerl argues that this effect is related to the lower amounts of oxygen present in the atmosphere at lower pressures. Nevertheless, Hatch who carried out similar work on alloy Ti-5Al-2.5Sn claims that even very low pressures of air (1.3×10^{-5} bar) will allow hot-salt cracking (Hatch 1966).

The only study of hot-salt stress-corrosion of titanium alloys at high pressures available in the literature was carried out by Gray and Johnston (Gray 1969b). The authors tested alloy Ti-8Al-1Mo-1V in a dynamic air apparatus where a total environmental pressure of 3.6 bars was imposed. They report an increase of the threshold stress at this pressure, principally at the lower temperature of 316 °C and mention that creep limitations of the alloy prevented testing at the higher stresses required to produce a typical HSSCC brittle fracture at this temperature (Figure II.h). Although no definite explanation is given for this beneficial effect, Gray and Johnston suggest two possibilities:

-1- The chemical corrosion reactions that lead to embrittlement of the material are inhibited in some manner at high pressures.

-2- The increased availability of oxygen results in rapid repair of the naturally protective surface oxide.

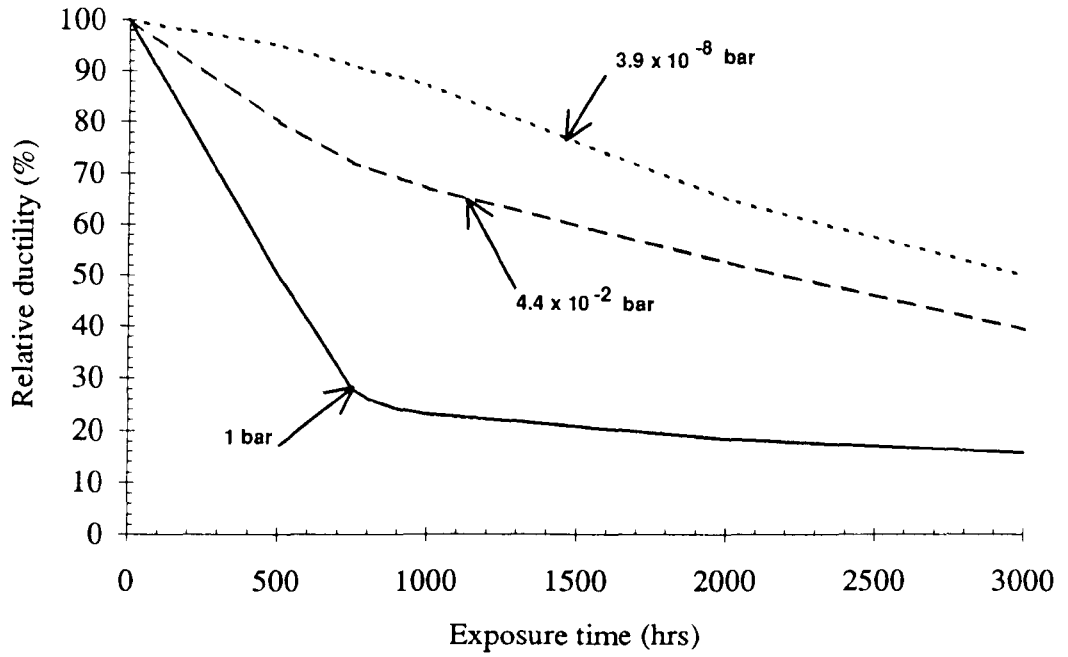

Figure II.g. Effect of low air pressure on HSSCC of Ti-8Al-1Mo-1V alloy sheet at 288 °C (Heimerl 1966).

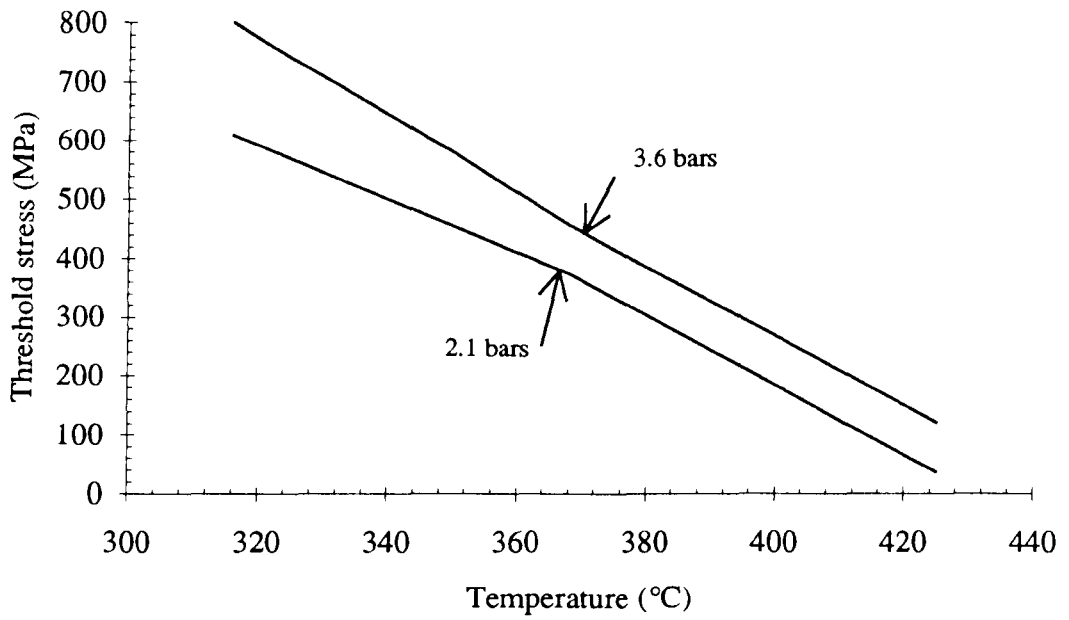

Figure II.h. Effect of high air pressure on threshold curve of Ti-8Al-1Mo-1V (Gray 1969b)

II.c.6. Air flow

There has been a lot of speculation in the literature on whether the high air velocities encountered in a typical gas-turbine engine during flight would be able to sweep away the salt or any damaging gaseous corrosion products (Petersen 1971). Heimerl et al. subjected self-stressed specimens made of Ti-8Al-1Mo-1V to a Mach 3 air stream at 238 °C and observed that although some of the salt had been swept away after a 1 minute test, enough remained on the surface to produce cracking during subsequent oven exposure at 377 °C (Heimerl 1966).

The first study that achieved close to in-service conditions was carried out by Weber and Davis, using Lockheed's supersonic wind tunnel (Weber 1967). They achieved hot-salt stress-corrosion testing in a Mach 2.5 air flow, together with a pressure equivalent to an altitude of about 23,000 m on Ti-6Al-4V and Ti-8Al-1Mo-1V. Control tests run in still air creep furnaces showed that although cracking was not inhibited by air velocities, substantial amounts of salt were removed from the surface of the specimens during the first few hours of the test, reducing HSSCC damage. However, 80% of the initial salt deposits were retained by the material after these tests.

Similarly, Gray and Johnston noticed only a minor effect of a Mach 1 dynamic air stream on the hot-salt stress-corrosion cracking of Ti-8Al-1Mo-1V, this effect being virtually non-existent at higher temperatures as shown on Figure II.i (Gray 1969b).

II.c.7. Cyclic operating conditions.

Another major argument, for the non-occurrence of hot-salt stress-corrosion cracking in service, centres around the cyclic conditions encountered by titanium alloys in gas-turbine engines. Thus, if titanium parts are exposed to high loads at elevated temperatures during flight, they may benefit from "zero load, room temperature" conditions when the aircraft is not in use. The observation that general corrosion always precedes HSSCC suggested to some investigators that the corrosion process may well be inhibited by these dwells in still conditions.

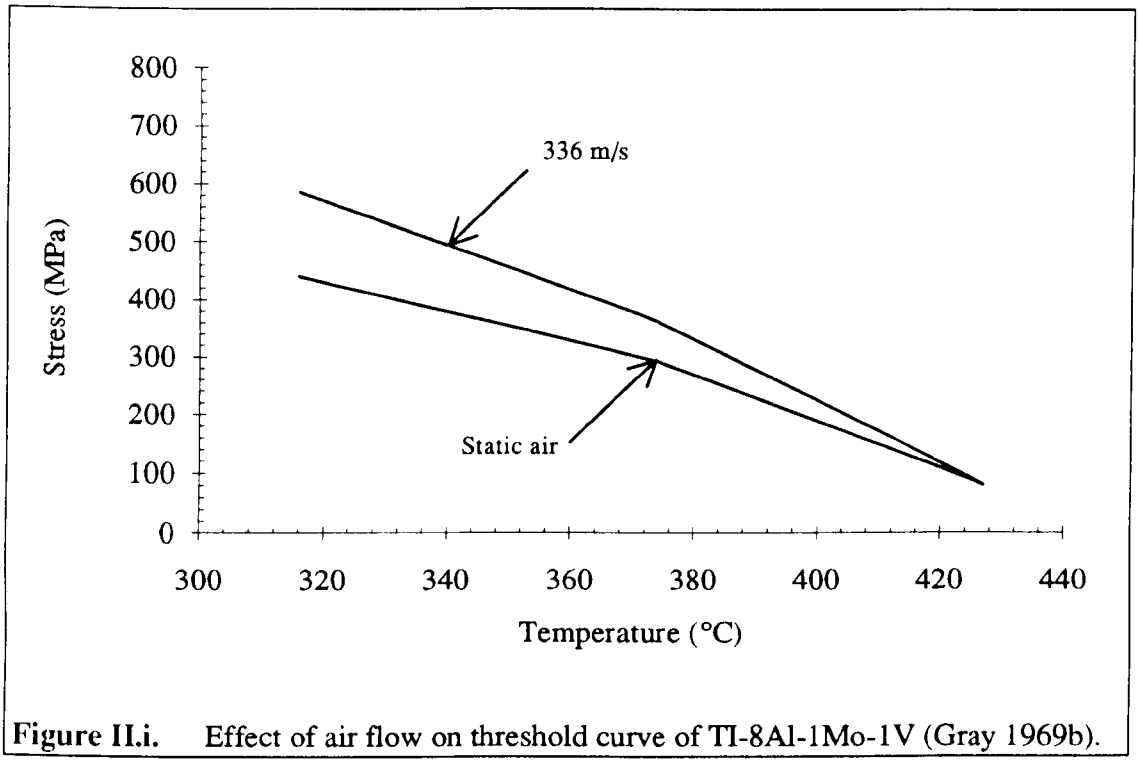

Figure II.i. Effect of air flow on threshold curve of TI-8Al-1Mo-1V (Gray 1969b).

Numerous workers noticed a decrease in hot-salt stress-corrosion damage in titanium alloys when cyclic conditions were used (Martin 1966, Gray 1973, Kolachev 1977). Heimerl et al. even demonstrated that if the temperature alone were cycled, the severity

of cracking could be directly related to the time-at-temperature portion of the cycle (Heimerl 1966). This result encouraged investigators to determine incubation times for HSSCC. Stone reports that such incubation periods are strongly alloy dependent (Stone 1967), and successful temperature cycles were used to retard HSSCC of several titanium alloys in laboratory investigations (Piper 1966, Stone1967). However such cycles proved to be less efficient at higher temperatures, and the cycles used successfully were not representative of service conditions.

Gray attempted to reduce hot-salt stress-corrosion damage by cycling the load imposed on the material (Gray 1973). A substantial improvement was obtained for the lower end of his temperature range (320 °C) but again, this effect tended to disappear when a higher temperature of 400 °C was used. He also reports that the use of both thermal and stress cycles resulted in no additional benefits when compared with the use of either temperature or load cycles only. These results were confirmed in a later study by Lapasset (Lapasset 1979).

II.c.8. Fatigue.

Several investigators who studied the influence of a pre-existing crack on hot-salt stress-corrosion of titanium report that when precracked fatigue specimens were salt-coated and tested, rapid failure initiated away from the precrack (Turley 1966, Martin 1966, Stone 1967, Kolachev 1977). Furthermore, it has been reported that attack at a specific location during one HSSCC exposure is not continued at the same point during subsequent exposures (Hatch 1966). Petersen concludes from these results that HSSCC is not controlled solely by fracture mechanics since new cracks nucleate and grow in preference to the existing one (Petersen 1971).

Salt-corrosion studies were also carried out with both low cycle (LCF) and high cycle (HCF) fatigue conditions. Turley et al. report no differences in the life of several titanium alloys for air fatigue with and without salt when relatively low temperatures are employed (316 °C), but they also claim a significant decrease in the life of the material when this temperature is exceeded (Turley 1966). Weaver and Winstone carried out a detailed study where in some cases the life of some alloys was reduced from 10^5 cycles without salt to only a few hundred cycles in the presence of salts (Weaver 1982). Therefore it would appear that salt deposits on titanium alloys have similar effects in fatigue testing to those under static load tests.

From the above considerations, one can conclude that not only the conditions which induce hot-salt stress-corrosion of a titanium alloy are met during flight but that environmental parameters encountered in service which are significantly different to those used in classic laboratory testing do not inhibit the phenomenon. The presence of an air flow and the existence of cyclic conditions are beneficial to the material, but are unable to protect it fully from hot-salt cracking. With regard to the possible influence of environmental pressure, testing has been limited to a value of 3.6 bars. This demonstrated an effect but it is not possible to determine whether the partial improvement noticed at this pressure would be extended or increased for higher pressures more representative of real flight conditions. Therefore with a view to eliminating the HSSCC problem, it is of primary importance to study the influence of parameters directly related to the material.

II.d. Effect of material

If it is difficult to compare the results obtained by different workers for the hot-salt stress-corrosion of the same titanium alloy, the task is even more complicated when several alloys in a wide range of metallurgical conditions are used.: Besides the use of different testing techniques which induce a considerable scatter, one must also consider parameters such as alloy composition, microstructure, texture and heat treatment, as well as surface conditions. In addition, most of the testing achieved to date has been carried out using the two alloys Ti-8Al-1Mo-1V and Ti-6Al-4V. However, as seen in Chapter I, there is a wide range of titanium alloys, most of which have been HSSCC tested in one work only.

II.d.1. Effect of alloy composition.

It is generally admitted that commercially pure grades of titanium are immune to hot-salt stress-corrosion cracking (TML 1957, Crossley 1960), but that all alloyed grades are susceptible. It has also been demonstrated that α and near α alloys are usually more sensitive to HSSCC than the heat treatable ($\alpha+\beta$) and β alloys. This feature led investigators to study the influence of the most common alloying elements on the phenomenon.

There is some controversy on the importance of alloying additions in the HSSCC process, but a few trends are nevertheless noticeable when abstraction of heat treatment is made. Work achieved at Dupont showed that aluminium present in alpha and near alpha alloys is preferentially attacked by hot-salt (Ondrejcin 1968). This behaviour is shown in figure II.j where the time taken for cracking to occur under HSSCC conditions is related to the aluminium content of five different titanium alloys. This preferential attack of aluminium is also reported by Rideout (Rideout 1966). There is speculation about the reasons for this apparent negative effect of aluminium towards hot-salt stress-corrosion cracking and it is not clear yet whether this phenomenon is related to chemical mechanisms or not.

Ondrejcin also reports that molybdenum (Mo), vanadium (V), and tin (Sn) are not preferentially attacked by hot-salt, explaining therefore the very good resistance of the Beta III alloy (Ti-11.5Mo-6Zr-4.5Sn) to HSSCC (Ondrejcin 1968). Finally, a study of the hot-corrosion of titanium alloys (i.e. without load) carried out by Dumas and St

John reports the outward diffusion of aluminium and zirconium (Zr) from the alloy into the internal and external oxide scales (Dumas 1976).

It appears therefore that if hot-salt stress-corrosion seems unavoidable for alloyed titanium, the degree of susceptibility of the material is partially related to its composition. Hence, careful alloy selection is necessary when titanium parts are likely to be subjected to HSSCC conditions.

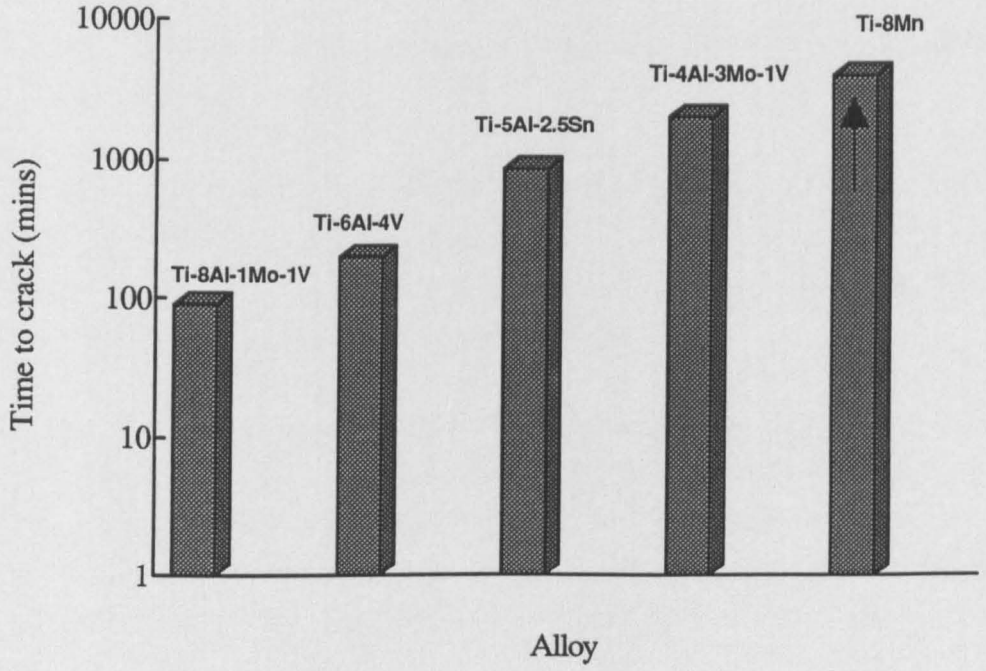

Figure II.j. Effect of alloy composition on time to initiate cracking by NaCl at 343 °C (Rideout 1968).

II.d.2. Effect of microstructure.

There is some disagreement in the literature about the importance of microstructure on the extent of damage caused by hot-salt stress-corrosion in titanium alloys. In fact, it would seem that this influence depends upon the alloy, which helps to explain the differences in the results obtained for different investigations. However there is no doubt that the respective amounts and the organisation of the α and β phases do influence the resistance of titanium to HSSCC (Turley 1966, Garfinkle 1973). Gray in a

most detailed study, noticed differences in the resistance to HSSCC of alloy Ti-8Al-1Mo-1V according to three microstructural features related to the amount and form of the beta phase (Gray 1973):

-1- A microstructure consisting of equiaxed primary α in a continuous transformed β matrix (i.e. processing of the alloy high in the $(\alpha+\beta)$ field) is the most resistant.
-2- A microstructure formed of equiaxed β phase in a continuous matrix of primary α phase (i.e. processing of the alloy low in the $(\alpha+\beta)$ field) exhibits intermediate resistance.
-3- A microstructure consisting of acicular transformed β (i.e. processing above the β transus) is very sensitive.

Furthermore several investigators report the extreme sensitivity of alloys containing more than 6% aluminium when the Ti_3Al phase is allowed to form (Petersen 1966, Gray 1973, Myers 1977), and Mahoney suggests an increase in susceptibility to HSSCC with an increasing grain size (Mahoney 1976).

Whether the influence of microstructure on the hot-salt stress-corrosion of titanium alloys is related to changes in mechanical properties such as fracture toughness or to the mechanisms of HSSCC themselves is a debatable question. In any case, it means that suitable heat treatments dependent on alloy composition must be employed in order to optimise the material 's performance in hot-salt stress-corrosion environments.

II.d.3 Heat treatment.

The investigations reported in the literature on the development of suitable heat treatments to increase the resistance of titanium alloys to HSSCC are somewhat difficult to compile, as heat treatments which may be beneficial for one alloy may be disastrous for another (Petersen 1971). Nevertheless there are two essential rules which must be observed in heat treating a titanium alloy likely to be exposed to HSSCC conditions.

First of all, titanium alloys containing more than 6% aluminium and processed relatively high in the $(\alpha+\beta)$ field should be cooled in a rapid manner in order to avoid the precipitation of the α_2 phase (Ti_3Al) which is particularly detrimental (Petersen 1966).

Secondly, processing of the alloy above the β transus should be avoided, as it results in an acicular transformed β phase with a low salt-cracking threshold (Donachie 1966).

Table II.b. and Figure II.k. show the dramatic effects of heat treatment on the hot-salt stress-corrosion threshold curves of two titanium alloys, Ti-8Al-1Mo-1V and Ti-5Al-6Sn-2Zr-1Mo-0.25Si. The results illustrate the extent to which the use of heat treatments to improve HSSCC resistance is alloy dependent. While duplex and triplex annealing treatments were used successfully for the Ti-8Al-1Mo-1V alloy, different heat treatments had to be employed for the second alloy tested (Gray 1973).

In any case, there is evidence that process control can minimise the sensitivity of alloyed titanium to hot-salt stress-corrosion cracking. This should include relatively short annealing times, low processing temperatures, adequate cooling rates, and preferentially the use of a controlled atmosphere (i.e. vacuum or argon) in order to avoid oxygen and hydrogen contamination of the material (Petersen 1966, Heimerl 1966).

II.d.4. Influence of texture.

The first report of the role played by texture in HSSCC was made by Stone and Freedman who noticed that most titanium alloys were actually more sensitive in the transverse direction than in the longitudinal direction (Stone 1967). This was confirmed later by Mahoney who reports that in some cases, the resistance to hot-salt cracking in the transverse direction can be reduced by as much as five times when compared with longitudinal direction loading (Mahoney 1976).

According to Lapasset, the influence of texture results from the existence of a crystallographic plane usually perpendicular to the direction of the load, which enhances cleavage (Lapasset 1979). The author even proposes a model for cleavage-assisted crack propagation based on the statistical repartition of suitably oriented grains resulting from the texture of the alloy. This model may actually help to elucidate some controversy between Lapasset and Mahoney: The former argues that a strong texture enhances resistance to hot-salt stress-corrosion cracking, while the latter claims the opposite effect. In fact it would appear that texture itself is not a valid parameter to evaluate HSSCC resistance if it is not related to the alloy microstructure.

Therefore texture has got to be considered as yet another parameter which can considerably complicate metallurgical studies of HSSCC of alloyed titanium. However it is still unclear whether this effect is related purely to the mechanical properties and fracture mechanics aspects of the material or to the mechanisms of the phenomenon themselves.

Alloy	Heat treatment	Microstructure
Ti811 Mill anneal	As-received (790 °C, 1 hr, air cool)	7% equiaxed β 93% continuous primary α
Ti811 Mill anneal	As received + (900 °C, 1 hr, furnace cool)	7% equiaxed β 93% continuous primary α
Ti811 Duplex anneal	As received + (650 °C, 24 hrs, air cool)	7% equiaxed β 93% continuous primary α
Ti811 Triplex anneal	As received +(1010 °C, 1 hr, air cool) +(590 °C, 8 hrs, air cool)	50% equiaxed primary α 50 % continuous transformed β
5621S (1)	As-received (980 °C, roll, 980 °C, 1 hr, air cool, 590 °C, 2 hrs, air cool)	10 % equiaxed primary α 90 % continuous transformed β
5621S (2A)	As-received (980 °C, roll, 1040 °C, 1 hr, air cool, 590 °C, 2 hrs, air cool)	100% transformed β (Widmanstätten)
5621S (2B)	As-received (1040 °C, roll, 1040 °C, 1 hr, air cool 590 °C, 2 hrs, air cool)	100% acicular transformed β
5621S (2C)	(2B) +(980 °C, 1 hr, air cool) +(590 °C, 2 hrs, air cool)	100% acicular transformed β

Table II.b. Heat treatments and microstructure used in conjunction with Figure II.k.

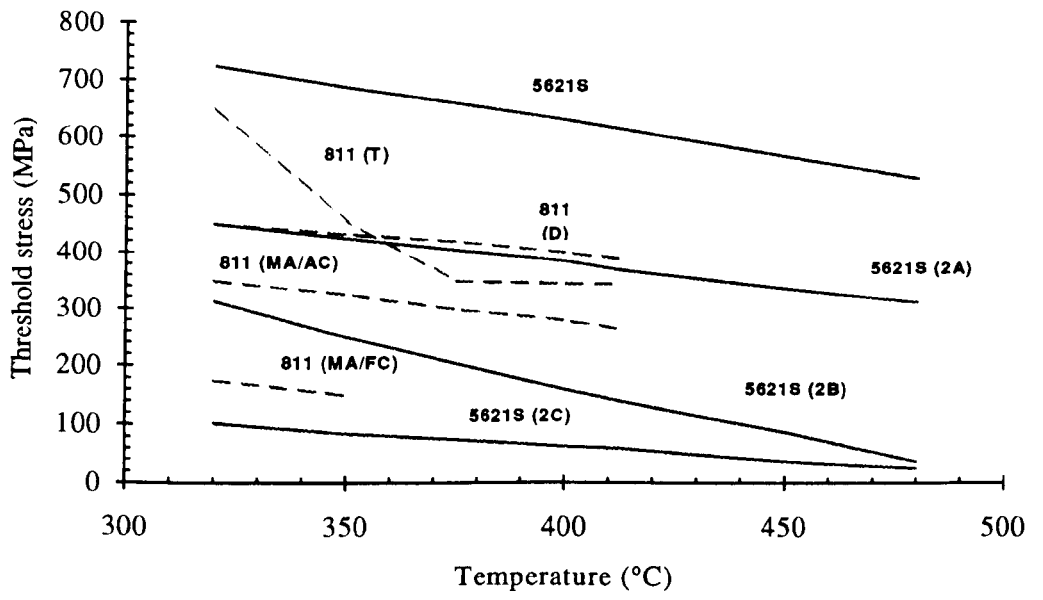

Figure II.k.: Effect of heat treatment on 96 hours crack threshold curves of titanium alloys Ti-8Al-1Mo-1V (------) and Ti-5Al-6Sn-2Zr-1Mo-0.25Si (——). The corresponding heat treatment are indicated in table II.b.(Gray 1973)

II.d.5. Surface conditions and processing effects.

If hot-salt stress-corrosion is insensitive to surface roughness or cracks (see paragraph II.b.2.), it appears to be strongly dependent on surface residual stresses which are induced by machining operations. Gray reports that the stress threshold curves obtained for stress-relieved specimens lay substantially below these obtained for test pieces in the as-machined condition. After an analysis of the stresses remaining after machining, he concludes that the effect is due to residual compressive stresses induced by shearing and milling (Gray 1971a). The author also argues that if machining or processing of the alloy were to induce residual tensile stresses, then the resistance of the alloy to HSSCC would be lowered. This was confirmed by Simenz et al. who prestrained tension specimens with a view to induce tensile residual stresses and noticed a decrease in the resistance of the alloy to hot-salt stress-corrosion during subsequent testing (Simenz 1966).

Turley also reports a decrease in HSSCC resistance when the material is fusion welded. According to him, the occurrence of severe cracking both in the heat affected zone and in the base material suggests that stress-relieving itself lowered the threshold stress in

this case (Turley 1966). Further studies showed that bolted and riveted joints, spotwelded joints and brakes, and roll formed angles are all at least as susceptible to hot-salt stress-corrosion as the plain alloy, and can sometimes exhibit dramatic reductions in life (Simenz 1966).

II.d.6. Protective treatments.

The first protective treatment to be investigated is obviously the growth of a protective oxide layer at the surface of the material, as rutile (TiO_2) is known to be extremely stable. Heimerl et al. report that oxide layers up to 600 Å formed on the alloy prior to HSSCC testing have no effect on either the rate or the amount of hot-salt stress-corrosion damage (Heimerl 1966). Indeed, the general opinion is that although removal of the oxide layer seems to encourage HSSCC, only very slight improvements in resistance can be achieved when a preoxidation treatment is employed (Mahoney 1972). There are two reasons for the inability of rutile layers to protect the material under HSSCC conditions: Firstly the oxide layer is destroyed by stresses and corrosion products. Secondly thermodynamical conditions above 300 °C may be such that the activity of the salt may be able to activate the passive oxide layer (Crossley 1960, Dinnappa 1988). Nevertheless the mechanisms of the activation of oxides by chlorides have not yet been established. Despite these results, a recent study at Rolls Royce plc. seems to have shown that high temperature oxidation treatments prior to hot-salt stress-corrosion testing enhances the resistance of the alloy (Cuningham 1993). This work which is still under development partly agrees with the results obtained by Siniglia who found that preoxidation of the material prior to HSSCC increases substantially the initiation times to crack for Ti-13V-11Cr-3Al and Ti-6Al-4V, while Ti-5Al-2.5Sn and Ti-8Al-1Mo-1V were unaffected (Siniglia 1978).

Because of the influence of surface residual stresses on HSSCC (see § II.d.5.), shot peening represents an attractive way of protecting the material. Indeed, shot peening constitutes means of providing substantial residual compressive stresses to the surface of the alloy by glass beads bombardment. This treatment was found to be effective by several workers in moderate hot-salt stress-corrosion environments (Stein 1968, Boudreau 1968, Webster 1992). However when tests are carried out at higher loads and temperatures, this beneficial effect tends to disappear (Petersen 1971).

Numerous coatings have also been used in an attempt to protect titanium alloys from HSSCC. Stein showed that electrophoretic aluminium coatings and nickel electroplating were both successful in retarding hot-salt stress-corrosion (Stein 1968). However nickel electroplating provoked a significant decrease in ductility of the base material. Later studies showed the same behaviour for chromium, silicon, iron, and magnesium based coatings (Groves 1973, Wright 1974). Resin based coatings also proved to be inadequate due to spalling of the protective layer after prolonged exposure at elevated temperatures (Petersen 1971).

Other protection techniques studied include zinc dipping (Petersen 1966) and cladding of the material with unalloyed titanium, also called autocladding (Petersen 1971). However it is doubtful that these processes are totally efficient , and the ease of their use for gas turbine engine components is still to be demonstrated.

II.e. Conclusion

Titanium alloys suffer from hot-salt stress-corrosion (HSSCC) when contaminated by salts and exposed to high stresses at elevated temperature. This results in drastic reductions of their mechanical properties and cracking. A wide amount of research has been carried out on this phenomenon. However, there is considerable scatter in the results available in the literature due to the lack of standardised testing techniques, threshold considerations, and the nature of HSSCC itself.

The extent of damage induced in a titanium alloy by hot-salt stress-corrosion depends mainly on temperature, load, and exposure time. Present in minute quantities, a wide range of salts and other contaminants, can induce HSSCC in a titanium alloy. Water vapour and oxygen are prerequisite of hot-salt stress-corrosion of titanium alloys. However, the existence of an oxygen threshold below which the resistance to HSSCC would be considerably improved is probable.

Cyclic operating conditions and the presence of a high velocity airstream provide slight improvements to the resistance of the material. Limited hot-salt stress-corrosion testing has been achieved at high environmental pressures. However a marked beneficial effect was noticed up to 4 bars.

Pure titanium is immune to HSSCC. The resistance of titanium alloys to hot-salt stress-corrosion is strongly influenced by their aluminium content. Microstructure, texture, and surface conditions influence the resistance of titanium alloys to HSSCC but this effect depends strongly on alloy composition.

Protective treatments have been, and still are being investigated. However, complete protection of the material has not yet been achieved.

CHAPTER III

HOT-SALT STRESS-CORROSION OF TITANIUM ALLOYS: MECHANISMS AND MODELING ASPECTS

" At intervals researchers gather
And on mechanisms all palaver
Each to his own work will refer
Ignoring those who don't concur."

S.P.Rideout,
Savannah River Laboratory.

III.a. Introduction

The understanding of the mechanisms by which titanium alloys become embrittled as a result of hot-salt stress-corrosion has been, and still is, a major problem for the researcher: First of all, the reactions between titanium, water, oxygen, and halide salts at elevated temperatures are of an incredible complexity and some of the likely corrosion products such as oxychlorides are still relatively unknown. Secondly, the presence of alloying elements makes the task even more complicated: If aluminium and to a lesser extent, vanadium are believed to act as accelerators in the HSSCC process, there is also speculation that zirconium and molybdenum have the opposite effect.

But the most argued feature of hot-salt stress-corrosion cracking of titanium alloys concerns the role of hydrogen which is regarded as being responsible for the embrittlement of the material and therefore, for stress-assisted crack initiation and propagation. Although hydrogen is actually the most likely candidate to explain HSSCC failures, it is nevertheless not totally realistic when one considers its diffusion rate in titanium at elevated temperatures. Furthermore, the observation of titanium hydrides under SEM and TEM conditions is unlikely, as the energy supplied by the electron beam is sufficient to dissolve these precipitates.

The importance of modeling the hot-salt stress-corrosion of titanium alloys is of two practical interests: Firstly, if a suitable model is eventually developed, the lack of in-service failures must be explained, and the possibility of their occurrence in more sophisticated engines should be addressed. Secondly if HSSCC of titanium based components is likely to become a problem, protective treatments could be investigated in a more systematic manner. A number of models have been developed to date. Although none of them is entirely satisfactory, they point out some of the probable steps of HSSCC of titanium alloys and they are worth a thorough investigation.

III.b. Identification of reactions between hot-salts and titanium alloys.

III.b.1. Identification of corrosion products

The chemical reactions which may take place during the hot-salt stress-corrosion cracking of titanium alloys involve a wide range of reactants which are contained either in the material itself (titanium, aluminium, vanadium, tin, etc.), in the halide salt deposits (Sodium, magnesium, potassium, lithium, chlorine...), or in the atmosphere (oxygen, water). Therefore numerous reactions are possible, especially at the elevated temperatures at which HSSCC occurs.

Unfortunately, information is still scarce on a number of potential corrosion products which can also be hardly detected with current analysis tools. This is particularly true for oxychlorides which may appear as a result of the reactions between hot-salt and oxygen, but which can not be assumed to have an active part in the process. Therefore, they have been left out of the potential steps of the mechanisms, although their possible presence is usually mentioned (Petersen 1966, Travkin 1979).

The identification of corrosion products is an essential step in order to restrict the large number of potential reactions (more than two hundred according to Travkin) to just a few, and several techniques have been extensively used to achieve this goal:

The analysis of X ray diffraction patterns of hot-salt stress-corroded specimens indicate that titanium dioxide, present both as anastase and rutile is one of the end products and appears as a blue/grey stain (Logan 1964, Martin 1966). Using hot-stage optical microscopy, Rideout was able to observe that staining occurs almost immediately, and in any case a lot earlier than cracking. The staining, which he also attributed to both forms of titanium dioxide is non adherent, flaky, and completely removed by a water-rinse (Rideout 1968). This tends to show that rutile and anastase would be left as deposits on the surface of the material rather than embedded in the corrosion scale (Logan 1964). X ray diffraction techniques also showed the presence of hydroxide (Martin 1966, Hatch 1966) and sodium titanate (Petersen 1966).

In order to verify which species are absorbed by materials undergoing HSSCC, radioactive tracer studies and electron microprobe analysis have both been employed by several workers (Garfinkle 1973, Rideout 1967, Ondrejcin 1967). They revealed that

both sodium and chlorine ions are actually absorbed by the alloy. However, sodium was detected only at the mouth of stress-corrosion cracks, while chlorine was found to be present in decreasing concentrations from the crack mouth to the crack tip. This implies that a diffusion mechanism must have taken place in order to transport the chloride ions from the surface of the oxide scale into the base material (Rideout 1967). These studies also showed segregations of alloying elements such as aluminium, molybdenum, and vanadium along such cracks (Martin 1966). Furthermore, the dissolution of corrosion products collected on the surface of the material revealed an increased ratio of aluminium to titanium content as compared to the base alloy composition (Rideout 1966). Therefore, these alloying elements must have an active role in the transport mechanisms.

The identification of gaseous species produced during the hot-salt stress-corrosion process is yet another difficult task. This has been achieved through gas mass spectrometry of samples taken from the atmosphere close to specimens undergoing HSSCC. This technique can provide valuable information only if substantial amounts of each gaseous product are present, and some attempts have proved unsuccessful (Logan 1966). However, both hydrochloric acid and chlorine were identified in several studies (Petersen 1966, Hatch 1966, Ondrejcin 1970). In this respect it is worth mentioning that cracking similar to this observed in HSSCC was obtained when unsalted specimens were tested in gaseous hydrochloric acid (Rideout 1966, Hatch 1966). Ondrejcin and Rideout also detected the presence of hydrogen gas and water vapour (Ondrejcin 1967, Rideout 1966), while Hatch claims to have identified titanium dichloride (Hatch 1966). His finding was confirmed by Heimerl who reports that $TiCl_2$ is one of the gaseous species which evolved during the dissolution of corrosion products collected on the surface of hot-salt stress-corroded specimens (Heimerl 1966).

III.b.2. Chemical reactions

The studies described above lead to a restricted number of proposed chemical reactions for the successive steps of the HSSCC process. Indeed they involve titanium oxides and sodium hydroxides (or sodium titanate) as solid species, and hydrochloric acid, oxygen, water vapour, and titanium dichloride as gaseous reactants and products. Table III.a. presents these reactions which can be classified in four categories: Chlorination of titanium metal, oxidation of salt, hydrolysis of both titanium chloride and salts oxides, and exchange reactions between oxygen and chlorine gas. Of course, this list is not

exhaustive and alloying elements may also be substituted for titanium metal. However, when one considers the current knowledge of the hot-salt stress-corrosion cracking of titanium alloys, these reactions constitute the most realistic options.

Chlorination of titanium:

$Ti + 2HCl \longrightarrow TiCl_2 + 2H$	**(III.1)**	(Gray 1969a, Hatch 1966)
$Ti + Cl_2 \longrightarrow TiCl_2$	**(III.2)**	(Hatch 1966)
$Ti + 2NaCl + \frac{1}{2}O_2 \longrightarrow TiCl_2 + Na_2O$	**(III.3)**	(Boyd 1964)
$Ti + 2NaCl + \frac{1}{2}O_2 + H_2O \longrightarrow TiCl_2 + 2NaOH$	**(III.4)**	(Hatch 1966, Martin 1966)

Oxidation of salt:

$NaCl + H_2O \longrightarrow HCl + NaOH$	**(III.5)**	(Hatch 1966)
$2NaCl + \frac{1}{2}O_2 + TiO_2 \longrightarrow Na_2TiO_3 + Cl_2$	**(III.6)**	(Crossley 1960)

Hydrolysis:

$TiCl_2 + H_2O \longrightarrow TiO + 2HCl$	**(III.7)**	(Hatch 1966, Gray 1969a)
$\frac{1}{2}Na_2O + \frac{1}{2}H_2O \longrightarrow NaOH$	**(III.8)**	(Boyd 1964)

Exchange reaction:

$TiCl_2 + O_2 \longrightarrow TiO_2 + Cl_2$	**(III.9)**	(Heimerl 1966, Hatch 1966)

Table III.a. Chemical reactions proposed for the hot-salt stress-corrosion cracking of titanium alloys.

Travkin et al. carried out a systematic thermodynamical analysis of more than two hundred possible reactions of metals, salts, and oxides in the solid state with water vapour and gases (Travkin 1979). These calculations confirm that complex oxides

scales are ultimately formed from titanium and its alloying elements at HSSCC temperatures. However, intermediate reactions involving the formation of volatile metallic chlorides are thermodynamically favourable especially for the alloying elements zirconium, molybdenum, and aluminium. The subsequent pyrohydrolysis of these metal chlorides which is accompanied by the production of gaseous hydrochloric acid is also probable, particularly with $MoCl_4$ and $AlCl_3$. Furthermore, the pyrohydrolysis of halide salts is accelerated by the presence of alumina and vanadium pentoxide which may be present within the oxide scales formed at temperature on titanium alloys (Rideout 1966).

Regarding the reactions between salts and water, Travkin claims that oxidation and hence the production of chlorine is more likely than their pyrohydrolisis (i.e. production of HCl). The formation of hydroxide is also reported as probable.

Finally Travkin mentions that exchange reactions of chlorides with oxides give no cause for doubt but that the conditions in which they are triggered are not fully understood. However, he also claims that sodium chloride is acting as a catalyst in such processes.

From the above considerations, the most likely chemical reactions of the hot-salt stress-corrosion cracking of titanium alloys can therefore be described as follows:

-1- Chlorination of metallic species and oxidation of salt deposits. The salt oxides may combine with metallic oxides to produce amphoteric salts such as sodium titanate, and chlorine is formed.

-2- Pyrohydrolysis of metallic chlorides accelerated by oxides catalysts accompanied by the formation of gaseous hydrochloric acid.

-3- Exchange reactions between metallic chlorides and oxides accelerated by the presence of halide salts.

III.c. Hydrogen and hot-salt stress-corrosion cracking of titanium.

The chemical reactions mentioned earlier were derived from both analytical and theoretical considerations. However, although they allow one to predict a number of possible mechanisms, they include two potential gaseous cracking agents: Chlorine and hydrochloric acid. In order to find out if hydrochloric acid is the cracking agent during HSSCC exposure, a study of the effects of free hydrogen in titanium alloys is therefore required.

III.c.1 Hydrogen embrittlement of titanium alloys.

The loss of ductility of titanium alloys due to the presence of small amounts of hydrogen (less than 200 ppm) can be classified in two categories (Williams 1963).

Impact embrittlement: Impact embrittlement in hydrogen contaminated alloys is caused by the precipitation of a hydride phase and is mostly observed in α alloys. Its effects increase with increasing hydrogen contents, increasing strain rates, decreasing temperatures, and the presence of notches on the surface of the material. The plate-like hydride phase precipitates in regions of high stress concentrations where the hydrogen solubility limit of the alloy is exceeded, and is followed by cleavage (Cotterill 1961).

Slow strain rate embrittlement: This form of hydrogen embrittlement is mostly observed in (α+β) alloys but has also been reported in α and β alloys (Williams 1960). It is absent at high strain rates and is most severe at room temperature. However there is some controversy on the manner in which slow strain rate embrittlement affects the mechanical properties of titanium alloys: Livanov claims that hydrogen atoms are dragged by moving dislocations until an obstacle is reached where dislocations pile up (Livanov 1973), whereas Shih proposes a model based on the direct influence of hydrogen on the dislocations' velocity (Shih 1988). Other studies suggest the precipitation of microhydrides in the alpha phase or at the α/β interface (Meyn 1974).

Based on these mechanisms, it seems doubtful that hydrogen embrittlement constitutes the final step of hot-salt stress-corrosion cracking of titanium: Impact embrittlement is transgranular while HSSCC failures are predominantly intergranular, and low strain rate embrittlement is not considered as a problem at high temperature. However

experimental evidence obtained by previous workers seem to imply that hot-salt stress-corrosion of titanium alloys is indeed a hydrogen embrittlement phenomenon.

III.c.2 Hydrogen and HSSCC.

In spite of the facts presented above, there is a general consensus that free hydrogen produced during hot-salt stress-corrosion is actually responsible for the failures observed in laboratory (Ondrejcin 1971, Gray 1971a, Plekhanova 1976, Dinnappa 1988).

In this respect, the mechanical testing techniques developed by Gray whereby the material is initially exposed to HSSCC for about 100 hours prior to a residual tensile test are of particular interest (Gray 1969b). Indeed, Gray noticed that the loss of ductility detected during the post-exposure test is strongly dependent on the strain rate and the ambient temperature. In fact, this loss of ductility is maximum for slower strain rates and at room temperature. This is of course very similar to the phenomenon of slow strain rate embrittlement and indicates that hydrogen may well be active in HSSCC of titanium.

Further indication that hydrogen must be considered come from the testing of unsalted titanium alloy specimens at elevated temperatures in hydrochloric acid gas and high pressure hydrogen gas atmospheres (Rideout 1967, Ondrejcin 1968). The features of the fracture surfaces obtained were similar to HSSCC failures, and cracking occurred more rapidly in HCl than during hot-salt stress-corrosion. Ondrejcin attributes this faster embrittlement to the continuous supply of hydrochloric acid which does not require an initiation stage. He also considers that the high pressures of hydrogen required to produce cracking indicate that the oxide layer present on the surface of the material must first be permeated. Ondrejcin also obtained cracking by bombarding a stressed sample of unsalted titanium alloy with H^+ ions.

Observation and analyses of fracture surfaces also tend to support the theory of hydrogen embrittlement: Firstly, Gray noticed the existence of a brittle, non-corroded zone ahead of the crack tip (Gray 1974). He concludes that cracking of the material is caused by a diffusable specie and is independent of the main corrosion process. Ondrejcin observed evidence of dislocation movement and claims that the fracture mode does not involve the precipitation of hydrides (Ondrejcin 1968). Furthermore, the

use of radioactive tracer studies revealed the presence of hydrogen in salt-corroded areas (Gray 1971b). In order to show the predominance of free hydrogen, Garfinkle carried out a study of the influence of salt pH on the initiation of cracking (Garfinkle 1972). His results show that lowering the pH (i.e. increasing the surface concentration of H^+) promotes cracking, whereas raising the pH has the opposite effect.

But the major argument supporting the theory of hydrogen embrittlement for the hot-salt stress-corrosion of titanium alloys has been obtained using analytical methods developed by Gray (Gray 1971c). Hydrogen concentrations which had been measured in titanium alloy specimens previously exposed to HSSCC conditions using vacuum fusion techniques were two to three times higher than these measured in the as-received condition (Gray 1971a). However, these measurements represented average bulk concentrations, and it was thought that local concentrations near the fracture surface could be significantly higher. Ion and laser microprobe analyses elaborated by Gray confirmed this hypothesis and revealed local hydrogen concentrations of several thousands ppm compared with an initial value of 70 ppm in the as-received condition (Gray 1973, Plekhanova 1976).

Following this work, several significant experiments were carried out in order to demonstrate the predominant role of hydrogen. Firstly, Gray inserted a vacuum annealing treatment between HSSCC exposure and post-exposure tensile testing. As expected, vacuum annealing reduced drastically the high hydrogen concentrations detected after hot-salt stress-corrosion. Furthermore, full recovery of the alloy's mechanical properties was demonstrated in the post-exposure tensile test (Gray 1973). Of course, this also meant that no permanent damage, such as that due to cracking, had been induced during HSSCC exposure. However, specimens exposed to the same conditions for the same length of time were significantly embrittled. Other studies also showed that the extent of embrittlement could be related to the amount of hydrogen pick-up by the material during HSSCC exposure (Plekhanova 1976). In fact, these concentrations tend to be so high, that the initial hydrogen content of the alloy can be considered as irrelevant (Gray 1971d).

Ondrejcin provided further evidence that hydrogen is absorbed during the hot-salt stress-corrosion of titanium alloys by measuring its penetration into the material. He concludes that not only does free hydrogen diffuse a minimum of 10 μm into the metal, but that the amounts absorbed are proportional to the amount of water vapour available (Ondrejcin 1970, Ondrejcin 1971).

Therefore, it seems that free hydrogen is indeed produced during the hot-salt stress-corrosion of titanium alloys and diffuses into the metal which is subsequently embrittled. However, the final step of the process which would describe the mechanisms of crack initiation and propagation (i.e. impact embrittlement or slow strain rate embrittlement) is still unknown. The argument that hydrogen may be present in titanium alloys exposed to HSSCC conditions simply as a result of general corrosion is also difficult to reject. Hence, with the current knowledge of hot-salt stress-corrosion cracking mechanisms, hydrogen embrittlement is implicit and constitutes the most plausable cause of HSSCC embrittlement.

III.d. Current models.

Numerous models have been proposed to describe the mechanisms of hot-salt stress-corrosion cracking of titanium alloys, but only three of them can be considered to be realistic possibilities. They are Rideout's pyrohydrolysis model (Rideout 1966), Logan's stress sorption model (Logan 1969), and Myers' electrochemical model (Myers 1977).

III.d.1. Rideout's pyrohydrolysis model

Rideout claims that direct salt/atmosphere/substrate reactions are responsible for the cracking, and that the primary role of corrosion, which is electrochemical in nature, is to produce free hydrogen. The model, which considers also the importance of aluminium in the process, proposes the following reactions:

-1- Chlorination of the alloy and oxidation of salt deposits:

$$Ti + 2NaCl + 2H_2O \longrightarrow TiCl_2 + 2NaOH + 2H \qquad \textbf{(III.10)}$$

$$Al + 3NaCl + 3H_2O \longrightarrow AlCl_3 + 3NaOH + 3H \qquad \textbf{(III.11)}$$

-2- Pyrohydrolysis of metal chlorides:

$$TiCl_2 + 2H_2O \longrightarrow TiO_2 + 2HCl + 2H \qquad \textbf{(III.12)}$$

$$2AlCl_3 + 3H_2O \longrightarrow Al_2O_3 + 6HCl \qquad \textbf{(III.13)}$$

-3- Reaction of the base alloy with hydrochloric acid:

$$Ti + 2HCl \longrightarrow TiCl_2 + 2H \qquad \textbf{(III.14)}$$

$$Al + 3HCl \longrightarrow AlCl_3 + 3H \qquad \textbf{(III.15)}$$

The model concludes that much of the hydrogen produced by these reactions is readily absorbed by the base alloy which becomes subject to embrittlement. The main criticisms addressed to the mechanism of Rideout are that reaction (III.10) is thermodynamically unfavourable, and that hydrochloric acid which forms would be neutralised by hydroxide ions (Garfinkle 1973, Myers 1977). However, the pyrohydrolisis reactions are of interest, and the influence of aluminium as observed by most workers (see chapter II) is explained by the greater amounts of hydrogen produced for the pyrohydrolisis of this alloying addition.

III.d.2. Logan's stress sorption model.

Logan suggests that a solid state reaction between the crystalline salt, the oxidised layer, and the base alloy occurs at elevated temperatures. This reaction, which could be assisted by water vapour, produces oxygen and chloride ions, and possibly hydrogen. Referring to studies showing that titanium dioxide is very slightly oxygen deficient (Wallwork 1959), Logan proposes a model whereby chloride ions diffuse down a stress and oxygen concentration gradient in the oxide layer to be present at the surface of the material. Following this, chloride ions react with the alloy to destroy the atomic bonds in the metal and thus form stress-corrosion cracks. Logan also suggests that any hydrogen produced during HSSCC would also dissolve in the alloy.

However, this stress sorption model does not specify which chemical reactions are occurring during the hot-salt stress-corrosion of titanium alloys and lacks experimental support. Furthermore, it is not consistent with stress and temperature cycling studies which showed that a non cumulative initiation period is required for HSSCC (see chapter II) since it does postulates that chlorine is the cracking agent.

III.d.3. Myers' electrochemical model.

Myers' electrochemical model is based on the existence of a oxygen differential aeration cell at the surface of the material, the anode being located under the salt deposits where oxygen is scarce. Once the oxide film has failed, it can not be repaired because of the high chloride concentrations and dissolution of the metal occurs:

$$Ti \longrightarrow Ti^{n+} + ne^- \qquad \textbf{(III.16)}$$

The cathodic reaction occurs in the higher oxygen containing electrolyte adjacent to the salt crystals, associated with an absorbed moisture layer:

$$O_2 + 2H_2O + 4e^- \longrightarrow 4OH^- \qquad \textbf{(III.17)}$$

After a pit has formed, it is filled with the electrolyte by capillary action. As a positive charge due to the dissolution of the metal develops in the pit, chloride ions diffuse through the electrolyte. Titanium ions then react with chloride ions and produce titanium chlorides which are subsequently pyrohydrolysed in the pit:

$$TiCl_n + nH_2O \longrightarrow Ti(OH)_n + nH^+ + nCl^- \qquad \textbf{(III.18)}$$

The high H^+ concentration which is therefore created in the pit would permit a secondary cathodic reaction which provokes the reduction of hydrogen ions:

$$H^+ + e^- \longrightarrow H \qquad \textbf{(III.19)}$$

Hence, the model provides a source of free monoatomic hydrogen which is required for cracking to occur. However, it is based on the presence of an electrolyte. Furthermore, it does imply that this liquid medium is going to fill the crack by capillary action. This assumption is actually not consistent with studies carried out by Kirchner who observed that stress-corrosion cracks were empty of any liquid (Kirchner 1966). Furthermore the extremely low amounts of water vapour which are necessary for HSSCC to occur seem to preclude the hypothesis of the existence of an electrolyte.

It can be concluded from these studies that none of the models proposed to date to describe the hot-salt stress-corrosion of titanium alloys are entirely satisfactory. However some of the concepts mentioned such as pyrohydrolysis of metal chlorides,

stress sorption, or electrochemical mechanisms initiated by an oxygen differential aeration cell are of interest and are representative of the different steps that may occur, as identified by a number of workers.

III.e. Conclusion

The chemical reactions which may take place during the hot-salt stress-corrosion of titanium alloys are extremely complex. They may involve oxychlorides but this aspect can unfortunately not be modeled.

The corrosion product which have been identified during HSSCC are:

Solids: Titanium dioxide, Sodium hydroxide, and Sodium titanate

Gases: Hydrochloric acid, and chlorine.

Chlorine and sodium ions are adsorbed by the material during HSSCC:

Na^+ ions concentrates near the crack mouth

Cl^- ions are present along cracks in decreasing concentrations towards the crack tip

There is evidence that titanium alloys failures under HSSCC conditions are provoked by hydrogen embrittlement. However it is not clear whether the mechanism involved relates to impact embrittlement or slow strain rate embrittlement.

None of the proposed models for the hot-salt stress-corrosion of titanium alloys are entirely satisfactory, but some of their concepts are nevertheless of considerable interest. They include the pyrohydrolysis of metal chlorides, stress sorption mechanisms, and electrochemical mechanisms caused by an oxygen different aeration cell.

CHAPTER IV

EXPERIMENTAL METHODS

IV.a. Introduction

Numerous studies on the hot-salt stress-corrosion cracking of titanium alloys have been carried out during the past thirty five years. However although great progress has been made, the mechanisms of HSSCC are still not completely understood (see Chapter III), and the lack of in-service failures is still to be explained.

Chapter II showed that many parameters which could have a beneficial effect on the behaviour of titanium alloys in hot-salt stress-corrosion environments lead to only minor improvements in the life of the materials. However there are two aspects which have so far received limited attention from past workers: Firstly, hot-salt stress-corrosion testing of titanium-base alloys at high pressures has been understudied because of the difficulties to combine loads, high temperatures, and high pressures in a corrosive environment. Indeed, the only results currently available on this topic come from Gray and have been obtained for pressures less than these commonly encountered in aero gas turbine engines (Gray 1969b). The comparison of the oxidation of titanium alloys in air and in hot-salt environments in the absence of an applied stress are also scarce. However Dumas showed that they could provide valuable information regarding the formation of corrosion scales on the surface of the material (Dumas 1976).

The aim of this study was to further investigate these two aspects of HSSCC of titanium alloys using a unique high temperature, high pressure, servo-hydraulic testing facility and a thermogravimetric apparatus. The material used is IMI 834 and this chapter will describe the cleaning, salting, and testing procedures used throughout this work.

IV.b. Material

II.b.1 IMI 834

The alloy used throughout this study is titanium alloy IMI 834 which is a near alpha alloy possessing increased tensile strength and creep resistance up to 600 °C together with good fatigue strength. The main alloying elements are aluminium, tin, zirconium with smaller additions of niobium, molybdenum, and silicon (see table IV.a.).

Photograph IV.a. shows the typical microstructure of the as-received material that is, after all heat treatments have been carried out. It can be noticed that the microstructure of this forged alloy is equiaxed and contains about 12% to 15% of primary alpha phase (white grains), together with Widmanstatten beta phase and alpha phase due to transformed beta. This primary alpha phase content which is desirable for an optimum compromise between creep and fatigue properties for aero gas turbine applications is obtained by heat treating the alloy high in the $\alpha+\beta$ field. This is possible because of carbon additions which extend the temperature range over wich this treatment can be carried out. The good mechanical properties of IMI 834 (see Chapter 1, table I.d.) and the fact that this alloy is also weldable makes it an ideal candidate for discs and blades in the initial and intermediate stages of gas turbine engines' compressors, and its use has become increasingly common in the past few years.

	Al (%)	Sn (%)	Zr (%)	Nb (%)	Mo (%)	Si (%)	C (%)	Fe (%)	O_2 ppm	N_2 ppm	H_2 ppm	Others
Min	5.5	3.0	3.0	0.50	0.25	0.20	0.04	-	750	-	-	-
Max	6.1	5.0	5.0	1.00	0.75	0.60	0.04	-	1500	-	-	-
Real	4.8	4.0	3.2	0.62	0.63	0.38	0.04	0.09	-	-	-	-

Table IV.a. Chemical composition of titanium alloy IMI 834 (IMI 1990)

IV.b.2.Specimens

The material was received as barstock cut out from an isothermally forged high pressure compressor disc designed and heat treated to be used in the 4th stage of a gas turbine's compressor. The material was solution treated for 2 hours at 1032 °C and oil quenched, and aged at 700 °C for two hours and air cooled. A simulated post weld heat treatment for two hours at 640 °C in vacuum was also carried out. Photograph VI.a. shows that in fact the microstructure of this material is unsatisfactory for engine use because of a non uniforme repartition of the primary alpha grains. However, this microstructure was not seen as a problem for this study.

This material was used in two forms: Fatigue test pieces were manufactured according to the drawing showed in figure IV.a. and were used for high pressure studies. Round coupons of 11.1 mm in diameter and 1.8 mm in thickness were also produced for the thermogravimetric oxidation and salt-corrosion studies.

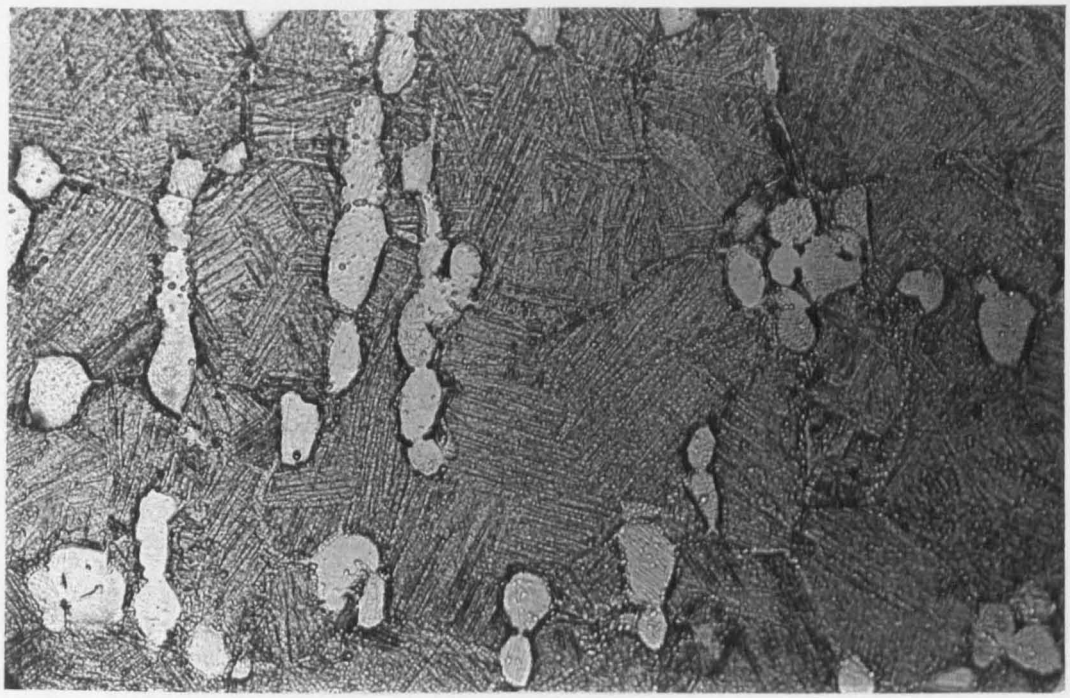

Photograph IV.a.: Acicular microstructure of the as-received alloy showing 12% to 15% primary alpha phase. Magnification: × 400.
Etchant: 2% HF, 8% HNO_3, 90% H_2O.

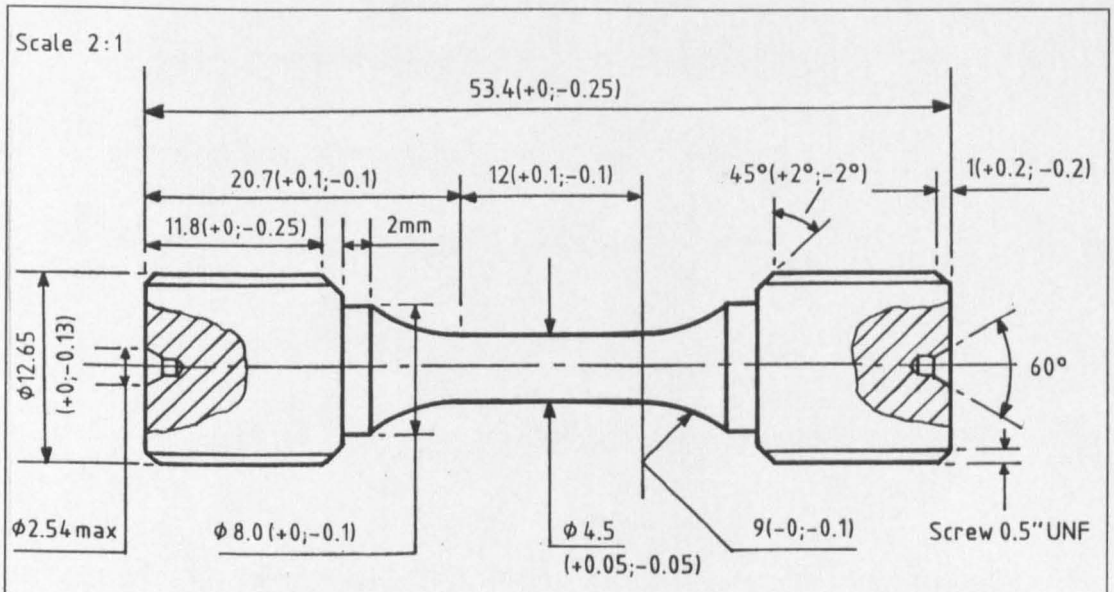

Figure IV.a. Technical drawing of the fatigue test piece geometry, used for stress-corrosion tests in this study

After machining, all specimens were cross-hatch polished using 800, 1000, and 1200 grid abrasive papers in order to remove all turning marks and to provide a uniform surface finish with no deep machining or grinding marks.

IV.c. Cleaning procedure

When one considers the nature of this work, it seems obvious that a reliable procedure to clean any testing material is of considerable importance to ensure a satisfactory quality of testing: Indeed, specimen surface preparation before salt coating is critical in order to provide optimum adherence between the salt and the test piece. Furthermore in the case of thermogravimetric oxidation studies, contamination of the specimen must be avoided. Hence all the material used throughout this study was cleaned before being salt-coated in the case of hot-salt stress-corrosion studies. The same method was also applied before each thermogravimetric oxidation test.

-1- Initial cleaning with methanol and drying

-2- Cleaning in ultrasonic bath with inhibisol

-3- Flushing with clean inhibisol

-4- Flushing with clean isopropyl alcohol

-5- Cleaning in ultrasonic bath with isopropyl alcohol

-6- Flushing with clean isopropyl alcohol

-7- Flushing with Analar isopropyl alcohol

-8- Vapour degreasing in cleaning column charged with Analar isopropyl alcohol

During all the cleaning procedure, as during any subsequent operation, the material is handed with surgical gloves in order to avoid recontamination of the surface. The specimens are then kept in a dessicator isolated from any contact with uncleaned surfaces.

IV.d. Salting procedure

IV.d.1 Salting

Both the fatigue test pieces used for hot-salt stress-corrosion studies and the coupons used in the thermogravimetric work were salted in a salt-fog atmosphere at elevated temperatures using the apparatus showed in figure IV.b.. The salt solution was made according to British Standard 3900 part F4 (see table IV.b.) and was sprayed on the material using the following procedure:

-1- The specimens are screwed into the turntable

-2- The furnace is lowered, clamped, and switched on.

-3- The peristaltic pump is switched on, and the pipes are purged with the salt solution.

-4- When the specimens have reached the spraying temperature (225 to 250 °C), the salt solution inlet pipe is connected to the spraying nozzle.

-5- The furnace is raised away from the turntable and clamped, the spraying chamber is raised over the specimens, and the air supply pipe is connected to the nozzle. The chamber is covered, and the turntable switched on.

-6- The specimens are exposed to the salt-fog atmosphere for a time determined previously (typically 200 s).

-7- The spraying chamber is lowered, and the specimens are allowed to cool.

-8- The specimens are unscrewed from the turntable and put individually in a small closed plastic vial which is kept in a dessicator.

-9- One specimen is soaked with water overnight in order to carry out its salt content analysis the following day.

Chemical product	Symbol	Quantity per litre of solution (g)
Sodium Chloride	NaCl	26.5
Magnesium Chloride	$MgCl_2$	4
Magnesium Sulphate	$MgSO_4$	3.3
Potassium Chloride	KCl	0.73
Sodium Hydrogen Carbonate	$NaHCO_3$	0.28
Calcium Chloride	$CaCl_2$	1.1

Table IV.b. Composition of salt spraying solution (BS3900)

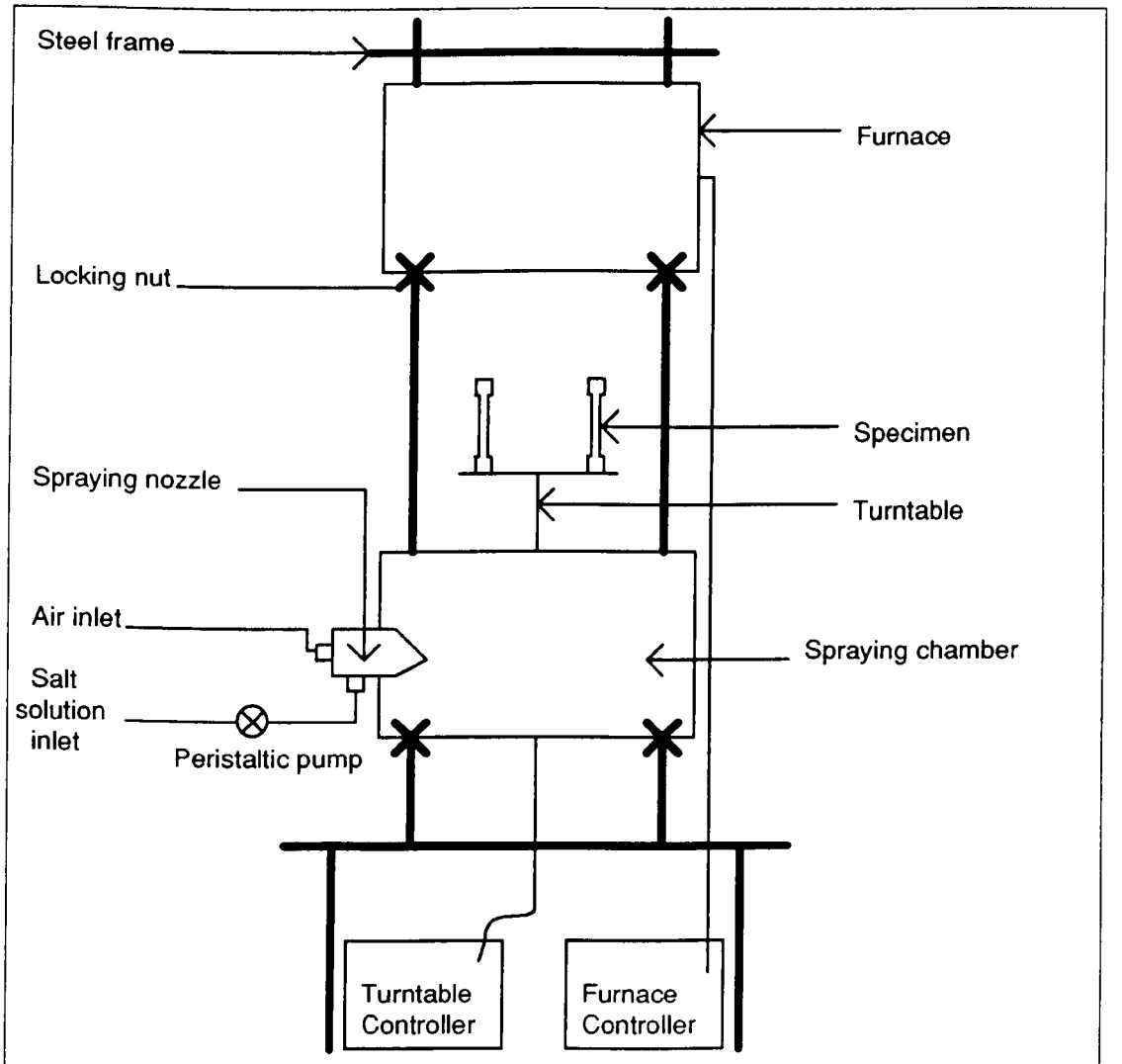

Figure IV.b. Salt spraying apparatus

IV.d.2. Salt analysis

The surface salt concentration of one specimen per salted batch is measured using titration techniques. The analysis equipment consists of an expandable ion analyser (Orion EA 940) linked to a single junction reference electrode (Orion 90-01) and a silver sulfide electrode. The solution obtained after soaking the specimen is thus analysed as follows:

-1- The solution is poured from the vial into a 20 ml volumetric flask. The specimen and the vial are washed with deionised water which is added to the contents of the flask. Deionised water is added to make up the solution to 20 ml.

-2- The solution is poured in a clean, dry, wide-form pyrex beaker. One milliliter of low level ionic strength adjuster (Orion 94-011) is added.

-3- The solution is placed on a magnetic stirrer and stirring is adjusted in order to be sufficiently vigorous, but without creating a vortex.

-4- The electrodes are immersed into the liquid.

-5- The voltage is recorded in millivolts.

-6- A volume of 0.1 ml of silver nitride ($AgNO_3$) 0.005N is added from a microburette.

-7- Steps 5 and 6 are repeated until a total of 1.5 mls of silver nitride has been added.

-8- The electrodes are removed and thoroughly rinsed.

-9- Steps 1 to 8 are repeated with20 mls of deionised water to serve as a reference.

IV.d.3. Calculation of salt concentration

For both solutions, the voltage recorded (y axis) is plotted versus the volume of silver nitride added (x axis) on volume-corrected plot paper, thus producing two straight lines. The titre of the salt solution is defined as the difference between the intercepts on the x axis for the solution analysed and for deionised water (the intercept for deionised water should be zero). The following calculations give the concentration of the salt coating on the specimen:

Mass of Cl- deposited:

$$m_{Cl^-} = \frac{Titre \times M_{Cl^-} \times M(AgNO_3)}{1000} \quad \text{in grammes} \qquad \text{(IV.1)}$$

where M_{Cl^-} is the molar weight of chlorine ions in grammes
$M(AgNO_3)$ is the molarity of the silver nitride solution.

Mass of salt deposited:

Using the composition of the spraying salt solution which is indicated in table IV.b., the ratio of chlorine to salt weights can be calculated:

$$\frac{m_{Cl^-}}{m_{salt}} = \frac{\left(\frac{m_{NaCl}}{M_{NaCl}} + 2\frac{m_{MgCl_2}}{M_{MgCl_2}} + \frac{m_{KCl}}{M_{KCl}} + \frac{m_{CaCl_2}}{M_{CaCl_2}}\right) \times M_{Cl^-}}{m_{NaCl} + m_{MgCl_2} + m_{MgSO_4} + m_{KCl} + m_{NaHCO_3} + m_{NaBr} + m_{CaCl_2}} \qquad \text{(IV.2)}$$

where m_i is the weight of species i per litre of solution in grammes
M_i is the molar weight of species i in g/mol.

For the salt composition used in this study, this calculation gives a result of $\frac{m_{Cl^-}}{m_{salt}} = 0.55$. Therefore, the mass of salt deposited on the material is:

$$m_{salt} = \frac{Titre \times M_{Cl^-} \times M(AgNO_3)}{550} \quad \text{in grammes} \qquad \text{(IV.3)}$$

Salt coating concentration:

The salt coating concentration on the specimen is given by:

$$[Salt] = \frac{m_{salt}}{A} \quad \text{in grammes/cm}^2 \qquad \textbf{(IV.4)}$$

where A is the specimen's surface area in cm^2.

For the fatigue test pieces used in the high pressure studies, the surface area was calculated according to the technical drawing's specifications (Figure IV.a.). A value of A=6.08 cm^2 was thus obtained. The exact dimensions of each salt-corrosion coupon were measured before cleaning, and the surface area was then calculated.

IV.d.4. Reliability of the salting procedure

Many different designs and procedures have been used by past workers in order to deposit salt coatings on test pieces in a sufficiently uniform manner. They vary from simply dipping the specimens in a salt solution of known concentration, to complex hot-air stream apparatus (Turley 1966, Donachie 1966, Gray 1970).

The ability of depositing relatively uniform salt coatings is a major concern. In this work, it was found that it could be best achieved when only three specimens were sprayed at the same time, and photographs IV.b. and IV.c. show typical salt coatings obtained for fatigue test pieces and thermogravimetric coupons with this method.

However, as only one of the three test pieces is subjected to the salt content analysis, one has to ensure that all three specimens have similar levels of salt deposited on their surface. Three batches of fatigue test pieces and three batches of salt-corrosion coupons were therefore salted. All three specimens per batch were analysed, and the results which are shown in table IV.c. show that the error induced by the salting procedure is relatively low.

The reproducibility of salt coatings from one batch to another was found to be average, and several specimens had to be entirely recleaned and recoated. However

this salting procedure has the double advantage of being reliable in terms of salt coating quality and uniformity, and relatively simple to use. Furthermore, it is representative of the conditions in which salt may be deposited in service (i.e. projection of salt droplets on components followed by the evaporation of water). Therefore, it was considered to be entirely satisfactory for the purpose of this study.

Test and Specimens numbers	Nature of specimens	Salt level mg/cm^2	Mean value mg/cm^2	Standard deviation mg/cm^2	Batch salt level mg/cm^2
Test 1 084A/49 084A/50 084A/54	Fatigue test pieces	0.0306 0.0364 0.0317	0.0329	0.0031	0.0329 ±0.64%
Test 2 084A/65 084A/78 084A/108	Fatigue test pieces	0.0295 0.0306 0.0317	0.0308	0.0014	0.0308 ±4.54%
Test 3 084A/109 084A/122 084A/129	Fatigue test pieces	0.0356 0.0264 0.0306	0.0309	0.0046	0.0309 ±15.21%
Test 4 084A/40/1 084A/40/2 084A/40/3	Coupons	0.0630 0.0596 0.0609	0.0612	0.0017	0.0612 ±2.94%
Test 5 084A/40/4 084A/40/5 084A/40/6	Coupons	0.0230 0.0279 0.0295	0.0268	0.0034	0.0268 ±14.18%
Test 6 084A/40/7 084A/40/8 084A/40/9	Coupons	0.0302 0.0302 0.0303	0.0302	0.00006	0.0302 ±0.33%

Table IV.c. Reliability of the salting procedure.

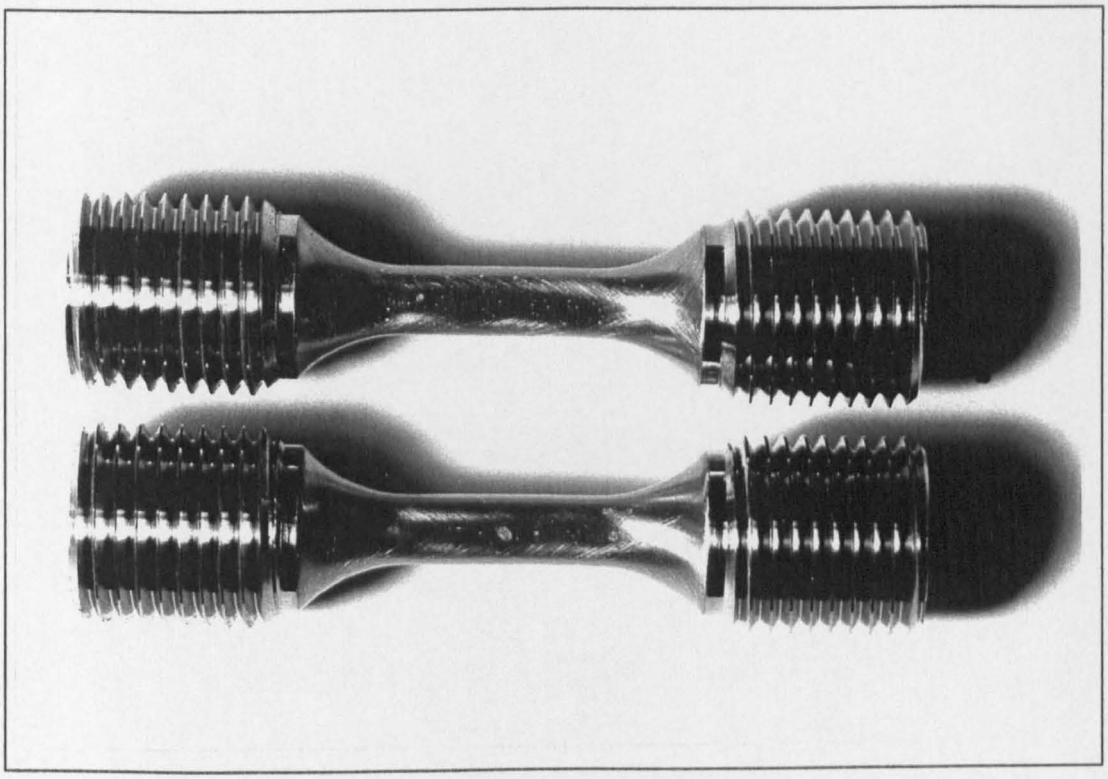

Photograph IV.b. Salt coated fatigue test pieces.

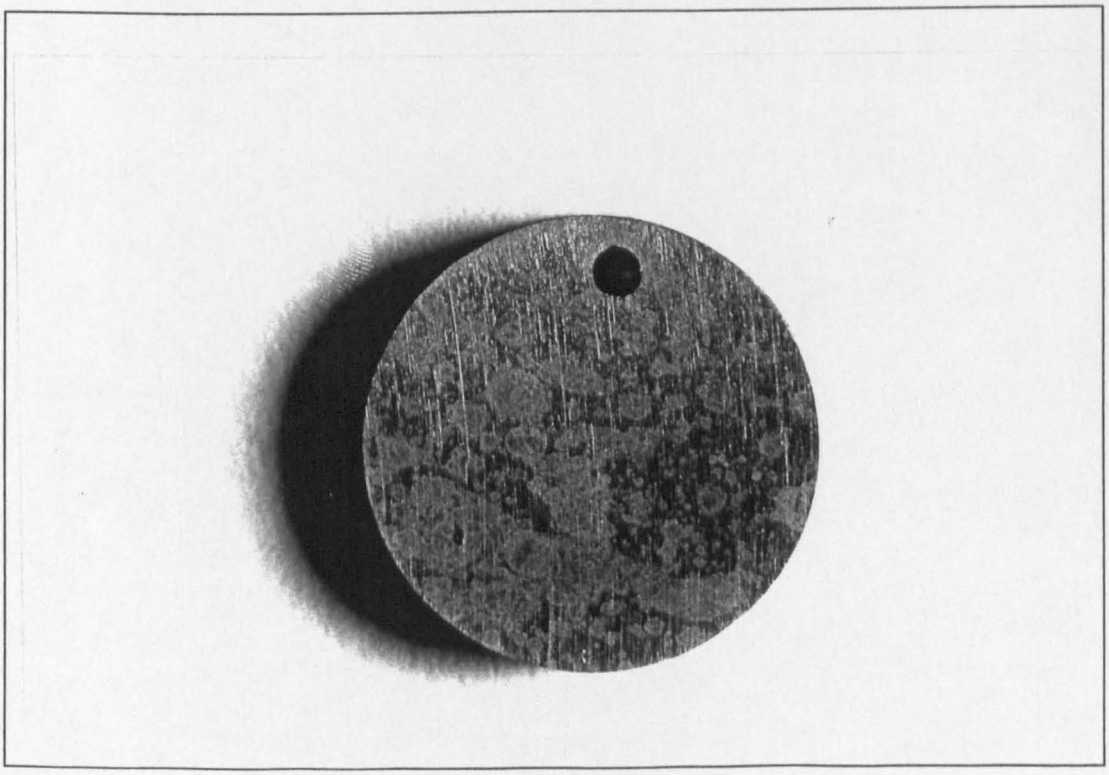

Photograph IV.c. Salt coated corrosion coupons

IV.e. High pressure studies

The main goal of this work was to develop a new mechanical test in order to carry out hot-salt stress-corrosion testing in high pressure, high temperature environments. This in itself is of significant interest as the only similar study encountered in the literature used tubular test pieces whose bore was pressurised (Gray 1969b). This means that the outside of the test piece is subjected to atmospheric pressure, and that parameters such as the presence of a fatigue notch could not be investigated. Secondly, Gray's apparatus allowed testing at pressures up to 3.6 bars which is significantly below the operating pressures encountered by titanium parts in service (up to 16 bars).

IV.e.1. Experimental apparatus

This study was carried out after upgrading a unique high pressure, high temperature, servo-hydraulic vessel built in the late seventies which is shown in photograph IV.d. and represented in figure IV.c.. This testing facility consists of four main parts:

The testing chamber: The chamber has been designed according to British Standard Code of Practice BS 5500 and can operate at maximum conditions of 33 bars and 600 °C. It is in fact comprising two chambers, allowing one to impose a differential pressure of about three bars in order to contain corrosive gases at the center and to avoid corrosion of the external walls. A three zone resistance heating furnace is wired on the outside wall of the inner chamber. Thermal insulation is provided by material packed between the resistors and the outside wall which is also water cooled. The loading train consists of two rods, the higher rod being attached to the top of the vessel, and the mobile lower rod being hydraulically controlled. The test piece is contained between two cans which retain any salt spalling from its surface or debris dropping during fracture. The testing gas is injected in the rig through two gas inlets situated at the top of the vessel and is withdrawn at its base. The testing chamber is closed with sixteen bolts.

Pressure control apparatus: All the testing gases were of pure dry quality. They were premixed and stored in bottles which were subsequently connected to the gas inlets. The gas inlets and outlets are controlled through a series of pressure gauges, valves and flow meters, allowing one to work at any pressure between 1 and 33 bars.

However, due to the mechanical nature of the pressure control loop, the working pressure can only be maintained under dynamic gas flow conditions.

Load control apparatus: A servo-hydraulic facility allows one to load the test piece outside the vessel through the lower pulling rod. This implies that a sufficient pressure seal must be achieved on the bottom part of the testing chamber where the rod is fed through the outer pressure vessel wall. Furthermore, the pressure difference between the inside and the outside of the vessel means that a pressure load is exerted on the loading rod. Hence, calibration of the load apparatus has to be achieved prior to testing, and an accurate control of the environmental pressure is required in order to ensure load stability.

Temperature control apparatus: Each of the furnace's three zones is connected to a temperature control unit. The median zone controller which is programmable acts as a master controller, while the top and bottom zones control units act as slaves. This allows one to compensate for temperature differences on the vertical axis of the furnace which are due to the cold gas inlets located at the top of the chamber. This implies that temperature control also had to be calibrated for each test pressure, in order to avoid temperature differences due to the variable gas thermomass in each high pressure environment.

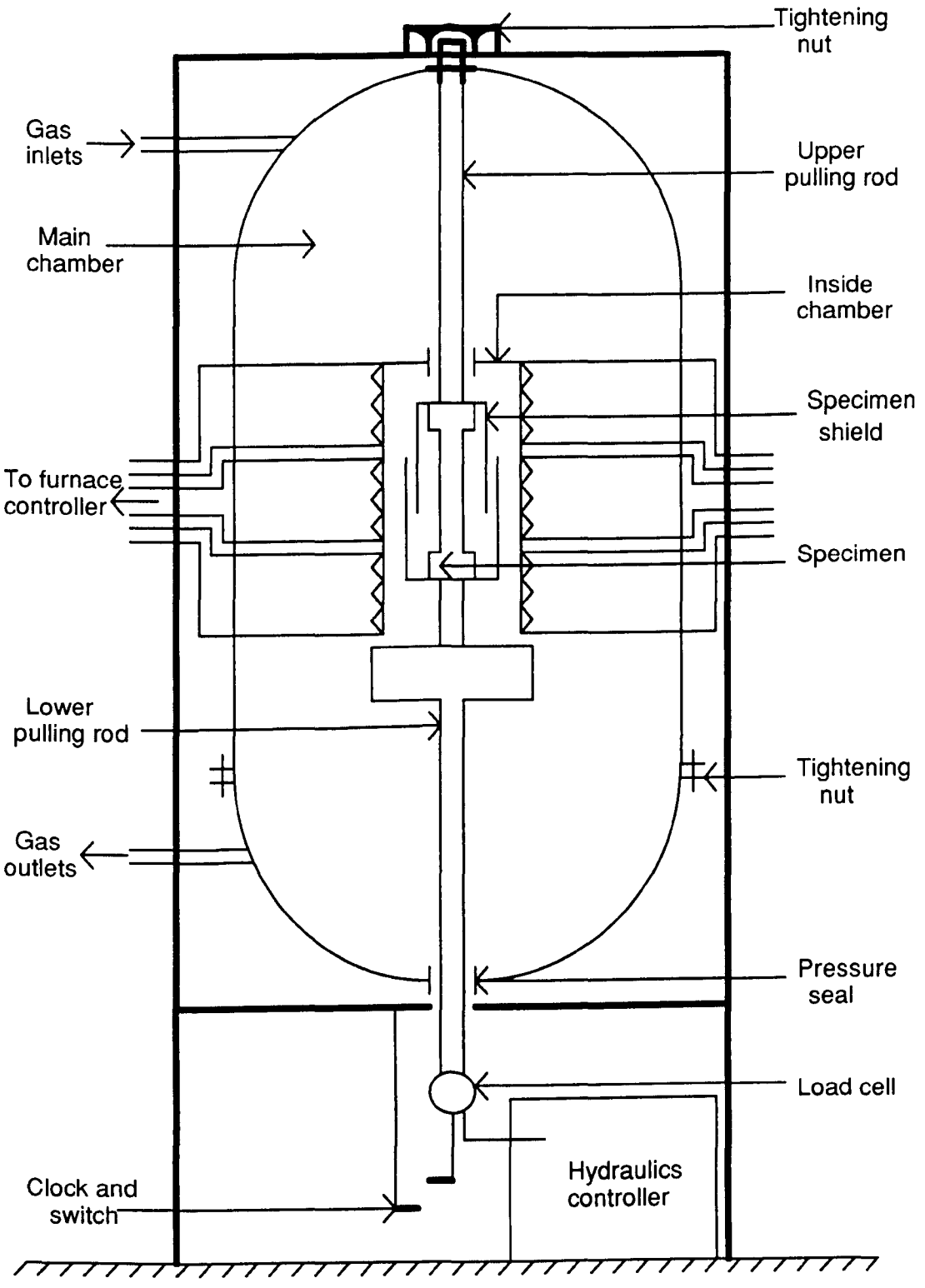

Figure IV.c. Sketch of high pressure vessel.

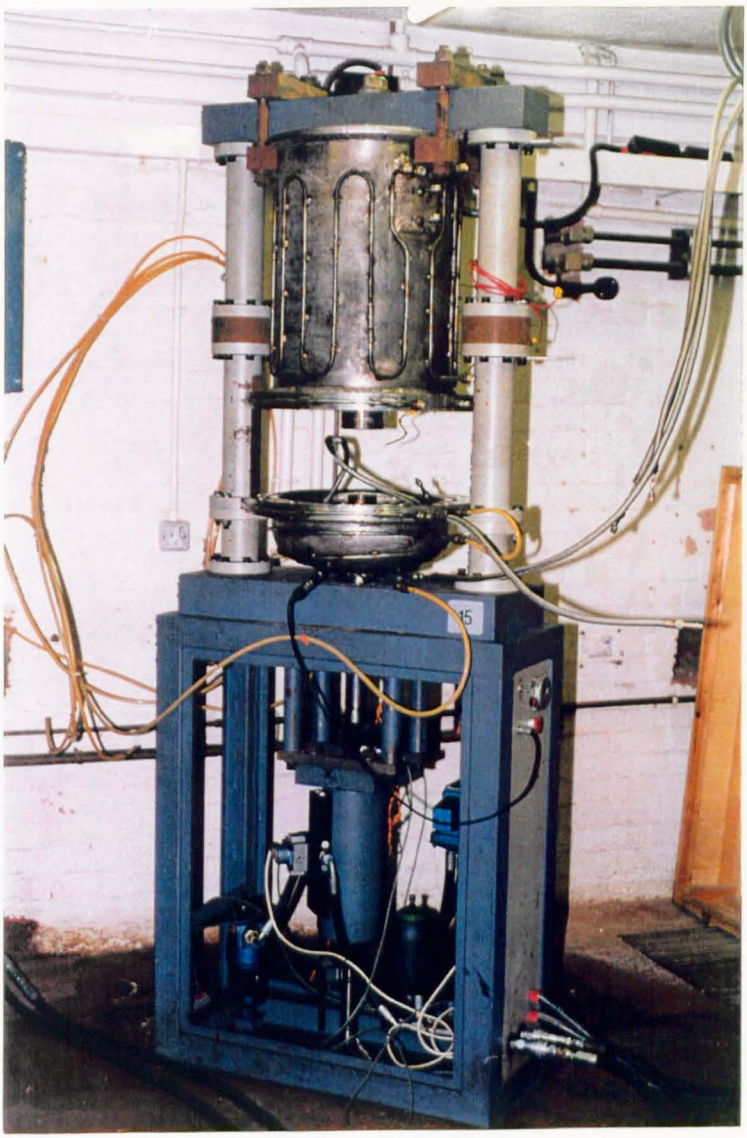

Photograph IV.d. High pressure, high temperature, servo-hydraulic facility used in this study.

IV.e.2. Pressure load calibration

As mentioned previously, it is necessary to know exactly how the pressure present inside the vessel is going to influence the load seen by the specimen. This pressure load can be calculated theoretically or measured experimentally.

Theoretical calibration: To calculate the pressure load theoretically, it is necessary to measure the area A on which the pressure is going to act (i.e. the section of the lower pulling rod). Thus if P is the vessel's gauge pressure, the pressure load is given by:

$$L(P) = P \times A \qquad \textbf{(IV.5)}$$

Measurements gave a total surface area A=2030 mm^2. Using equation (IV.5), a theoretical calibration curve was calculated. The results are given in table IV.d. where they are compared with the experimental measurements.

Experimental calibration: The experimental calibration was achieved with the lower pulling rod moving freely (i.e. without a test piece in the vessel). For each working pressure considered, the force necessary to counteract the pressure load is determined by bringing the lower pull rod to a standstill and measuring the load thus applied by the hydraulics. All measurements up to a pressure of 16 bars are given in table IV.d.

Both theoretical and experimental calibration curves are represented in figure IV.d.. It can be noticed that these two curves are slightly different due to an effect of friction in the hydraulics and gas seals. Therefore it is important to measure the pressure load experimentally, as considering the theoretical calibration alone would result in significant errors on the imposed load, especially during low pressure tests.

The true area on which the pressure load is applied can also be deduced from the slope of the experimental calibration curve as being 1992 mm^2, which is 38 mm^2 lower than the measured lower pulling rod. This decrease in effective area is due to the action of the pressure seals on the lower pulling rod.

Vessel gauge pressure (bars)	Absolute pressure (bars)	Theoretical pressure load (kN)	Experimental calibration (kN)
1	2	0.203	-
2	3	0.406	0.482
3	4	0.609	0.680
4	5	0.812	0.863
5	6	1.015	1.096
6	7	1.218	1.281
7	8	1.421	1.459
8	9	1.624	1.618
9	10	1.827	1.861
10	11	2.030	2.062
11	12	2.233	2.268
12	13	2.436	2.468
13	14	2.639	2.686
14	15	2.842	2.862
15	16	3.045	3.068
16	17	3.248	3.267

Table IV.d. Pressure load calibration measurements.

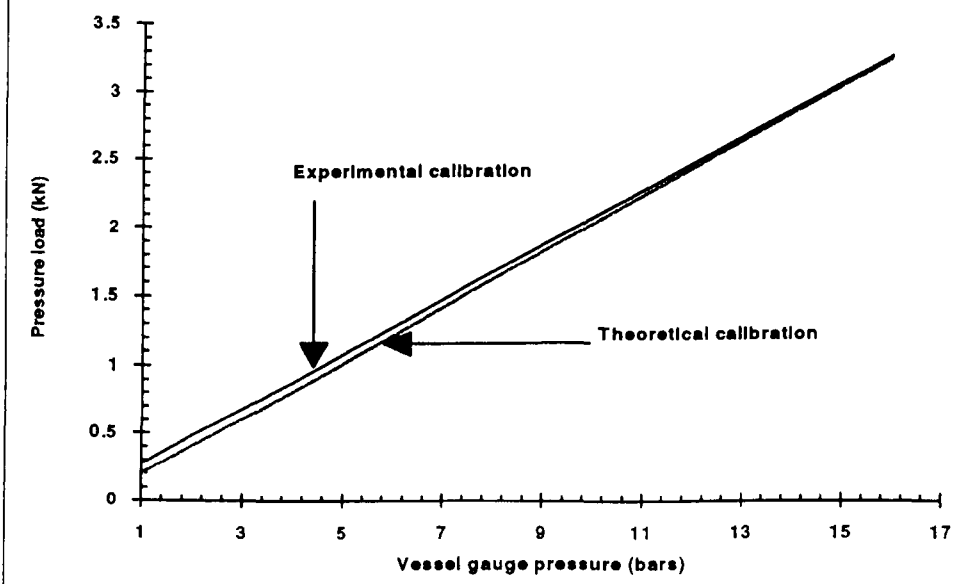

Figure IV.d. Pressure load calibration curves.

IV.e.3. High pressure testing procedure

After calibration, the high pressure vessel is actually ready for testing. A thermocouple is welded on the flat surface between the thread and the shoulder of the specimen (see Figure IV.a.). The test piece is then loaded inside the pressure chamber, and the vessel is closed. Starting a test takes between four and six hours and it is important to ensure that hot-salt stress-corrosion conditions are not met during this period. The main delay regarding the start of a test consists in the time necessary to reach the desired temperature under dynamic gas flow conditions. Thus the load is applied on the specimen only when all of the other experimental conditions have been reached. However it is equally impoortant to counteract the effects of the pressure load during the early stages by applying a calculated compressive load which corresponds to the values measured during calibration. In regard to these considerations, the following test procedure was developed:

-1- The vessel gas pressure is set to 4 bars and the chamber is purged. This ensures that any gas contained in the rig is of pure dry quality.

-2- The water cooling is switched on and the furnace is started.

-3- The vessel is pressurised to a pressure slightly below the operating conditions in order to allow gas expansion during heating.

-4- A calculated compressive load is applied in order to counteract the effects of the pressure load.

-5- When the test temperature is reached, the pressure is adjusted and the dynamic gas flow is set.

-6- Once the temperature, pressure, and gas flow conditions have stabilised, the clock is switched on and the load is applied to the test piece. The test has now started and the clock will switch off automatically when failure occurs.

IV.f. Thermogravimetric studies

Thermogravimetric studies have been designed in order to gather information on the mechanisms of hot-salt attack of titanium alloys. The aim of this work was to achieve continuous weight gain measurements to study the kinetics of the phenomenon, using an apparatus similar to this mentioned by Birks and Meier (Birks 1983). However before any salt-corrosion data can be exploited, it is necessary to know the oxidation behaviour of the material which will serve as a baseline. Since oxidation of titanium at HSSCC temperatures is relatively low, the use of an accurate experimental procedure is essential, and the following section will deal with this matter.

IV.f.1. Experimental apparatus

This work was carried out using a C.I. electronic microbalance comprising an MKII vacuum head and a C.I. Robal Control Unit, and a small cylinder-shaped resistance furnace which can be raised or lowered by mean of a hydraulic actuator. Data acquisition was computerised using a 286 IBM-compatible microcomputer and a Blue Chip ADC-16 data acquisition card. This necessitated the building of a buffer amplifier in order to resolve impedance problems between the control unit and the computer, and the elaboration of a Turbo Pascal data acquisition programme (see Appendix I). The overall experimental design is shown in figure IV.e..

A special reaction tube showed in figure IV.f. was designed for this study. The head of the balance is protected by a continuous flow of argon in order to avoid corrosion of the beam. Furthermore corrosive gases escaping from the reaction tube will also tend to condense when they reach the water jacket. A small pump was also connected in order to draw both the argon and the reaction gases out of the reaction tube. This ensures in particular that argon is not going to "fall" around the specimen. Finally, the reaction gas is introduced at a constant flow reasonably close to the specimen, at the bottom of the rection tube. The testing material is hooked on a long platinum wire (which will not oxidise) which is attached to the beam.

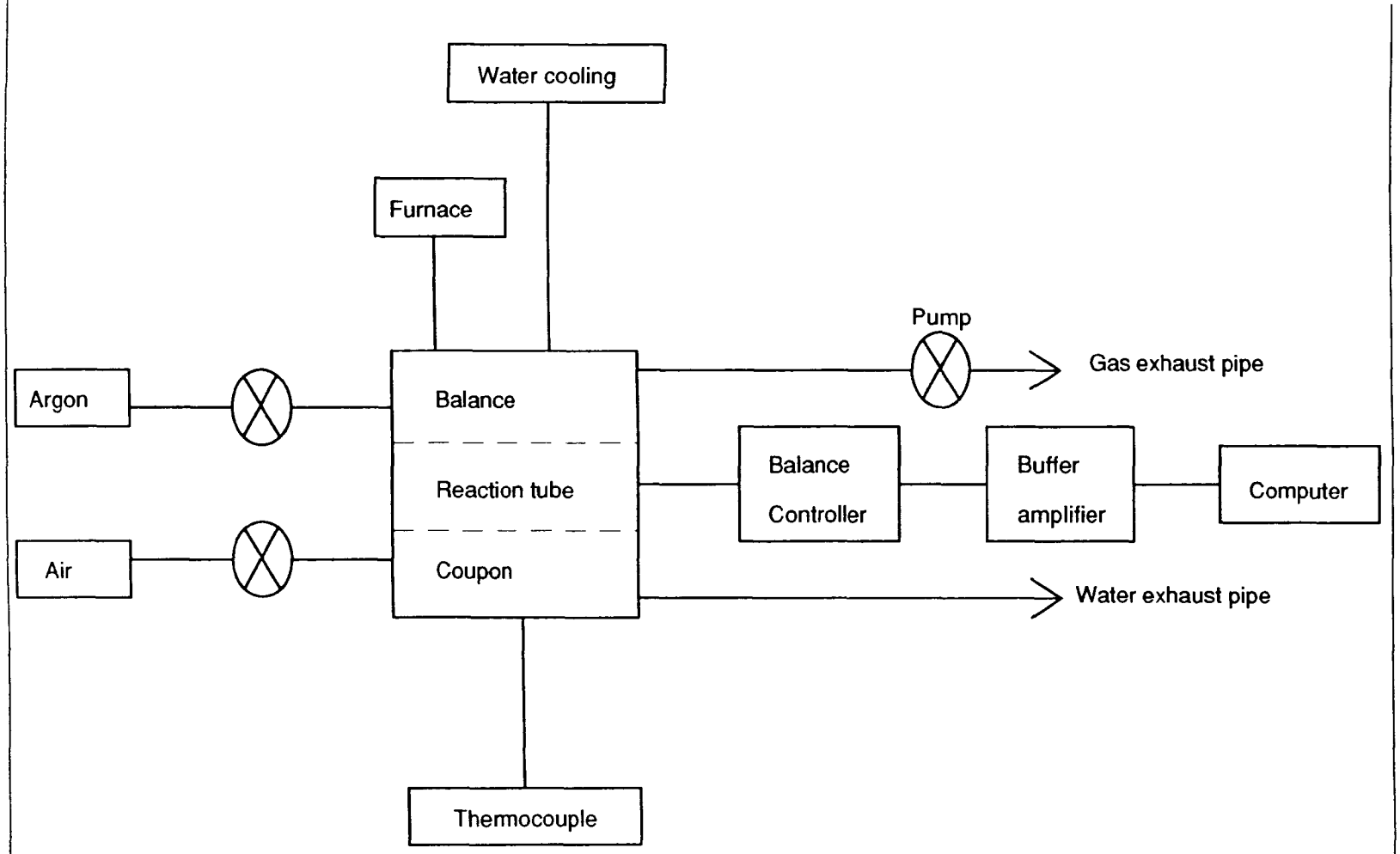

Figure IV.e. Overall apparatus used for thermogravimetric studies

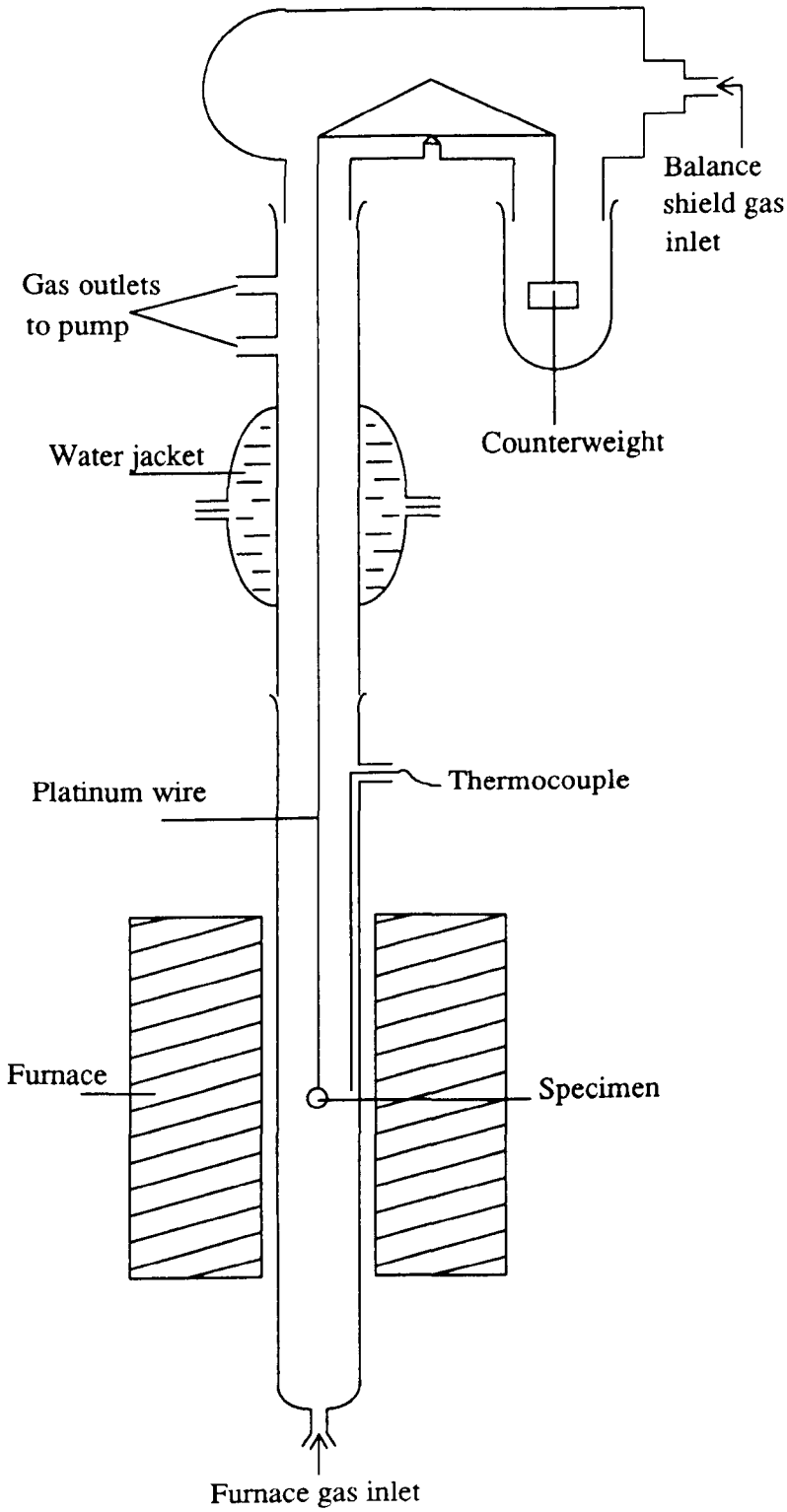

Figure IV.f. Reaction tube designed for this study

IV.f.2 Buoyancy effects and resolution

Because of the existence of two gas flows inside the reaction tube, transient buoyancy effects are induced during the first few hours of the test. In order to ensure that the weight gains recorded were due to the oxidation of the material alone, these effects were measured using a volume of alumina platelets similar to the average volume of the oxidation and salt-corrosion coupons. Three repeat measurements were carried out at each temperature of 500°C, 550 °C, and 600 °C. Table IV.e. indicates the average result obtained for each temperature. Figure IV.g. shows that the buoyancy effects can be considered as constant in the useful temperature range as the error induced by taking an overall average value is less than 20 µg, which is within the apparatus' resolution capability. Figure IV.g. also shows that these effects are stabilised after about three hours to a value of 60 µg.

Therefore the buoyancy effects measured through this method can not be neglected during the analysis of the results. Indeed they were systematically deduced from the weight gains measured before any further work was carried out on the data.

The manufacturer of the microbalance head certifies an accuracy of the weight measurements equal to ±1 µg at room temperature. However considering the two gas flows injected into the reaction tube, as well as the elevated temperatures used in this study, the overall resolution has been estimated to about ±20 µg which is entirely satisfactory for this work.

IV.f.3. Experimental procedure

The procedure used throughout this work is as follows:

-1- Rigorous calibration of the microbalance is necessary before each test in order to ensure the required precision of the results.

-2- To obtain a uniform surface finish , each sample is polished to 1200 grit. This ensures that oxidation at preferential sites constituted by surface defects is avoided.

500 °C		550 °C		600 °C		Average	
Time (hrs)	Buoyancy (µg)	Time (hrs)	Buoyancy (µg)	Time (hrs)	Buoyancy (µg)	Buoyancy (µg)	Max. error (µg)
0.00	0.00	0.00	0.00	0.00	0.00	0.00	0.00
0.17	80.95	0.17	78.53	0.17	50.23	69.90	19.67
0.33	102.94	0.33	87.13	0.33	72.50	87.52	15.42
0.50	97.81	0.50	91.31	0.50	68.54	85.89	17.35
0.67	91.73	0.67	91.26	0.67	67.98	83.66	15.68
0.83	89.50	0.83	85.33	0.83	71.70	82.18	10.48
1.00	78.83	1.00	77.13	1.00	65.66	73.87	8.21
1.17	75.21	1.17	76.82	1.17	61.33	71.12	9.79
1.33	83.56	1.33	67.84	1.33	55.60	69.00	14.56
1.50	76.71	1.50	69.62	1.50	53.62	66.65	13.03
1.67	71.61	1.67	63.20	1.67	48.64	61.15	12.51
1.83	73.08	1.83	66.78	1.83	47.31	62.39	15.08
2.00	70.38	2.00	62.10	2.00	48.85	60.44	11.59
2.17	66.10	2.17	60.54	2.17	46.65	57.76	11.11
2.33	61.11	2.33	51.37	2.33	51.54	54.67	6.44
2.50	65.73	2.50	58.52	2.50	61.06	61.77	3.96
2.67	57.59	2.67	61.62	2.67	55.91	58.27	2.36
2.83	60.87	2.83	61.39	2.83	58.10	60.12	2.02
3.00	63.99	3.00	53.79	3.00	63.51	60.43	6.64

Table IV.e. Buoyancy effect measurements

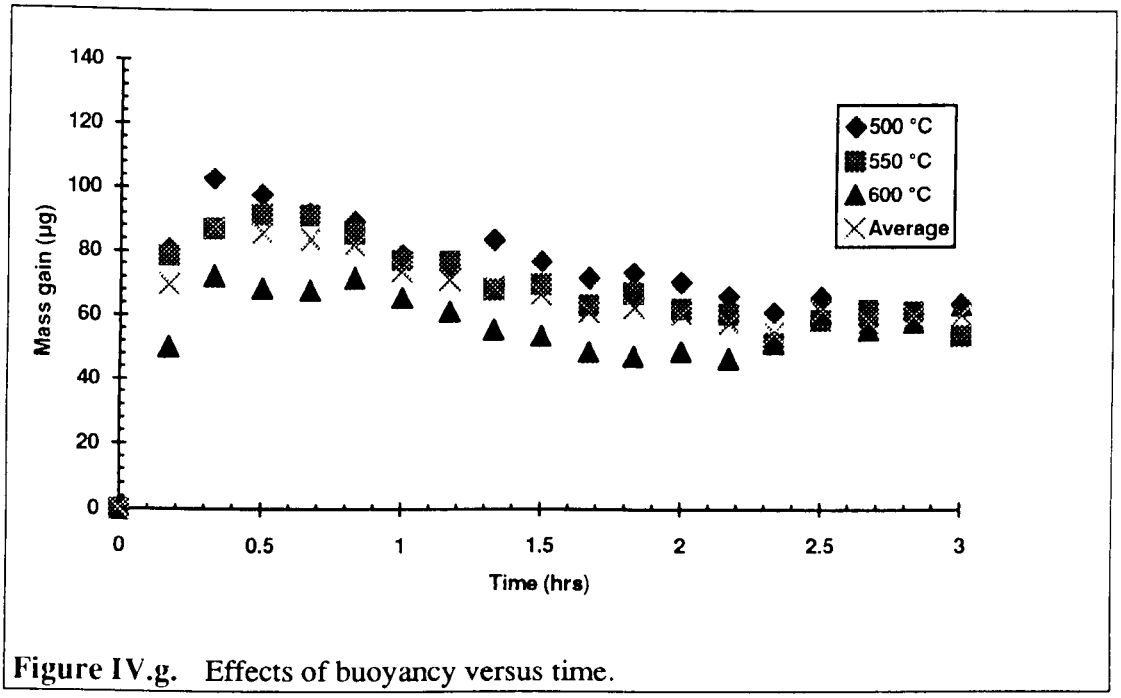

Figure IV.g. Effects of buoyancy versus time.

-3- The coupon is cleaned prior to the measurement of its dimensions (weight, diameter, thickness).

-4- The sample is cleaned again, in order to avoid chemical contamination which would considerably affect the oxidation data. From this moment onwards, the coupon has to be handled with surgical gloves or tweezers.

-5- The coupon is salted if required.

-6- The specimen is loaded into the reaction tube and its weight is tared to zero.

-7- The furnace is raised, the gas flows are opened, and the computer's programme is reset.

-8- The test is started from room temperature, and the test temperature is attained within ten minutes. The overshoot of the furnace is kept within ±3 °C and the temperature finally stabilises after about one hour.

IV.g. Analytical studies

Both optical microscope studies and Scanning Electron Microscope studies (SEM) were undertaken in order to support the model for the hot-salt stress-corrosion of titanium alloys which was developed in the course of this work. The tasks which were carried out can be summarised as follows:

1. Observation of oxidation scales, corrosion scales, and stress-corrosion cracks using the optical microscope.

2. Measurements of the depth of oxygen solution (α case) on thermogravimetric coupons.

3. Observation of oxidation scales, corrosion scales, and stress-corrosion cracks using the SEM.

4. Observation of HSSCC fracture surfaces on the SEM.

5. ZAF analyses along features observed on thermogravimetric coupons. ZAF analyses are a measurement of the X rays emissions of the material which are corrected according to the atomic number Z of the various elements of the alloy, as well as their adsorption and fluorescence characteristics.

IV.g.1. Metallographic preparation

Thermogravimetric coupons: Both oxidation and hot-salt corrosion coupons were sectioned and mounted in conductive bakelite in order to examine their oxidation or corrosion scales. After polishing, the samples were etched using two chemical solutions. The first solution which consisted of 2% hydrofluoric acid (HF), 8% nitric acid (HNO_3), and 90% distilled water was used to reveal the microstructure. The second solution was a colouring etchant made of lactic acid (3 ml), hydrofluoric acid (3 ml), and distilled water (400 ml) which was used to carry out α case depth measurements (the base material is darkened while the alpha case remains white).

Hot-salt stress-corrosion test pieces: The fracture surface of HSSCC tensile specimens was carbon coated and mounted on a stud. The gauge length close to the fracture surface was mounted in conductive bakelite. The mounted gauge length was then ground in order to produce a flat surface where cracks could be detected. After polishing, the material was etched.

IV.g.2. Alpha case depth measurements

Alpha case depth measurements were carried out using an optical microscope. Twenty measurements were made for each sample and the average was calculated and taken as the depth of oxygen solution for the sample. Attempts were made in order to complement these visual measurements using micro hardness profiles. However this method proved to be unsatisfactory, due to the low thickness of the alpha case layers produced on the samples during the short exposure times and for the low temperatures used in this study. In any case, chapter V will show that the resolution of the visual measurements was entirely satisfactory.

IV.g.3. Scanning Electron Microscope studies

The fracture surfaces of hot-salt stress-corroded test pieces were examined qualitatively using the SEM in order to observe the typical features mentioned by other workers (stress-corroded brittle zone, ductile zone, crack branching).

Both oxidation scales and hot-salt corroded scales were also examined on the SEM in order to observe the differences between the two processes. Some oxide thickness measurements were carried out on oxidation coupons, and ZAF analyses were made in particular places of hot-salt corroded specimens.

CHAPTER V

RESULTS

"Fifteen years ago the possibility of stress-corrosion cracking of titanium on exposure to ordinary salt seemed as likely as corrosion of gold in ice.

J.A.King (King 1966)

V.a. Introduction

Chapter II showed that the dramatic failures exhibited by titanium alloys subjected to hot-salt stress-corrosion cracking conditions during laboratory testing have been extensively studied for the past forty years. However HSSCC of titanium alloys has not yet been established as a cause of any in-service failure, which implies that one (or several) environmental parameter which is not encountered during laboratory testing must have a beneficial effect on the life of the material. Hence numerous environmental factors were investigated by previous workers and considerable data was gathered. However none of the candidates for such an improvement have been successfully identified to date. After an examination of the service conditions within a typical gas turbine engine, one can speculate that the high pressures encountered in the compressor environment where titanium parts are used may actually improve the life of this class of materials when they are subjected to HSSCC conditions.

The purpose of this work was to develop a new mechanical test using the unique high temperature, high pressure, servo-hydraulic facility described in chapter IV. Hence this experimental apparatus was used to study the combine effects of three parameters on the behaviour of titanium alloy IMI 834 undergoing hot-salt stress-corrosion: Load, environmental pressure, and atmosphere composition.

Along with these high pressure mechanical tests, continuous thermogravimetric studies were carried out with a view to compare the kinetics of the oxidation and hot-salt corrosion of the material. This chapter will present the results obtained for each of the tests achieved.

V.b. High pressure studies

V.b.1. Testing conditions

Hot-salt stress-corrosion testing relies on the ability to control a wide range of parameters such as mechanical load, salt coating concentration, temperature, surface finish, etc. Hence it is desirable to use relatively severe tests conditions in order to

reduce scatter in the data. The following general conditions were therefore used throughout this study:

Temperature: The temperature used during these tests was aimed to be 500 °C which is in the upper temperature range where HSSCC of titanium alloys occurs. However due to the varying gas thermo-mass encountered at different working pressures, differences in temperature were detectable from one test to another. Hence the fracture temperatures which will be quoted for each test vary from 464 °C to 513 °C. These variations were later found to be irrelevant due to the severity of the test which renders them neglectable.

Dynamic gas flow: Due to the mechanical nature of the gas control system, a dynamic gas flow of 250 l/h had to be used in order to maintain the operating pressure inside the vessel. However this flow, which is extremely low compared with those used by Gray (Gray 1969b), is not seen by the test piece which is shielded by two cans (see chapter IV).

Salt level: The test pieces used for this study were salted to a nominal level of 0.03 mg/cm^2 which is considered as a low salt level (Wing 1990). The actual salt concentrations deposited varied from 0.018 to 0.04 mg/cm^2 and are indicated for each test. These differences in the salt coating concentrations were found to be entirely satisfactory for the purpose of this work.

Pressure: The pressure could be monitored over the length of a test to a precision of ±1 bar. However, as it was readjusted every ten to twelve hours, the same variations in pressure were seen by each test. These variations can in fact be observed in the scatter of the results obtained at lower gas pressures and lower loads. This scatter being within reasonable limits, the variations in pressure were considered as being satisfactory.

Load: As variations in pressure occur inside the vessel, the load seen by the specimen is affected and this results in fluctuations of the imposed stress over the length of the test. These variations which were kept within ±5% were also similar for each test and did not affect the reliability of the results.

V.b.2. Influence of stress on the hot-salt stress-corrosion cracking of IMI 834 at atmospheric pressure

The stress level used for hot-salt stress-corrosion testing of titanium alloys is extremely important to ensure that the results are contained within a reasonable scatter, and that the test is going to meet practical requirements. HSSCC testing has always produced significant scatter in the past . Therefore it is desirable to avoid testing at very high stresses which will result in short test periods and will affect the reproducibility of the results. On the other hand, the low stresses that have been used in previous studies can produce considerably long material's lives up to several thousand hours (Martin 1966). As one specimen at a time can only be used with the experimental apparatus of this study, it is obvious that testing at low stresses would be very impractical.

Five different stress levels ranging from 540 MPa to 620 MPa were therefore initially investigated. The test conditions are described in Table V.a. while figure V.a. shows the influence of static load on the hot-salt stress-corrosion cracking of IMI 834.

Test piece number	Salt level (mg/cm^2)	Temperature (°C)	Stress (MPa)	Life (hrs)
084A/66	0.04	464	620	0.33
084A/123	0.0338	464	600	1.00
084A/121	0.0338	464	580	4.50
084A/54	0.031	507	560	12.12
084A/52	0.0285	464	540	45.80

Table V.a. Tests achieved at different static stresses at atmospheric pressure

V.b.3. Influence of environmental pressure

Five tests were carried out at high environmental pressures in a normal air composition atmosphere (i.e. 21% O_2 and 79% N_2). Test conditions which are indicated in Table V.b. all produced failures apart from the test at 540 MPa and 16 bars which was stopped after 200 hours and was considered as a "run out'. An immediate effect of the environmental pressure can be seen on figure V.b. where the tests carried out at stresses of 560 MPa and 580 MPa have been plotted together with

the points obtained at atmospheric pressure (see Table V.a.). By looking at Figure V.b. it becomes obvious that at one given stress , the relationship between total pressure and the life of the material is linear. This figure also explains why the test piece number 084A/107 did not produce any failure, as the life of the alloy is dramatically increased with a 20 MPa drop on the stress under high pressure testing conditions.

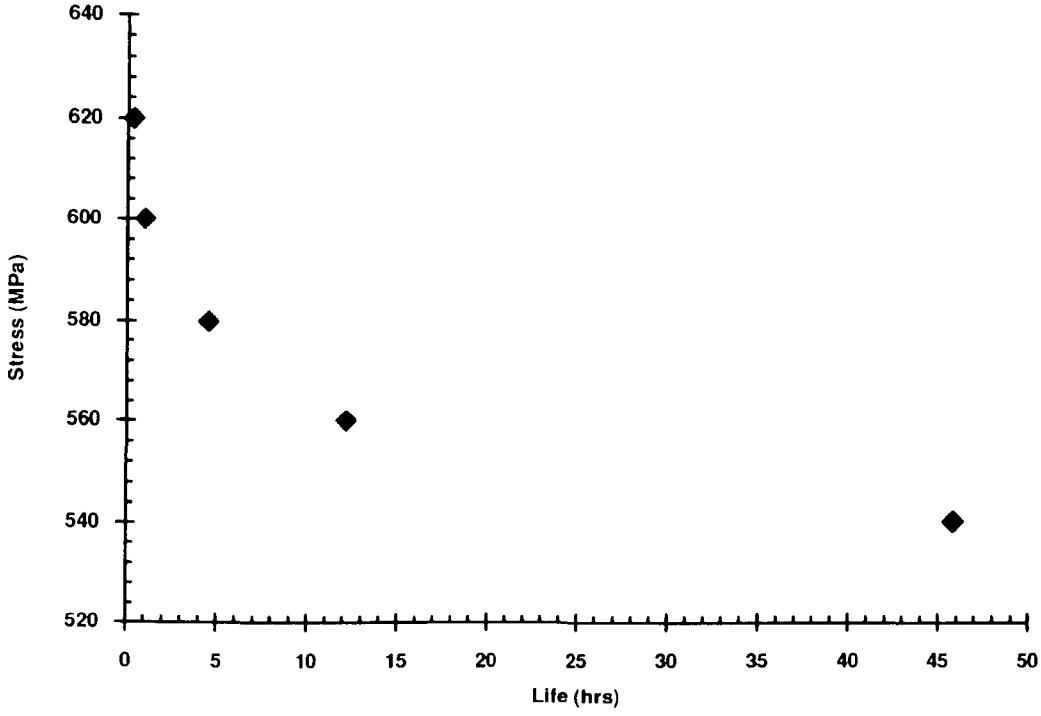

Figure V.a. Influence of static stress on the hot-salt stress-corrosion of IMI 834 at atmospheric pressure

Test piece number	Salt level (mg/cm^2)	Temperature (°C)	Stress (MPa)	Pressure (bars)	Life (h)
084A/107	0.0317	506	540	16	>200
084A/87	0.0232	492	580	16	66.40
084A/88	0.0232	501	580	4	16.90
084A/149	0.0310	500	560	4	62.08
084A/108	0.0180	500	560	2.5	46.9

Table V.b. Tests achieved at high pressures in normal air compositions

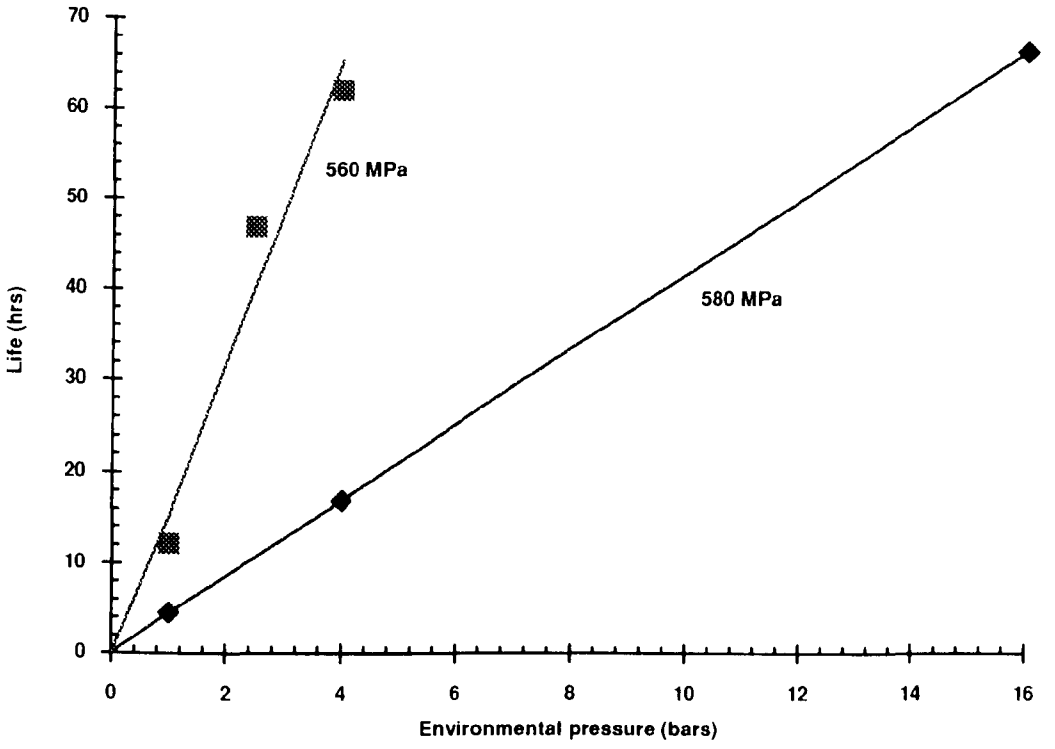

Figure V.b. Effect of environmental pressure on the hot-salt stress-corrosion of IMI 834 tested in normal air compositions

V.b.4. Influence of atmospheric composition

Five tests were also carried out in order to study the influence of atmospheric air compositions: It is worth mentioning at this point that this task is a lot easier to carry out with low oxygen contents that with high oxygen contents. Hence oxygen enriched gas mixtures can only be dealt with using grease free pipes, valves and regulators cleaned for oxygen use in order to avoid oxygen fires. The risk is limited for mixes containing up to 40% oxygen, but it becomes increasingly worrying above this level. This explains why only one test was achieved at the beginning of this study with a mixture containing more than 40% oxygen.

Table V.c. shows the tests which were carried out at atmospheric pressure using special air compositions. The results obtained for a stress of 560 MPa are plotted in Figure V.c., together with the point obtained using normal air (i.e. test piece number 084A/54 in table V.a.). It can be seen that both rare oxygen compositions and oxygen

enriched compositions seem to have a beneficial effect on the life of IMI 834 subjected to hot-salt stress-corrosion cracking conditions. Actually the life of the alloy was found to be minimum in the range 15% to 21% oxygen content. Furthermore the beneficial effect of gas composition on the HSSCC of IMI 834 was found to be more pronounced for rare oxygen mixtures than for oxygen enriched mixtures (see Figure V.c.). These results are consistent with these obtained by Heimerl et al. (see chapter II).

Test piece number	Salt level (mg/cm^2)	Temperature (°C)	Stress (MPa)	Pressure (bars)	Oxygen (%)	Life (hrs)
084A/130	0.0350	500	560	1	10.5	84.3
084A/75	0.0350	507	560	1	40	39.7
084A/86	0.0380	508	560	1	15	21.6
084A/64	0.0264	499	580	1	84	23.4

Table V.c. Tests carried out with special air compositions at atmospheric pressures

V.b.5. Combined influence of environmental pressure and atmosphere composition

Three more tests were carried out in order to study the simultaneous effects of environmental pressure and rare oxygen or oxygen enriched atmospheres at two different stress levels. One of the tests presented in table V.d. was considered as a 'run out' when no failure occurred after 120 hours. However the two other tests which were carried out at a stress of 560 MPa produced interesting results. Hence it seems that at low oxygen contents, no further improvement of the life of IMI 834 is obtained (i.e. test pieces 084A/86 in table V.c. and 084A/75 in table V.d. failed after similar exposure times). However, for oxygen enriched compositions, the tests carried out on specimens 084A/75 (Table V.c.) and 084A/78 (Table V.d.) demonstrate a further improvement of the life of the material when high environmental pressures are used with oxygen enriched air compositions. These observations will be studied in detail during the discussion.

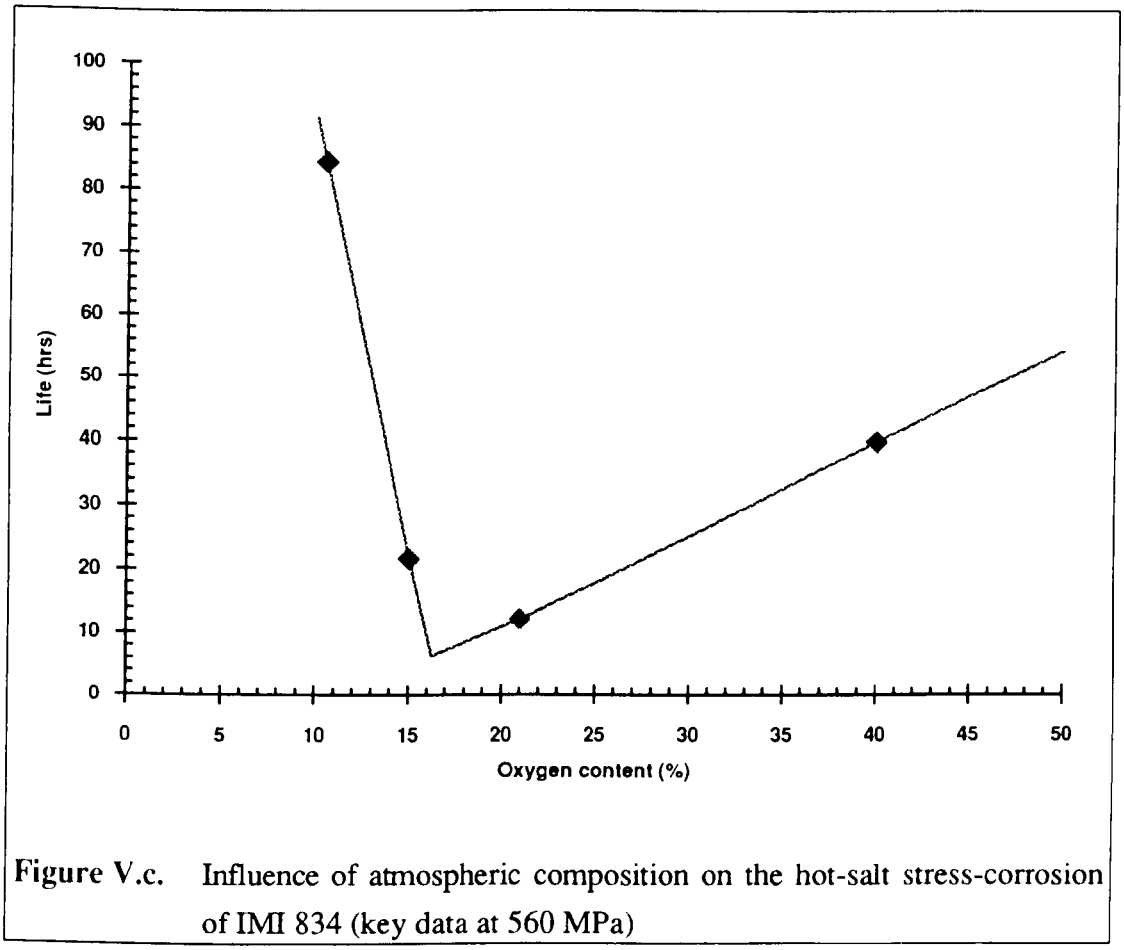

Figure V.c. Influence of atmospheric composition on the hot-salt stress-corrosion of IMI 834 (key data at 560 MPa)

Test piece number	Salt level (mg/cm^2)	Temperature (°C)	Stress (MPa)	Pressure (bars)	Oxygen (%)	Life (hrs)
084A/77	0.0264	513	580	16	5.25	>120
084A/122	0.0380	506	560	4	15	17.4
084A/78	0.035	504	560	4	40	63.7

Table V.d. Tests achieved showing the combine effects of high environmental pressures and atmosphere composition

V.c. Thermogravimetric studies

V.c.1. Introduction

Thermogravimetric studies were carried out in order to gather information on the mechanisms of hot-salt attack of titanium alloy IMI 834. The aim of this work was to produce continuous weight gain measurements for relatively short exposure times (100 hours) with a view to study the kinetic aspects of the phenomenon. Indeed, the extreme rapidity of hot-salt stress-corrosion failures occurring in the laboratory showed the extent of damage which can be produced sometimes after a few minutes only. The interest of continuous measurements is obvious: Firstly, the specimen does not have to be removed at regular intervals in order to be weighed, and thermal cycles are therefore avoided while only one test piece is used per test temperature. Secondly, because handling of the specimen is not required, spalling and damage of the oxidation or corrosion scales is avoided. In any case, if spalling occurs during the test, it would be detected through the continuous weight measurements.

Before any salt-corrosion data could be gathered, oxidation data had to be obtained in order to act as a reference. These oxidation studies were extremely difficult because of the low temperatures (525 °C to 675 °C) and the short exposure times (100 hours) which were employed. Hence the temperature at which thermogravimetric studies were carried out constitute the upper range where hot-salt stress-corrosion cracking of titanium alloys occurs (i.e. before the material becomes creep limited). However oxidation tests at lower temperatures for such short exposure times were not possible, as the weight gain detected would have come too close to the experimental apparatus' resolution.

V.c.2. Oxidation tests

Oxidation tests were performed every 25 °C increments from 525 °C to 675 °C generally for a test duration of 100 hours. Control of the test temperature was possible within ±2 °C. Table V.e. shows the conditions of each of these oxidation tests as well as the total weight gain obtained after exposure and the depth of oxygen solution (i.e. depth of alpha case) measured on a cross section of the sample after test.

The alpha case depth was estimated to be measured with a precision of ±0.75 µm (photographs V.a. to V.g.).

Figure V.d. shows a typical continuous thermogravimetric curve obtained after test for a temperature of 625 °C (the other curves obtained are presented in Appendix 2). Weight gains were measured and stored in the computer every ten minutes for the first four hours of the test. After this period, measurements were carried out every ten minutes but were recorded only every hour, unless a significantly higher weight gain than this expected was detected.

Test number	Temperature (°C)	Time of exposure (hrs)	Total mass gain ($\mu g/cm^2$)	Alpha case depth x (µm)	Log (Kp) ($mg^2.cm^{-4}.s^{-1}$)	Log (x^2/t) ($\mu m^2.hr^{-1}$)
ON252	525	99.48	65.56	5.2	-7.92	-0.57
ON355	550	89.00	94.75	9.2	-7.55	-0.02
ON257	575	100.00	168.64	13.3	-7.10	0.25
ON260	600	100.00	151.03	15.1	-7.20	0.36
ON162	625	100.00	365.21	22.9	-6.43	0.72
ON165	650	100.00	472.31	35.1	-6.21	1.09
ON167	675	99.00	614.51	43.6	-5.97	1.28

Table V.e. Results of thermogravimetric oxidation tests

Since the oxidation of titanium alloys is known to follow a parabolic law in this temperature range (see Chapter I), the weight gain data were entered in a spreadsheet package in order to carry out parabolic regression analyses leading to the calculation of the parabolic rate constant Kp for each test temperature. These calculations confirmed that the oxidation of IMI 834 in the temperature range 525 °C to 675 °C is indeed parabolic. The decimal logarithm of the parabolic rate constant which is given in table V.e. was then plotted on an Arrhenius plot (i.e. versus $\frac{10^4}{T}$ in K^{-1}) as shown in Figure V.e. which shows that Log (Kp) varies in a linear manner with $\frac{10^4}{T}$.

Similarly, the logarithm of the parabolic rate constant was also calculated from the depths of alpha case measured on the sample's cross section for each temperature and

was plotted on an Arrhenius plot. The straight line which can be seen on Figure V.f. shows that the scatter associated with this method is very satisfactory.

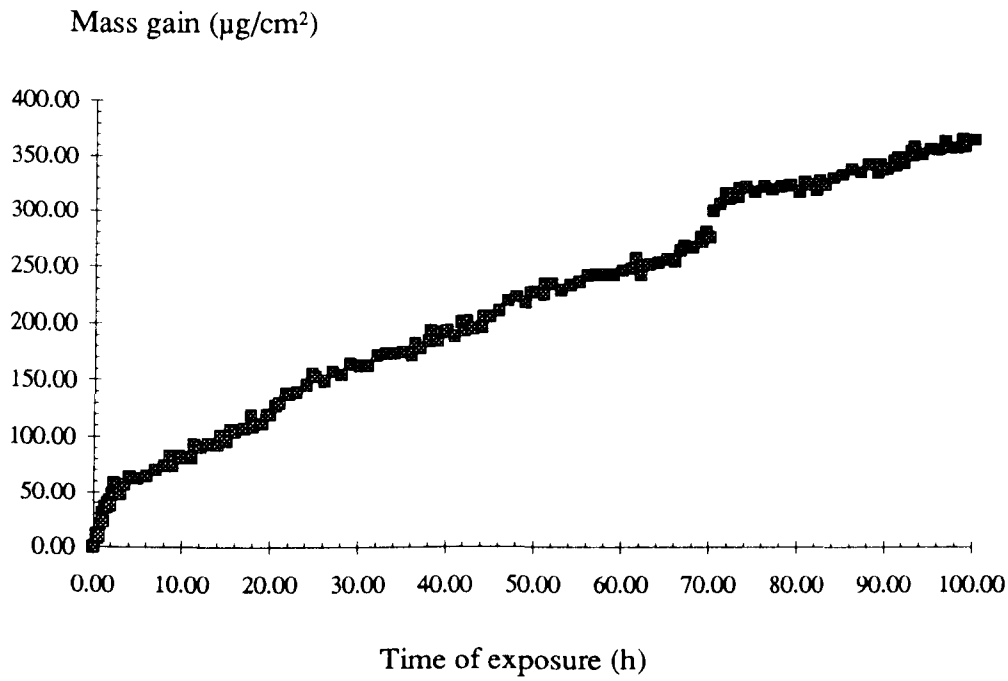

Figure V.d. Thermogravimetric curve for the oxidation of IMI 834 at 625 °C

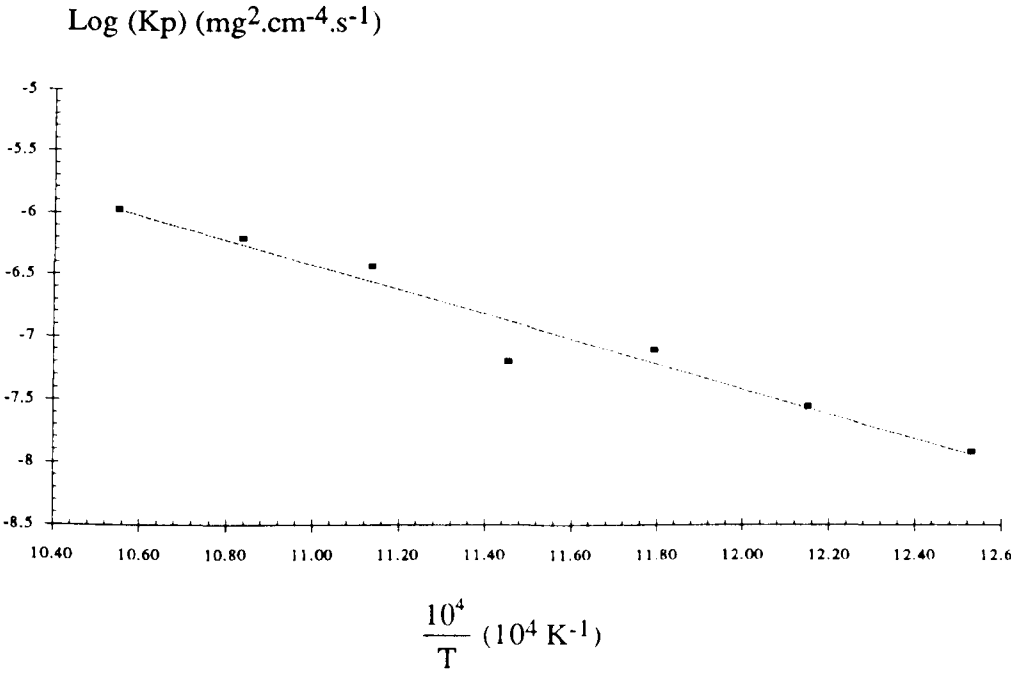

Figure V.e. Arrhenius plot based on total weight gains for the oxidation of IMI 834 between 525 °C and 675 °C

Photographs V.a. to V.g.
Evolution of the depth of oxygen solution with exposure conditions for the oxidation of IMI 834 between 525 °C and 675 °C
Magnification: × 400

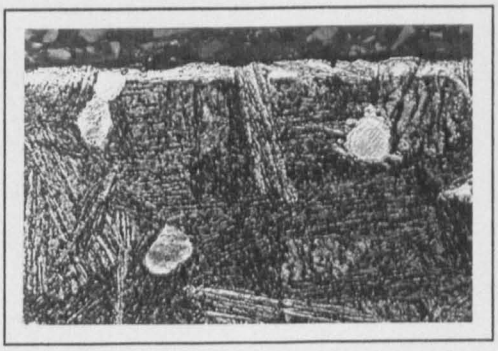

Photograph V.a. 525 °C, 99.48 h

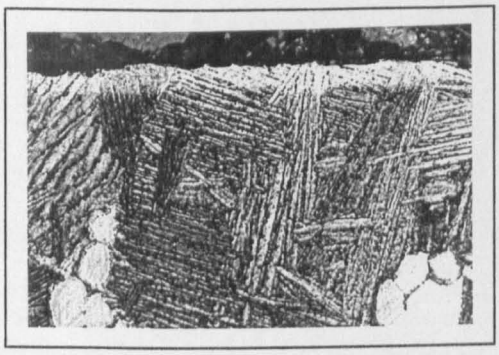

Photograph V.b. 550 °C, 89 h

Photgraph V.c. 575 °C, 100 h

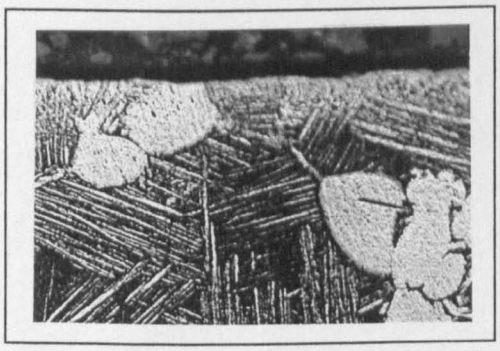

Photograph V.d. 600 °C, 100 h

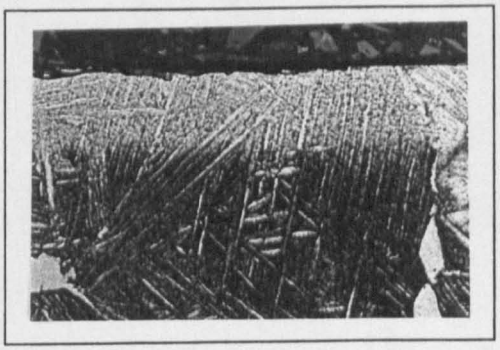

Photograph V.e. 625 °C., 100 hours

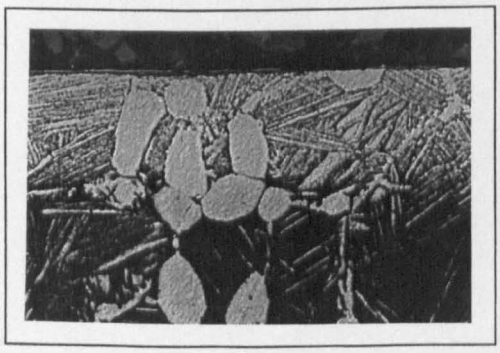

Photograph V.f. 650 °C, 100 h

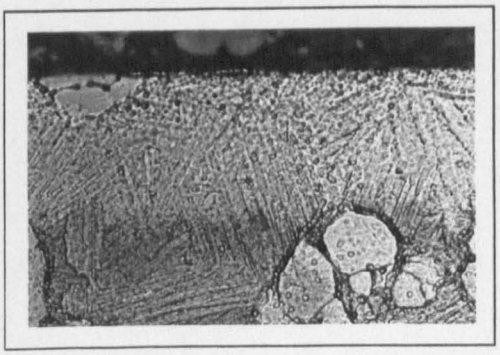

Photograph V.g. 675 °C, 99 h

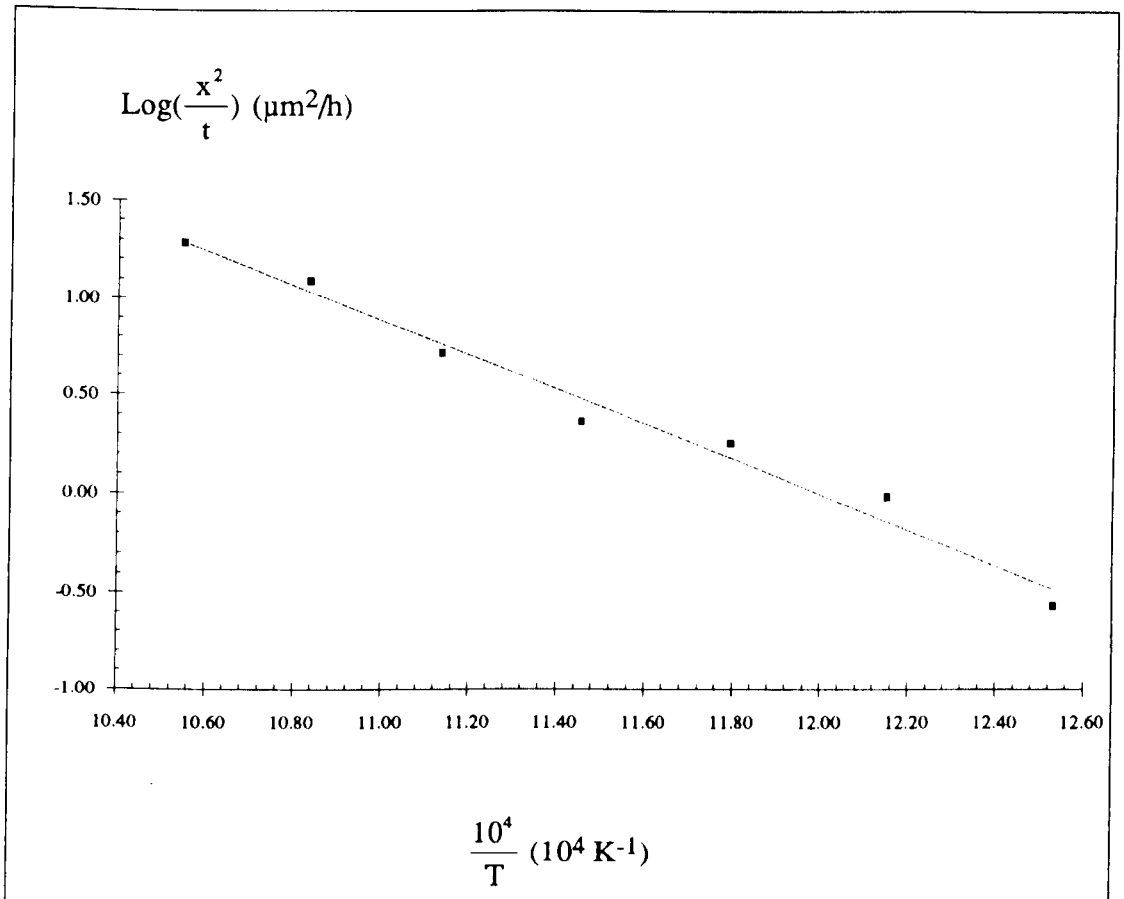

Figure V.f. Arrhenius plot based on measurements of alpha case depth for the oxidation of IMI 834 between 525 °C and 675 °C

V.c.3. Salt-corrosion tests

Hot-salt continuous thermogravimetric tests were carried out under the same test conditions as the oxidation tests, but the lower part of the temperature range was extended to 500 °C. Table V.f . shows the experimental parameters for each of the tests, while Figure V.g. shows the thermogravimetric curve obtained at a temperature of 625 °C.

Obviously, the shape of this curve is not parabolic during the first ten hours of exposure. However, a value of the parabolic rate constant Kp based on the total mass gain after exposure was calculated as a first approximation for each test. These values are indicated in Table V.f. and are plotted on an Arrhenius plot in Figure V.h. A straight line was thus obtained, though the resulting scatter is considerably higher than this observed for the case of the oxidation runs. Nevertheless this seems to indicate

that the behaviour of IMI 834 under hot-salt attack remains predominantly parabolic, in spite of the initial non-parabolic behaviour observed during the first few hours of exposure.

Test number	Temperature (°C)	Salt level (mg/cm^2)	Time of exposure (h)	Total mass gain ($\mu g/cm^2$)	Log (Kp) ($mg^2.cm^{-4}.s^{-1}$)
SN150	500	0.0299	100	237.89	-6.80
SN152	525	0.0229	100	259.75	-6.73
SN155	550	0.0229	100	277.6	-6.67
SN157	575	0.0299	100	537.3	-6.10
SN257	575	0.0297	100	250.33	-6.76
SN160	600	0.0230	99.17	489.12	-6.17
SN162	625	0.0297	100	537.43	-6.10
SN165	650	0.0297	100	831.12	-5.72
SN167	675	0.0297	99.5	791.23	-5.76

Table V.f. Results of hot-salt corrosion thermogravimetric tests

As can be seen in Photographs V.h. to V.o., alpha case was not detected on the edge of the specimens' cross section. Hence, one can assume that either oxygen was not dissolved into the alloy, or that if it was dissolved, it was subsequently transformed or consumed.

From these results, one can see that the thermogravimetric behaviour of IMI 834 undergoing hot-salt attack is significantly different from its oxidation behaviour: The mass gains obtained are higher, the thermogravimetric curve is not purely parabolic, and the alpha case was not clearly detected at the surface of the sample after exposure. These facts will be explored in greater depth in the discussion, with the help of Scanning Electron Microscope examinations.

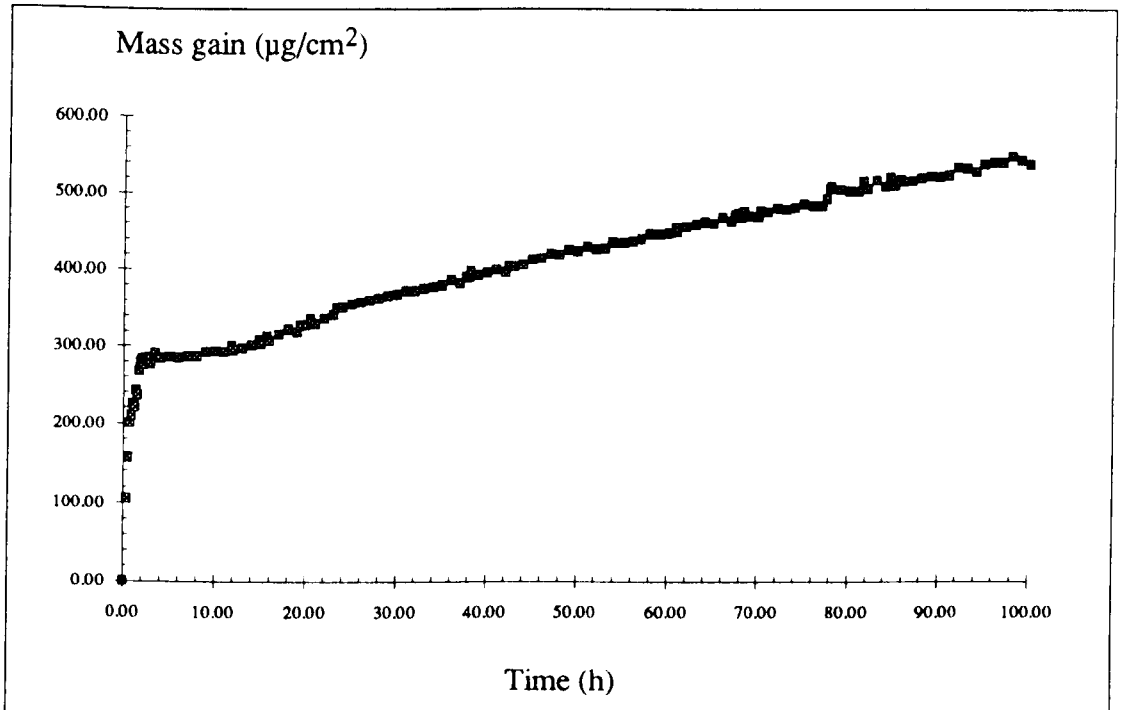

Figure V.g. Thermogravimetric curve for the hot-salt corrosion of IMI 834 at 625 °C

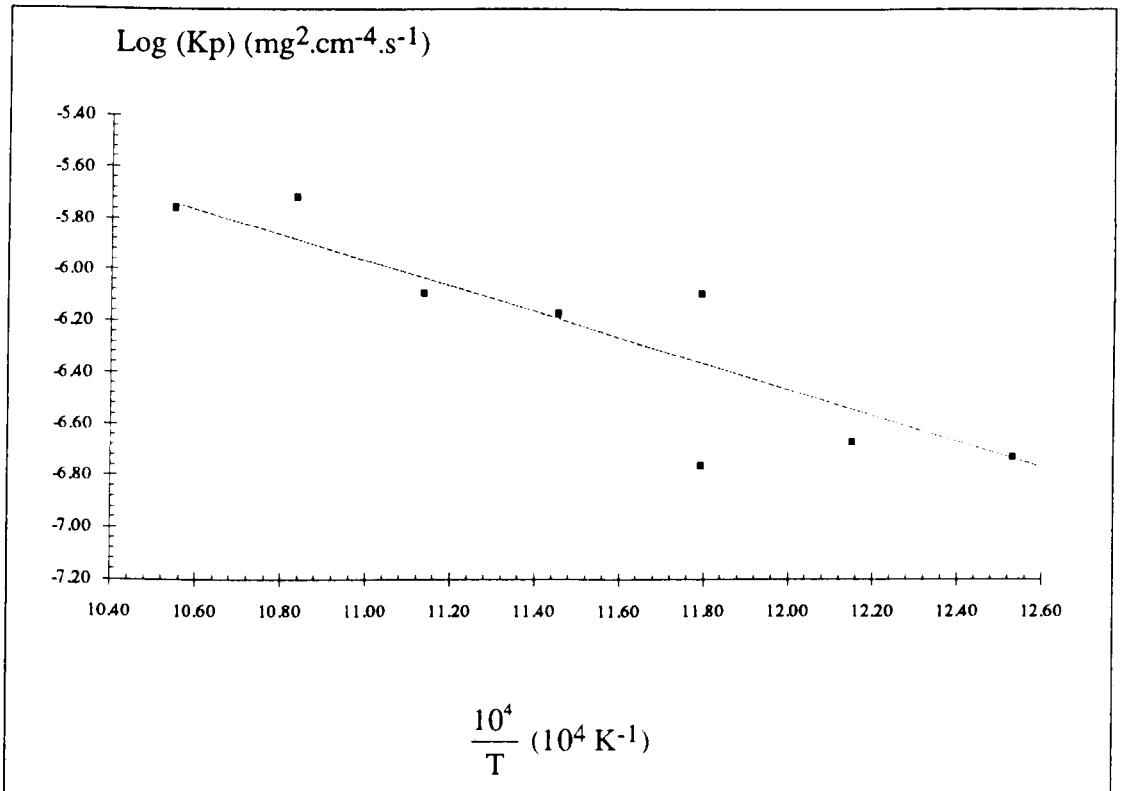

Figure V.h. Arrhenius plot based on total weight gain for the hot-salt corrosion of IMI 834 between 500 °C and 675 °C

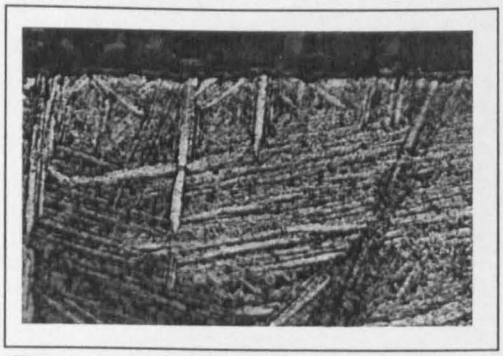

Photograph V.h. 500 °C, 100 h

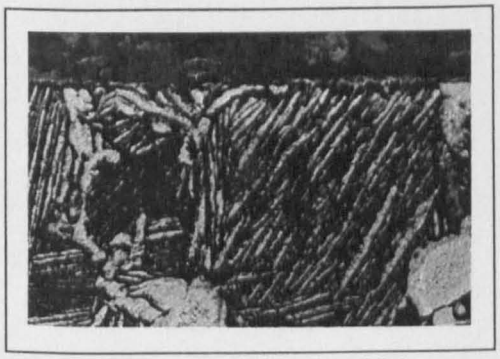

Photograph V.i. 525 °C, 100 h

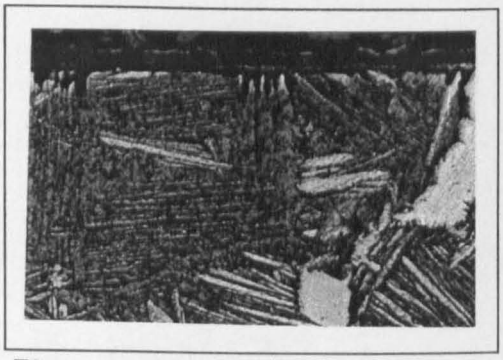

Photograph V.j. 550 °C, 100 h

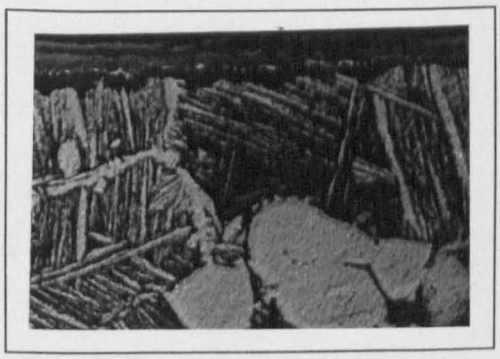

Photograph V.k. 575 °C, 100 h

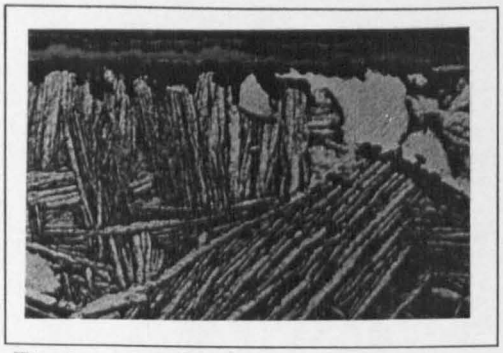

Photograph V.l. 600 °C, 99.17 h

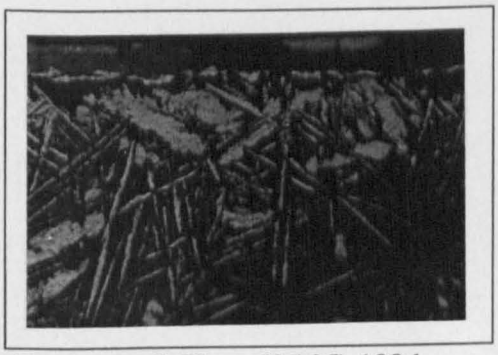

Photograph V.m. 625 °C, 100 h

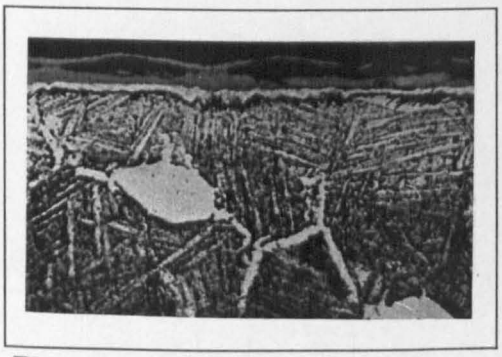

Photograph V.n. 650 °C, 100 h

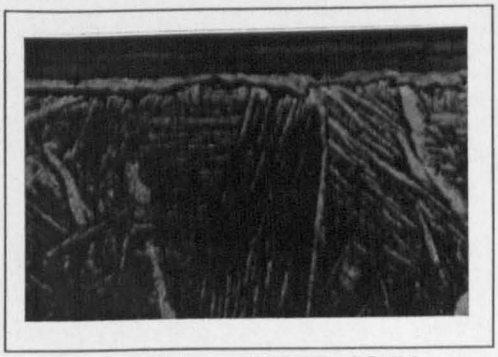

Photograph V.o. 675 °C, 99.5 h

Photograph V.h. to V.o.: Photographs showing no clear α case during salt-corrosion

Magnification: × 600

CHAPTER VI

DISCUSSION AND MODELLING

VI.a. Introduction

Chapter V showed the existence of significant pressure effects on the hot-salt stress-corrosion cracking of titanium alloys and highlighted the differences in the thermogravimetric behaviour of IMI 834 in oxidising and hot-corrosion environments. Although high environmental pressures are beneficial for the life of the material under HSSCC conditions, it is now necessary to examine further these effects and to study the mechanisms by which they interact with the phenomenon. Therefore it is crucial to model the different aspects of HSSCC and to develop an understanding of the manner by which hot-salt can initiate cracks in the material. In the course of this study, two tools were used to achieve this goal: Metallographic studies were carried out on both hot-salt stress-corroded test pieces and thermogravimetric coupons exposed to oxidising and hot-salt environments. Furthermore, thermodynamical studies were undertaken in order to provide information on the mechanisms of crack initiation during HSSCC exposure.

The first part of this chapter will discuss the beneficial effects of pressure which have been presented in chapter V. Metallographic studies will be used to identify the main characteristics of hot-salt stress-corrosion failures. In the second part, a comprehensive analysis of thermogravimetric data will be carried out and the differences observed between material exposed to oxidation and material exposed to hot-salt corrosion will be presented and discussed using metallographic evidence. Finally, theoretical studies using thermodynamical phase stability diagrams will be presented and a new model for the hot-salt stress-corrosion cracking of titanium alloys will be derived.

VI.b. High pressure studies

It has been shown in the preceding chapter that pressure effects are beneficial to the life of a titanium alloy undergoing hot-salt stress-corrosion cracking. However it appeared that the influence of high pressure was far from simple and seemed to interact with atmosphere composition: Hence, at high oxygen volume contents, high pressures resulted in a further improvement in the life of the material, but this effect vanished for rare oxygen contents. This change in behaviour must therefore be characterised and explained.

VI.b.1. Influence of load at atmospheric pressure and normal air compositions

In the course of this study testing was carried out with stresses ranging from 540 MPa to 620 MPa. However it is necessary to standardise these tests in order to characterise the interactions between stress and pressure. As mentioned in chapter II, this has usually been achieved by using either the Larsen-Miller parameter or the Orr-Sherby-Dorn parameter (Turley 1966, Royster 1968). Both of these parameters are in fact dependent on the test temperature and the logarithm of the time to failure. Since testing temperature can be considered as being constant for this study, it was decided to express the stress dependence with the logarithm of the time to failure.

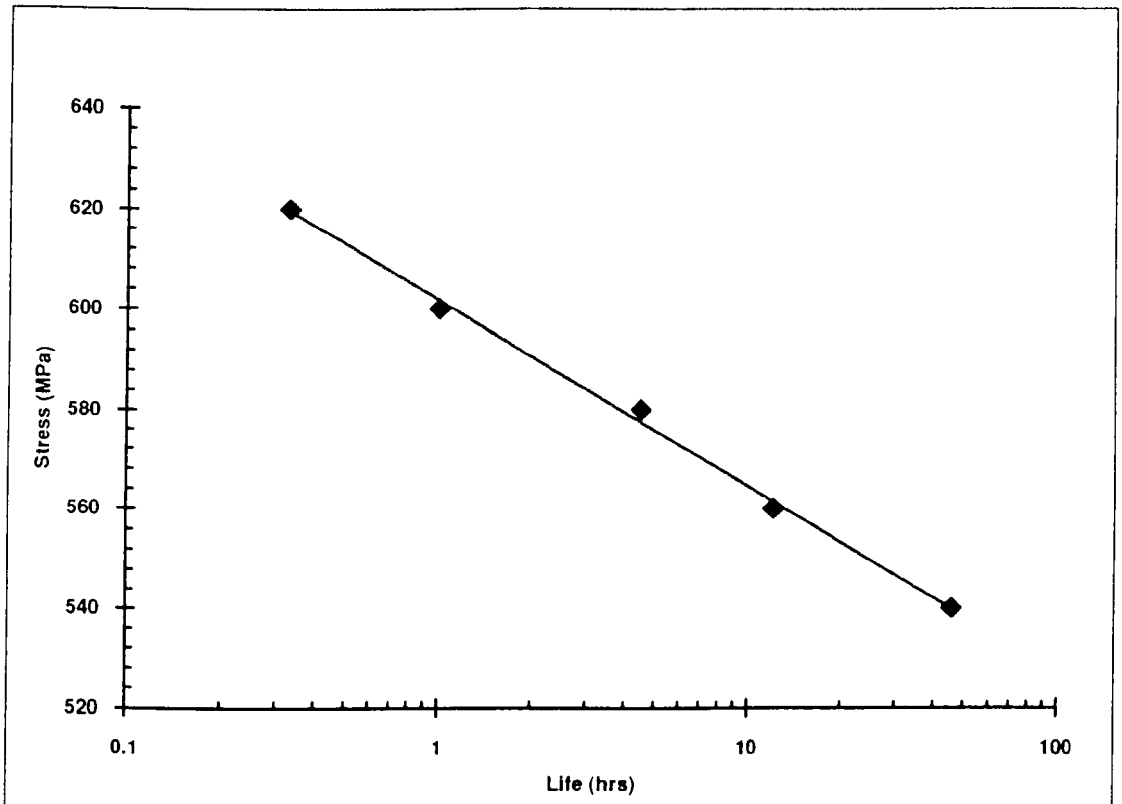

Figure VI.a. Plot showing a linear dependence of the testing stress versus Log (t) at atmospheric pressure.

Figure VI.a. shows a plot of the testing stress versus the logarithm of the time to failure for atmospheric pressure conditions. It can be seen that a straight line was thus obtained. Hence, the influence of the imposed stress on the life of IMI 834 subjected to hot-salt stress-corrosion cracking conditions can be described by the following law:

$$\sigma = \sigma_0 + aLog\left(\frac{t}{t_0}\right) \qquad \textbf{(VI.1)}$$

where σ_0 is the intercept with the y axis for t_0=1 hour
a is the slope of the line in MPa
σ is the testing stress in MPa
t is the time to failure in hours

A linear regression on the data points obtained through testing gave the following values for a coefficient of determination of 0.997:

σ_0=601.66 MPa
a=-37.15 MPa

Therefore, at atmospheric pressure, the testing stress and the life of the material can be accurately related with the following relationship:

$$\sigma = 601.7 - 37.15Log(t) \qquad \textbf{(VI.2)}$$

VI.b.2. Interaction between static load and total environmental pressure

Chapter V showed that for normal air compositions the influence of total pressure on the time to failure of IMI 834 in HSSCC environments was linear. Knowing also the effect of load on the life of the material at atmospheric pressure, the interaction between the stress imposed on the test piece and the total pressure can now be examined. Figure VI.b. was obtained from Figure VI.a. by adding all the results at high pressure for normal air atmospheres. It was found that testing at four bars resulted in a line parallel to that obtained at atmospheric pressure. Therefore a series of discontinuous parallel lines obtained by extrapolation were plotted on this graph. This implies that the total pressure actually changes the value of σ_0 in equation (VI.1), as the slope of these lines remains constant from one testing pressure to

another. Therefore σ_0 and a (equation VI.a.) can be used to characterise the life of IMI 834 subjected to hot-salt stress-corrosion cracking environments at a given temperature: Lower values of σ_0 represent dramatically short lives, while increasing life times obtained with increased pressures result in higher values of σ_0. The stress dependence is determined by the value of a in conjunction with σ_0.

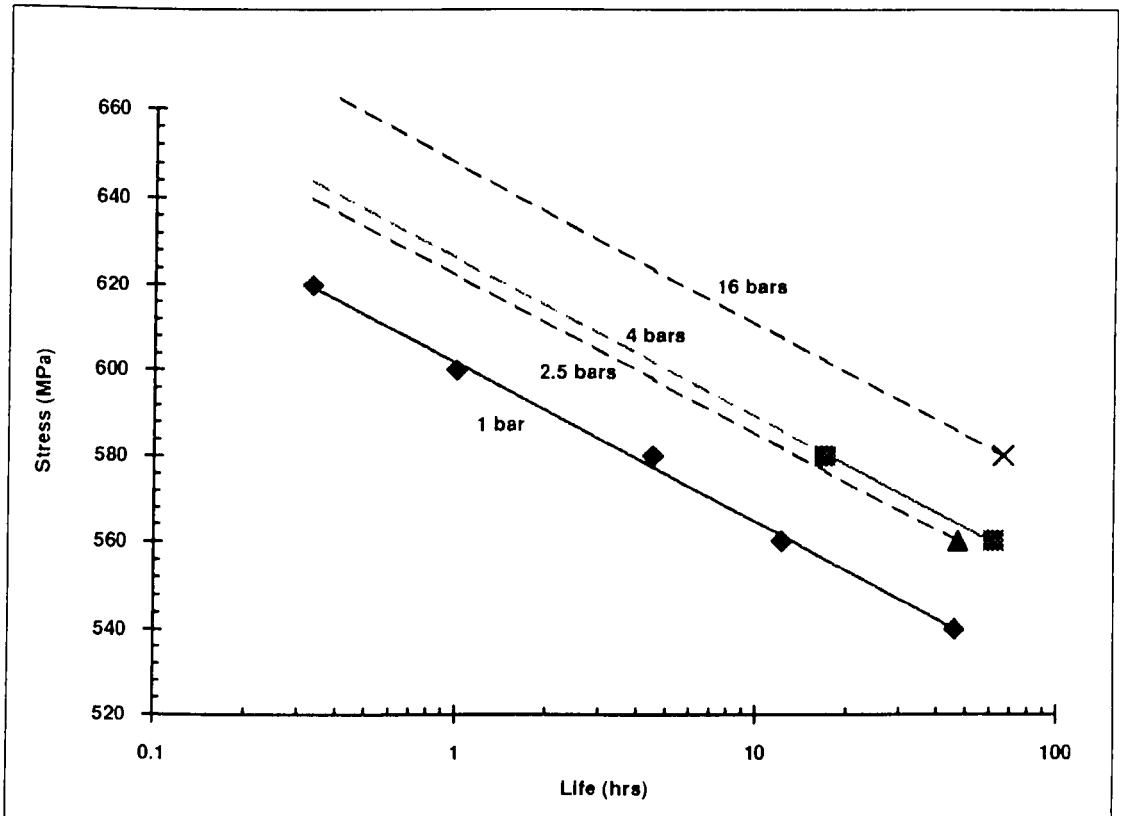

Figure VI.b. Interaction between load and total pressure

However since the number of high pressure data points shown in Figure VI.b. is limited, one could argue that their extrapolation is inaccurate and that the use of σ_0 to characterise the effect of total pressure, independently of load, on the life of the material is unreliable. Therefore it is necessary to validate this model through another analysis. This was done by studying the influence of pressure on σ_0 for all testing stresses. Figure VI.c. shows a plot of σ_0 versus total pressure for the whole range of stress used in this study. This plot actually shows that the influence of pressure on the life of the material can indeed be defined by a linear increase of σ_0 with the logarithm of total pressure, irrespective of the test's stress.

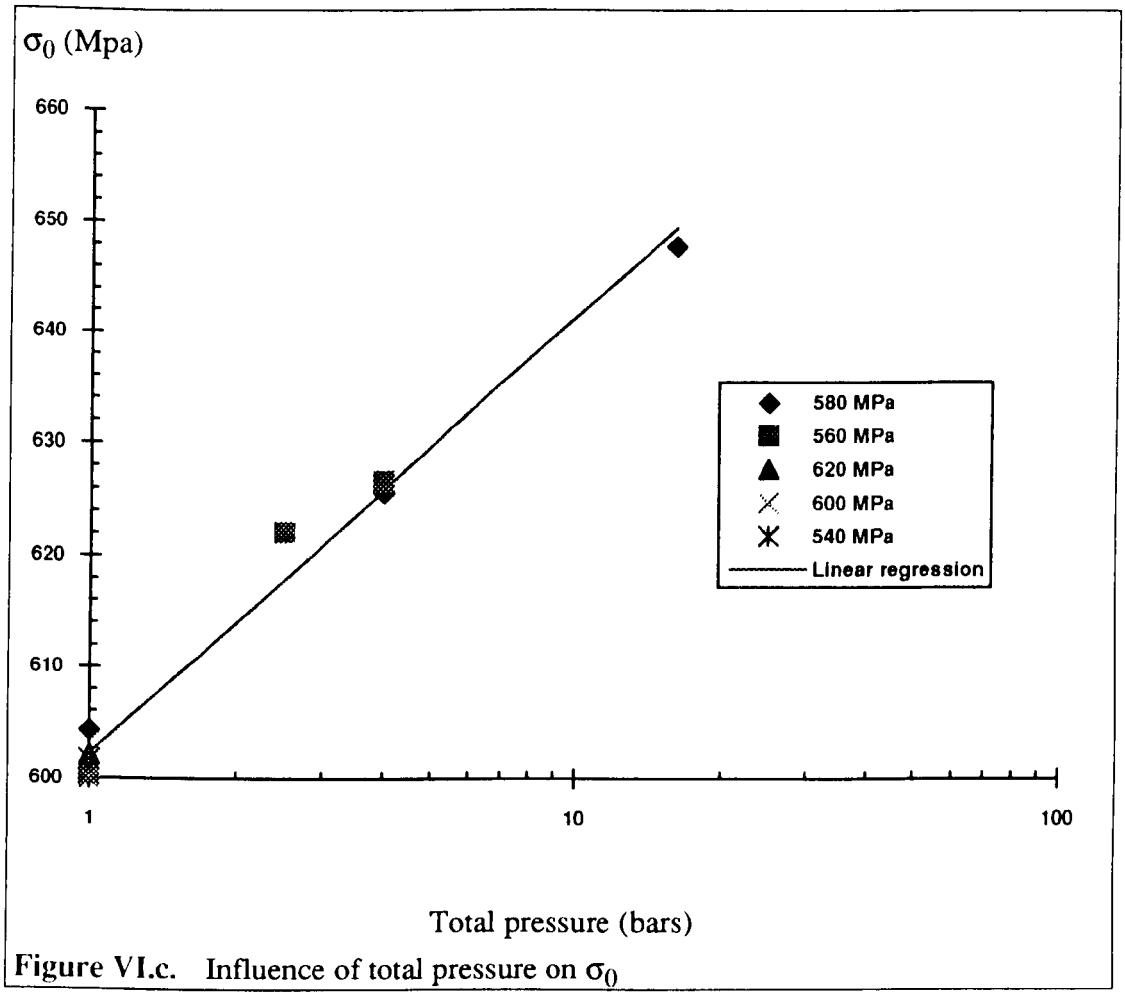

Figure VI.c. Influence of total pressure on σ_0

Therefore the relationship between σ_0 and the environmental pressure is of the form:

$$\sigma_0 = \sigma_{0atm} + bLog\left(\frac{P}{P_{atm}}\right) \qquad \text{(VI.3)}$$

where σ_{0atm} is the value of σ_0 at P_{atm} in MPa
b is the slope of the line in MPa
P is the testing pressure
P_{atm} is the atmospheric pressure

Regression analysis carried out on the data points gave a coefficient of determination of 0.98 for this relationship and the following values for σ_{0atm} and b:

σ_{0atm}=602.3 MPa

b=39.1 MPa

Substituting equation (VI.3) in equation (VI.1) the combined influence of load and pressure on the life of IMI 834 in HSSCC environments at a constant temperature of 500 °C can therefore be described by:

$$\sigma = \sigma_{0atm} + 39.1 Log\left(\frac{P}{P_{atm}}\right) - 37.15 Log\left(\frac{t}{t_0}\right) \qquad \text{(VI.4)}$$

Rearranging this formula, one obtains:

$$Log\left(\frac{t}{t_0}\right) = \frac{\sigma_{0atm} - \sigma}{37.15} + \frac{39.1}{37.15} Log\left(\frac{P}{P_{atm}}\right) \qquad \text{(VI.5)}$$

and

$$\frac{t}{t_0} = \left(\frac{P}{P_{atm}}\right)^{1.05} \times (1.06)^{(\sigma_{0atm} - \sigma)} \qquad \text{(VI.6)}$$

where t is the time to failure

t_0=1 h for this study

P is the total pressure

P_{atm} is atmospheric pressure (i.e. 1 bar for this study)

σ is the testing stress in MPa

σ_{0atm}=602.3 MPa is the value of σ_0 for a time to failure of $t=t_0$ at $P=P_{atm}$

Table VI.a. compares the experimental values of the time to failure t with these obtained by injecting the testing stress and the total pressure in equation (VI.6) for each test. The last column of this table also gives the error made when measuring the life of the material . This error was estimated from equation (VI.6) and the calculation of Δt in hours was done using the general equation:

$$\Delta t = \Delta P \left|\frac{\partial t}{\partial P}\right| + \Delta\sigma_{0atm} \left|\frac{\partial t}{\partial \sigma_{0atm}}\right| + \Delta\sigma \left|\frac{\partial t}{\partial \sigma}\right| \qquad \text{(VI.7)}$$

Hence one obtains:

$$\Delta t = \Delta P\left[1.05\times(P)^{0.05}\times(1.06)^{\sigma_{0atm}-\sigma}\right]+\Delta\sigma_{0atm}\left[(P)^{1.05}\times\ln(1.06)\times(1.06)^{\sigma_{0atm}-\sigma}\right] + \Delta\sigma\left[(P)^{1.05}\times\ln(1.06)\times(1.06)^{\sigma_{0atm}-\sigma}\right] \quad \text{(VI.8)}$$

where:

ΔP is the error made when setting the pressure at the desired value and was estimated to be 0.25 bar. It is worth noticing that the fluctuations of pressure throughout the test are not taken in account as they are similar for all the tests and were contained within ±1 bar (see Chapter V, paragraph V.b.1).

$\Delta\sigma_{0atm}$ is the error made by using the value σ_{0atm}=602.3 MPa which was calculated through linear regression analysis (see equation VI.1), paragraph VI.b.1.). Hence the true values of σ_{0atm} for each test at atmospheric pressure was calculated and are indicated in Table VI.a. for all the tests considered.

$\Delta\sigma$ is the error made when stressing the specimen and is given by the precision of the load cell which is guaranteed to be ±1% by the manufacturer. Again, this term does not consider the periodic fluctuations of the load which are due to the fluctuations of the total pressure (see Chapter V, paragraph V.b.1)

When calculating Δt, one has also to consider the pressure conditions at which each test was carried out: Hence tests at atmospheric pressure can not result in a negative contribution of the pressure term in Δt. Therefore both the positive and negative errors are indicated in Table VI.a.

Figure VI.d. shows a plot of the time to failure measured through testing versus the life calculated with equation (VI.6). The straight line shown on this graph represents an ideal situation where the result of each test could be predicted exactly with equation (VI.6). The error bars corresponding to the last column of Table VI.a. were added to the graph. They show that significant errors can be induced by using stresses in the lower range (i.e. 540 and 560 MPa). Indeed, by examining equation (VI.6), one can notice that the calculated lifetime is extremely stress sensitive. In order to visualise this effect, the two lines corresponding to the errors induced by the load cell (±1%) were plotted on the graph. It can be seen that in most cases, the error induced by these small stress variations constitute the major part of the total error of the test. One can also see that the test which produces the biggest error is that carried out at a total pressure of 2.5 bars. This is actually expected as pressure control in this range is

extremely difficult and is at the limit of the gauges' resolution. Table VI.a. shows that test 084A/107 which was stopped after 200 hours would in fact have failed in about 693 hours. This gives an example of the dramatic influence of the combined effects of stress and total environmental pressure on the life of IMI 834 subjected to hot-salt stress-corrosion cracking conditions in air .

Test piece number	Pressure (bars)	Stress (MPa)	t_{calc} (h)	t_{exp} (h)	σ_{0atm} (MPa)	Δt (h)
084A/66	1	620	0.36	0.33	602.1	+0.22 -0.13
084A/123	1	600	1.14	1.00	600.0	+0.85 -0.55
084A/121	1	580	3.67	4.50	604.3	+2.63 -1.67
084A/54	1	560	11.76	12.12	600.2	+8.37 -5.28
084A/52	1	540	37.72	45.80	601.7	+23.09 -13.19
084A/108	2.5	560	30.78	46.90	606.5	+20.80 -20.80
084A/149	4	560	50.42	62.08	603.1	+22.11 -22.11
084A/88	4	580	15.72	16.90	602.1	+6.52 -6.52
084A/87	16	580	67.40	66.40	600.6	+30.57 -30.57
084A/107	16	540	693	>200	-	-

Table VI.a. Comparison between the results of equation (VI.6) and the experimental life of IMI 834 subjected to HSSCC in normal air compositions

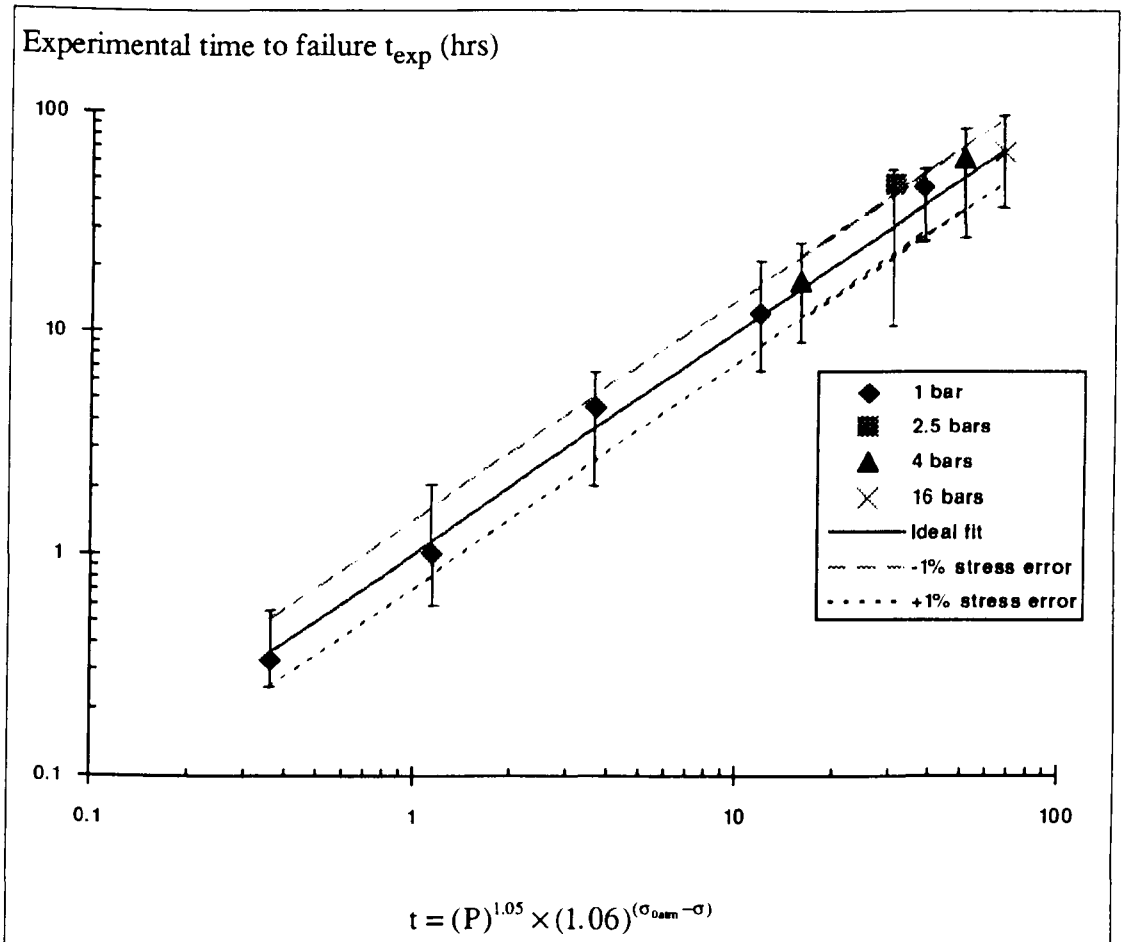

Figure VI.d. Experimental life versus expected life for the HSSCC of IMI 834 in normal air composition

VI.b.3. Influence of atmospheric composition at atmospheric pressure

It has been shown in paragraph VI.b.2. that any test undertaken in air can be characterised by a single parameter representing a normalised stress:

$$\sigma_0 = \sigma + 37.15 Log\left(\frac{t}{t_0}\right)$$

where σ is the stress in MPa

t is the time to failure in hours

t_0=1 hour

This parameter was also used in order to evaluate the influence of atmosphere composition on the hot-salt stress-corrosion cracking of IMI 834 at atmospheric pressure. Table VI.b. gives the calculated values of this normalised stress for all the tests carried out at 1 bar in atmospheres containing 10.5% to 84% volume fraction of oxygen. The values calculated for σ_0 are also plotted versus the volume fraction of oxygen in Figure VI.e.

Test piece number	Stress (MPa)	Volumetric oxygen content (%)	Life (h)	σ_0 (MPa)
084A/130	560	10.5	84.3	631
084A/86	560	15.0	21.6	610
084A/66	620	21.0	0.33	602
084A/123	600	21.0	1.0	600
084A/121	580	21.0	4.5	604
084A/54	560	21.0	12.12	600
084A/52	540	21.0	45.8	602
084A/75	560	40.0	39.7	619
084A/64	580	84.0	23.4	631

Table VI.b. Values for the normalised stress in different atmosphere compositions at atmospheric pressure

One can see from Figure VI.e. that the influence of atmosphere composition on the normalised stress σ_0 and thus on the life of the material is rather complex: Indeed, both high volumetric oxygen contents and low volumetric oxygen contents extend the life of IMI 834 subjected to hot-salt stress-corrosion cracking. Although it is difficult to draw a precise curve through the limited number of data points present in this graph, it is possible to approximate these effects by drawing two lines which result in a "dip" around normal air composition. In any case, Figure VI.e. shows that the most severe hot-salt stress-corrosion cracking environment is unfortunately close to normal air composition. This correlates well with the results published by Heimerl which have been presented in Chapter II (see paragraph II.c.4.): Indeed, Heimerl noticed that the beneficial effects of rare oxygen atmospheres on the hot-salt stress-corrosion of titanium alloy TI-8Al-1Mo-1V were more effective than these observed for enriched oxygen compositions (Heimerl 1966). The same observation can be made for IMI 834

in this study, since the slope of the line on the left side of the "dip" is steeper than this on the right side.

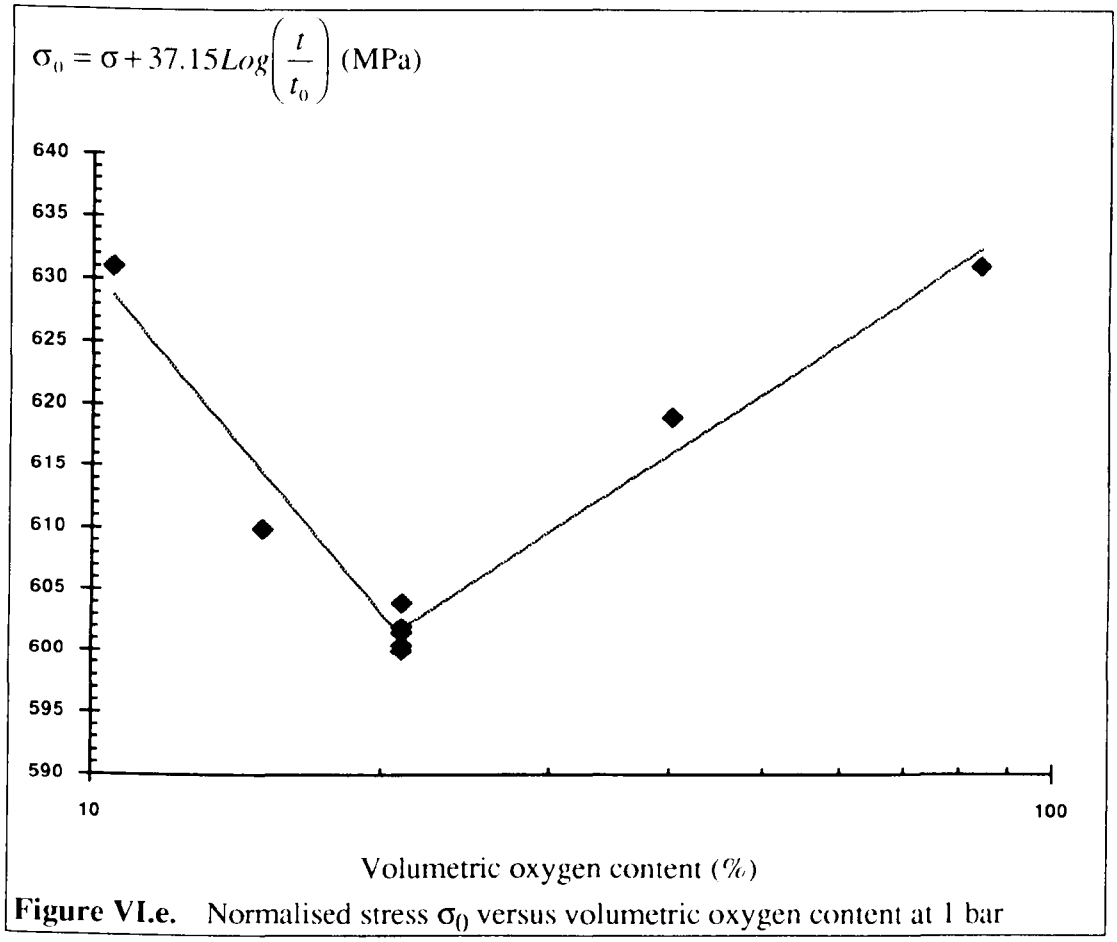

Figure VI.e. Normalised stress σ_0 versus volumetric oxygen content at 1 bar

VI.b.4. Combined effects of total pressure and atmospheric composition

The preceding paragraph showed that atmosphere composition influences dramatically the behaviour of IMI 834 subjected to hot-salt stress-corrosion cracking conditions at atmospheric pressure. However in a given environment, the volumetric fraction of oxygen and the partial pressure of oxygen are related by the following relationship:

$$Vol\%\ (O_2) = \frac{P(O_2)}{P_{tot}} \qquad \textbf{(VI.9)}$$

where Vol % (O_2) is the volumetric oxygen content in %

$P(O_2)$ is the partial pressure of oxygen in bars

P_{tot} is the total pressure in bars

Hence, it is not possible to determine from Figure VI.e. whether the beneficial effects of rare oxygen and enriched oxygen compositions are due to volumetric oxygen contents or to partial pressures of oxygen. Therefore, the interaction between total pressure and atmosphere composition have to be examined. This was also possible using the normalised stress σ_0 to characterise the life of the material. Table VI.c. gives such values for each of the tests carried out in the course of this study.

Test piece number	Stress (MPa)	O_2 content (Vol %)	Total pressure (bars)	$P(O_2)$ (bars)	Life (h)	σ_0 (MPa)
084A/77	580	5.25	16	0.84	>120	>657
084A/130	560	10.5	1	0.105	84.3	631
084A/86	560	15.0	1	0.15	21.6	610
084A/122	560	15.0	4	0.6	17.4	606
084A/66	620	21.0	1	0.21	0.33	602
084A/123	600	21.0	1	0.21	1	600
084A/121	580	21.0	1	0.21	4.5	604
084A/54	560	21.0	1	0.21	12.12	600
084A/52	540	21.0	1	0.21	45.8	602
084A/108	560	21.0	2.5	0.525	46.9	622
084A/149	560	21.0	4	0.84	62.08	627
084A/88	580	21.0	4	0.84	16.9	626
084A/87	580	21.0	16	3.36	66.4	648
084A/107	540	21.0	16	3.36	>200	>625
084A/75	560	40.0	1	0.4	39.7	619
084A/78	560	40.0	4	1.6	63.7	627
084A/64	580	84	1	0.84	23.4	631

Table VI.c. Values of the normalised stress σ_0 for all test conditions

By rearranging equation (VI.9), one can see that the partial pressure of oxygen does in fact represent the interaction between atmosphere composition and total pressure:

$$P(O_2) = Vol\%(O_2) \times P_{tot} \qquad (VI.10)$$

Therefore the values of the normalised stress σ_0 were plotted versus the partial pressure of oxygen for each test, thus producing Figure VI.f. which was obtained from the tests carried out in rare oxygen content atmospheres, and Figure VI.h. which considers enriched oxygen compositions. The values of σ_0 for normal air compositions at atmospheric pressure are represented on each graph for reference.

It is not possible to define a clear relationship between the life of the material (or its normalised stress) and the partial pressure of oxygen from Figure VI.f. Indeed, on inspection of Table VI.c. one can notice that no increase in life could be achieved at a volume fraction of oxygen of 40% when the total pressure was increased from 1 bar to 4 bars. In this reduced oxygen regime, lifetimes seem to be controlled by the volumetric fraction of oxygen and this can readily be observed in Figure VI.g.

This behaviour does not constitute a problem in view of gas turbine engine applications, since the air compositions encountered in service present a volume fraction of oxygen of 21%. However one can conclude that the behaviour of IMI 834 subjected to hot-salt stress-corrosion cracking in low oxygen content atmospheres is dictated solely by the environment's oxygen content, that is, by the interactions between total pressure and oxygen partial pressure. The implications of this on the hot-salt stress-corrosion mechanism will be discussed in section VI.e.2.

To the contrary, for high oxygen volume fractions a net improvement of the life of the material with increasing partial pressure of oxygen is evident from Figure VI.h. Indeed, the life of IMI 834 in enriched oxygen atmospheres can be related to the partial pressure of oxygen through a logarithmic relationship. Although these effects will also be discussed in more details in the final part of this chapter when a mechanism for the hot-salt stress-corrosion process is presented, it is worth mentioning that the life of the material for the air compositions considered in Figure VI.h. is thought to be controlled by a chemical process involving oxygen gas. Indeed, the equilibrium rate constant of any chemical reaction involving oxygen will depend on oxygen activity that is, oxygen partial pressure. If oxygen partial pressure is increased, then the activity of oxygen is increased, and some of the possible reactions involving oxygen in the HSSCC mechanism would be encouraged (i.e. their rate constant would increase).

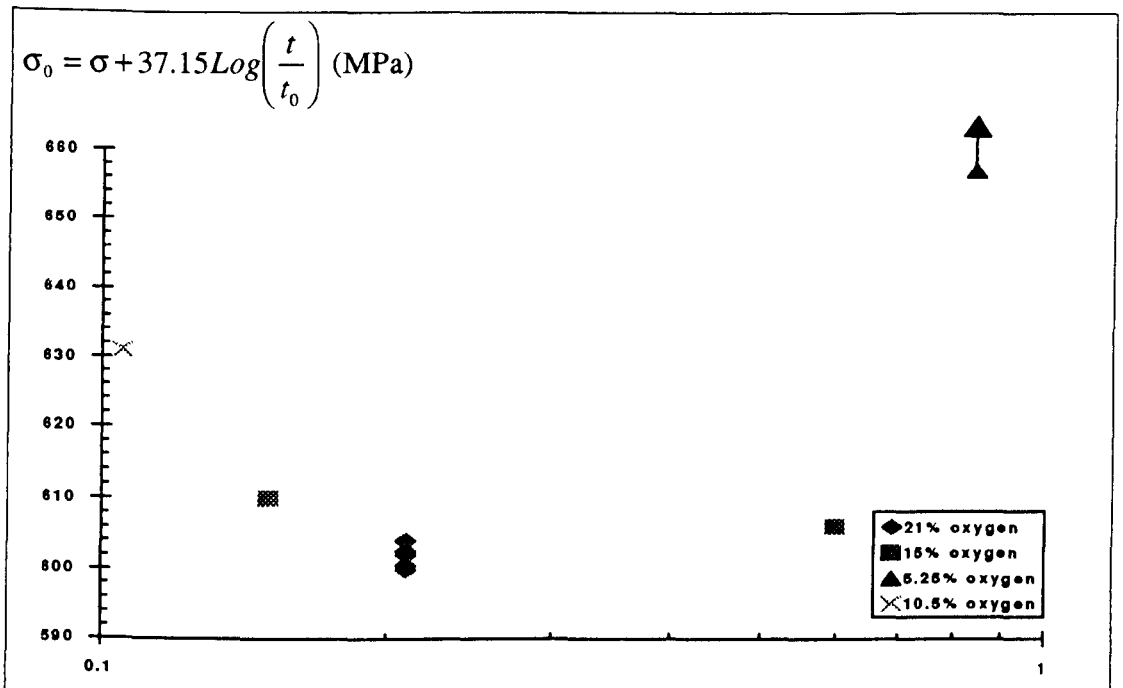

Figure VI.f. Plot of the normalised stress σ_0 versus partial pressure of oxygen for tests carried out in low oxygen content air compositions

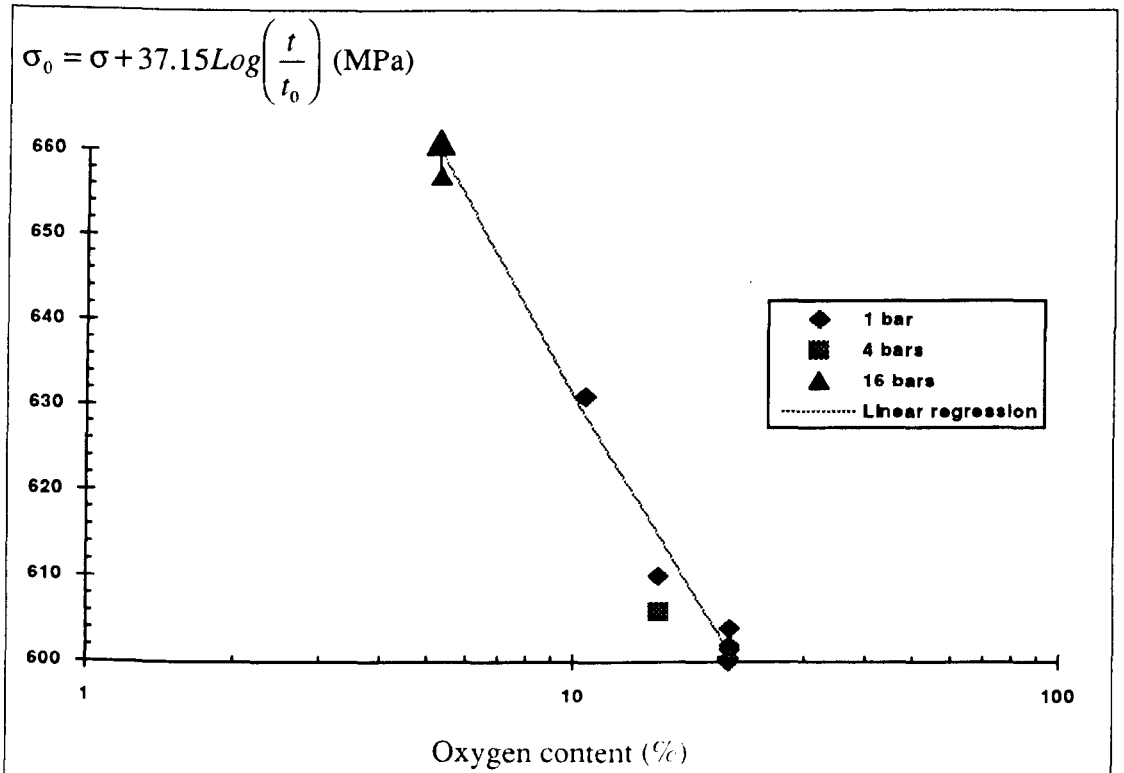

Figure VI.g.: Plot of the normalised stress σ_0 versus volume fraction of oxygen for tests carried out in low oxygen air compositions

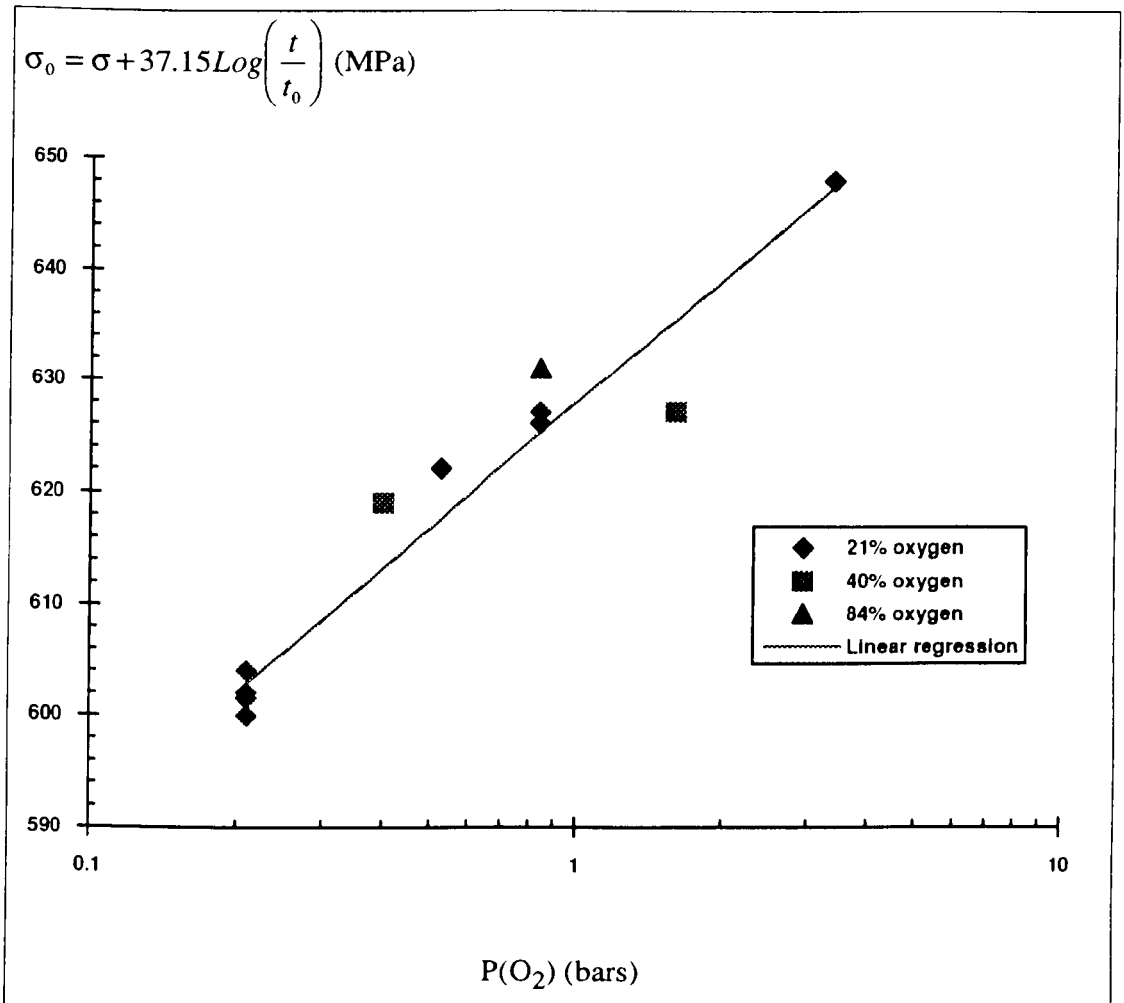

Figure VI.h. Plot of the normalised stress σ_0 versus partial pressure of oxygen for tests carried out in enriched oxygen air compositions.

Since the relationship between σ_0 and the partial pressure of oxygen is logarithmic, one can now establish a new law for the life of IMI 834 in enriched oxygen, hot-salt stress-corrosion cracking environments. From Figure VI.h. the relationship between the normalised stress σ_0 and $P(O_2)$ is of the form:

$$\sigma_0 = \sigma^* + cLog(P(O_2)) \qquad \text{(VI.11)}$$

Where σ_0 is the normalised stress for the test in MPa

σ^* is the normalised stress in MPa at $P(O_2)$=1 bar

$P(O_2)$ is the partial pressure of oxygen in bars

c is the slope of the line in MPa

A linear regression analysis on the data of Figure VI.h. gives a coefficient of correlation of 0.96 and:

$$\sigma^* = 628.3 \text{ MPa}$$
$$c = 37.01 \text{ MPa}$$

By substituting equation (VI.11) in equation (VI.1), one obtains:

$$\sigma = \sigma^* + 37.01 Log(P(O_2)) - 37.15 Log t \qquad \text{(VI.12)}$$

This can be approximated as:

$$t = (1.06)^{\sigma^* - \sigma} \times P(O_2) \qquad \text{(VI.13)}$$

with little error.

The error made by predicting the time to failure with equation (VI.13) can be estimated by substituting equation (VI.10) in equation (VI.13):

$$t = (1.06)^{\sigma^* - \sigma} \times P_{tot} \times Vol\%(O_2) \qquad \text{(VI.14)}$$

The error made when calculating t is therefore:

$$\Delta t = \Delta Vol\%(O_2)\left|\frac{\partial t}{\partial Vol\%(O_2)}\right| + \Delta Ptot\left|\frac{\partial t}{\partial Ptot}\right| + \Delta\sigma^*\left|\frac{\partial t}{\partial \sigma^*}\right| + \Delta\sigma\left|\frac{\partial t}{\partial \sigma}\right| \qquad \text{(VI.15)}$$

Hence the total error is given by:

$$\begin{aligned}\Delta t = {} & \Delta Vol\%(O_2) \times \left[(1.06)^{\sigma^* - \sigma} \times Ptot\right] + \Delta Ptot\left[(1.06)^{\sigma^* - \sigma} \times Vol\%(O_2)\right] \\ & + (\Delta\sigma^* + \Delta\sigma) \times \left[\ln(1.06) \times (1.06)^{\sigma^* - \sigma} \times Vol\%(O_2) \times Ptot\right]\end{aligned} \qquad \text{(VI.16)}$$

where:

$\Delta Vol\%(O_2)$ is the error made when blending the gas mixture. This term is equal to zero for normal air compositions (i.e. 21% oxygen) and is estimated to be ±2% for other mixes.

ΔP_{tot} is the error made on the mean pressure of the test (see paragraph VI.b.2.) and is assumed to be 0.25 bar

$\Delta\sigma^*$ is the error made by using σ^*=628.3 MPa which was calculated through linear regression analysis (see equation (VI.11)). The true value of σ^* for each test considered is indicated in table VI.d.

$\Delta\sigma$ is the error made in measuring the mean stress of the test (see paragraph VI.b.2) and relates to the precision of the load cell which is ±1%

Table VI.d. compares the time to failure t_{calc} as calculated with equation (VI.13) with the lifetime t_{exp} measured experimentally and gives the error value for t_{calc}. This error takes into consideration that pressure errors can only be positive for atmospheric pressure tests, and that no error is made on blending normal air compositions.

Figure VI.i. shows a plot of the experimental time to failure versus the calculated lifetime, and indicates the ideal situation where they would be equal. The error bars which are shown on this graph represent the error values featuring in the last column of Table VI.d. The lines representing errors of +1% and -1% on the testing stress are also drawn on this figure. Once again one can notice that the lifetime law is very stress sensitive. However, there are now three tests which are not contained within this stress error band. One of these tests is the run which was carried out at a pressure of 2.5 bars where pressure control is the most difficult (i.e. at the limit of the pressure gauges' resolution), and it is therefore possible that the error on the mean pressure of the test was more than 0.25 bar. The two other tests were carried out with special gas blends, and an extra error term is thus added. One can also notice that test 084A/107 which was stopped after 200 hours should have lasted about 576 hours if it is assumed that the life of the material is governed by equation (VI.13).

The results which have been discussed in the final part of this section provide an explanation for the lack of in-service failures of titanium base components: Indeed, the high pressures encountered in the compressor parts of gas turbine engines (typically 8 to 16 bars) can extend significantly the lifetime of such components before the onset of hot-salt stress-corrosion cracking. From the results obtained in this study, it has been possible to model the lifetime of IMI 834 in high pressure environments. This model has been found to be extremely stress sensitive, but gave satisfactory lifetime predictions. For example, at 580 MPa, increasing the pressure from 1 bar to 16 bars would increase the life to failure by sixteen times. A mechanism by which pressure effects extend these lifetimes will be discussed in details in the last part of this chapter.

Test piece number	Stress (MPa)	O_2 content (%)	P_{tot} (bars)	$P(O_2)$ (bars)	t_{exp} (h)	σ^* (MPa)	t_{calc} (h)	Δt_{calc} (h)
084A/66	620	21	1	0.21	0.33	627.2	0.34	-0.14 +0.48
084A/123	600	21	1	0.21	1	625.1	1.09	-0.58 +0.81
084A/121	580	21	1	0.21	4.5	629.3	3.50	-1.38 +2.31
084A/54	560	21	1	0.21	12.12	625.3	11.23	-5.66 +8.02
084A/52	540	21	1	0.21	45.8	626.8	36.03	-14.49 +23.5
084A/108	560	21	2.5	0.525	46.9	632.4	28.09	-19.45 +19.45
084A/149	560	21	4	0.84	62.08	629.4	44.94	-20.53 +20.53
084A/88	580	21	4	0.84	16.9	628.4	14.01	-5.69 +5.69
084A/87	580	21	16	3.36	66.4	628.2	56.05	-20.14 +20.14
084A/107	540	21	16	3.36	>200	-	576.6	-
084A/75	560	40	1	0.4	39.7	634.1	21.03	-15.47 +22.97
084A/78	560	40	4	1.6	63.7	619.5	85.61	-77.59 +77.59
084A/64	580	84	1	0.84	23.4	633.7	14.01	-9.60 +10.80

Table VI.d. Comparison of t_{calc} with t_{exp} for the hot-salt stress-corrosion of IMI 834 in rich oxygen air compositions

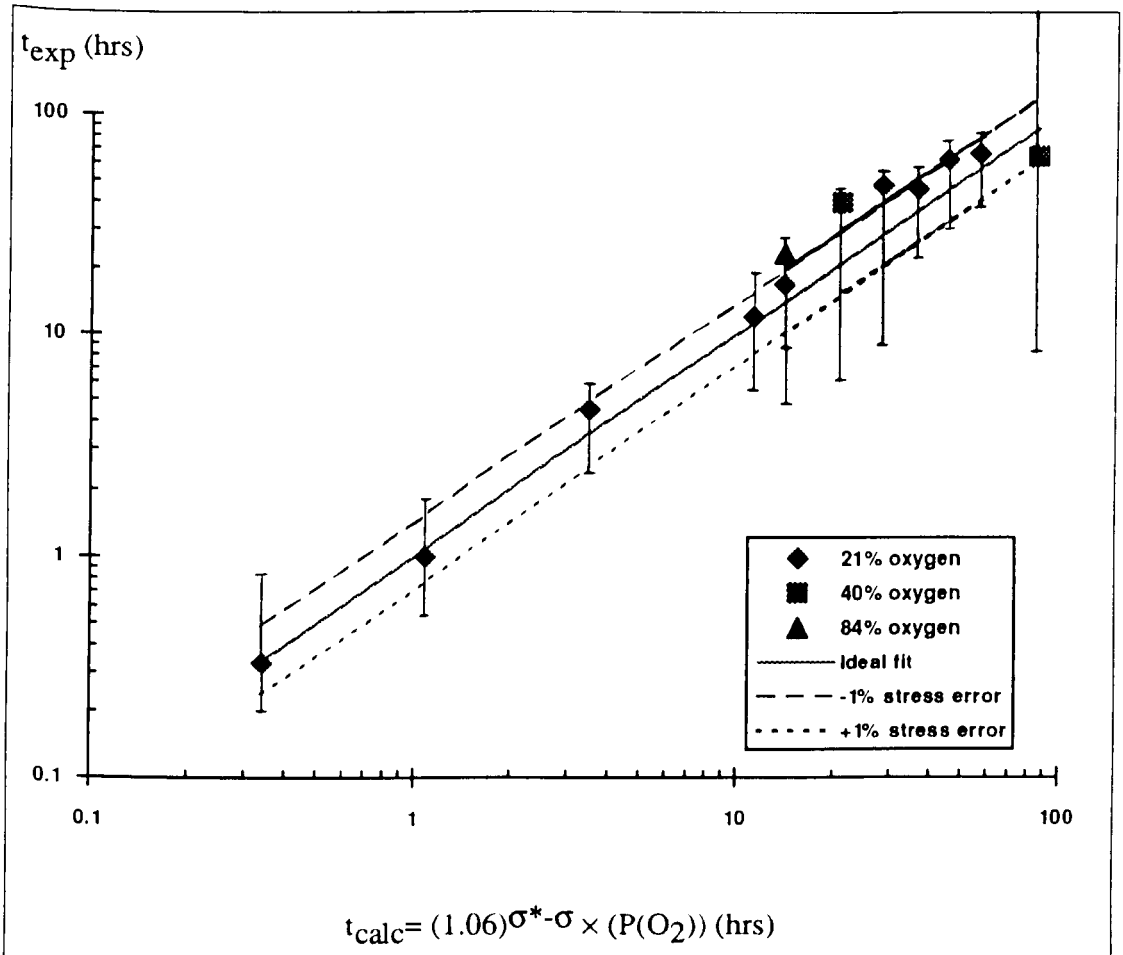

Figure VI.i. Plot of t_{exp} versus t_{calc} as calculated with equation (VI.13) for the hot-salt stress-corrosion cracking of IMI 834 in enriched oxygen air compositions

VI.b.5. Metallographic studies

Photograph VI.a. shows a general view of a typical hot-salt stress-corrosion failure. General corrosion and pitting were observed on the gauge length, and crack propagation was found to be generally intergranular and was accompanied by limited transgranular cleavage. Photograph VI.b. shows the existence of crack branching. These features are in good agreement with the observations made for other titanium alloys by previous workers (Turley 1966, Hatch 1966).

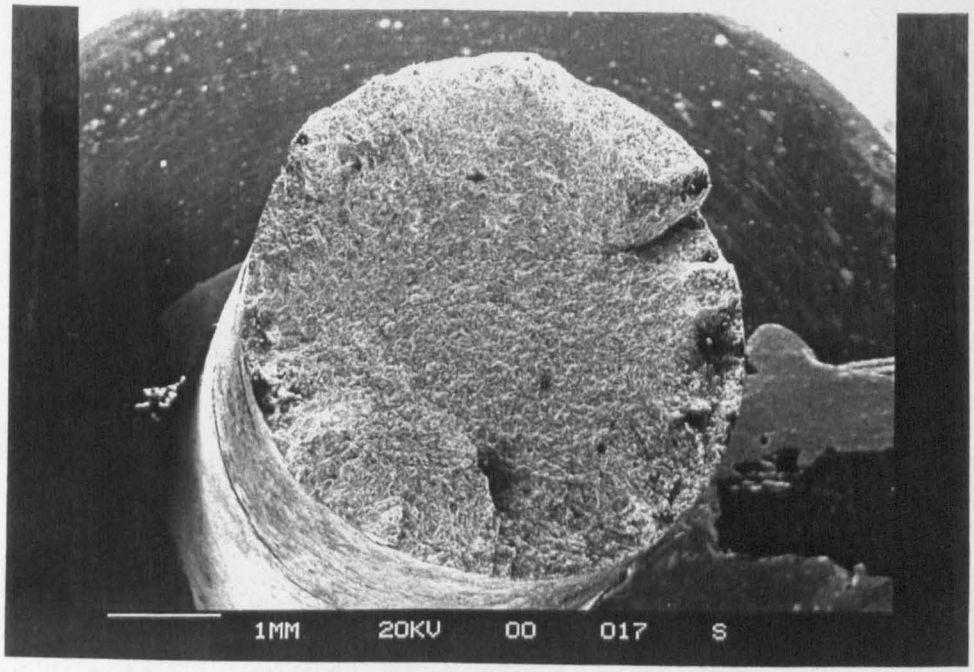

Photograph VI.a.: General view of a hot-salt stress-corrosion fracture surface.

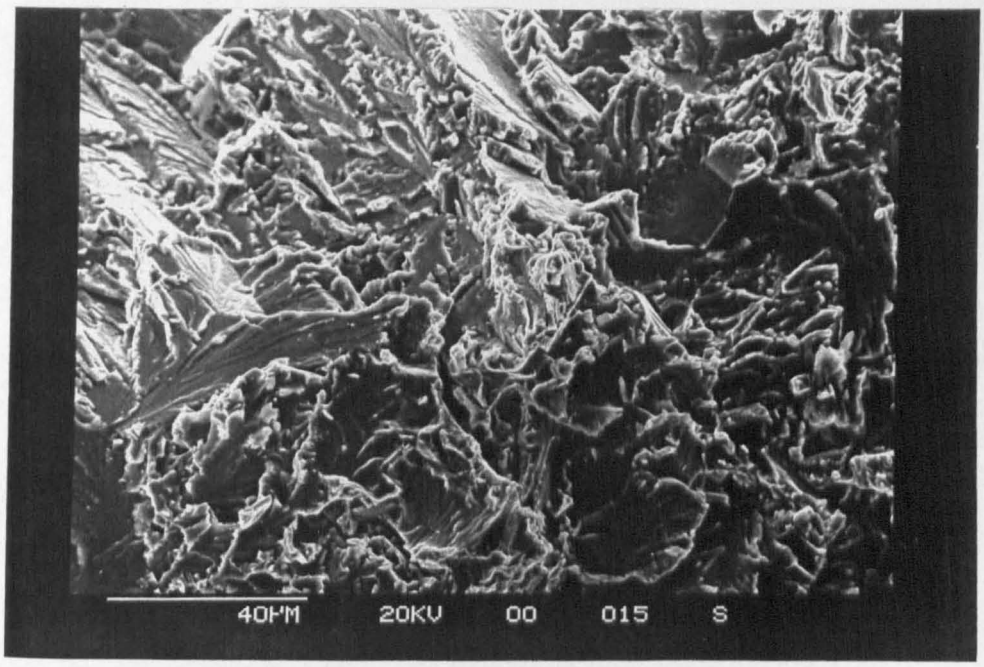

Photograph VI.b.: Evidence of crack branching during crack propagation.

Photograph VI.c. shows a view of the brittle outer zone which was formed during the early stages of crack initiation and propagation. The nucleus of the crack was found to be beneath a salt deposit, and this area is actually typical of the HSSCC process. Photograph VI.d. shows that away from this zone, fracture is accompanied by the formation of dimples and is therefore ductile. This zone is in fact produced by overloading after the HSSCC mechanism has reduced the load bearing area of the specimen and is therefore not linked to the hot-salt stress-corrosion phenomenon itself. Further metallographic studies on hot-salt stress-corroded samples will be discussed in a later part of this chapter, since it is necessary at this point of the study to introduce other metallurgical concepts which have been revealed by the thermogravimetric studies before discussing fully the fracture mechanisms observed in the presence of an applied stress.

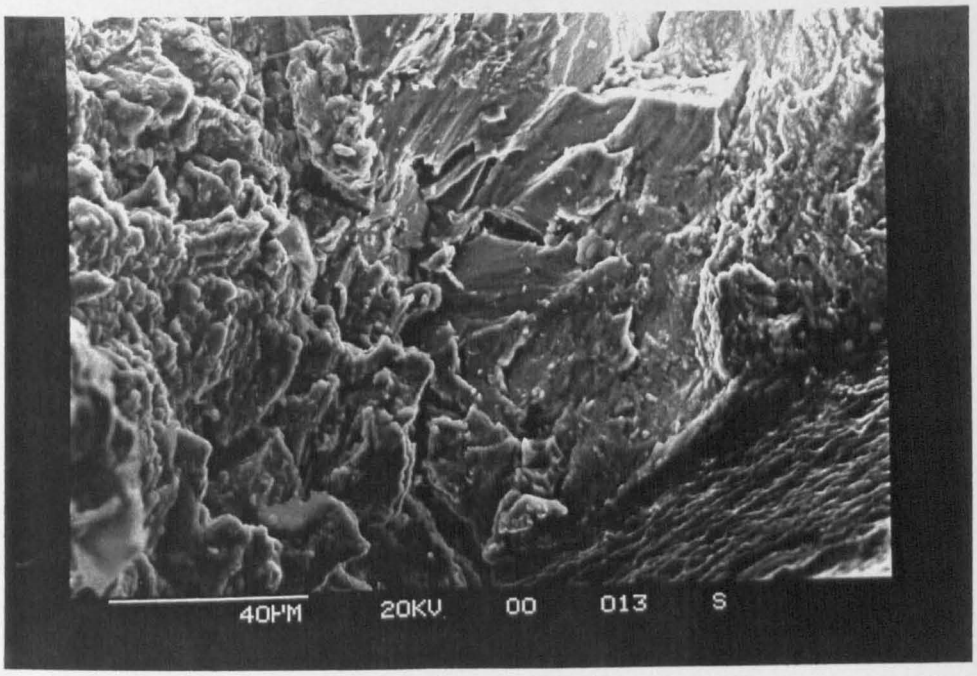

Photograph VI.c.: View of the outer brittle zone produced by HSSCC mechanisms.

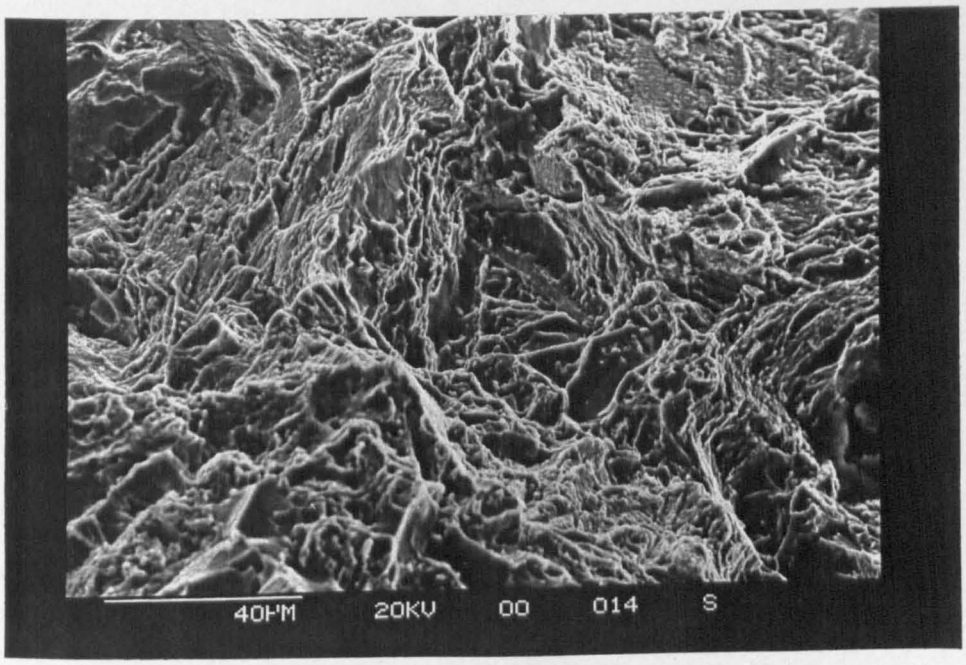

Photograph VI.d.: View of the ductile zone produced by overload of the specimen after HSSCC

VI.c. Thermogravimetric studies

VI.c.1. Introduction

The thermogravimetric studies were designed in order to gather information on the kinetics of salt attack of titanium alloy IMI 834 at elevated temperatures. Chapter V showed that the oxidation of the material in the range 525 °C to 675 °C is governed by a parabolic rate law and that significant differences exist between the mechanisms of oxidation and hot-salt attack: Indeed, the mass gains measured with IMI 834 contaminated by salts exhibited an initial period which does not follow a parabolic law, and metallographic analysis of the corroded coupons showed that no alpha case could clearly be detected at the surface of the sample, for samples removed over this period.

These initial results show therefore the need for a more detailed analysis. The oxidation behaviour of IMI 834 as determined in the course of this study will be characterised further and compared with this observed by other workers for other titanium base materials. A more accurate analysis of the hot-salt characteristics of IMI 834 will then be carried out. These results will be discussed using metallographic evidences in order to provide information on the mechanisms by which titanium alloys are attacked by hot-salt.

VI.c.2. Oxidation studies

Chapter V showed that the oxidation behaviour of IMI 834 follows a classic parabolic law of the form:

$$X^2=Kp\times t+C \qquad \textbf{(VI.17)}$$

where:

X represents the mass gain in mg/cm^2

Kp is the parabolic rate constant in $mg^2.cm^{-4}.s^{-1}$

C is a constant in $mg^2.cm^{-4}$ (in this case, C=0 since $\Delta m=0$ at t=0)

Parabolic oxidation of titanium involves in fact two simultaneous processes: They are the growth of a stable oxide scale (i.e. TiO_2 also called rutile) at the surface of the material, and the solution of oxygen into the base metal (i.e. formation of alpha case).

Since both mechanisms are parabolic, the overall behaviour of pure titanium during oxidation above 600 °C is also parabolic (Kofstad 1966). Hence the thermogravimetric measurements carried out during this study represent the overall oxidising process, that is formation of rutile and formation of alpha case, while alpha case measurements describe the amount of oxygen dissolution involved during each exposure.

The oxidation of titanium alloys is similar to that of pure titanium. However it has been mentioned in the literature that for alloyed titanium, and especially when aluminium constitutes the main alloying addition, the temperature range over which oxidation is governed by a parabolic rate law is extended to lower temperatures (Chaze 1990). It is therefore expected that in the case of IMI 834, parabolic oxidation should occur at temperatures below 600 °C, since the alloy comprises about 6 %wt aluminium. In fact the results described in Chapter V showed that parabolic oxidation was observed at temperatures as low as 525 °C.

Figure VI.j. shows a superposition of the two arrhenius plots shown previously in Chapter V which were obtained through mass gain data (see Figure V.f.) and alpha case measurements (see Figure V.g.). These two lines can be compared by comparing their slopes observed in Figure V.j. which characterise the activation energy of titanium for the process considered through the following relationship:

$$\frac{d(Log(Kp))}{d\left(\frac{1}{T}\right)} = -\frac{\Delta G}{2.303R} \times 10^4 \qquad \textbf{(VI.18)}$$

where:

ΔG is the activation energy for the process characterised by the line in J/mole

R=8.32 J/mole/°K is the gas constant

Although several physical interpretations for the meaning of the activation energy have been given by previous workers, the relationship between ΔG and the physical oxidation process is still not fully understood. However as a rule, the activation energy remains constant as long as the same rate-determining oxidation process prevails.

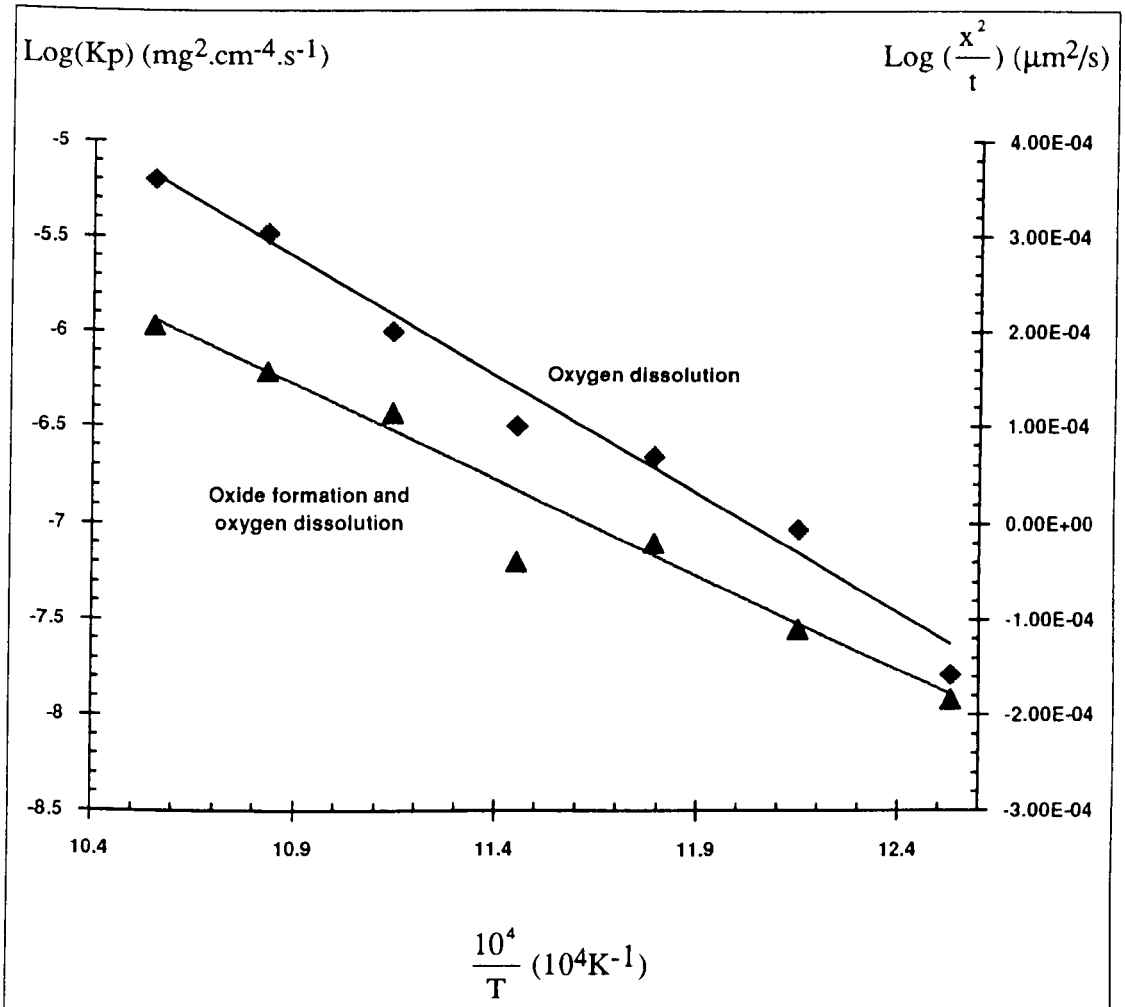

Figure VI.j.: Superposition of arrhenius plots for oxygen solution and total oxidation behaviour for the oxidation of IMI 834 between 525 °C and 675 °C.

The activation energies corresponding to the two lines obtained in Figure VI.j. were calculated through regression analysis. The following values were thus obtained:

ΔG_{tot}=-190 kJ/mole for the total oxidation process (i.e. for mass gain data)
ΔG_{α}=-171 kJ/mole for oxygen solution (i.e. for alpha case data)

One can therefore conclude that oxygen solution represents an essential part of the oxidation of IMI 834 between 525 °C and 675 °C. This correlates well with the theoretical calculations mentioned by Kofstad (Kofstad 1988).

The value obtained for the activation energy based on mass gain data of IMI 834 was compared to these obtained by other workers. Figure VI.k. shows mass gain data on

the oxidation of titanium and its alloys available from the literature. Although no data is currently available in the open literature on IMI 834, one can observe that apart from the point obtained at the lower temperature of 525 °C, the results of the current study are contained within the general scatter associated with continuous thermogravimetric techniques on other titanium materials (pure titanium, CP 130, IMI 685).

Since oxygen solution is not the only oxidation process occurring in IMI 834 for the temperature range studied, Scanning Electron Microscope studies were carried out in order to verify the presence of oxide at the surface of the material. Photographs VI.e. to VI.g. show the surface of coupons exposed to 525 °C, 600 °C, and 675 °C respectively. One can notice that a thin oxide layer is produced at the surface of IMI 834 during exposure at these temperatures. Although these oxide layers are fairly irregular, their thickness was evaluated. Measurements gave values of about 0.29 μm, 1.9 μm, and 2.5 μm for 525 °C, 600 °C, and 675 °C respectively. As expected, the thickness of the oxide layer formed at the surface of the material during oxidation increases therefore with increasing exposure temperatures. The activation energy for the oxide growth during exposure was also calculated as an aproximation from theses data. The value obtained is:

ΔG_{oxi}=-184 kJ/mole for the formation of a stable oxide layer

This activation energy is closer to the activation energy for the overall oxidation process than that of oxygen solution. This means that the formation of a stable oxide layer is the predominant process occurring during oxidation of IMI 834 in the temperature range considered.

The results discussed above show that the oxidation mechanism for IMI 834 is similar to that of pure titanium or other titanium systems, although the rates of oxidation will vary from alloy to alloy. The overall oxidation kinetics of the material in the temperature range 525 °C to 675 °C is governed by a parabolic rate law. Oxygen solution constitutes a significant part of the overall oxidation process at these temperatures and increases with increasing temperature. During oxidation, a thin oxide layer is formed at the surface of the material. The thickness of this layer also increases with increasing temperature, with the mass associated to oxide scale formation increasing more rapidly with increasing temperature, than for oxygen solution.

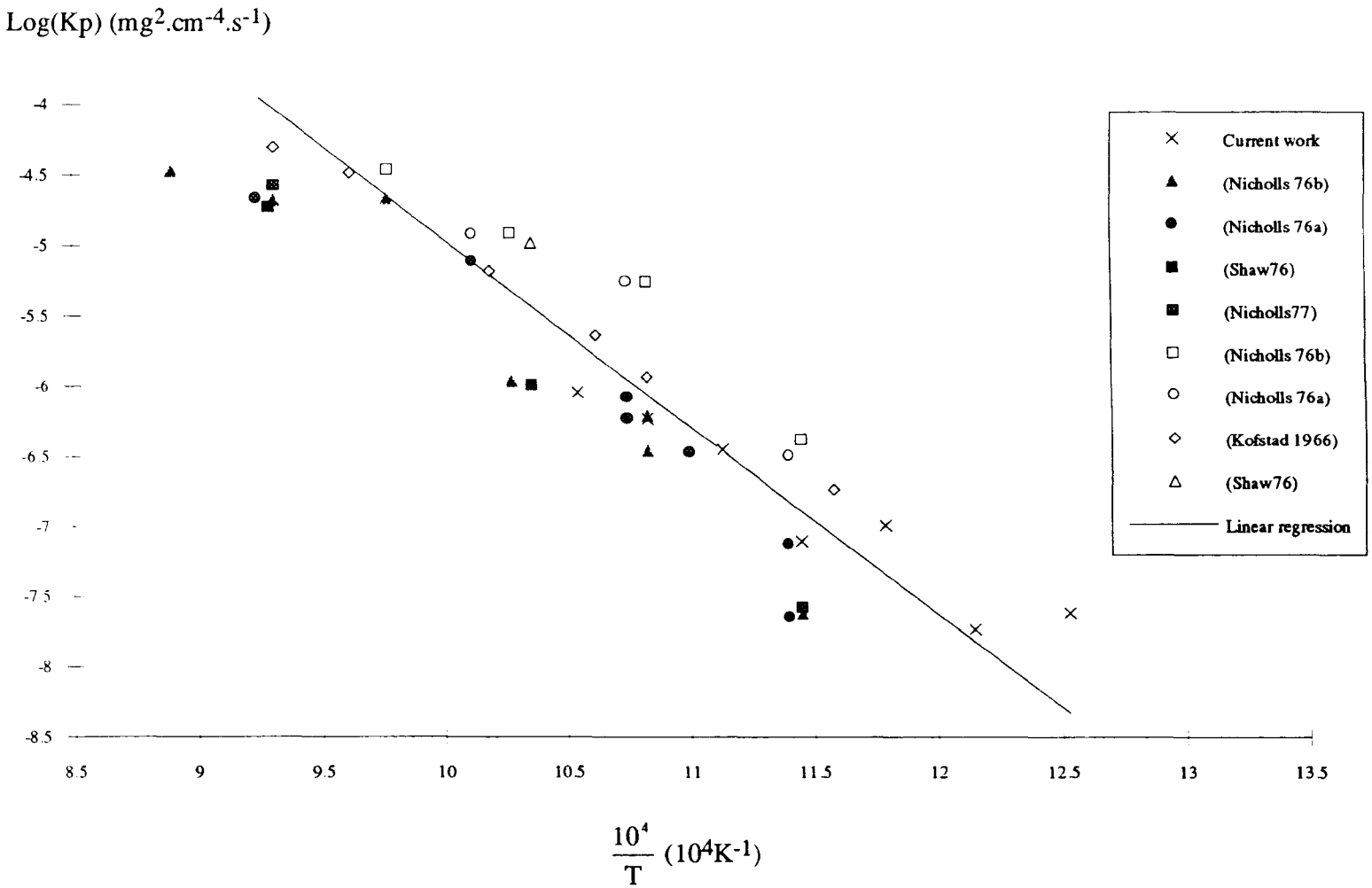

Figure VI.k.: Comparison of the oxidation mass gain data obtained during this study with data obtained by previous workers. The filled markers represent data points for IMI 685, and the unfilled markers for commercially pure titanium.

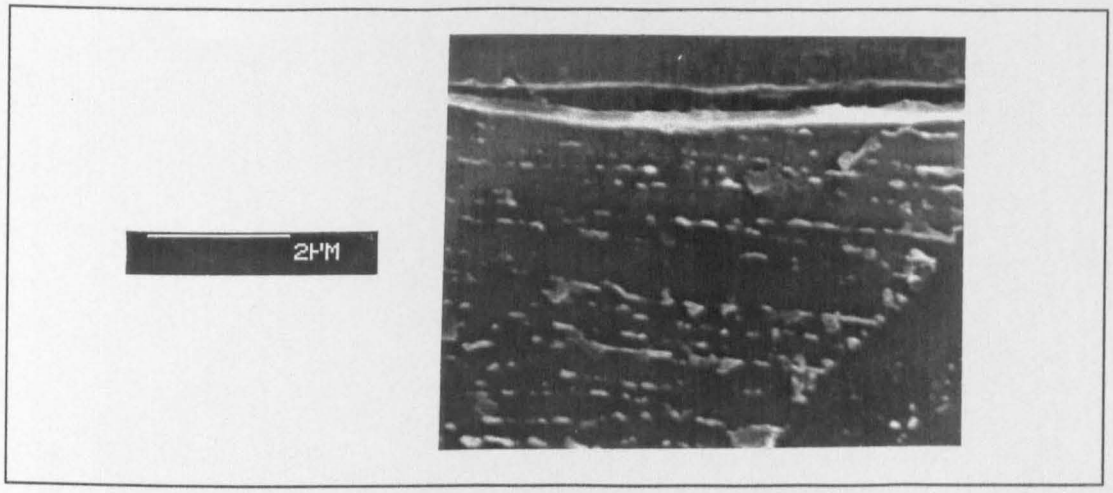

Photograph VI.e.: Oxide layer (0.25 µm) formed during 100 h exposure at 525 °C

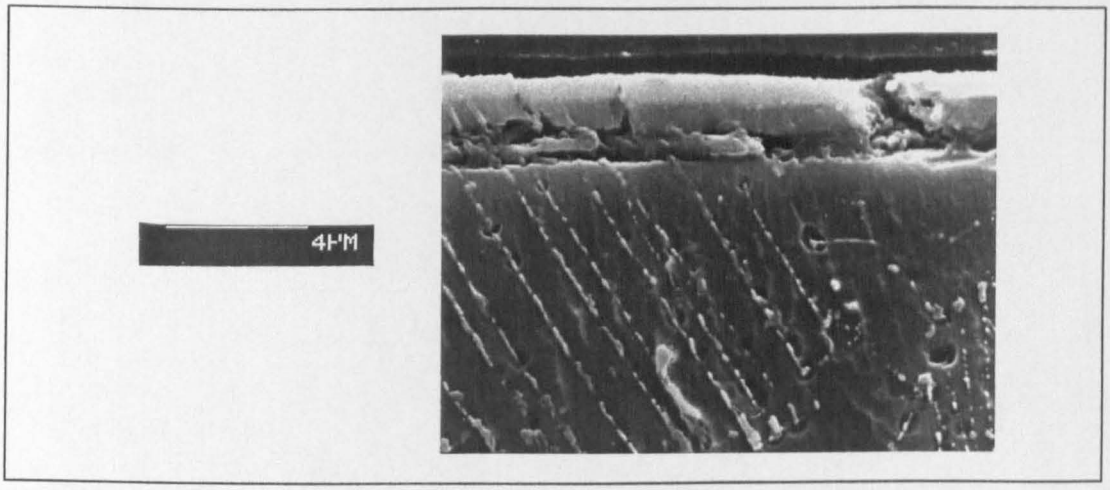

Photograph VI.f.: Oxide layer (1.9 µm) formed during 100 h exposure at 600 °C

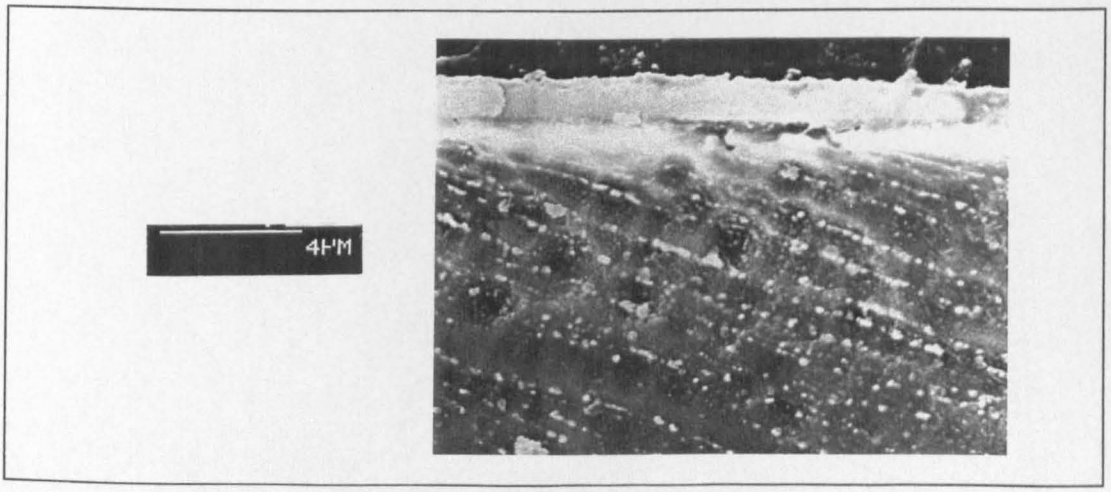

Photograph VI.g.: Oxide layer (2.5 µm) formed during 100 h exposure at 675 °C

VI.c.3. Salt-corrosion studies

Chapter V showed that the hot-salt corrosion characteristics of IMI 834 differed from its oxidation characteristics. The two main features which were identified were that:

-1- Salt-corrosion is not governed by a classic parabolic law, especially during the first few hours of exposure.

-2- No alpha case formation was detected on the sample, implying that oxygen solution does not constitute a significant part in the salt-oxidation process, or that alpha case was consumed at some stage during exposure.

The differences between the continuous thermogravimetric behaviours of IMI 834 in oxidising and salt-corrosion atmospheres are obvious from Figure VI.l. which shows a superposition of the two curves obtained. Indeed, the curve representing hot-salt corrosion conditions can be separated in three main parts:

-1- An initial accelerated mass gain which is not governed by a parabolic law and which is extremely rapid (two to four hours).

-2- Between four and fifteen hours of exposure, the mass gains observed are extremely low. They seem to stabilise at the beginning of this period, and then, present a steady increase

-3- After about fifteen hours, the mass gain seems to be governed by a parabolic rate law similar to that observed during classic oxidation, but at increased rates.

The same characteristics were observed on all the continuous thermogravimetric curves obtained for the salt-corrosion of IMI 834 in the temperature range 500 °C to 675 °C. These effects can be more readily observed on Figure VI.m. which presents a plot of the square of mass gain versus time of exposure for the test carried out at a temperature of 625 °C.

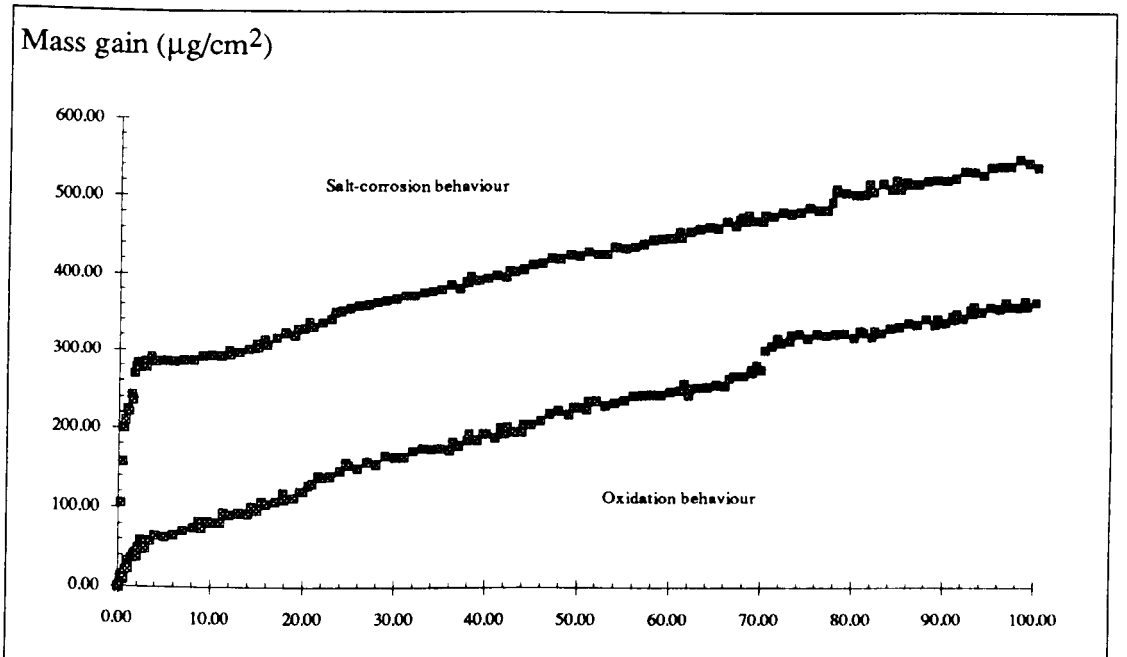

Figure VI.l.: Superposition of the continuous thermogravimetric curves obtained for the oxidation and the salt-corrosion of IMI 834 at 625 °C

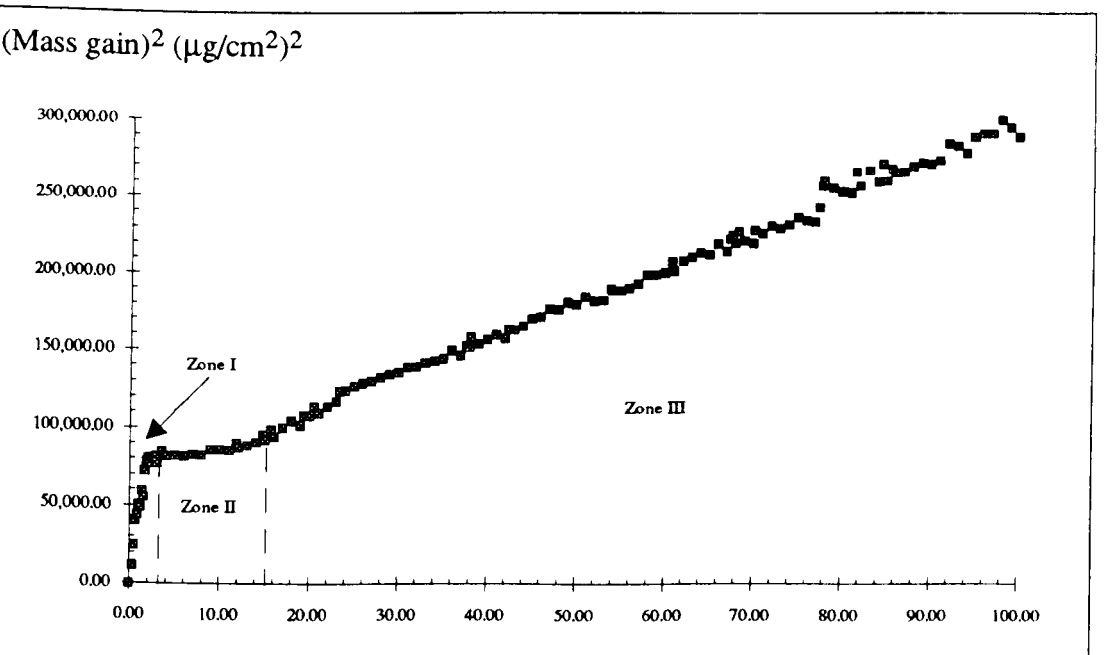

Figure VI.m. Plot of the square of mass gains versus time of exposure for the salt-corrosion of IMI 834 at 625 °C

A detailed thermogravimetric and metallographic analysis of zones I and III was carried out for each exposure temperature in order to define more accurately the characteristics of the hot-salt attack of IMI 834. Again, the same features were observed for all temperature in the range 500 °C to 675 °C :

Zone I: The first two to five hours of exposure constitute the main difference between the oxidation and the salt-corrosion behaviour of the material. Hence, the mass gains observed during this initial process are typically between six to ten times these detected for similar exposure times during normal oxidation. Attempts were made to determine whether these mass gain differences between oxidation and salt-corrosion observed during this early period could be related to the test temperature, but they proved unsuccessful, probably due to the scatter encountered in the oxidation data measured.

Attempts were also made to try to identify whether a classic oxidation rate law prevails in zone I. Regression analysis on the data points tend to show that mass gains are actually governed either by a parabolic or by a linear rate law in this region. However due to the small amount of measurements available during this initial exposure, it was not possible to identify accurately either of these two processes as rate controlling.

Photograph VI.h. and VI.i. show typical features encountered on a salt-corroded coupon exposed for only one hour only in a still air furnace at 600 °C and provide extremely important information on the processes that are prevailing during the initial stage of hot-salt attack on IMI 834. Indeed, one can observe the existence of long, straight, and narrow voids, or channels which extend deep into the alloy. Photograph VI.i. also shows that these channels change direction and can occasionally form a network in heavy salt-corroded areas. This "tunnelling" characteristic has been observed in recent studies of the high temperature oxidation/chlorination of binary nickel/chromium alloys (Al Khyat 1991) and is here extremely developed.

The importance and formation of these channels will be discussed in the final part of this chapter. However, their existence constitute a unique and preferential path for volatile species to gain immediate access to the base alloy. This is of particular interest with regards to the extent of damage that can be caused during hot-salt stress-corrosion cracking of IMI 834 in extremely short times: The shortest life recorded during this work was indeed of 20 minutes. This indicates that the initial stages of the

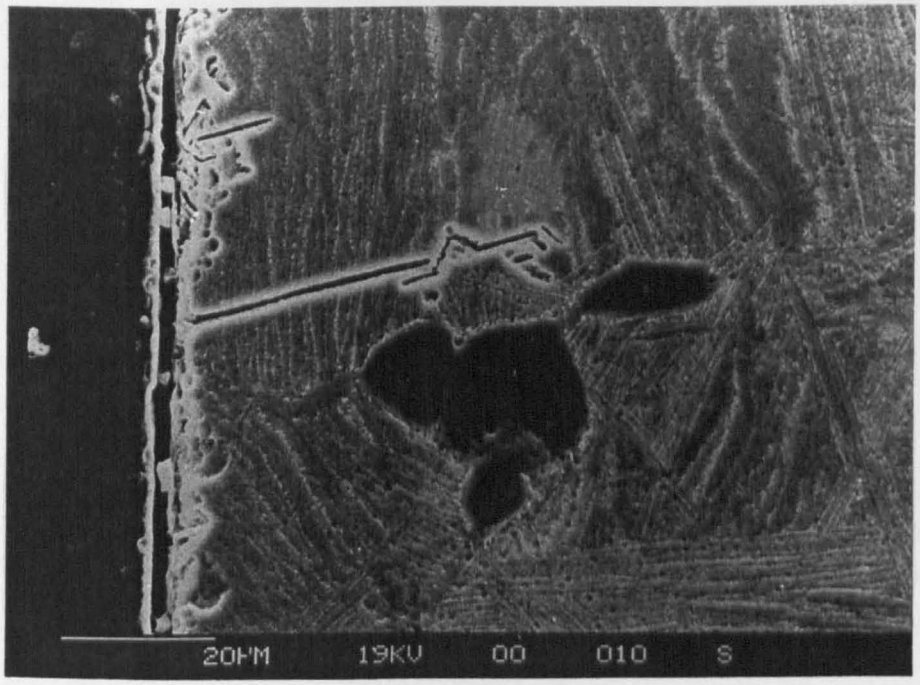

Photograph VI.h.: Cross section of salt corrosion coupon exposed for 1 h at 600 °C showing the presence of channels formed during the initial stage of hot-salt attack of IMI 834.

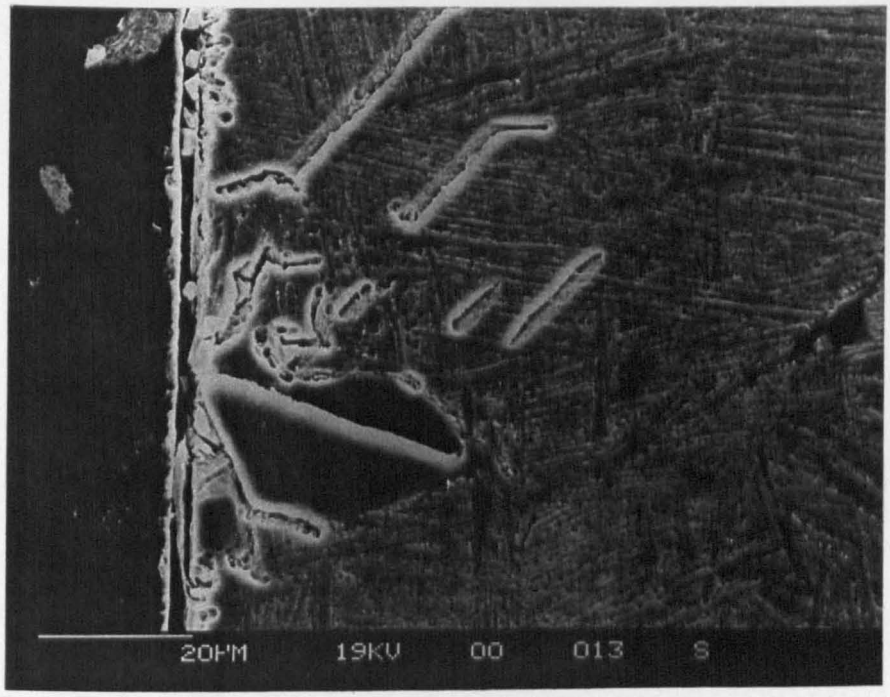

Photograph VI.i.: Cross section of salt corrosion coupon exposed for 1 h at 600 °C showing a network of channels in a heavy salt-corroded area

corrosion process have to provide ways of damaging the material very quickly. The coexistence of chlorides and diffusion channels which extend deep into the alloy provide a most likely explanation for the dramatic failures observed under stress.

Zone 3: The preceding paragraph showed the importance of the first few hours of the corrosion process in the hot-salt attack of IMI 834. It is now of interest to observe the mechanisms prevailing after longer exposures. One can notice in Figure VI.l. that in zone 3, the thermogravimetric behaviour of IMI 834 undergoing salt attack is remarkably similar to this prevailing during oxidation in air. Figure VI.m. also clearly shows that after about a fifteen hours exposure, the mass gains recorded are actually governed by a parabolic rate law (i.e. a plot of the square of the mass gains versus the time of exposure reveals a straight line).

A detailed analysis of the mass gains observed in zone 3 was therefore carried out for each of the temperatures used in the course of this study. Parabolic rate constant were calculated for each test through regression analysis, and an Arrhenius plot for the parabolically dominated part of thermogravimetric hot-salt corrosion curves was produced. This plot was superposed on that obtained for the oxidation studies as shown in Figure VI.n.

This superposition actually shows that although both processes are parabolic, their activation energies are different. This difference in the activation energy of IMI 834 between oxidation in air and zone III salt-corrosion seems therefore to point out that although both phenomena are parabolic, they are not controlled by the same rate limiting process. Hence the existence of channels in hot-salt corroded specimens would mean that the diffusion of gases into the base metal is significantly faster than for the normal oxidation process. This explains why the mass gains observed during zone III salt-corrosion are significantly higher than for oxidation, and why the temperature dependence of zone III salt-corrosion is less marked. Hence, if the mass gains become similar at higher temperatures, the presence of channels during salt-corrosion will allow the material to acquire higher mass gains for similar exposure times than during oxidation in the lower temperature range.

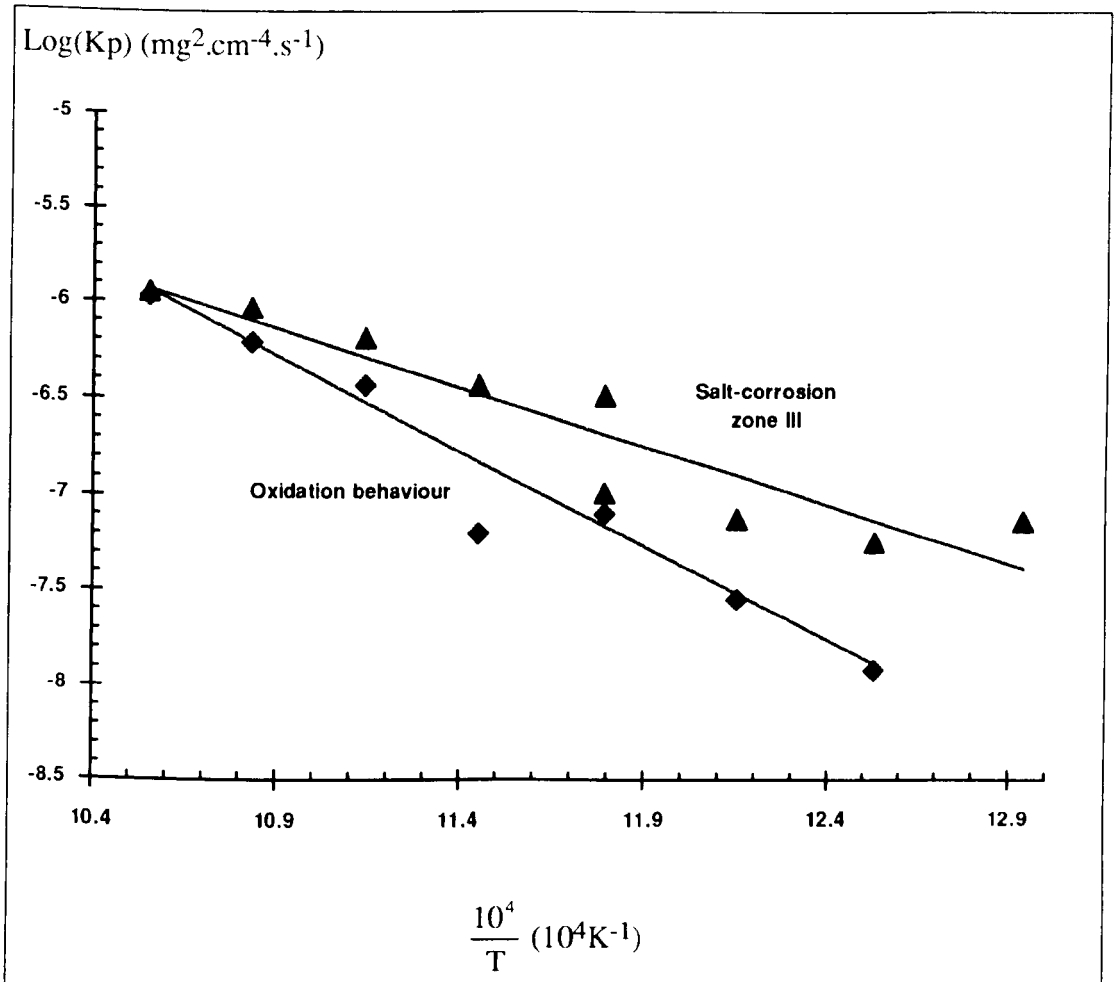

Figure VI.n.: Superposition of Arrhenius plots obtained from mass gain data for oxidation and zone III salt-corrosion of IMI 834 between 525 °C and 675 °C.

Furthermore similar metallographic studies to these described above were completed on salt corrosion coupons exposed for one hundred hours. Hence it can be seen in photographs VI.j. and VI.k. that after one hundred hour exposure at 600 °C, a thick oxide layer is formed at the surface of the material. This oxide layer showed evidence of cracking and is porous. This observation, and the fact that alpha case was not clearly detected on these samples clearly show that the process is now dominated by the formation of a stable oxide at the surface of the material rather than oxygen solution which constituted the prevailing process in the case of oxidation in air.

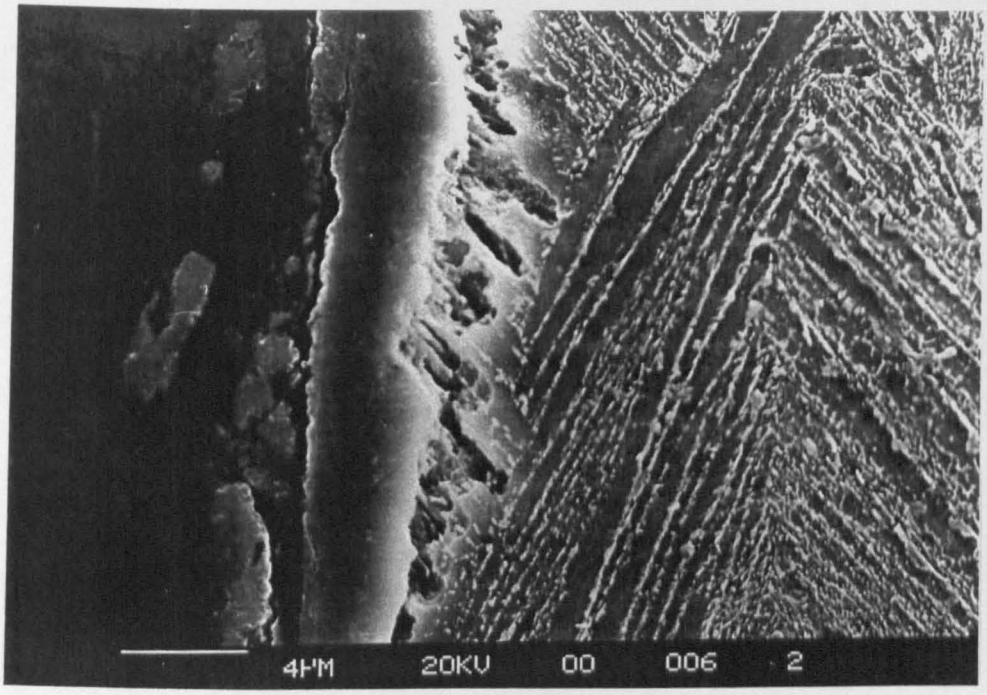

Photograph VI.j.: Photograph of the corrosion scale after 100 h exposure to salt-corrosion at 600 °C showing the formation of a stable oxide and the presence of channels.

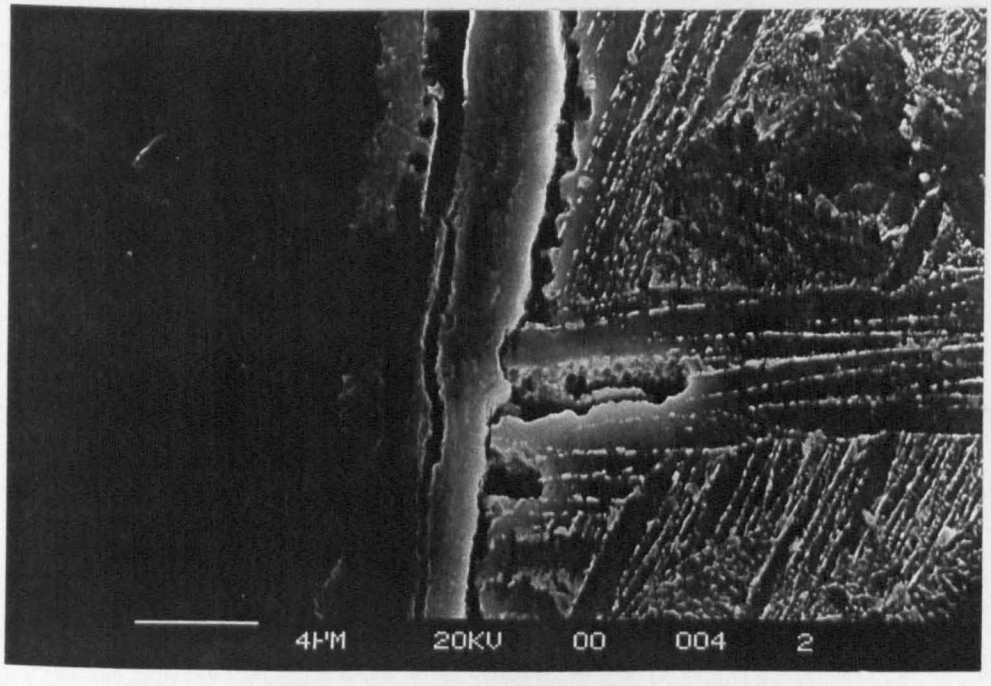

Photograph VI.k.: Typical channel observed after 100 hours exposure to salt-corrosion at 600 °C

Another remarkable feature which can be noticed on Figures VI.l. and VI.m. relates to the aspects of the channels discussed previously: Firstly, it is obvious that these pores are considerably shorter (in fact one tenth to one twelth of the length) than these observed in zone I of the thermogravimetric curve. Actually, no pore that extend deep into the alloy could be detected after the one hundred hours exposure at any temperature. Secondly, these pores now look rough edged, and their surface is oxidised. These characteristics seem to indicate that the channels formed during the first few hours of exposure have been blocked by the precipitation of stable oxides and consumed from the surface as the salt-corrosion process progressed.

Zone II: The information gathered on zones I and III processes suggest that the pores formed during the first few hours of exposure have a limited depth penetration into the alloy. When this limit is reached, stable oxides will precipitate and the channels will be consumed from the surface. Zone two can be interpreted as a transition period between zone I and zone III. This would also explain why the mass gains measured during this time are extremely low.

The thermogravimetric studies which were carried out in the course of this study accompanied by basic metallography have been extremely useful and allowed a detailed characterisation of the processes which are controlling the salt attack of IMI 834 at elevated temperature. An obvious correlation can be made between continuous mass gain measurements and the features observed on the cross section of hot-salt corroded samples. They showed the importance of the first few hours of exposure of the material to hot-salt environments where channels which extend deep into the base alloy are formed. These channels can therefore constitute preferential rapid diffusion paths which could provide vapour chlorides with a way to gain access extremely quickly to the base material. This is of considerable interest when one considers the rapidity of hot-salt stress-corrosion failures as observed during laboratory testing.

VI.d. Thermodynamic studies

So far this work has been focused on two major aspects of the hot-salt stress-corrosion cracking of IMI 834: Firstly, high pressure studies demonstrated that partial pressure of oxygen has a significant effect on the life of the material. Secondly, kinetic studies showed that salt attack of the alloy is extremely rapid and results in the formation of channels which constitute a unique diffusion path for volatile species to migrate from deep within the alloy to the oxide/metal interface.

With a view to proposing a model for the HSSCC of IMI 834, it is now necessary to examine closely the chemical reactions which may be involved during exposure. Hence some of the questions which have to be raised are:

-1- What is the role of oxygen and water vapour?

-2- Why is pure titanium immune to HSSCC?

-3- Are any volatile products produced during HSSCC and what are they?

-4- How are the pores formed?

-5- Why does increased partial pressure of oxygen extend the life of the material?

To answer these questions, theoretical studies involving the calculation of Phase Stability Diagrams (PSD) from thermodynamic data available in the open literature were carried out. Phase stability diagrams are commonly used in the aerospace industry to characterise metallurgical equilibria involving reactions between a solid metal and a two gas atmosphere but have not yet been applied to corrosion phenomena related to titanium.

The first part of this paragraph gives a brief reminder of basic principles of the thermodynamics of gas/metal reactions while the second part will explain the construction of PSD's. The last part will present the phase stability diagrams which have been calculated for the systems $Ti/O_2/Cl_2$, $Al/O_2/Cl_2$, and $Sn/O_2/Cl_2$ and discuss the information which can be obtained from these PSD's with a view to developing a model for the hot-salt stress-corrosion cracking of titanium alloys.

VI.d.1 Basic thermodynamics of gas/metal reactions

A number of basic thermodynamic functions can be used to characterise the reactions occurring between gases and metals. They include the free energy of formation of metallic species, the activity of reactants and products of a given equilibrium, and the equilibrium constant of such reactions.

If a chemical reaction between a solid metal and a given gas involves the production of solid compounds, it can be described by:

$$xM_{(s)} + yX_{2(g)} \longrightarrow xMX_{z(s)} \qquad \textbf{(VI.19)}$$

where $z = \frac{2y}{x}$

Spontaneous formation of $MX_{c(s)}$ will occur if the free energy of formation ΔG^0 is negative and equilibrium will be reached when $\Delta G^0=0$. Positive values of Gibbs energy imply that the reaction considered is thermodynamically impossible. The value of ΔG^0 can in fact be calculated for reaction (VI.19) as follows:

$$\Delta G^0 = x\Delta G^0(MX_{z(s)}) - x\Delta G^0(M_{(s)}) - y\Delta G^0(X_{2(g)}) \qquad \textbf{(VI.20)}$$

where $\Delta G^0(MX_{z(s)})$, $\Delta G^0(M_{(s)})$, and $\Delta G^0(X_{2(g)})$ can be obtained from tabulated data. Reaction (VI.19) is also characterised by its equilibrium constant:

$$K = \frac{a(MX_{z(s)})^x}{a(M_{(s)})^x \times a(X_{2(s)})^y} \qquad \textbf{(VI.21)}$$

where $a(MX_{z(s)})$, $a(M_{(s)})$, $a(X_{2(g)})$ are the activities of the species involved in the reaction. At the equilibrium, the standard free energy of formation and the equilibrium constant are related by the following relationship:

$$\Delta G^0 = -2.303RT \times Log(K) \qquad \textbf{(VI.22)}$$

where

R=8.314 J/°K.mole is the gas constant

T is the temperature in °K

Substituting (VI.21) in (VI.22), one obtains:

$$\Delta G^0 = -2.303RT \times Log\left(\frac{a(MX_{z(s)})^x}{a(M_{(s)})^x \times a(X_{2(g)})^y}\right) \qquad \textbf{(VI.23)}$$

When the reacting metal and the product form in their standard state, $a(M_{(s)})=1$ and $a(MX_{z(s)})=1$. Furthermore, the activity of the reacting gas is $a(X_{2(g)})=P(X_{2(g)})$. Thus equation (VI.23) can be re-written as:

$$\Delta G^0 = 2.303RT \times Log(P(X_{2(g)})^y) \qquad \textbf{(VI.24)}$$

VI.d.2. Thermodynamic consideration for the system $M/O_2/Cl_2$ and calculation of Phase Stability Diagrams

The phase stability diagram for the system $M/O_2/Cl_2$ is a plot of the thermodynamically stable phases formed by the three reactants as a function of the two gas atmosphere composition. Hence, they represent the most stable reactions that are likely to occur when the metal is exposed to a two gas mixture environment. This approach, which was developed by Giggins (Giggins 1980) has been used for this study in order to characterise the likeliness of chemical reactions put forward by previous workers for the hot-salt stress-corrosion of titanium alloys.

Formation of solid metallic oxides and chlorides:

These reactions can be described as follows:

Oxidation: $$M_{(s)} + \frac{1}{2}O_{2(g)} \xrightarrow{T} MO_{(s)} \qquad \textbf{(VI.25)}$$

Chlorination: $$M_{(s)} + Cl_{2(g)} \xrightarrow{T} MCl_{2(s)} \qquad \textbf{(VI.26)}$$

At the equilibrium, one can write using equation (VI.24):

$$\Delta G^0 = 2.303RT \times Log(P(O_2)^{\frac{1}{2}}) \qquad \textbf{(VI.27)}$$

and: $$\Delta G^0 = 2.303RT \times Log(P(Cl_2)) \qquad \textbf{(VI.28)}$$

Rearranging these equations, one obtains:

$$Log(P(O_2)) = \frac{2\Delta G^0}{2.303RT} \qquad \textbf{(VI.29)}$$

and:
$$Log(P(Cl_2)) = \frac{\Delta G^0}{2.303RT} \qquad \textbf{(VI.30)}$$

where the standard free energy of formation for each of the reactions considered can be calculated using equation (VI.20) from tabulated values. Therefore, the partial pressure of oxygen at which the metal will start forming a stable solid oxide MO can be calculated. Similarly, the partial pressure of chlorine at which the metal starts forming a stable solid chloride MCl_2 is obtained. The next transitions which can be calculated can be described for example by the following reactions:

Oxidation:
$$2MO_{(s)} + \frac{1}{2}O_{2(g)} \xrightarrow{T} M_2O_{3(s)} \qquad \textbf{(VI.31)}$$

Chlorination:
$$MCl_{2(s)} + \frac{1}{2}Cl_{2(g)} \xrightarrow{T} MCl_{3(s)} \qquad \textbf{(VI.32)}$$

Using similar calculations to those described above one will obtained the values for the partial pressure of oxygen and chlorine where M_2O_3 and MCl_3 respectively will start forming.

Exchange reactions between solid oxides and solid chlorides:

These reactions occur when for example, the conditions become favourable to form a stable oxide from a solid chloride compound:

$$2MCl_{2(s)} + \frac{3}{2}O_{2(g)} \xrightarrow{T} M_2O_{3(s)} + 2Cl_{2(g)} \qquad \textbf{(VI.33)}$$

Using equation (VI.23) one obtains:

$$\Delta G^0 = -2.303RT \times Log\left(\frac{P(Cl_2)^2}{P(O_2)^{\frac{3}{2}}}\right) \qquad \textbf{(VI.34)}$$

and therefore:

$$\frac{3}{2}Log(P(O_2)) - 2Log(P(Cl_2)) = \frac{\Delta G^0}{2.303RT} \qquad \textbf{(VI.35)}$$

Rearranging this equation, one obtains the equation of a straight line:

$$Log(P(O_2)) = \frac{2\Delta G^0}{3 \times 2.303RT} + \frac{4}{3} Log(P(Cl_2)) \qquad \textbf{(VI.36)}$$

By calculating Log($P(O_2)$) for different Log($P(Cl_2)$), this line can be drawn on a Log($P(Cl_2)$) versus Log($P(O_2)$) plot.

Production of volatile chlorides in equilibrium with solid oxides:

When a solid oxide is stable in an oxygen/chlorine mixture environment, volatile metallic chlorides can be formed in equilibrium with the solid phase. The kind of reactions which must then be considered are of the form:

$$M_{(s)} + Cl_{2(g)} \xrightarrow{T} MCl_{2(g)} \qquad \textbf{(VI.37)}$$

By using equation (VI.23), one obtains:

$$\Delta G^0 = -2.303RT \times Log\left(\frac{P(MCl_2)}{P(Cl_2)}\right) \qquad \textbf{(VI.38)}$$

and therefore:

$$Log(P(Cl_2)) = \frac{\Delta G^0}{2.303RT} + Log(P(MCl_2)) \qquad \textbf{(VI.39)}$$

Therefore, by imposing an arbitrary value for the activity of $MCl_{2(g)}$, one can draw a line on a plot of Log($P(Cl_2)$) versus Log($P(O_2)$) where significant amounts of volatile metallic chlorides are formed in equilibrium with the stable oxide.

Figure VI.o. shows the typical trends of a phase stability diagrams for the system $M/O_2/Cl_2$. The transitions described above are indicated on this graph.

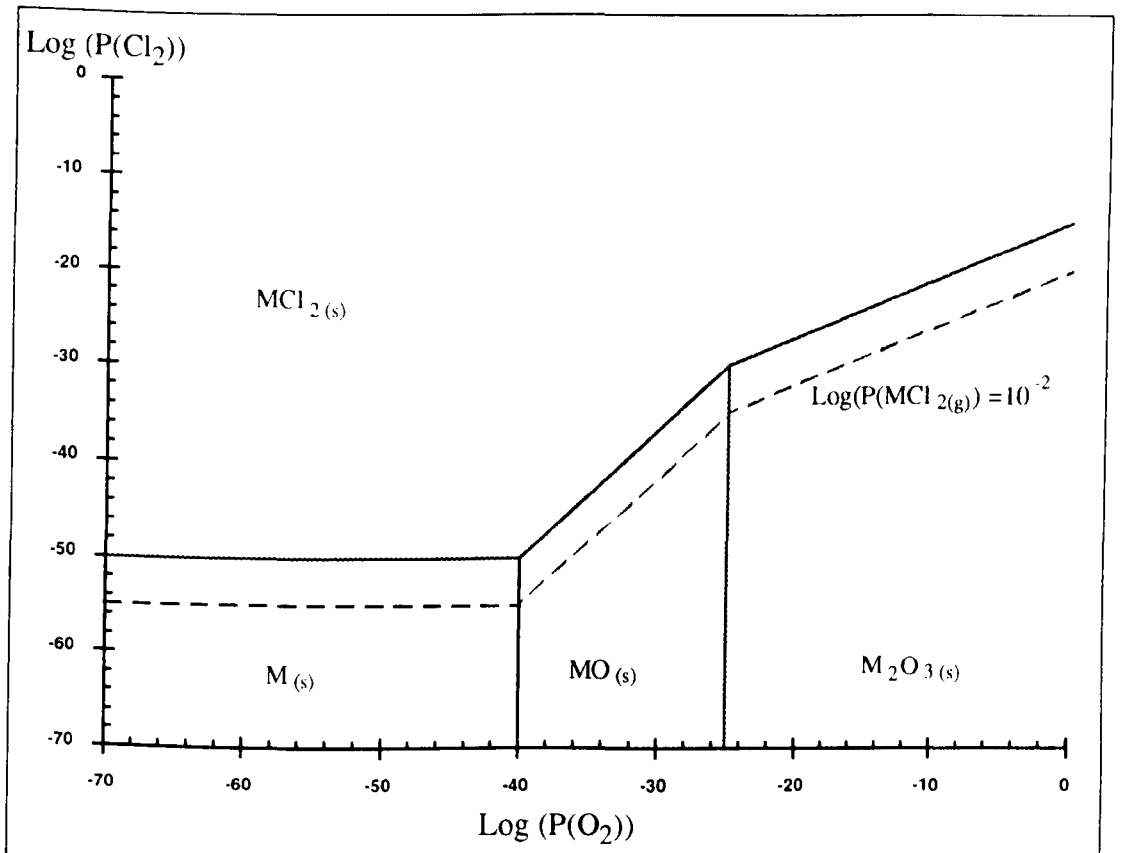

Figure VI.o.: Typical features of a phase stability diagram for the system $M/O_2/Cl_2$

VI.d.3. Thermodynamic analysis for the systems $Ti/O_2/Cl_2$, $Al/O_2/Cl_2$, and $Sn/O_2/Cl_2$

In order to identify the phases which titanium, aluminium, and tin may form during exposure to oxygen and chlorine, the phase stability diagrams for the systems $Ti/O_2/Cl_2$, $Al/O_2/Cl_2$, and $Sn/O_2/Cl_2$ were calculated. The temperature which was considered for this work is 500 °C, and the activities of the metals were taken as their weight content in IMI 834, that is 0.9 for titanium, 0.058 for aluminium, and 0.035 for tin. The data used to calculate these PSD's has been taken from one source only in order to ensure compatibility of the tabulated values of the standard free energy of formation of the phases considered (JANAF 1975).

System $Ti/O_2/Cl_2$:

Figure VI.p. shows the phase stability diagram obtained for the system $Ti/O_2/Cl_2$. The calculation of the different boundaries have been carried out using the procedures described in the preceding paragraph. Figure VI.p. shows that upon exposure to an

oxygen/chlorine gas mixture, titanium will form a series of stable solid oxides ranging from TiO to TiO_2 as well as solid titanium dichloride and trichloride. However, it clearly shows that at the surface of the material, that is around $Log(P(O_2))=0$, a stable layer of rutile should be produced. The series of diagonal transitions on the diagram show that solid $TiCl_2$ or $TiCl_3$ are thermodynamically stable, provided that the partial pressure of oxygen is reduced significantly. This means that titanium dichloride or trichloride can therefore not be produced at the surface of the material, where high partial pressures of oxygen prevail.

However, titanium dichloride and trichloride could actually be thermodynamically stable as one travels inwards through the oxide scale and towards the bare metal. Hence, the oxygen activity nearer the metal/scale interface is expected to be reduced significantly by the presence of the oxide scale/metal equilibria, while the chlorine activity is expected to remain largely unaffected. This means that the formation of solid $TiCl_2$ or $TiCl_3$ will progressively be thermodynamically encouraged at the expenses of solid oxides. In particular, this will be the case at the metal/scale interface if the chlorine activity is greater than 10^{-27} atmospheres. Unfortunately, the calculation of chlorine activity through the corrosion scale of hot-salt stress-corrosion exposed specimens is not possible since chlorine is produced from the salt deposits at the scale/atmosphere interface. However, this diagram allows one to characterise the nature of the scale formed in a qualitative way that is useful in terms of chemical reactions' prediction.

The dotted line which was drawn on Figure VI.p. represents the amount of volatile titanium tetrachloride formed in equilibrium with solid titanium trichloride. For this work, a reference level for the activity of volatile chloride species of 10^{-2} atmospheres (equivalent to 10,000 ppm at 1 bar total pressure) was assumed to represent the onset of potential damage for titanium alloy IMI 834. The lines corresponding to the same levels of $TiCl_{2(g)}$ and $TiCl_{3(g)}$ formed in equilibrium with solid stable titanium oxides were also calculated but showed that these amounts of volatile titanium dichloride and trichloride would thermodynamically not be expected. Hence, one can conclude that the only vapour phase titanium chloride formed near the metal/scale interface is $TiCl_{4(g)}$. As mentioned in paragraph VI.c.3., the presence of preferential channel-like diffusion paths in the substrate of salt-corroded material underlined the possibility of rapid vapour chloride induced damage when the alloy is exposed to hot-salt corrosion. Substantial amounts of titanium chlorides that would form during the salt-attack of titanium are therefore of considerable interest. Although these calculations can seem

approximate, they clearly indicate that the formation of vapour phase chlorides in titanium is limited. Furthermore, the immunity of pure titanium to hot-salt stress-corrosion cracking indicates that this assumption is correct.

System $Al/O_2/Cl_2$:

Figure VI.q. shows the phase stability diagrams which was obtained for the system $Al/O_2/Cl_2$. As expected, a stable layer of alumina should be formed at the scale/atmosphere interface. As the partial pressure of oxygen is reduced when one travels through the oxide scale, liquid aluminium trichloride becomes increasingly stable at the expense of Al_2O_3. However this hypothetical formation of $AlCl_{3(l)}$ can not be assumed to be the cause of damage in the alloy during exposure to hot-salt stress-corrosion environments.

The most interesting feature of the system $Al/O_2/Cl_2$ is its ability to form vapour phase aluminium chlorides all through the scale. Indeed, substantial amounts of $AlCl_{3(g)}$ can be formed in equilibrium with alumina or even with the bare metal, provided that the activity of chlorine is greater than 10^{-25} atmospheres. As mentioned previously, the actual chlorine activity encountered during hot-salt stress-corrosion can not be calculated. However, it is thought that these levels could be attained deep within the pores in the substate where the oxygen activity is considerably reduced by the presence of an oxide layer. Therefore, there is a possibility that aluminium vapour chlorides would form and induce significant damage in the material. This feature is extremely important when one considers the recognised influence of aluminium additions on the life of titanium alloys subjected to hot-salt stress-corrosion environments (see paragraph II.d.1). Hence, this characteristic alone could partly explain why pure titanium is immune to HSSCC and why all titanium alloys are susceptible, since aluminium additions are present in virtually all commercial titanium base alloys.

System $Sn/O_2/Cl_2$:

The phase stability diagram for the system $Sn/O_2/Cl_2$ is indicated in Figure VI.r. and shows that tin is extremely stable up to partial pressures of oxygen of about 10^{-27}

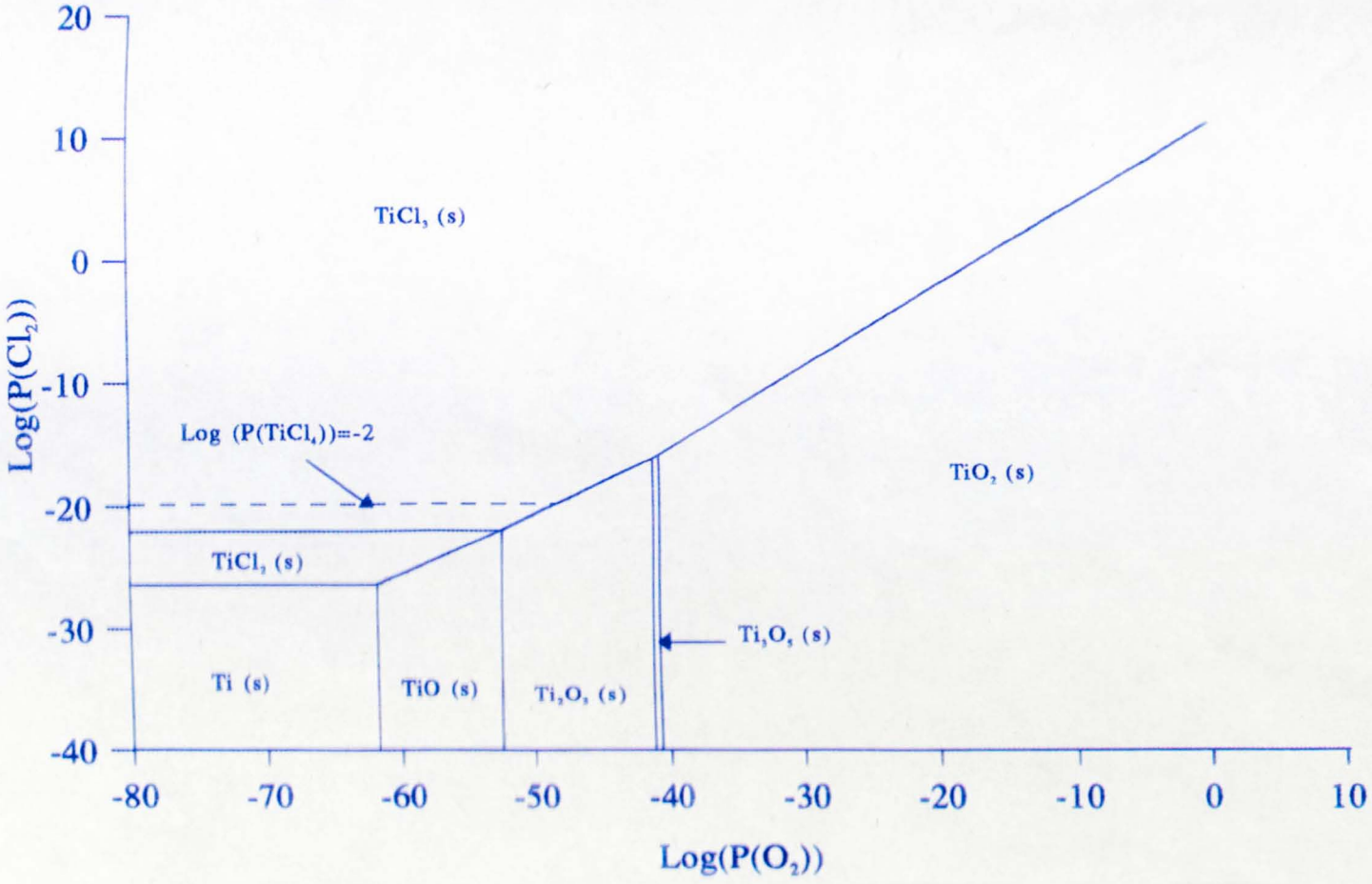

Figure VI.p.: Phase stability diagram for the system $Ti/O_2/Cl_2$ at 500 °C
Titanium activity: 0.9

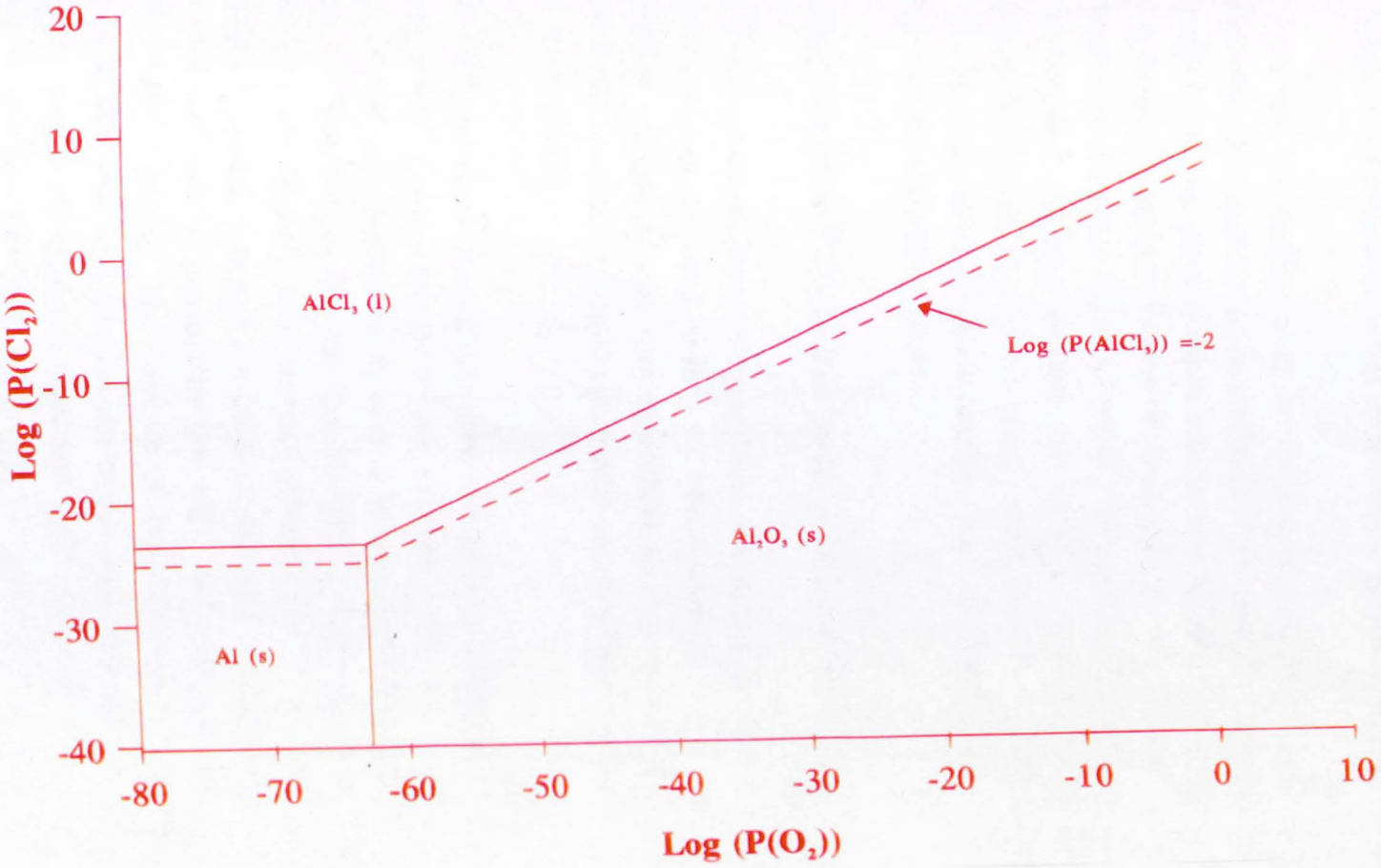

Figure VI.q.: Phase stability diagram for the system $Al/O_2/Cl_2$ at 500 °C
Aluminium activity: 0.058

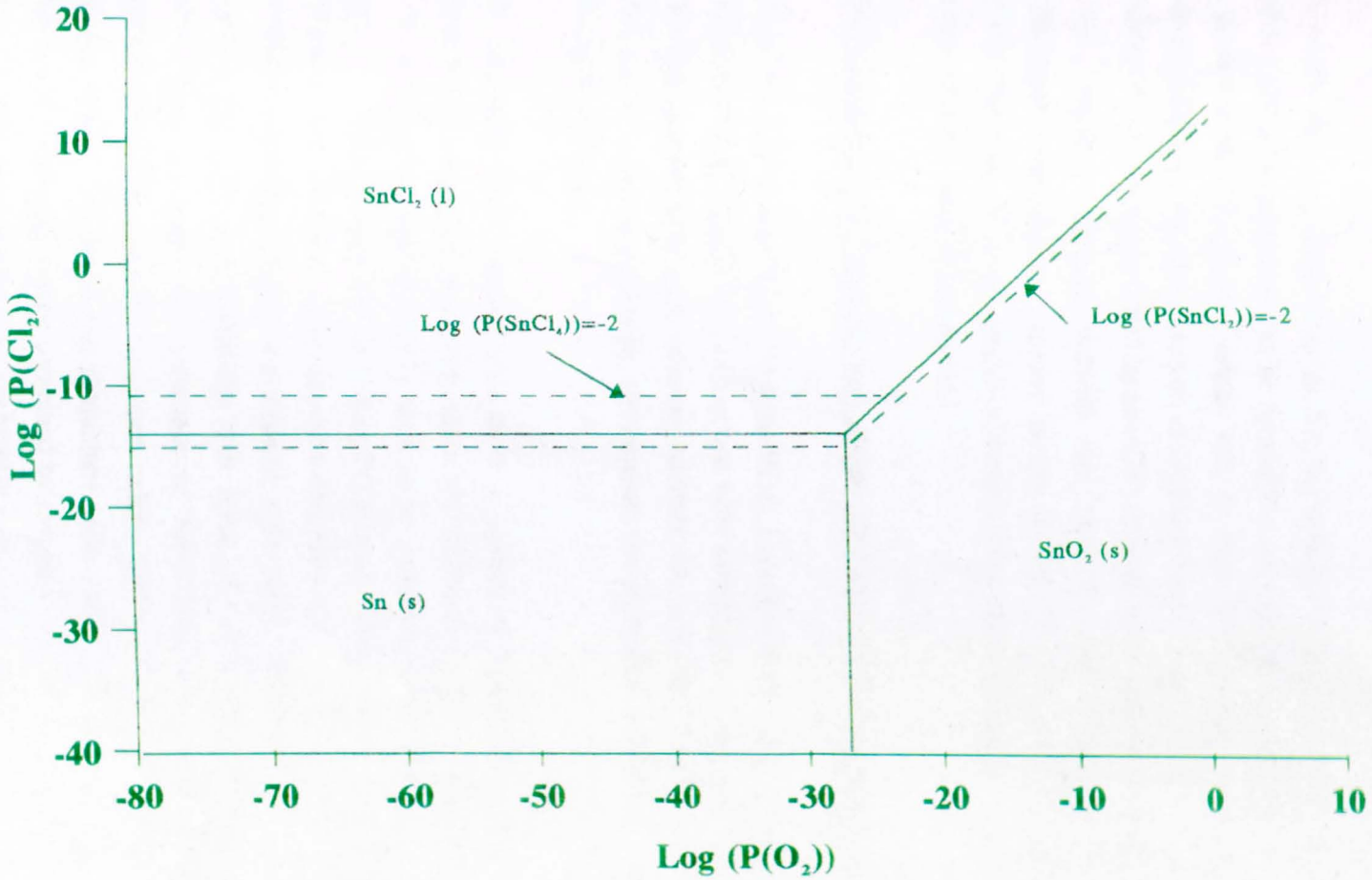

Figure VI.r.: Phase stability diagram for the system $Sn/O_2/Cl_2$ at 500 °C
Tin activity: 0.035

atmospheres. After this limit, a solid tin dioxide becomes thermodynamically stable, while significant chlorine activities are required in order to form liquid tin dichloride.

However one can notice that as for the system $Al/O_2/Cl_2$, significant amounts of vapour phase tin chlorides can be produced at any depth in the oxide scale. Hence, it is probable that tin plays a similar role to that of aluminium and induces damage during the hot-salt stress-corrosion of titanium alloys. Work carried out at Cambridge University on transverse TEM sections of titanium alloy material subjected to hot-salt stress-corrosion cracking showed that both tin and aluminium were actually significantly depleted in selective places within the alloy and sub-scale (Nicholls 1993). The formation of volatile chlorides from these elements would provide an explanation for these observations.

Superposition of the PSD's for the systems $Ti/O_2/Cl_2$, $Al/O_2/Cl_2$, and $Sn/O_2/Cl_2$:

When one superposes Figure VI.p. to VI.q., a picture of the alloy's, behaviour can be obtained. Hence, the three systems are now considered at the same time, and the respective amounts of each alloying addition are described by the activities of the three metals considered. Useful information can therefore be reliably obtained from this superposition.

The superposition of these PSD's show a number of critical points where solid or liquid oxides/chlorides transition lines are intersecting. For example, if only the systems $Ti/O_2/Cl_2$ and $Al/O_2/Cl_2$ were to be considered, this critical point could be seen for $Log(P(O_2))=-18$ and $Log(P(Cl_2))=-3$. This shows that before these conditions are reached, solid titanium chlorides (i.e. $TiCl_2$ and $TiCl_3$) and solid aluminium oxide (i.e. Al_2O_3) can coexist in the scale. Above this point, the trend is reversed and there is a possibility that rutile and solid aluminium trichloride are formed simultaneously. The existence of these intersection points indicates that exchange reactions between titanium oxides and aluminium or tin chlorides, or titanium and tin chlorides and aluminium oxides are likely to occur. Indeed, these exchange reactions have been examined by previous workers, and have been found to be accelerated when halide salts are present (see paragraph III.b.2.).

These exchange reactions become extremely interesting when vapour phase chlorides are considered. Indeed, one can actually see from the superposition of the three phase stability diagrams that a number of points exist where exchange reactions are likely to

occur between tin or aluminium vapour phases and titanium oxides. This is of particular interest when one considers the diffusion channels which have been identified in paragraph VI.c.3. Hence, if vapour phase chlorides are formed, and if they travel along one of these channels, they could be precipitated as solid oxides when the partial pressure of oxygen is increased, that is nearer the scale/metal interface. Chlorine would therefore react with another element, and produce a different volatile metallic chloride.

This complex behaviour and the essential role of alloying additions mean that it would be extremely difficult to model the hot-salt stress-corrosion of IMI 834 in an accurate way through the use of phase stability diagrams only as numerous elements are present in this alloy. Furthermore, this technique does not consider kinetics aspects which may change some of the processes involved in the phenomenon. However, it provides one with a range of possible chemical mechanisms which are likely to occur when titanium alloys are exposed to HSSCC environments. Furthermore, it can account for the immunity of pure titanium to hot-salt stress-corrosion cracking and indicates that any commercial alloy should be susceptible to different extents, as the mechanisms of HSSCC are closely linked to the nature and the quantity of alloying additions. Finally, the production of metallic vapour phase chlorides accompanied by their diffusion along preferential paths and their deposition as solid oxides indicates that the depletions and segregations of alloying additions at selected points within the alloy, sub-scale, and scale which were observed in recent work at Cambridge University are thermodynamically expected (Nicholls 1993).

VI.e. Modelling of the hot-salt stress-corrosion of titanium alloys

This chapter has focused so far on two main objectives: Firstly, the beneficial effects of high partial pressures of oxygen on the life of IMI 834 subjected to hot-salt stress-corrosion cracking environments. Secondly, thermogravimetric studies and theoretical studies which introduced basic concepts which are likely to be involved in the HSSCC of titanium alloys. This section proposes a new and improved model for the hot-salt stress-corrosion cracking of titanium alloys and will discuss these mechanisms in view of gas turbine engine applications.

VI.e.1. A new model for the HSSCC of titanium alloys

The model which is proposed is based on the assumption that the mechanisms of the hot-salt stress-corrosion of titanium alloys lead to hydrogen embrittlement of the material. Indeed, chapter III showed that if hydrogen embrittlement of titanium alloys exposed to HSSCC environments has not been proven, sufficient indications exist that imply that hot-salt stress-corrosion cracking of titanium results in this mode of fracture (see paragraph III.c.2.). For all the models which have been proposed to date by other workers which lead to hydrogen embrittlement of the material, none of them describes how vast amounts of hydrogen may actually be injected into the alloy. The model which is presented below actually addresses this problem.

Hot-salt stress-corrosion of titanium alloys is in fact a two stage process: Crack initiation is driven by surface chemistry, while crack propagation is controlled by corrosion kinetics, fracture mechanics, and material's properties.

Crack initiation:

It has been shown that under hot-salt stress-corrosion crack initiation is not dependent on defects that may be present at the surface of the material, but is usually originating beneath salt beads which have been deposited on the oxide scale (see paragraph II.b.2.). If one considers a salt bead present at the surface of the alloy, the following will occur:

When the material is exposed to elevated temperatures in the presence of salts, its oxide scale will be disrupted. This was suggested by the thermogravimetric studies carried out during this study which showed that alpha case was not present at the surface of the material after salt exposure (see paragraph VI.c.3.). This observation suggests a rapid consumption of the alloy from the surface.

A differential oxygen aeration cell may well form between the scale/salt interface and the scale/atmosphere interface (Garfinkle 1973, Myers 1977). Therefore, as oxygen is consumed under the salt bead, the oxygen activity at this point is lowered. This implies that the activities of water vapour or any volatile chloride species will be raised.

At elevated temperatures, rutile is likely to react with the salt and water vapour to produce sodium titanate according to the following reaction:

$$TiO_{2(s)} + 2NaCl_{(s)} + H_2O_{(g)} \xrightarrow{T} Na_2TiO_{3(s)} + 2HCl_{(g)} \qquad \textbf{(VI.40)}$$

Petersen actually reported the detection of sodium titanate in the scale of hot-salt stress-corroded samples (Petersen 1966). This reaction results in the production of gaseous hydrochloric acid.

This means that gaseous hydrochloric acid which has been produced by reaction (VI.40) can gain access to the bare metal by diffusing through micro-channels and imperfections in the oxide scale (Hancock 1978, Jacobson 1990) and can readily react with titanium, or to a larger extent with aluminium and tin according to the following reactions:

$$Ti_{(s)} + 4HCl_{(g)} \longrightarrow TiCl_{4(g)} + 4H \qquad \textbf{(VI.41)}$$

$$Al_{(s)} + 3HCl_{(g)} \longrightarrow AlCl_{3(g)} + 3H \qquad \textbf{(VI.42)}$$

$$Sn_{(s)} + 4HCl_{(g)} \longrightarrow SnCl_{4(g)} + 4H \qquad \textbf{(VI.43)}$$

These reactions would therefore inject free hydrogen into the material, but would also remove atoms from the base material. This results in the formation and extension of the pores at the surface of the material. Indeed, photographs VI.l. and VI.m. show the presence of similar channels to these observed during thermogravimetric studies near stress-corrosion cracks produced in IMI 834.

The study of phase stability diagrams for the systems $Ti/O_2/Cl_2$, $Al/O_2/Cl_2$, and $Sn/O_2/Cl_2$ showed that reactions (VI.42) and (VI.43) are more likely to occur than reaction (VI.41) (see paragraph VI.d.3.). Hence, the corrosion mechanisms are accelerated by the presence of aluminium and tin as alloying additions. The influence of aluminium content on the life of titanium alloys exposed to HSSCC environments has been demonstrated by several workers (see paragraph II.d.1.).

The volatile metallic chlorides formed through these reactions are then able to diffuse along the pore formed within the alloy towards the scale/alloy and then scale/salt interfaces under concentration gradients. Nearer the surface, they are hydrolysed and deposited as solid oxides, either along the pores, or at the surface of the material according to the following reactions:

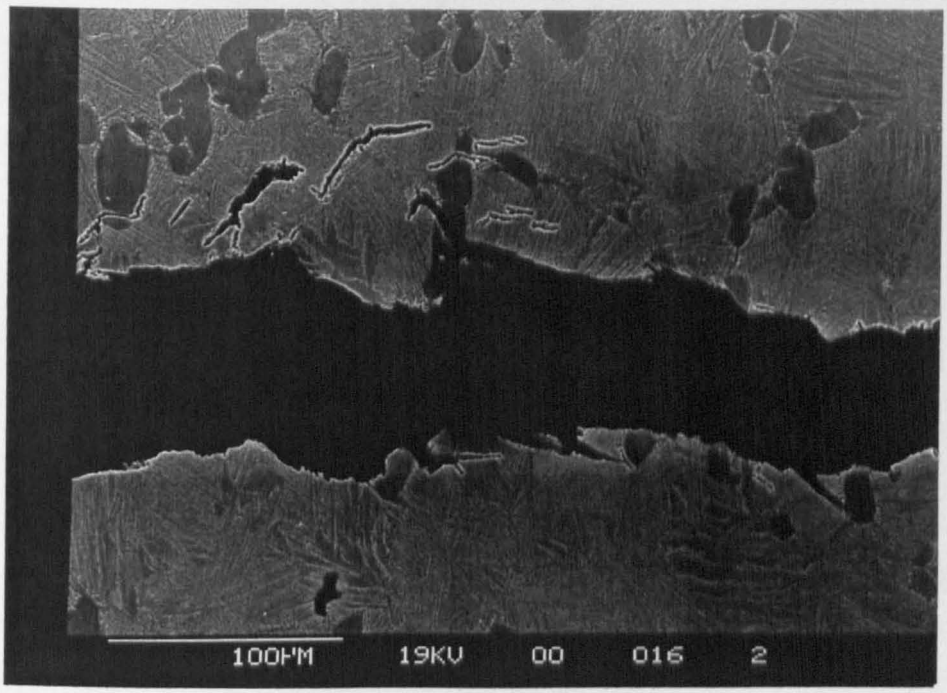

Photograph VI.l.: Stress-corroded area showing the presence of diffusion channels in the area near the crack.

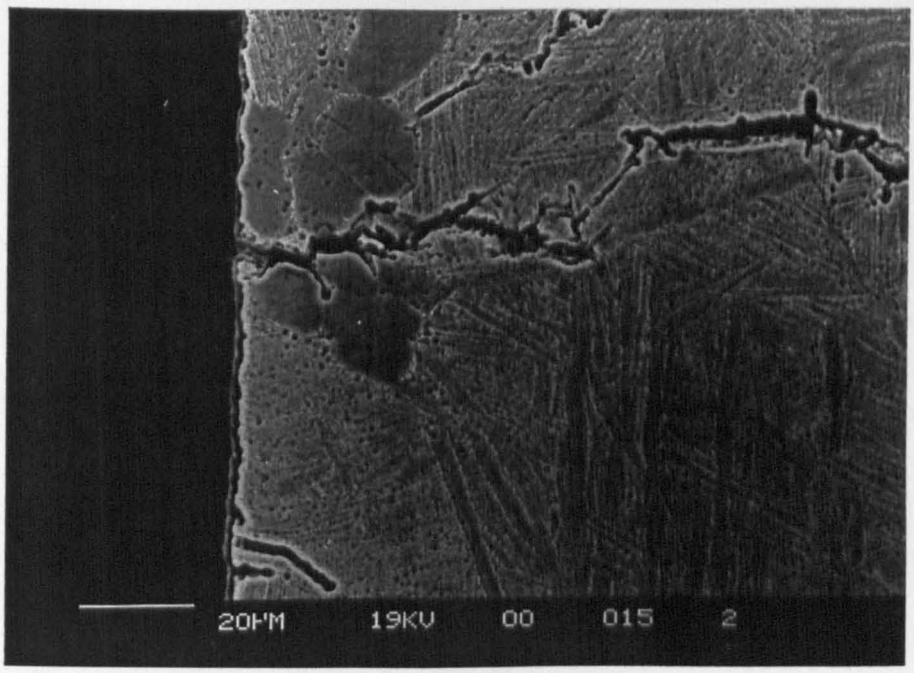

Photograph VI.m.: Stress-corroded area showing the presence of diffusion channels in the area near the crack.

$$TiCl_{4(g)} + 2H_2O_{(g)} \xrightarrow{T} TiO_{2(s)} + 4HCl_{(g)} \quad \textbf{(VI.44)}$$

$$2AlCl_{3(g)} + 3H_2O_{(g)} \xrightarrow{T} Al_2O_{3(s)} + 6HCl_{(g)} \quad \textbf{(VI.45)}$$

$$SnCl_{4(g)} + 2H_2O_{(g)} \xrightarrow{T} SnO_{2(s)} + 4HCl_{(g)} \quad \textbf{(VI.46)}$$

There is considerable evidence for the existence of these pyrohydrolysis reactions which have been extensively discussed in the literature (see chapter III). Since the activity of oxygen is considerably reduced along the pore and beneath the salt bead at the surface of the material, the activity of water vapour is likely to increase. Furthermore, heat will act as a catalyst. This reaction would also explain why water vapour is required to produce hot-salt stress-corrosion cracking in titanium alloys. It is difficult at this stage to predict at which depth in the pore these reactions are likely to occur and it is probable that this would depend on which of the reactions showed above is considered (see paragraph VI.d.3.). ZAF analysis were carried out along some of the pores observed in hot-salt corroded samples on the Scanning Electron Microscope in order to verify this matter. As indicated in photographs VI.n. and VI.o., they show that aluminium has been depleted significantly along these pores while tin contents have been slightly increased. In fact these slight increases in tin may indicate that aluminium has been removed, as shown by the depletions.

Reactions (VI.44) to (VI.46) are accompanied by the production of gaseous hydrochloric acid. A self sustaining and accelerating cycle which can at the same time open channels penetrating deep in the material and inject hydrogen in the material is thus produced. This cycle is represented in Figure VI.s.

The high temperature hydrogen embrittlement of titanium alloys has been shown to depend to a large extent on the presence of stress concentrators (Livanov 1973). Therefore, it is probable that free hydrogen now present in the material will be diffusing to regions of high triaxal stress. When the hydrogen injected exceeds the hydrogen solubility of the alloy, a crack is initiated.

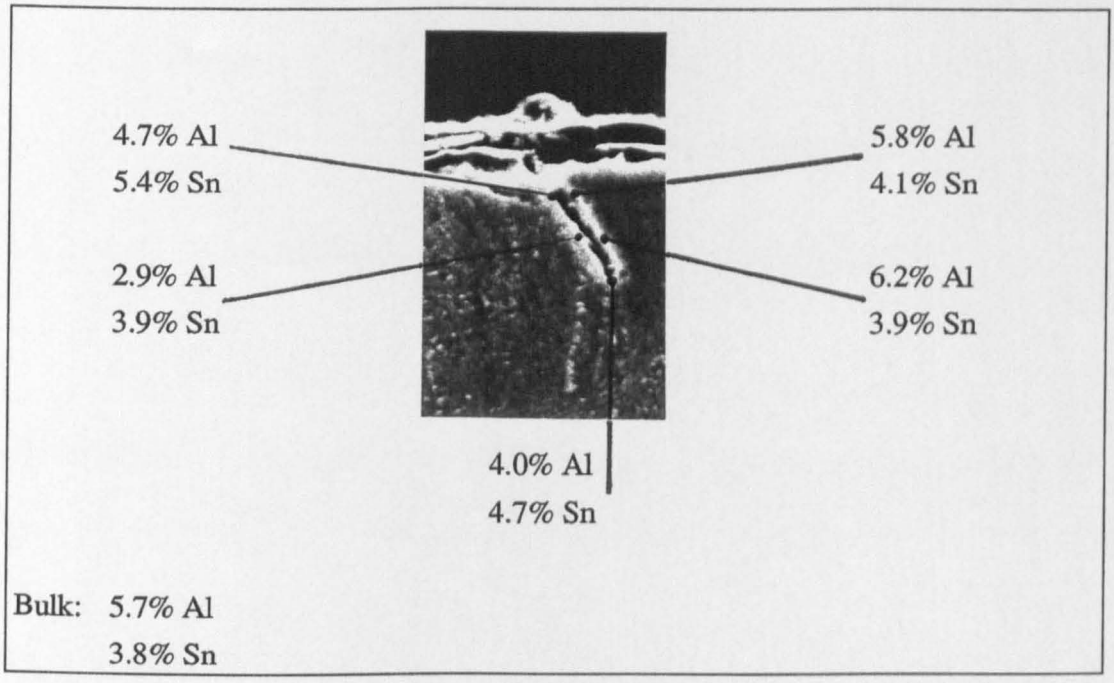

Photograph VI.n.: ZAF analyses carried out along a channel showing depletions in aluminium content (results in wt%). 1 hour exposure at 600 °C

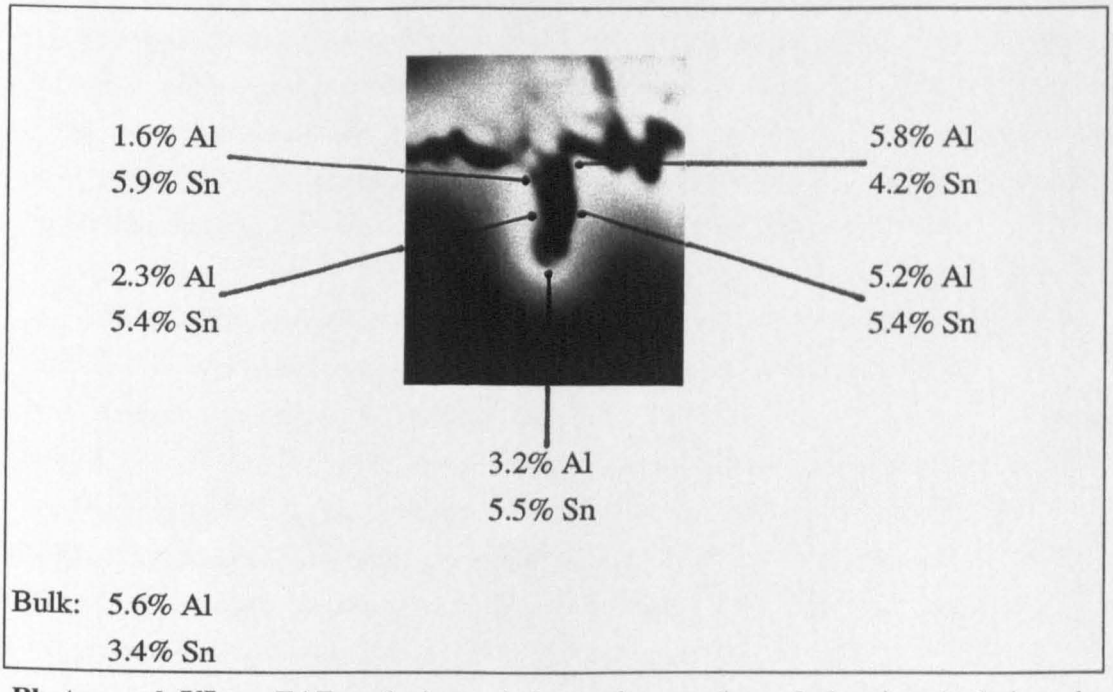

Photograph VI.o.: ZAF analysis carried out along a channel showing depletions in aluminium content (in wt%). 100 hours exposure at 600 °C

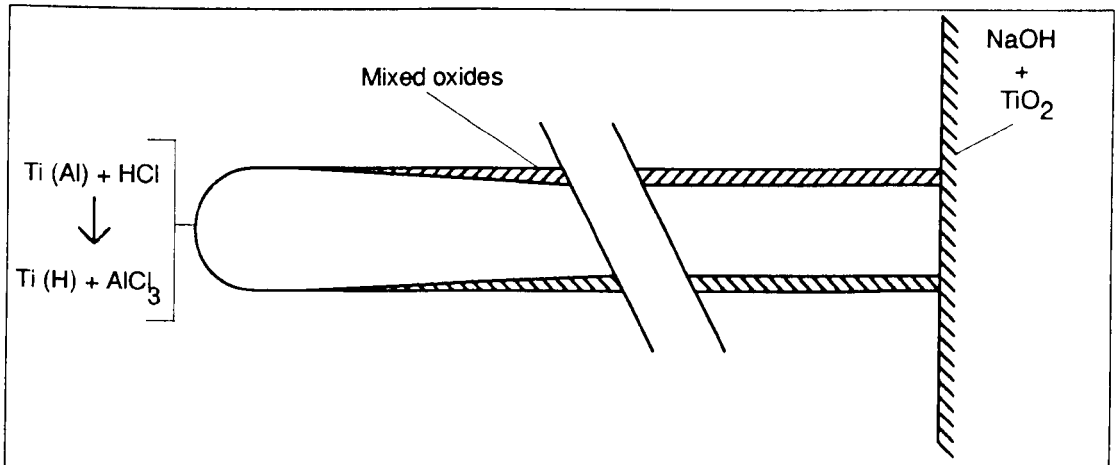

Figure VI.s.: Cycle established during the hot-salt stress-corrosion of titanium alloys.

Crack propagation:

The mode of cracking of titanium alloys exposed to hot-salt stress-corrosion environments has been assumed to be due to hydrogen embrittlement by most of the researchers working on this topic (see paragraph III.c.2.). However, the manner by which hydrogen embrittles titanium and its alloys at high temperatures is not yet fully understood. Some have postulated that hydrogen will precipitate hydrides or micro hydrides in titanium alloys (Coterill 1961). However recent in situ hydrogen embrittlement TEM studies carried out by Shih showed that hydrogen atoms could decrease significantly the velocity of dislocations in titanium (Shih 1988).

In any case, for the hot-salt stress-corrosion of titanium alloys the critical aspect is related to the amount of hydrogen which can be injected in the material in a rapid manner. Actually, hydrogen will diffuse quickly in titanium at elevated temperatures. However, a study by Waisman showed that diffusion rates of hydrogen in titanium alloys (and especially in the presence of aluminium) are influenced by composition, temperature, and stress gradients (Waisman 1973). Hence, it is necessary to be able to inject hydrogen into the material before it can diffuse away from the region ahead of the pore's or crack's tip. It is thought that the mechanisms described above can fulfil this condition, but Waisman's model which is based on the experimental determination of diffusion gradients under specific experimental conditions can not be applied directly to the phenomenon of hot-salt stress-corrosion. Furthermore, the

calculation of a hydrogen mass balance to support this model would imply that the amounts of hydogen which are injected into the material are known.

Once the crack has been initiated, the overall corrosion process will have to be repeated according to the schematic diagram presented in Figure VI.t. before the crack propagates. Hence, the reactions proposed for crack initiation will lead to the production of more hydrogen which will be injected ahead of the crack tip. When the solubility limit in regions of high triaxial stress is reached, cracking will occur and

the crack will propagate. This step like-pattern is enhanced by the presence of an applied stress which breaks the oxide forming at the tip of the crack and provides access for the volatile chloride species to the base metal.

When the crack has propagated sufficiently, the remaining area of the material can not bear the applied load any more, and ductile fracture occurs by overloading.

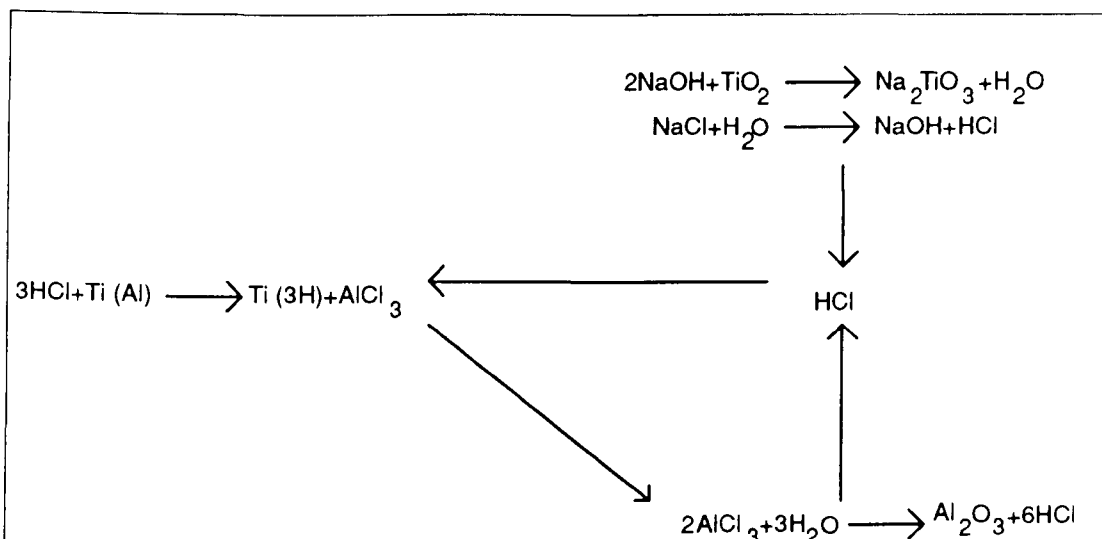

Figure VI.t.: Schematic of the mechanisms of the hot-salt stress-corrosion of titanium alloys

VI.e.2. Validity of the proposed model in view of gas turbine engine operation

The preceding paragraph proposed a new model for the hot-salt stress-corrosion cracking of titanium based alloys. The validity of these mechanisms can now be examined with a view to determine how the beneficial pressure effects revealed in the course of this study would relate to the proposed model.

The model which has been developed in this work has actually the merit to agree with the main features of the HSSCC of titanium alloys which have been observed by other workers over the years. It has been demonstrated in the literature that any halide salt apart from fluorides are able to cause cracking (see paragraph II.c.2.). This would in fact be expected from the proposed model, since fluorides can not be hydrolysed. Hence, reaction (VI.40) will not occur, and the corrosion controlled cycle will not be established. The importance of water vapour in the hot-salt stress-corrosion process is also evident from reactions (VI.44) to (VI.46).

$$TiO_{2(s)} + 2NaCl_{(s)} + H_2O_{(g)} \xrightarrow{T} Na_2TiO_{3(s)} + 2HCl_{(g)} \qquad \textbf{(VI.40)}$$

$$TiCl_{4(g)} + 2H_2O_{(g)} \xrightarrow{T} TiO_{2(s)} + 4HCl_{(g)} \qquad \textbf{(VI.44)}$$

$$2AlCl_{3(g)} + 3H_2O_{(g)} \xrightarrow{T} Al_2O_{3(s)} + 6HCl_{(g)} \qquad \textbf{(VI.45)}$$

$$SnCl_{4(g)} + 2H_2O_{(g)} \xrightarrow{T} SnO_{2(s)} + 4HCl_{(g)} \qquad \textbf{(VI.46)}$$

The immunity of pure titanium to HSSCC can also be explained with the proposed model: Thermodynamics studies and the examination of phase stability diagrams showed that reactions (VI.42) and (VI.43) are more likely to occur than reaction (VI.41). Hence, alloying elements act as hydrogen carriers through the scale and provide the main source of embrittlement by accelerating the cycle described by the model. This means that even if reaction (VI.41) does occur, it may not be sufficiently powerful, and the small amounts of hydrogen which could be injected in the material would be insufficient to cause cracking. Therefore, hydrogen could diffuse away from the crack tip before sufficient levels to cause cracking are reached.

$$Ti_{(s)} + 4HCl_{(g)} \longrightarrow TiCl_{4(g)} + 4H \qquad \textbf{(VI.41)}$$

$$Al_{(s)} + 3HCl_{(g)} \longrightarrow AlCl_{3(g)} + 3H \qquad \textbf{(VI.42)}$$

$$Sn_{(s)} + 4HCl_{(g)} \longrightarrow SnCl_{4(g)} + 4H \qquad \textbf{(VI.43)}$$

It has also been shown that cyclic operating conditions extend the lifetime of titanium alloys subjected to hot-salt stress-corrosion cracking conditions. Furthermore Livanov showed that hydrogen embrittlement of titanium alloys is reversible (Livanov 1973). As numerous workers mentioned, if the operating temperature is decreased to room temperature before a crack is initiated, then the alloy will show a complete recovery of its mechanical properties (Stone 1967). If the stress is cycled, then titanium hydrides may not precipitate or diffusion of hydrogen away from the pore's tip may be more rapid than in the presence of a constant stress. In any case, when both the temperature and the stress are cycled, no significant further improvement in the life of the material should be obtained, as hot-salt stress-corrosion will be controlled either by the necessity to precipitate hydrides which is stress related or by chemical reactions which are temperature dependent. This trend has been observed by previous workers (Gray 1973, Lapasset 1979).

This study showed the existence of significant pressure effects on the hot-salt stress-corrosion cracking of IMI 834 and these results have to be considered in conjunction with the proposed model. As mentioned in paragraph VI.b., these pressure effects are interacting with the composition of the gas atmosphere used for the test. The interesting part of the results in view of gas turbine engine applications is this obtained for atmosphere compositions containing about 21% volumetric ratio of oxygen.

For these compositions and at a constant stress, partial pressure of oxygen has been found to be a life determining parameter. This influence can actually be related to the model which has been described in paragraph VI.e.1. Indeed, increases in oxygen partial pressures would result in increases of the oxygen activity beneath the salt beads deposited at the surface of the material. Therefore three new reactions will have to be considered:

$$TiCl_{4(g)} + O_{2(g)} \longrightarrow TiO_{2(s)} + 2Cl_{2(g)} \qquad \textbf{(VI.47)}$$

$$2AlCl_{3(g)} + \frac{3}{2}O_{2(g)} \longrightarrow Al_2O_{3(s)} + 3Cl_{2(g)} \qquad \textbf{(VI.48)}$$

$$SnCl_{4(g)} + O_{2(g)} \longrightarrow SnO_{2(s)} + 2Cl_{2(g)} \qquad \textbf{(VI.49)}$$

As one can see, these reactions which are now competing with the pyrohydrolysis reactions (VI.47) to (VI.49) to control the corrosion process are producing chlorine gas rather than gaseous hydrochloric acid. This means that the self sustaining cycle described in paragraph VI.e.1. will now produce chlorine gas and that hydrogen will

not be injected into the material. Therefore, the main source for the embrittlement of the alloy is inhibited, and the life of the material is extended.

The data points corresponding to rare oxygen atmosphere compositions were actually obtained while trying to extend the range of the partial pressures of oxygen used in this study. The life of IMI 834 for these air compositions seems to be dependent on the oxygen content of the testing atmosphere, that is on the interactions between oxygen partial pressure and total pressure. This behaviour which is not fully understood may be caused by the growth of a thinner oxide which will take more time to grow to a critical thickness required to cause cracking of this protective layer. Therefore, this oxide layer may be more efficient in protecting the material. However more work is needed in order to verify this matter (see "Future work).

The model proposed in this work accounts for the observations made by previous workers and relates successfully to the beneficial effect of the partial pressure of oxygen on the life of IMI 834 in HSSCC environments containing at least 21% volumetric ratios of oxygen which were demonstrated in this study. This model which was developed from both thermogravimetric studies and thermodynamic studies is therefore suitable and describes satisfactorily the mechanisms of the hot-salt stress-corrosion cracking of titanium alloys. The beneficial effect of a reduced oxygen atmosphere which has been observed in this work is not fully understood, but is considered as being irrelevant in view of gas turbine engine applications.

CONCLUSION

The work which has been carried out in the course of this study contributes to a better understanding of the phenomenon of the hot-salt stress-corrosion cracking of titanium alloys:

1. Pressure was shown to increase substantially the life of IMI 834 subjected to hot-salt stress-corrosion cracking.

2. Pressure interacts very closely with the applied load and the composition of the testing atmosphere to determine the components life. For atmospheres containing 21% or more oxygen volumic ratios, the life of the material under hot-salt stress-corrosion conditions was found to depend on the partial pressure of oxygen. In view of aero gas turbine engine applications, this behaviour is particularly interesting and could account for the lack of in-service HSSCC failures. For rare oxygen content atmosphere, oxygen content is the determining parameter. However this behaviour is less relevant for the applications which are concerned by this study.

3. Thermogravimetric studies were undertaken to gather information on the kinetics of hot-salt attack of titanium. They highlighted the importance of the first few hours of exposure to hot-salt stress-corrosion cracking environments, and revealed the existence of diffusion channels that extend deep into the material.

4. Theoretical thermodynamics showed that metallic vapour phase chlorides are likely to form during HSSCC.

5. Alloying additions in titanium have a marked influence on the mechanisms of the hot-salt stress-corrosion of titanium alloys.

6. The production of HCl as a corrosion product may lead to hydrogen embrittlement of titanium based alloys.

7. A model was developed from both the thermogravimetric and thermodynamic studies achieved in the course of this study. It is based on the diffusion of metallic

vapour phase chlorides which are diffusing through the channels formed during salt attack.

8. These mechanisms may result in the injection of vast quantities of hydrogen into the alloy, based on the establishment of an accelerating and self sustaining cycle where vapour phase chlorides act as the transport agents, carrying hydrogen into the alloy and metallic chlorides away from the reaction front. The role played by alloying additions in this model is extremely important and is at the origin of the embrittling process.

9. The proposed model accounts for the observations made by previous workers. It also does explain why high partial pressures of oxygen do extend the life of IMI 834 in rich oxygen HSSCC environments. The behaviour of the alloy in rare atmosphere compositions was not studied in detail, since it does not present an interest in view of gas turbine engine applications.

FUTURE WORK

This study raises a number of questions and shows the need for further work:

Fatigue behaviour: The loading conditions used in this study were static. This means that the tests were actually extremely severe in comparison with the actual loading conditions encountered in service. This study, which showed that the life of IMI 834 in high pressure HSSCC environments is extremely sensitive to the stresses employed, underlines the need for fatigue studies. Hence, the testing conditions will be more representative of gas turbine engine compressor's operation and will definitely elucidate the lack of in-service failures.

Role of alloying elements: This study showed that alloying additions are extremely influent on the life of titanium alloys in HSSCC environments. However, due to the wide range of alloying elements present in commercial titanium alloys such as IMI 834, it is extremely difficult to determine their relative influence. This could be done by undertaking a study of the hot-salt stress-corrosion of model binary and ternary titanium alloys where the influence of each element could be characterised separately.

Rare oxygen atmosphere testing: The results of this study show an improvement of the life of IMI 834 for atmospheric low oxygen volumic contents. This behaviour which is not relevant in terms of aero gas turbine engine applications is nevertheless of interest for a better understanding of the mechanisms of the hot-salt stress-corrosion of titanium alloys. In particular, it may provide one with a better characterisation of the role of stress during HSSCC.

Titanium aluminides: There is growing interest in the aerospace industry for the use of titanium aluminides which would provide exceptional weight savings. However this study showed that aluminium is a major actor of the hot-salt corrosion cracking of titanium alloys. This shows therefore the need for a study of the HSSCC of titanium aluminides.

Protective treatments: Protective treatments against the hot-salt stress-corrosion of titanium alloys have been investigated in an empirical manner. With a better

understanding of the phenomenon of the HSSCC of titanium alloys, a systematic study could be carried out. However a more immediate study could involve the evaluation of shot peening which is widely used in the aerospace industry, and the evaluation of pre oxidation.

Appendix 1

Turbo pascal programme written for computerised data acquisition during the thermogravimetric studies

```
PROGRAM THERMOGRAVIMETRIC;
{Computerised data acquisition programme developed by Thierry Chevrot, Cranfield University
for use in continuous thermogravimetric studies}

uses crt,dos;
var
  daystart,timestart,testtime,duration,previoustime1,previoustime2,interval1,interval2: longint;
  {These are the time variables which give access to the clock and process the time's measurements}

  Day,average: byte;
  {Average is the number of measurement on which the final result is calculated}
  {Day indicates the number of days for which the test has been runing}

  dom,m,y:word;
  {day, month, and year the test started}

  span: integer;
  {Span is the number of full range weight gains for one test}

  sum: longint;
  {Sum allows the programme to calculate the average result of one series of measurements}

  Out, measure, store: boolean;
  {Out allows the user to exit the program at any time by pressing the "E" key}
  {Measure=true indicates that the programme has to take measurements from the ADC}
  {Store=true indicates that the measurement must be recorded}

  result, previousresult: longint;
  {Result is the combination of highbyte and lowbyte as read on the ADC 16}
  {Previousresult represents the previous measurement}

  voltage, startingweight, weight, weight2, weightgain, previousweight: real;
  {voltage is the output from the robal in Volts, Startingweight is the weight of the sample at the
  start of the test, Weight and Weight2 are the new weight of the sample, Previousweight is the
  weight given by the previous measurement}
```

```
    Filename: string[19];
    {Name of the file chosen by the user where the results will be saved}

    Resultsfile :text;
    {File were the results will be stored}
  {*************************************************************************}
  FUNCTION READTIME: longint;

  {Returns the time from the computer's clock}
  var
    Hour,minute,second: longint;     {Process the different time variables read on the clock}
    a,b,c,d: word;                   {Local time variables as in the clock}

  begin
      gettime(a,b,c,d);              {Reads the time from the clock}
      hour:=a;
      minute:=b;
      second:=c;
      readtime:=(60*hour+minute)*60+second;        {Calculates the current time in seconds}
  end;
  {*************************************************************************}
  PROCEDURE EXPERIMENT_TIME_PARAMETERS;

  {The user enters the duration of the test and the interval between measurements}
  begin
      writeln('How long do you want the test to last in minutes?');
      readln(Duration);
      duration:=duration*60;                       {The duration is calculated in seconds}
      writeln('At which interval (in seconds) do you want to measure the weight?');
      readln(interval1);
      writeln('At which interval (in seconds) do you want to record the measurements?');
      readln(interval2);
      writeln('On how many measurements do you want to average the results?');
      readln(average);
      clrscr;
  end;
  {*************************************************************************}
```

```
PROCEDURE ERROR_MESSAGE1;

{This procedure ensures that the filename given is valid under DOS}
begin
    writeln('Your file name is not valid.');
    writeln('Please enter another name. 1 character minimum, 8 characters maximum!');
end;
{*************************************************************************}
PROCEDURE ERROR_MESSAGE2;

{This procedure ensures that no file with the same filename has been saved previously}
begin
    writeln('This file name already exists; Please try another one');
    readln(filename);
end;
{*************************************************************************}
PROCEDURE CHOOSE_FILENAME;

{Asks the user for a filename with 8 characters maximum and adds a default directory name to the
file name}
begin
  chdir('d:\data');                                    {Changes to the data directory}
  writeln('Give the name of the file where your results will be saved.');
  writeln('8 characters maximum!');
  readln(filename);
  while (length(filename)>8) or (length(filename)=0) do begin   {Filename must be <8 characters}
    Error_message1;
    readln(filename);
  end;
end;
{*************************************************************************}
PROCEDURE START_TEST;

{Reads the date and time at the start of the test and initialises all date and time variables}
var
 a,b,c,d: word;                    {Local date variables as in the clock}
```

```
begin
    span:=0;                    {No previous weight gain data}
    voltage:=0;                 {Initialises the voltage recorded to zero}
    previousresult:=0;          {No previous measurement}
    out:=false;                 {Initialise the exit variable}
    store:=false;               {No storage necessary}
    Day:=0;                     {First day of test}
    testtime:=0;                {The test has not started yet}
    previoustime1:=0;           {No previous measurement taken}
    previoustime2:=10800;       {Initialises the time at which measurements have to be made}
    getdate(a,b,c,d);           {Reads the date on which the test is started}
    daystart:=d;                {First day of test}
    y:=a;                       {Stores the day of the week the test is started}
    m:=b;                       {Stores the month at which the test is started}
    dom:=c;                     {Day of the month at which the test is started}
    timestart:=readtime;        {Test starts now}
end;
{*************************************************************************}
PROCEDURE CREATE_FILE;

{This procedure creates a file where the results will be stored}
begin
{$I-}                                   {Turns the compiler off}
      assign(resultsfile,filename);     {Opens the file}
      reset(resultsfile);
      while ioresult=0 do begin         {Looks for a file with a similar name}
        Error_message2;
        assign(resultsfile,filename);
        reset (resultsfile);
      end;
{I+}
   rewrite(resultsfile);                {Creates the file in directory D:\DATA}
   writeln(resultsfile,'These are the results for the test: '+filename);   {Creates a file header}
   writeln(resultsfile,'It started on the ',dom,' ',m,' ',y);
end;
{*************************************************************************}
```

```
PROCEDURE EXPERIMENT_TIME;

{Reads the time and calculates the duration of the test}
var
  time: longint;
  a,b,c,d: word;                          {Local date variables as in the clock}

begin
   time:=readtime;                        {Gets the current time}
   getdate(a,b,c,d);                      {Gets current date from the clock}
   if d<>daystart then begin              {Checks that the day has not changed}
     day:=day+1;                          {The test has been runing for one day more}
     daystart:=d                          {Daystart is implemented for tests of more than 1 week}
   end;
   testtime:=86400*day+time-timestart;    {Total testing time is calculated in seconds}
end;
{*************************************************************************}
PROCEDURE ABORT_THE_TEST;

{Allows the user to abort the test at any time and to exit the program by pressing "e" or "E"}
var
  ch:char;

begin
   if keypressed then begin
     ch:=readkey;
     if (ch='E') or (ch='e') then out:=true;          {The program will stop running when}
   end;                                               "out" is pressed later in the program}
end;
{*************************************************************************}
PROCEDURE WAIT;

{This procedure orders to wait for one second before doing the next measurement}
var
  Currenttime: longint;
  {Currenttime is the time just before the procedure was called}
```

```
Begin
   currenttime:=testtime;
   repeat
      Experiment_time;
   until testtime>=(currenttime +1);
end;
{*************************************************************************}
PROCEDURE DO_YOU_WANT_TO_MEASURE;

{This procedure checks if it is time to take a measurement}
begin
   Experiment_time;
   if testtime<(previoustime1+interval1) then measure:=false
   else measure:=true;
end;
{*************************************************************************}
PROCEDURE DISPLAY_MESSAGE;

begin
   Writeln('Wait please; The next measurement will start in '
   ,(previoustime1+interval1-testtime),' seconds');
end;
{*************************************************************************}
PROCEDURE TAKE_MEASURE (var result: longint);

{Takes the measure on the ADC 16}
var
  Discard, Highbyte, Lowbyte: longint;
  {Discard's purpose is only to start the conversion}
  {Highbyte and lowbyte are the readings on the ADC 16}

begin
   result:=0;
   port[$30C]:=0;                    {Writes channel 0 as selected for measuring weight}
   discard:=port[$302];              {Start conversion}
   delay(1);                         {Gives time for the conversion to be finished}
   Highbyte:=port[$301];             {Reads high byte}
```

```
    Lowbyte:=port[$302];                {Reads low byte}
    result:=(highbyte*256)+lowbyte;     {Combines low byte and high byte to give the result}
 end;                                   {Result=4000 corresponds to 5V}
{*************************************************************************}
PROCEDURE CALCULATE_SUM;

{This procedure calculate the sum of all the measurements made for average measurements}
begin
    if (previousresult>2500) and (result<1000) then span:=span+1;
    if (previousresult<500) and (result>3500) then span:=span-1;
    sum:=sum+(result+(4000*span));
    previousresult:=result;
end;
{*************************************************************************}
PROCEDURE WORK;

{This procedure covers all the measurement tasks for average measurements}
var
  Firstmeasure: longint;
  {First time at which a measure is taken}

begin
    firstmeasure:=testtime;
    sum:=0;
    repeat
        Take_measure(result);
        writeln(result);
        Calculate_sum;
        wait;
   until testtime>(firstmeasure+average-1);
end;
{*************************************************************************}
PROCEDURE CALCULATE;

{This procedure calculates the weight gain from the measurements}
begin
   weight:=(sum/average)/4;
```

```
    voltage:=((sum/average)*5)/4000;
    weight2:=(voltage*1000)/5;
end;
{*************************************************************************}
PROCEDURE DISPLAY_RESULTS;

{This procedure displays the results on the screen}
begin
    writeln ;
    writeln('The average weight measured between t=',testtime-average,' s and t=',
    testtime,' s is');
    writeln(weight,' micrograms and total weight ',weight2,' micrograms');
    writeln('The weightgain so far is ',weight2-startingweight,' micrograms');
    writeln('The next measurement will be made in ',Interval1-average,' seconds');
    writeln;
end;
{*************************************************************************}
PROCEDURE DO_YOU_WANT_TO_STORE;

{This procedure decides whether the results have to be stored}
begin
   if (testtime-average)>=previoustime2+interval2 then
     begin
      store:=true;
      previoustime2:=testtime-average;
     end
   else store:=false;
   if (testtime-average)<=10800 then store:=true;
   if weight>(previousweight+20) then store:=true;
end;
{*************************************************************************}
PROCEDURE STORE_WEIGHT;

begin
   append(resultsfile);
   writeln(resultsfile,(testtime-average)/3600,',',weight,',',weight2,',',weight2-startingweight);
   close(resultsfile);
```

```
    previousweight:=weight;
end;
{*************************************************************************}
PROCEDURE FINISH_THE_TEST;

begin
    writeln;
    writeln('The test has been running for ',testtime,' seconds');
    writeln('Press return to exit the programme');
    readln;
end;
{*************************************************************************}
{THIS IS THE BEGINNING OF THE MAIN PROGRAM}

begin
    clrscr;
    Experiment_time_parameters;          {Returns the duration of the test and time interval}
    Choose_filename;
    Create_file;
    Start_test;                          {Initialises all time variables}
    work;
    calculate;
    startingweight:=weight;
    display_results;
    Store_weight;
    repeat
        Abort_the_test;                  {Tests if the user wants to abort the test}
        Do_you_want_to_measure;
        if measure=false then begin
          Display_message;
          Wait;
        end
        else begin
            Work;
            calculate;
            Display_results;
            Do_you_want_to_store;
```

```
        if store=true then Store_weight;
        previoustime1:=testtime-average;        {Time of the measurement is kept in memory}
      end;
  until (testtime=duration+average) or out;     {Test is finished or aborted}
  Finish_the_test;
end.
```

Appendix 2

Thermogravimetric curves

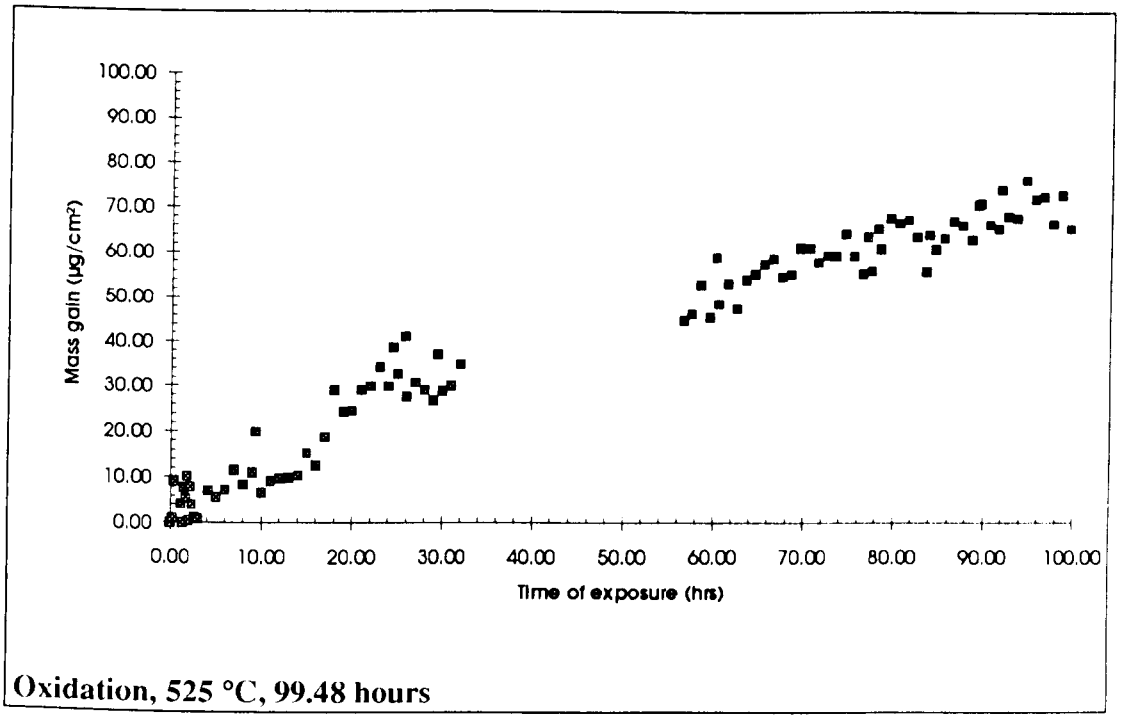

Oxidation, 525 °C, 99.48 hours

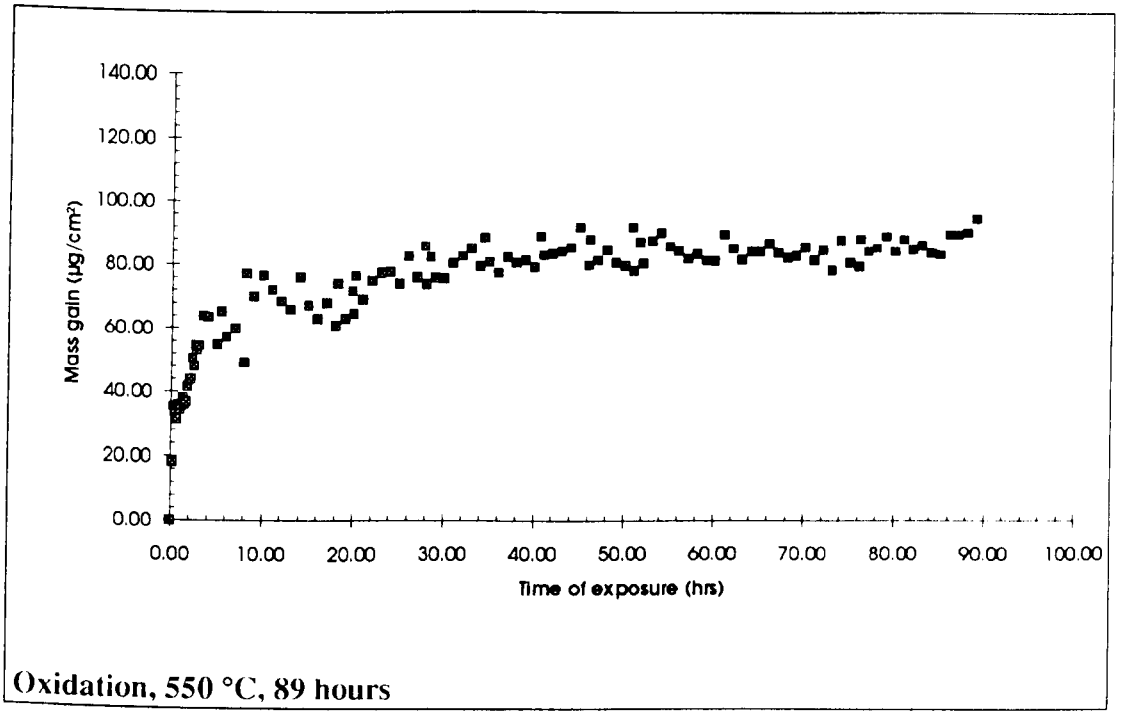

Oxidation, 550 °C, 89 hours

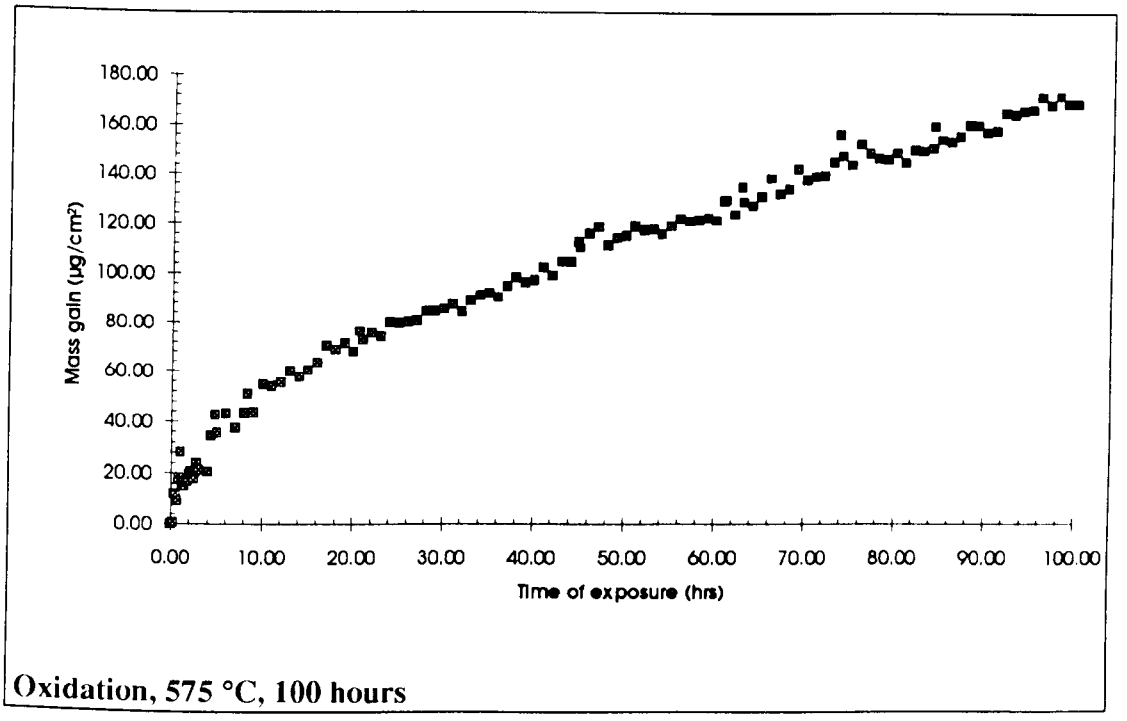

Oxidation, 575 °C, 100 hours

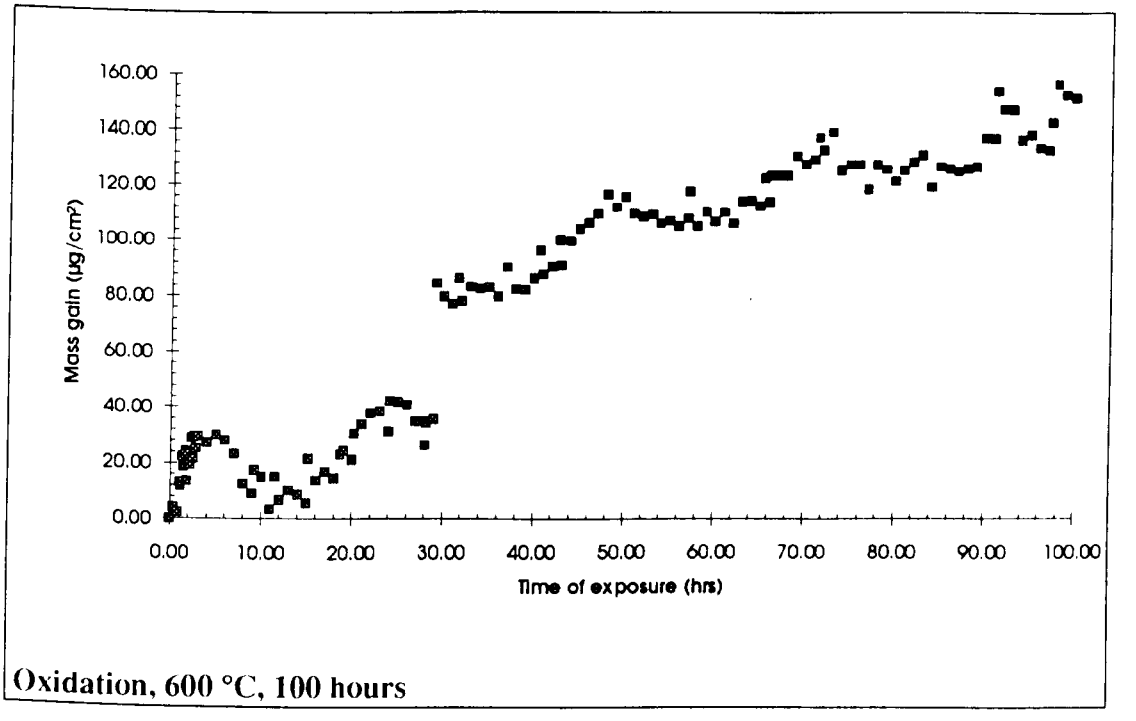

Oxidation, 600 °C, 100 hours

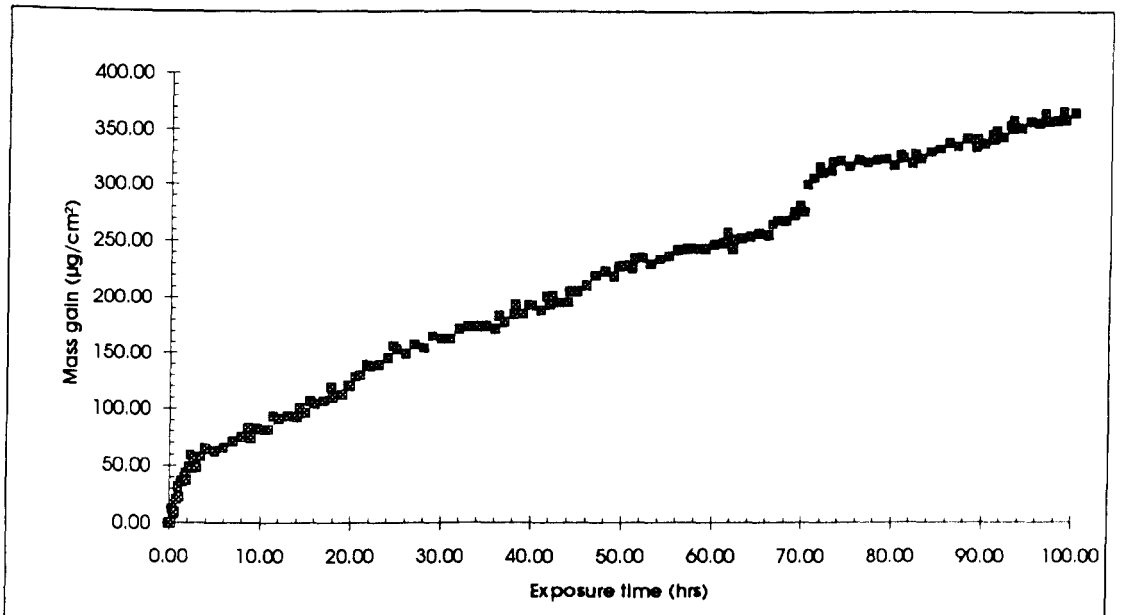

Oxidation, 625 °C, 100 hours

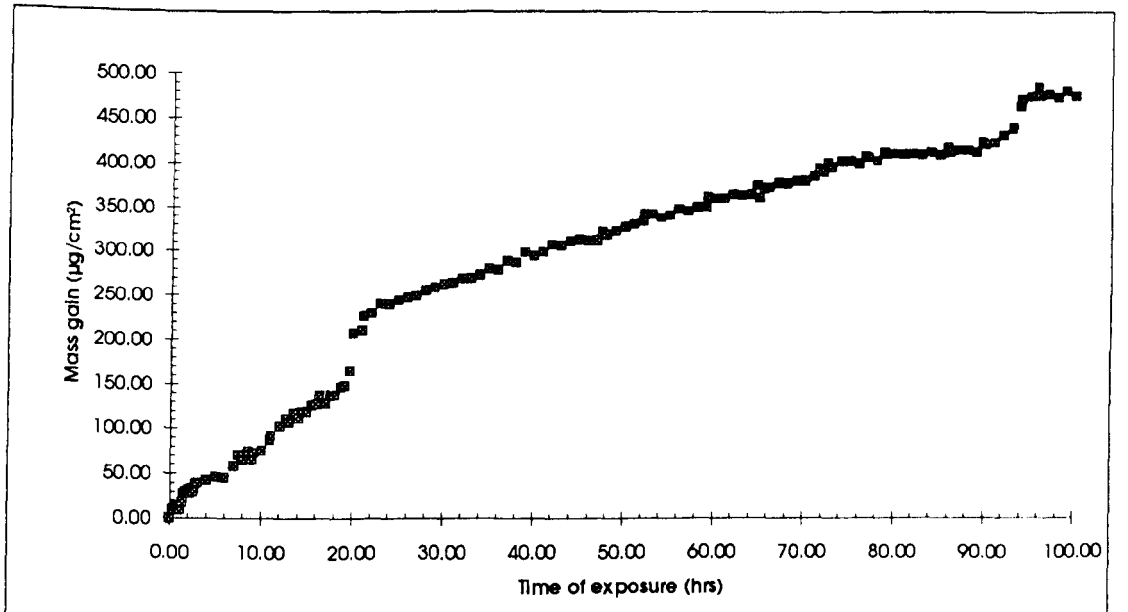

Oxidation, 650 °C, 100 hours

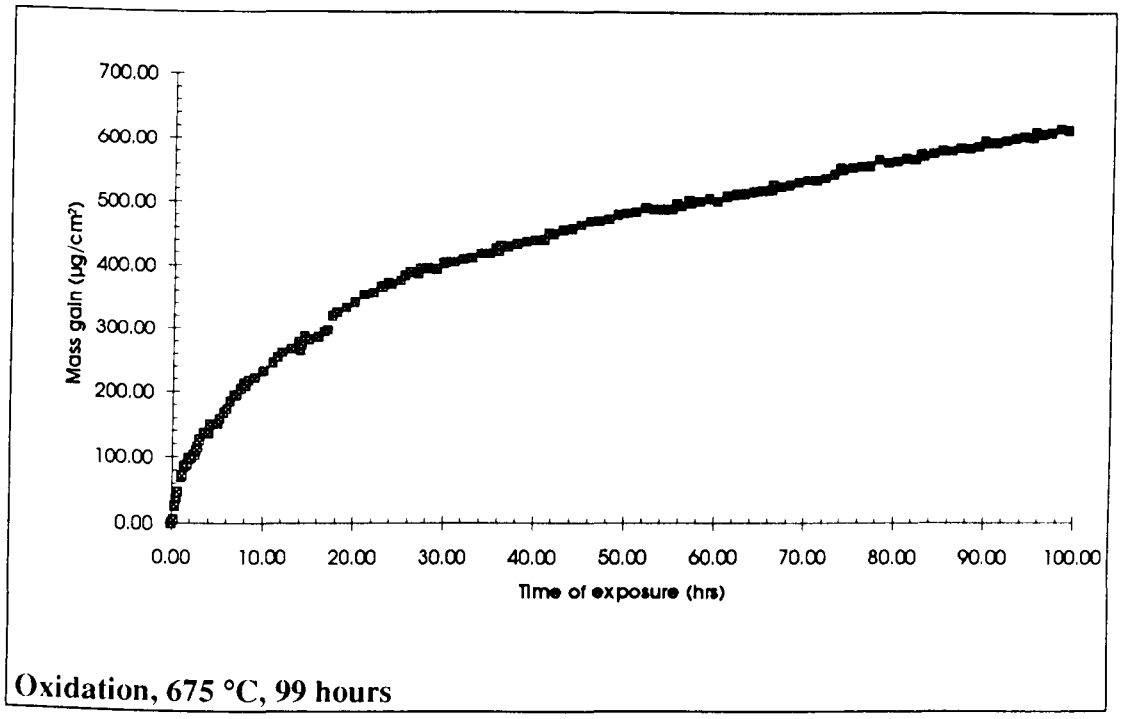

Oxidation, 675 °C, 99 hours

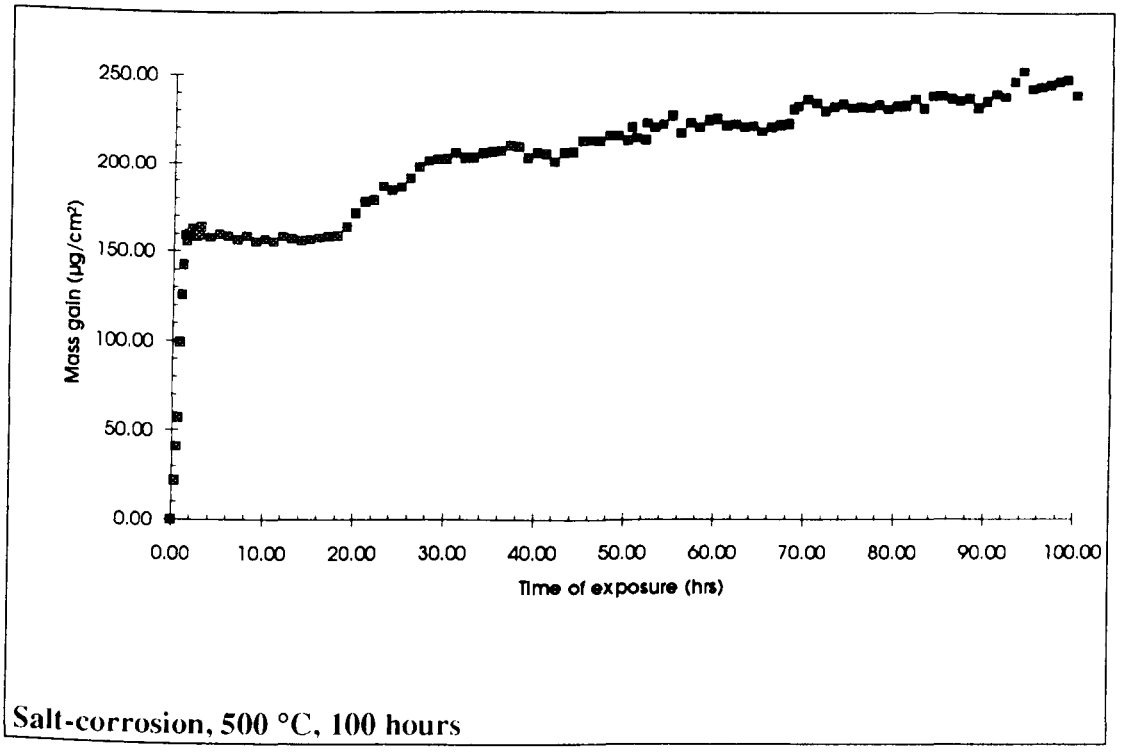

Salt-corrosion, 500 °C, 100 hours

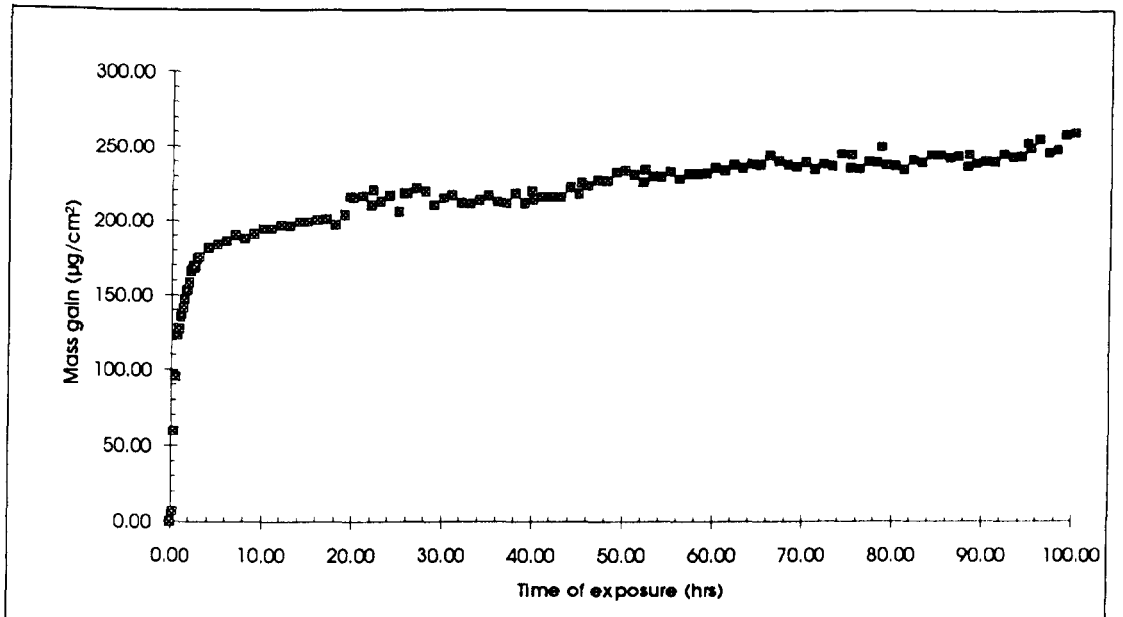

Salt-corrosion, 525 °C, 100 hours

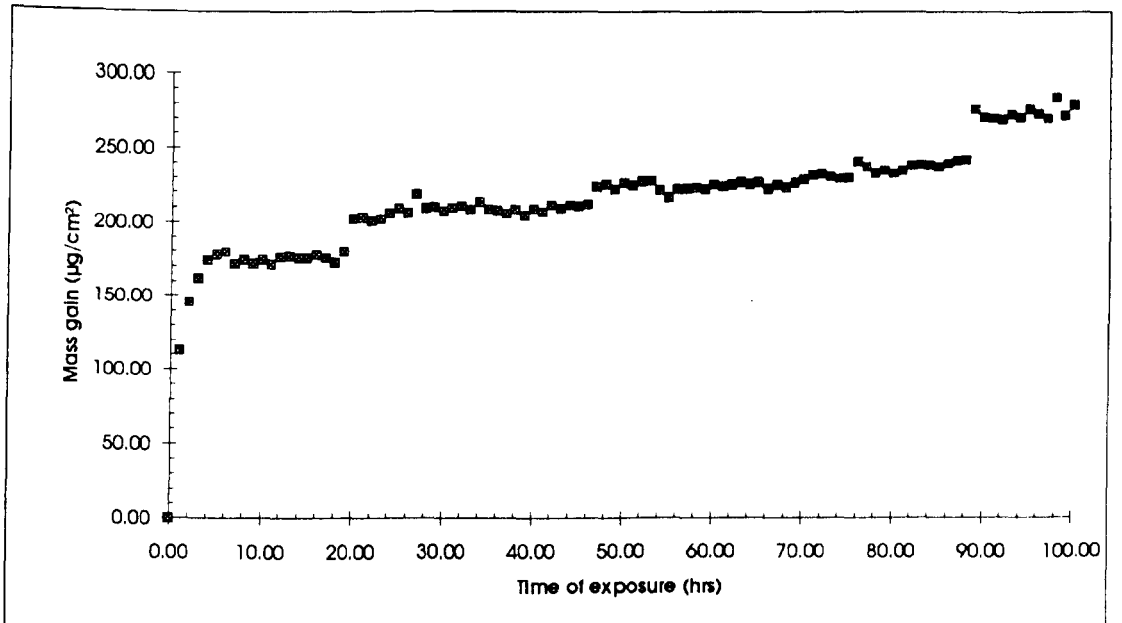

Salt-corrosion, 550 °C, 100 hours

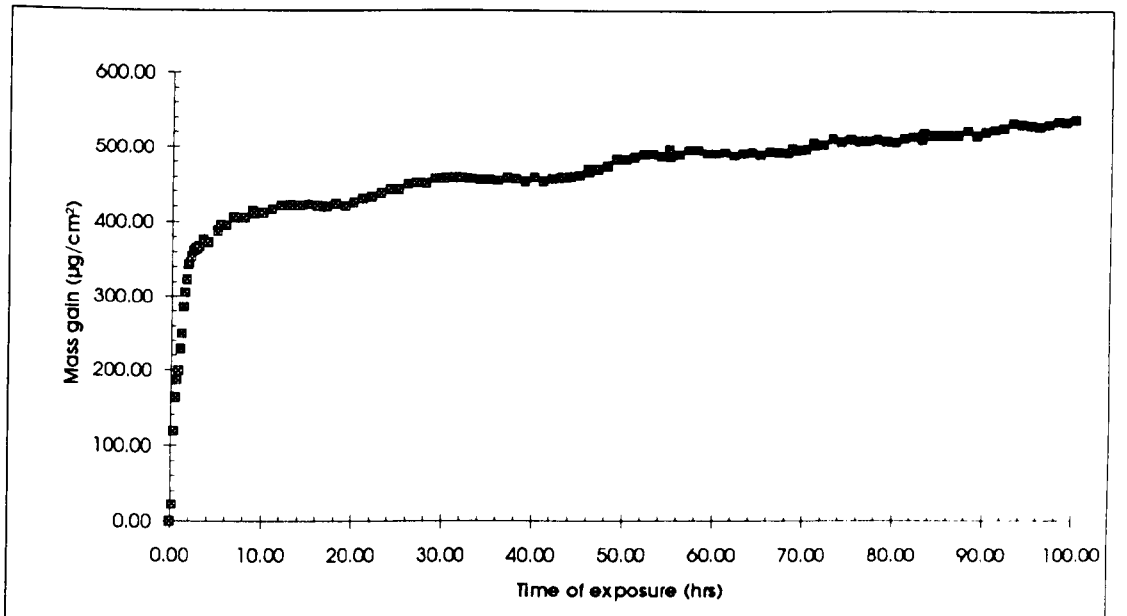

Salt-corrosion, 575 °C, 100 hours

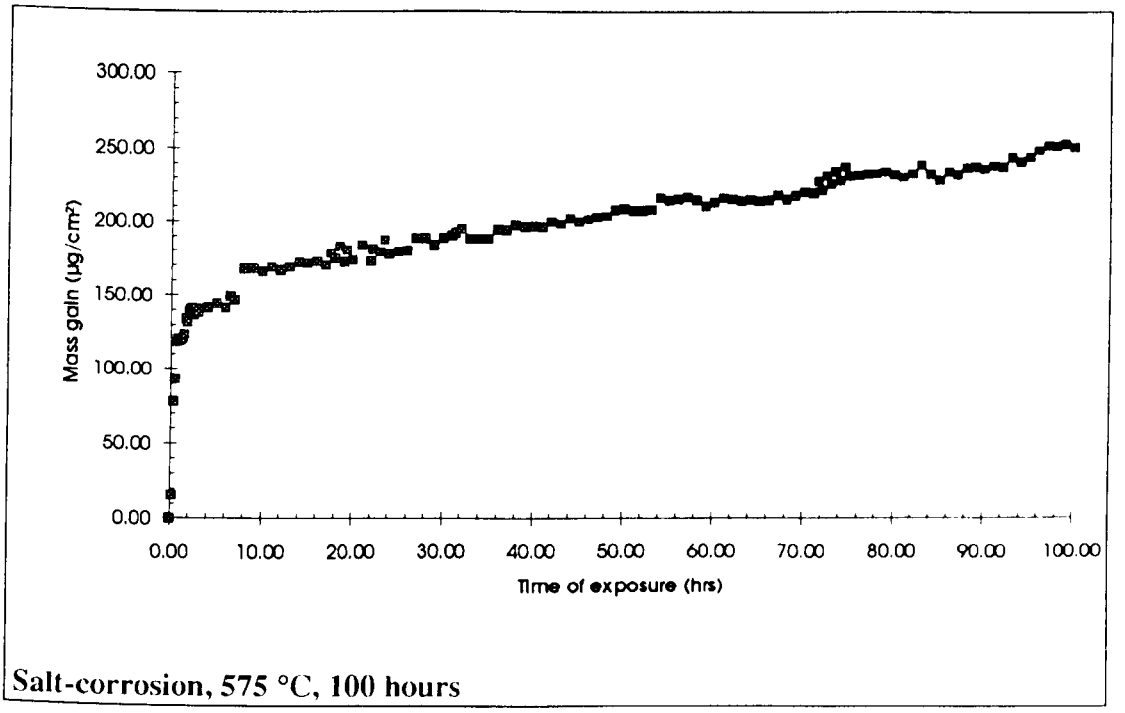

Salt-corrosion, 575 °C, 100 hours

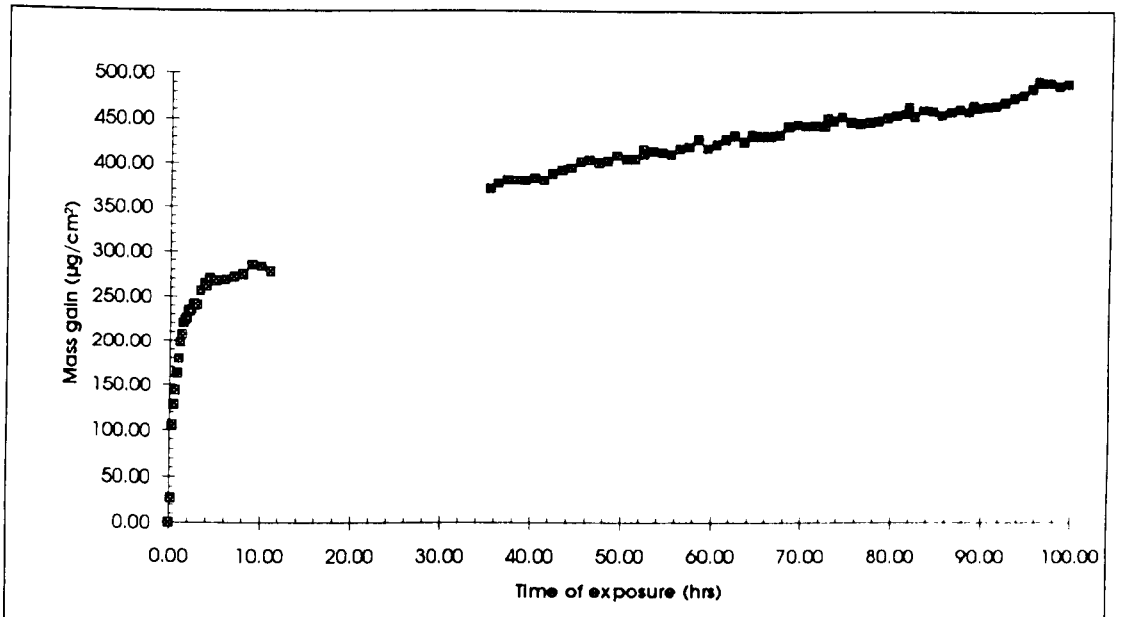

Salt-corrosion, 600 °C, 99.17 hours

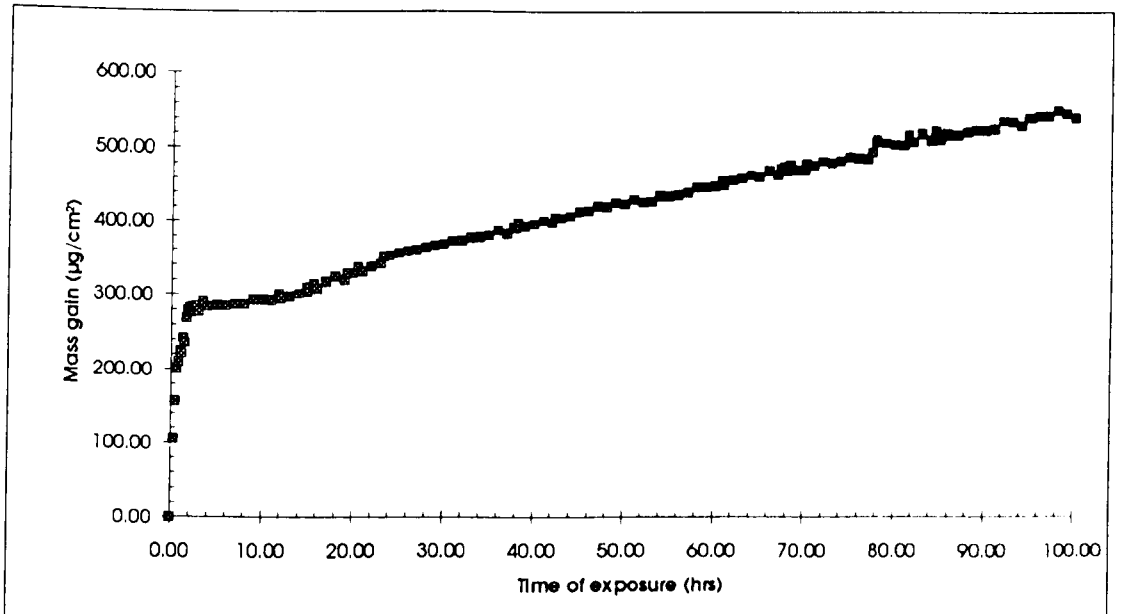

Salt-corrosion, 625 °C, 100 hours

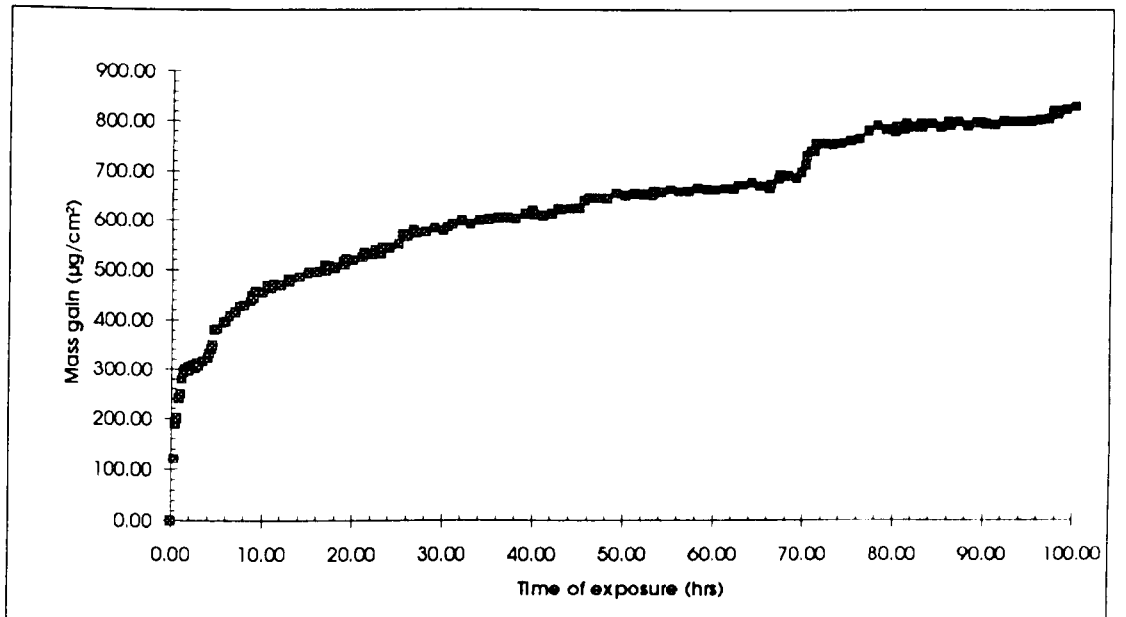

Salt-corrosion, 650 °C, 100 hours

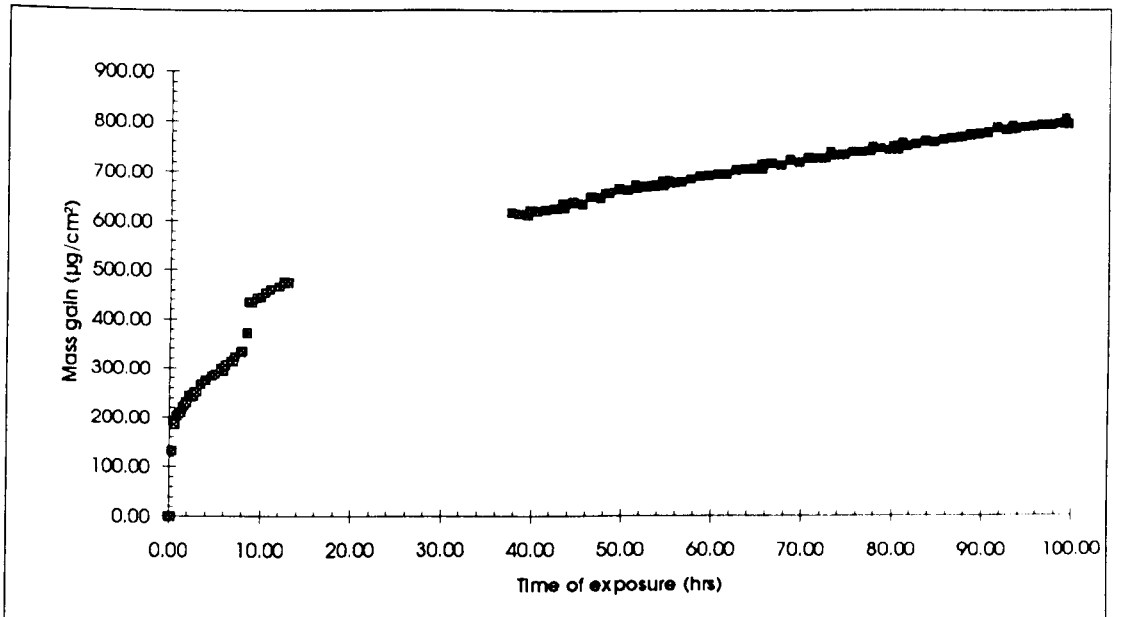

Salt-corrosion, 675 °C, 99.5 hours

REFERENCES

[ABKOWITZ 1955] "Titanium in Industry : Technology of Structural Titanium"
S. Abkowitz, J. J. Burke, R. H. Hiltz Jr.
D. Van Nostrand Company, New York, 1955.

[AL-KHYAT 1991] "High temperature chloride induced corrosion of nickel and nickel-based alloys"
A. I. Al-Khyat
PhD thesis, Cranfield Institute of Technology, August 1991

[ASHBROOK 1969] "A survey of salt deposits in compressors of flight gas turbine engines"
R. L. Ashbrook
NASA TN D-4999, 1969.

[ASTM 1966] Stress-corrosion cracking of titanium,
ASTM STP397, 1966

[ASTM 1972] "Microstructure of Titanium and Titanium Alloys"
ASTM comitee on Metallography of Titanium and Titanium Alloys
American Society for Metals
Metal handbook, 8th Edition, vol. 7, 1972.

[BECK 1969] "Electrochemical aspects of titanium stress-corrosion cracking"
T. R. Beck
in *Fundamental aspects of stress-corrosion cracking*
R. Staehle, A. J. Forty, D. Van Rooyen Eds
Nat. Assoc. of Corrosion Engineers
Houston, pp 605-619, 1969

[BIRKS 1983] "Introduction to high temperature oxidation of metals"
N. Birks, G. H. Meier
Edward Arnold publishers, 1983.

[BLACKBURN 1973] "Critical review: Stress-corrosion and hydrogen embrittlement"
M. J. Blackburn, W. H. Smyrl
in *Titanium Science and Technology*, Plenum Press, New York, 1973, pp 2577-2609

[BOMBERGER 1968] "The general corrosion resistance of titanium"
H. B. Bomberger
in *Titanium for the chemical engineer*
DMIC memorandum 234, pp 29-34, 1968.

[BOUDREAU 1968] "Stress-Corrosion behaviour of Titanium alloy 6-2-4-2 as related to engine operation"
Proceedings 8th Annual National Conference on Environmental Effects of Aircraft and Propulsion Systems
Inst. Environmental Sci., pp. 105-122, 1968.

[BOYD 1964] "The phenomenon of Hot-Salt Stress-Corrosion of Titanium Alloys"
W. K. Boyd, F. W. Fink
NASA CR-117, Battelle Memorial Institute, 1964.

[BOYD 1969] "Stress-corrosion cracking of titanium and its alloys"
W. K. Boyd
in *Fundamental aspects of stress-corrosion cracking*
R. Staehle, A. J. Forty, D. Van Rooyen Eds
Nat. Assoc. of Corrosion Engineers
Houston, pp 593-603, 1969

[BS 3900] "Methods of test for paints. Part F4: Resistance to continuous salt spray"
British Standards Institution, London, 1968

[CHAZE 1990] "Influence of aluminium on the oxidation of titanium between 550 and 750 °C"
A. M. Chaze, C. Coddet
Journal of the less common metals
No. 157, pp 55-70, 1990

[COTERILL 1961] "The hydrogen embrittlement of titanium alloys"
P. Coterill
Progress in Materials Science, Vol. 9, No. 4, 1961,
pp. 241-259.

[CROSSLEY 1960] "The determination of the effects of elevated temperatures on the stress-corrosion behaviour of structural materials"
F. A. Crossley, C. J. Reichel, C. R. Simcoe
WADD technical report 60-191, 1960.

[CUNINGHAM 1993] Private communication, Rolls Royce plc.

[DINNAPPA 1988] "Hot-Salt Stress-Corrosion Cracking of a Titanium Alloy : The phenomenon in view of Aero Gas Turbine operating conditions"
R. K. Dinnappa
Key Eng. Mat., vol. 3, pp. 2255-2271, 1988.

[DONACHIE 1966] "Effects of salt atmosphere on crack sensitivity of commercial titanium alloys at 600 to 900 F"
M. J. Donachie Jr., W. P. Danesi, A. A. Pinkowish
in *Stress-corrosion cracking of titanium*, ASTM STP397,
pp. 179-194, 1966.

[DONACHIE 1982] "Introduction to Titanium and Titanium Alloys"
M. J. Donachie Jr.
in *Titanium and Titanium Alloys : Source Book*
American Society for Metals, 1982, pp. 3-9.

[DUMAS 1976] "NaCl-induced accelerated oxidation of titanium alloys"
P. Dumas, C. St John
Oxidation of metals, Vol. 10, No. 2, 1976, pp. 127-134.

[EYLON 1984] "High Temperature Titanium Alloys - A review"
D. Eylon, S. Fujishiro, P. J. Postans, F. H. Froes
Journal of Metals, November 1984, pp. 55-62.

[JACOBSON 1990] "High temperature reactions of ceramics and metals with chlorine and oxygen"
N. S. Jacobson, M. J. McNallan, E. R. Kreidler
in *Materials chemistry at high temperatures*, Vol 2,
J. W. Hastie Ed., Humana, 1980, pp381-392

[JAFFEE 1980] "An overview on titanium development and application"
R.I.Jaffee
Titanium '80, Science and technology
TMS-AIME publications, 1980, pp. 53-74

[JANAF 1975] "JANAF thermochemical tables"
NSRDS-NBS-37, Dow Chemical Co, 1974 and 1975 supplements

[GARFINKLE 1972] " An electromechanical model for Hot-Salt Stress-Corrosion of Titanium alloys"
M. Garfinkle
NASA TN D-6779, 1972.

[GARFINKLE 1973] "An electrochemical model for hot-salt stress-corrosion of titanium alloys"
M. Garfinkle
Metallurgical Transactions, Vol. 4, 1973, pp.1677-1686.

[GIGGINS 1980] "Corrosion of metals and alloys in mixed gas environments at elevated temperature"
C. S. Giggins, F. C. Pettit
Oxidation of metals, Vol 14, No 5, 1980, pp 363-413

[GRAHLE 1991] "Protective coatings for Ti_3Al against high temperature oxidation"
P .Grahle, B .Heine, E .Fromm
Materials and corrosion, No 42, 1991, pp 12-18

[GRAY 1969a] "Hot-Salt Stress-Corrosion of Titanium Alloys"
H. R. Gray
in *Aerospace Structural Materials*, Proceedings,
NASA SP227, pp. 251-268, 1969.

[GRAY 1969b] "Hot-Salt Stress-Corrosion of a Titanium Alloy under a simulated turbine engine compressor environment"
H. R. Gray, J. R. Johnston
NASA TN D-5510, 1969.

[GRAY 1970] "Hot-Salt Stress-Corrosion of a Titanium Alloy in a air environment"
H. R. Gray, J. R. Johnston
Metallurgical Transactions, vol. 1, 1970, pp. 3101-3105.

[GRAY 1971a] " Relative susceptibility of titanium alloys to hot-salt stress corrosion"
H. R. Gray
NASA Technical Note TN D-6498, November 1971.

[GRAY 1971b] "Role of hydrogen in hot-salt stress-corrosion of a titanium alloy"
H. R. Gray
NASA TN D-6188, 1971.

[GRAY 1971c] "Ion and laser microprobes aqpplied to the measurement of corrosion produced hydrogen on a microscopic scale"
H. R. Gray
NASA TN D-6521, 1971.

[GRAY 1971d] "Effect of initial hydrogen content of a titanium alloy on susceptibility to hot-salt stress-corrosion"
H. R. Gray
NASA TM X-2404, 1971.

[GRAY 1973] "Hot-Salt Stress-Corrosion of Titanium Alloys as related to turbine engine operation"
H. R. Gray
in *Titanium Science and Technology*, Plenum Press,
New York, 1973, pp. 2627-2638.

[GRAY 1974] "Effect of exposure cycle on hot-salt stress-corrosion of a titanium alloy"
H. R. Gray, J. R. Johnston
NASA TM X-3145, 1974.

[GROVES 1973] "Environmental protection to 922 K for titanium alloy"
M. T. Groves
NASA CR-134537, 1373.

[HANCOCK 1978] "The role of halides in high temperature gas corrosion"
P. Hancock
Journal of Electrochemical Society, Vol 78, No 1, 1978,
pp 645-659

[HATCH 1966] "Effects of environment on cracking of titanium alloys"
A. J. Hatch, H. W. Rosenberg, E. F. Erbin
in *Stress-corrosion cracking in Titanium*, ASTM STP397,
pp. 122-136, 1966.

[HEIMERL 1966] "Salt-stress corrosion of Ti-8Al-1Mo-IV alloy sheet at elevated temperatures"
G. J. Heimerl, D. N. Braski, D. M. Royster, H. B. Dexter
in *Stress Corrosion Cracking of Titanium*, ASTM STP397, pp. 194-214, 1966.

[HURON 1988] "Titanium requirement for current and future military gas turbine engines"
E. S. Huron, J. A. Miller
2nd International SAMPE metals conference
August 2-4, 1988.

[IMI 1990] "High Temperature Alloys"
IMI Titanium Ltd., 1990.

[KING 1966] "The stress-corrosion threat"
J. A. King
Space/Aeronautics, October 1966, pp 61-67

[KIRCHNER 1966] "The diffusion of corrosion products in hot-salt stress-corrosion cracking of titanium"
R. L. Kirchner, E. J. Ripling
in *Stress-corrosion cracking of titanium*, ASTM, STP397, pp. 230-245, 1966.

[KOFSTAD 1966] "High temperature oxidation of metals"
P. Kofstad
John Wiley & Sons, inc. , 1966

[KOFSTAD 1988] "High temperature corrosion"
P.Kofstad
2nd Edition, Elsevier Applied Science, 1988

[KOLACHEV 1977] "Effect of Salt-Corrosion on the Endurance strength of pseudoalpha Titanium alloys"
B. A. Kolachev, V. V. Travkin, Y. N. Artsybasov
Sov. Mater. Sci., vol. 13, No. 4, pp.391-394, 1977.

[LAPASSET 1979] "Etude de la corrosion sous tension a chaud de l'alliage TA6V par le chlorure de sodium"
G. Lapasset
La recherche aérospatiale, No. 4, 1973, pp. 255-261.

[LINGWALL 1967] "Mechanisms of hot-salt stress-corrosion cracking of titanium base alloys"
R. G. Lingwall, E. J. Ripling
NASA CR-88979, Materials Research Lab., 1967.

[LIVANOV 1973] "Reversible hydrogen embrittlement of titanium alloys"
V. A. Livanov, B. A. Kolachev, R. M. Gabidullin, A. A. Buhanova
in *Titanium Science and Technology*, Plenum Press, pp. 2703-2717, 1973.

[LOGAN 1964] "The mechanisms of stress-corrosion of the titanium alloy Ti-8-1-1 exposed to salt environments at elevated temperatures"
H. L. Logan
National Bureau of Standards, R-130, May 1964.

[LOGAN 1966] "Chemical and Physical mechanisms of Salt-Stress Corrosion Cracking in the Titanium 8-1-1 alloy"
H. L. Logan, M. J. Mc Bee, C. J. Berchtoldt,
B. T. Sanderson, G. M. Ugiansky
in *Stress-Corrosion Cracking of Titanium*, ASTM STP397,
pp. 215-228, 1966.

[LOGAN 1969] "Studies of hot-salt cracking of the titanium 8%Al-1Mo-IV alloy"
H. L. Logan
in *Fundamental aspects of stress-corrosion cracking*,
NACE, Houston, 1969, pp. 662-672.

[MAHONEY 1972] "The effect of oxide thickness on the hot-salt stress-corrosion susceptibility of Ti-6Al-4 V"
M. W. Mahoney, N. E. Paton
Corrosion-NACE, Vol. 28, No. 10, October 1972,
pp. 374-377.

[MAHONEY 1976] "The effect of microstructure on the hot-salt stress-corrosion susceptibility of titanium alloys"
M. W. Mahoney, A. S. Tetelman
Metallurgical Transactions, Vol. 7, 1976, pp. 1549-1558.

[MARTIN 1966] "Investigation of long-term exposure effects under stress of two titanium structural alloys"
G. Martin
in *Stress corrosion cracking of Titanium*, ASTM STP397,
pp. 95-120, 1966.

[Mc QUILLAN 1951] "The Titanium-Hydrogen system for Magnesium-reduced Titanium"
A. D. Mc Quillan
Journal of the Institute of Metals, No 5, p 371, 1951

[MEYN 1974] "Effect of hydrogen on fracture and inert-environment sustained load cracking resistance of α/β alloys"
D. A. Meyn
Metallurgical Transactions, Vol. 5, 1974, pp. 319-328.

[MISKA 1974] "Titanium and its alloys"
K. H. Miska
Materials Engineering, July 1974, pp. 10-19.

[MOLCHANOVA 1964] "Phase diagrams of titanium alloys"
E. K. Molchanova
Israel Program for Scientific Translation, 1965

[MORTON 1976] "The Contribution of Physical Metallurgy to Engineering Practice"
P. H. Morton
Rosenhaim Centenary Conference, The Royal Society, 1976.

[MYERS 1977] "Hot-salt stress-corrosion cracking of titanium alloys : An improved model for the mechanism"
J. R. Myers, J. A. Hall
Corrosion-NACE, Vol. 33, No. 7, 1977, pp. 252-257.

[NEAL 1989] "IMI 834: A new high temperature capability titanium alloy for engine use"
D.F.Neal, M.J.Weaver
International Symposium on Air Breathing Engines,
American Institute for Aeronautics and Astronautics
Athens, 3-8 Sept. 1989, pp. 342-348.

[NICHOLLS 1993] Private communication, Cranfield University

[ONDREJCIN 1967] "Role of Chloride in Hot-Salt Stress-Corrosion Cracking of Titanium-Aluminium Alloys"
R. S. Ondrejcin, C. L. Selby, S. P. Rideout
NASA CR-87817, 1967. (or NASA DP-1116, 1967 ?)

[ONDREJCIN 1968] "Role of Hydrogen Chloride in Hot-Salt Stress-Corrosion Cracking of Titanium-Aluminium Alloys"
R. S. Ondrejcin, M. R. Louthan
NASA CR-1133, 1968.

[ONDREJCIN 1970] "Hydrogen in hot-salt stress-corrosion cracking of titanium aluminium alloys"
R. S. Ondrejcin
Metallurgical Transactions, Vol. 1, 1970, pp. 3031-3035.

[ONDREJCIN 1971] "The role of hydrogen in hot-salt stress-corrosion cracking of titanium-aluminium alloys"
R. S. Ondrejcin
NASA CR-1915, 1971.

[PETERSEN 1966] "The mechanism of salt attack on Titanium alloys"
V. C. Petersen, H. B. Bomberger
in *Stress Corrosion Cracking of Titanium*, ASTM STP397, pp. 80-94, 1966.

[PETERSEN 1971] "Hot-Salt Stress-Corrosion of Titanium"
V. C. Petersen
Journal of Metals, vol. 23, April 1971, pp. 40-47.

[PIPER 1966] "The relative Stress-Corrosion Susceptibility of Titanium Alloys in the presence of Hot-Salt"
D. E. Piper, D. N. Fager
in *Stress-Corrosion Cracking of Titanium*, ASTM STP397, pp. 31-52, 1966.

[PLEKHANOVA 1976] "Salt cracking of titanium alloys"
N. G. Plekhanova, E. A. Borisova, V. N. Modestova, T. V. Barysheva, N. D. Tomashov
Prot. Met., No. 12, 1976, pp. 559-563.

[POLMEAR 1989] "Light Alloys : Metallurgy of the light metals"
I. J. Polmear
2nd Edition
Edward Arnold publishers, London, 1989.

[REINSCH 1982] "Terminology for Titanium microstructures"
W. A. Reinsch
Metal Progress, February 1982, pp. 51-55.

[RIDEOUT 1966] "Basic mechanisms of stress-corrosion cracking of titanium"
S. P. Rideout, S. P. Louthan, C. L. Selby
in *Stress-Corrosion Cracking of Titanium*, ASTM STP397, pp. 137-151, 1966.

[RIDEOUT 1967] "The role of moisture and hydrogen in hot-salt cracking of titanium alloys"
S. P. Rideout, R. S. Ondrejcin, M. R. Louthan, D. E. Rawl
Symposium on fundamental aspects of stress-corrosion cracking, Ohio State University, September 1967.

[RIDEOUT 1968] "The initiation of hot-salt stress-corrosion cracking of titanium alloys"
S. P. Rideout
in *Applications related phenomena in Titanium alloys*,
ASTM STP432, 1968, pp. 205-217.

[ROSENBERG 1970] "Titanium alloying in theory and practice"
in *The Science, Technology, and Application of Titanium*
H. W. Rosenberg
Pergamon Press, New York, 1970, pp. 851-859.

[ROYSTER 1968] "Hot-Salt Stress-Corrosion Cracking and its effect on tensile properties of Ti-8Al-1Mo-IV Titanium alloy sheet"
D. M. Royster
NASA Technical Note TN D-4674, 1968.

[SCHOFIELD 1955] "The constitution of titanium-oxygen alloys in the range 0-35 weight per cent. oxygen"
T. H. Schofield, A. E. Bacon
Journal of the Institute of Metals, No 84, p 47, 1955

[SEAGLE 1968] "Physical Metallurgy and Metallography of Titanium Alloys"
S. R. Seagle, S. J. Bartlo
Metals Engineering Quaterly, vol. 8, August 1968, pp.1-10.

[SHIH 1988] "Hydrogen embrittlement of α titanium: In Situ TEM studies"
D. S. Shih, I. M. Robertson, H. K. Birnbaum
Acta Metall., vol 36, 1988, pp 111-124.

[SIMENZ 1966] "Environmental effects studies on selected titanium alloys"
R. F. Simenz, J. M. Van Orden, G. G. Wald
in *Stress-Corrosion Cracking of titanium*, ASTM STP397,
pp. 53-79, 1966.

[SINIGLIA 1978] "Hot-Salt Stress-Corrosion Cracking of Titanium Alloys"
D. Siniglia, G. Taccani, B. Vicentini
Corrosion Sci., vol. 18, pp. 781-796, 1978.

[SHIH 1988] "Hydrogen embrittlement of α titanium : *In situ* TEM studies"
D. S. Shih, I. M. Robertson, H. K. Birnbaum
Acta Metallurgia, Vol. 36, No. 1, 1988, pp. 111-124.

[SMITHELLS 1976] "Metals Reference"
C. J. Smithells
6th Edition, Butterworths, London, 1983.

[STEIN 1968] "Coatings and surface treatments for longtime protection of Ti-8Al-1Mo-IV alloy sheet from hot-salt stress-corrosion"
B. A. Stein, H. B. Dexter, D. M. Royster
NASA Technical Note TN D-4319, 1968.

[STONE 1967] "Cyclic hot-salt stress-corrosion of Titanium alloys"
L. H. Stone, A. H. Freedman
Northrop Corporation, AFML TR-67289, 1967.

[TML 1957] "Progress report on the salt-corrosion of titanium alloys at elevated temperature and stress"
TML report 88, Battelle Memorial Institute, 1957.

[TRAVKIN 1979] "Thermodynamic analysis of the chemical mechanisms for the hot-salt corrosion of titanium alloys"
V. V. Travkin, V. F. Pshirkov, B. A. Kolashev
Sov. Mater. Sci., No. 15, 1979, pp. 134-137.

[TURLEY 1966] "Elevated temperature static and dynamic sea-salt stress cracking of Titanium alloys"
R. V. Turley, C. H. Avery
in *Stress Corrosion Cracking of Titanium*, ASTM STP397,
pp. 1-30, 1966.

[WAISMAN 1973] "Diffusion of hydrogen in titanium alloys due to composition, temperature, and stress gradients"
J. L. Waisman, G. Sines, L. B. Robinson
Metallurgical transactions, Vol. 4, 1973, pp 291-302

[WALKER 1994] Private Communication, Rolls Royce plc., 1994

[WALLWORK 1959] "Oxidation of titanium, zirconium, and hafnium"
G. R. Wallwork, A. E. Jenkins
Journal of the Electrochemical Society, Vol. 106, No. 10,
1959.

[WEAVER 1982] "The influence of hot-salt on the properties of titanium alloys"
M. J. Weaver, M. R. Winstone
National Gas Turbine Establishment, Memorendum 82008, 1982.

[WEBER 1967] "Stress-corrosion of Titanium alloys under simulated supersonic flight conditions"
K. E. Weber, A. D. Davis
NASA CR-981, Lockheed Aircraft Corp., 1967.

[WEBSTER 1992] Private communication, Rolls Royce plc.

[WILLIAMS 1960] "Relationships between impact embrittlement and slow-strain-rate hydrogen embrittlement of titanium alloys"
D. N. Williams, R. I. Jaffee
J. Less Common Metals, No. 2, 1960, pp. 42-

[WILLIAMS 1963] "The hydrogen embrittlement of titanium alloys"
D. N. Williams
Journal of the Institute of Metals, Vol. 91, 1963, pp. 147-152

[WING 1990] Private communication, Rolls Royce plc.

[WRIGHT 1974] "Environmental protection of titanium alloys at high temperatures"
I. G. Wright, R. A. Wood, M. S. Seltzer
NASA CR-134681, 1974.